

Understanding MS/MS fragmentation pathways of small molecular weight molecules

Patricia Ann Wright [BSc (Hons), MPhil]

A thesis submitted in fulfilment of the requirements of the University of Greenwich for the Degree of Doctor of Philosophy

July, 2015

Department of Pharmaceutical, Chemical & Environmental Sciences
Faculty of Engineering & Science,
University of Greenwich (Medway Campus),
Chatham Maritime, ME4 4TB, UK



UNIVERSITY
of
GREENWICH

DECLARATION

I certify that this work has not been accepted in substance for any degree, and is not concurrently being submitted for any degree other than that of Doctor of Philosophy being studied at the University of Greenwich. I also declare that the work is the result of my own investigations except where otherwise identified by references and that I have not plagiarised the work of others.

SignedPatricia Wright (Candidate)

Date

.....

PhD Supervisor

Signed Prof. Francis Pullen

Date

ACKNOWLEDGEMENTS

This project would not have been possible without Prof. Frank Pullen (University of Greenwich) and Dr Alexander Alex (Evenor Consulting Limited). The scientific discussions we have had were both highly enjoyable and scientifically outstanding. I feel privileged to work with these exceptional scientists.

I would also like to thank Cris Laphorn for all the help he has given me. I am always impressed by his ability to remain cheerful even in adversity.

I wish to thank the Vice Chancellor's Office (University of Greenwich) for providing the studentship which enabled me to undertake doctoral studies and also the BMSS for supplying a small equipment grant for the purchase of the Spartan computational chemistry software.

ABSTRACT

Fragmentation of molecules by collision-induced dissociation (CID) is not well-understood, making interpretation of MS/MS spectra difficult and limiting the effectiveness of software tools intended to aid mass spectral interpretation. An approach is required which is tailored to each individual molecule and improves the 'chemical sense' of the software.

It was hypothesised that the bonds which break during CID of protonated molecules are the bonds which are elongated, and hence weakened, as a result of conformational changes induced by protonation. Bond length changes for a test set of molecules were calculated using quantum chemistry software. Density Functional Theory (DFT) or Austin Model 1 (AM1) or both were used to energy minimise the structures of the neutral molecules and their corresponding protonated molecules (protonated at all possible sites). Bonds which elongated to the greatest extent after protonation were compared to the bonds which were found to cleave to give the product ions in the CID spectra of these compounds. Quantum chemistry modelling was also applied to the deprotonated molecules.

AM1 calculated bond lengths were found to be similar to those generated by DFT and have the advantage of being rapidly obtained. All the polarised bonds which cleaved were calculated to elongate significantly, thus achieving a 100% success rate in the prediction of bond cleavage as a result of protonation on a heteroatom. The proton is mobile across the molecule, leading to fragmentation when the proton reaches a site where it causes significant bond elongation, provided the molecule has sufficient internal energy. Cleavage of carbon-carbon bonds was not predicted. The success rate for predicting bond cleavage in deprotonated molecules was 48%, suggesting this approach cannot be applied reliably for these anions.

AM1 calculated bond length change acts as a descriptor for predicting polarised bond cleavage in protonated pseudo-molecular ions having the potential to be incorporated in mass spectral interpretive software to increase the accuracy of prediction of CID spectra.

DEDICATION

I wish dedicate this thesis to my family: My husband Adrian for his continual help and support and without whom I would not be the person I am today; my intelligent, handsome sons Iain and Tom for the continual entertainment they supply, making sure I am never bored; and my late father, Len, who was always proud of me; he taught me to work hard and not to be limited by other people's expectations.

CONTENTS

DECLARATION	II
ACKNOWLEDGEMENTS	II
ABSTRACT	III
DEDICATION	IV
CONTENTS	V
TABLE OF FIGURES	IX
TABLES	XI
LIST OF ABBREVIATIONS	XV
PUBLICATIONS AND PRESENTATIONS	XVI
CHAPTER 1: INTRODUCTION	1
1.1. MASS SPECTROMETRY FOR SMALL MOLECULE ANALYSIS (LESS THAN 1000 DA) 1	
1.1.1. Overview	1
1.1.2. Ionisation sources	1
1.1.1. Mass Analysers	7
1.2. SOFTWARE TOOLS FOR ANALYTICAL SCIENTISTS	12
1.2.1. Overview	12
1.1.1. Software aids for the mass spectrometrist	15
1.1.1.1. Mass Frontier	16
1.1.1.2. MS Fragmenter	16
1.1.1.3. Mass Spec Calculator	16
1.1.1.4. Fragment iDentificator (FiD)	16
1.1.1.5. EPIC (Elucidation of product ion connectivity)	17
1.1.1.6. MetFrag	17
1.1.1.7. Mass Bank	17
1.1.1.8. Metabolite Specific Software	18
1.3. QUANTUM MECHANICAL APPROACHES	18
1.3.	21
1.4. INTRODUCTION TO COMPUTATIONAL CHEMISTRY	21
1.4.1. Molecular orbital calculations	22
1.4.2. Semi-empirical calculations	24
1.4.3. Basis sets	26
1.4.4. Density Functional Theory (DFT)	26
1.5. THERMODYNAMICS AND KINETICS OF IONS DURING ESI AND CID (COLLISION-INDUCED DISSOCIATION)	30

1.5.1. ESI and ion transmission	30
1.5.2. CID	32
CHAPTER 2: UNDERSTANDING COLLISION-INDUCED DISSOCIATION OF DOFETILIDE: A CASE STUDY IN THE APPLICATION OF DENSITY FUNCTIONAL THEORY AS AN AID TO MASS SPECTRAL INTERPRETATION	36
2.1. INTRODUCTION	36
2.2.1. Chemicals.....	40
2.2.2. High resolution MS/MS	40
2.2.3. Computational calculations	40
2.3. RESULTS AND DISCUSSION	41
2.3.1. Ionisation.....	41
2.3.2. Thermodynamics of Fragmentation	44
2.3.3. Proton migration/tunnelling	52
2.3.4. Stability of product ions	57
2.3.5. Mass Fragment Prediction of Dofetilide Product Ions.....	60
2.4. CONCLUSIONS	62
CHAPTER 3: PREDICTING COLLISION INDUCED DISSOCIATION (CID) SPECTRA: SEMI-EMPIRICAL CALCULATIONS AS A RAPID AND EFFECTIVE TOOL IN SOFTWARE-AIDED MASS SPECTRAL INTERPRETATION	63
3.1. INTRODUCTION	63
3.2. EXPERIMENTAL.....	66
3.2.1. Chemicals.....	66
3.2.2. LC/MS	67
3.2.3. Computational modelling.....	69
3.2.4. Assignment of product ions.....	69
3.3. RESULTS AND DISCUSSION	70
3.3.1. Comparison of AM1 and DFT for calculating bond length changes	70
3.3.2. Comparison of AM1 and DFT for calculating relative gas phase basicities.....	72
3.3.3. Prediction of bond cleavage on basis of calculated bond elongations	73
3.3.4. Prediction of product ion intensity	81
3.3.5. Proton migration	83
3.4. CONCLUSIONS	86
CHAPTER 4: THE USE OF AM1 FOR PREDICTING NEGATIVE ION CID FRAGMENTATION	88
4.1. INTRODUCTION	88
4.2. EXPERIMENTAL.....	90

4.2.1. Chemicals.....	90
4.2.2. LC/MS	90
4.2.3. LC/MS Computational modelling.....	91
4.2.4. Assignment of product ions.....	91
4.3. RESULTS AND DISCUSSION	91
4.3.1. Dofetilide	91
4.3.2. Sulpiride	95
4.3.3. Reserpine.....	98
4.3.4. Sildenafil.....	101
4.3.5. Carboxylic acids and phosphates	104
4.4. CONCLUSIONS	106
CHAPTER 5: COMPARING APCI AND ESI SPECTRA	109
5.1. INTRODUCTION	109
5.2. EXPERIMENTAL.....	110
5.2.1. Chemicals.....	110
5.2.2. LC/MS	110
5.2.3. Computational modelling.....	110
5.2.4. Assignment of product ions.....	110
5.3. RESULTS AND DISCUSSION	111
5.3.1. Compounds with APCI and ESI spectra are similar.....	111
5.3.1.1. Similar Gas and liquid phase basicities	111
5.3.1.2. Different gas and liquid phase basicities	112
5.3.1.3. Compounds for which APCI and ESI spectra differ	113
5.3.2. Relative intensity of APCI and ESI spectra.....	115
5.4. CONCLUSIONS	116
CHAPTER 6: EFFECT OF COLLISION ENERGY ON PROTON MIGRATION	117
6.1. INTRODUCTION	117
6.2. EXPERIMENTAL.....	121
6.2.1. Chemicals.....	121
6.2.2. LC/MS	121
6.2.3. Computational modelling.....	121
6.2.4. Assignment of product ions.....	122
6.2.5. Physicochemical properties	122
6.3. RESULTS	122
6.3.1. Interesting observation on fragmentation of desipramine.....	139
6.4. CONCLUSIONS	140
CHAPTER 7: CONCLUSIONS AND FUTURE WORK	142

REFERENCES.....	148
APPENDIX 1: THE PKA'S OF THE TEST COMPOUNDS	173
APPENDIX 2: THE RELATIVE STABILITIES OF THE CATIONS PROTONATED AT HETEROATOMS IN TEST COMPOUNDS	177
APPENDIX 4: THE WORK FLOW FOR CALCULATING THE BOND ELONGATIONS USING SPARTAN '10.....	191
APPENDIX 5: THE MAXIMUM INTERNAL ENERGY GAIN FOR EACH MOLECULE AT THE STATED COLLISIONS ENERGIES CALCULATED USING THE EQUATION S-2 IN CHAPTER 2.	193
APPENDIX 6: CALCULATING THE ACTIVATION ENERGIES FOR INTERNAL PROTON TRANSFER.....	194
APPENDIX 7. PROPOSED STRUCTURAL ASSIGNMENTS FOR PRODUCT IONS AND THEIR RELATIVE INTENSITIES	196
APPENDIX 8. PLOTS OF PHYSICOCHEMICAL PROPERTIES VERSUS CE₅₀ (THE COLLISION ENERGY AT WHICH THE SURVIVAL YIELD IS 50%)	208

TABLE OF FIGURES

Figure 1.1	Schematic representation of atmospheric pressure ionisation (APCI)....	2
Figure 1.2	Schematic representation of a) electrospray with ion evaporation;.....	4
Figure 1.3	Schematic Waters Synapt™ marketed by Waters	9
Figure 1.4	Schematic LTQ Orbitrap™ marketed by Thermo Fisher Scientific.	10
Figure 1.5	Overview of differences between computational methods.....	28
Figure 2.1	Structure of dofetilide highlighting the possible protonation sites	39
Figure 2.2	The structures of the four methylated analogues of dofetilide.	39
Figure 2.3	MS/MS (CID) spectrum of dofetilide.	46
Figure 2.4	MS/MS (CID) spectra of dofetilide analogues I to IV	48
Figure 2.5	Proposed scheme for the formation of the product ions of dofetilide. ...	56
Figure 2.6	Proposed formation of the product ion <i>m/z</i> 184	58
Figure 2.7	AM1 modelled configuration of dofetilide protonated at most basic centre.	59
Figure 2.8	AM1 modelled configuration of dofetilide product ion at <i>m/z</i> 255 protonated at most basic centre.	60
Figure 2.9	Screen shot of Waters MassFragment	61
Figure 3.1	The structures of the fifteen compounds analysed in this study.	68
Figure 3.2	Comparison of bond elongations calculated by both AM1 and DFT	70
Figure 3.3	CID product ion spectrum of protonated 1-methyl-2-pyrrolidinol.....	72
Figure 3.4	CID product ion spectrum of protonated ziprasidone.....	79
Figure 3.5	Structure of ziprasidone carbocation modelled by AM1	79
Figure 4.1	Structure of dofetilide with potential anionic sites designated A-1 to A-9.	92
Figure 4.2	The negative product ion spectrum of dofetilide.	92
Figure 4.3	The structure of sulpiride with the potential anionic sites designated A-1 to A-10.....	95
Figure 4.4	The negative product ion spectrum of sulpiride.	95
Figure 4.5	Structure of reserpine with potential anionic sites designated A-1 to A-13..	98
Figure 4.6	The negative product ion spectrum of reserpine.....	99

Figure 4.7 Structure of sildenafil with potential anionic sites designated A-1 to A-15.	101
Figure 4.8 The negative product ion spectrum of sildenafil.....	102
Figure 4.9. The structure of sildenafil anion A-4.	104
Figure 4.10 Structures of the four acidic compounds showing only the bonds observed to cleave in their CID spectra.....	105
Figure 5.1 The ESI and APCI spectra of sildenafil.....	112
Figure 5.2 The ESI and APCI spectra of desipramine	113
Figure 5.3 The structure of cortisone showing the most basic centre in solution and gas phase.....	114
Figure 5.4 The ESI and APCI spectra of cortisone (Waters' ESCi source).....	115
Figure 5.5 Schematic showing the polarity and molecular weight requirements for efficient APCI and ESI ionisation.	116
Figure 6.1 The product ions of desipramine, m/z 72 and m/z 193, formed by cleavage of N15 and C16.	139
Figure 6.2 The product at m/z 72 formed by heterolytic cleavage of N15-C1	140
Figure 7.1 Schematic illustrating the proposal that protonation induced bond elongation initiates bond cleavage.	147

All Figures are drawn by the author, Patricia Wright, unless otherwise referenced.

TABLES

Table 1.1. General characteristics of mass spectrometer ion sources commonly used for structural elucidation 1971 to 2015.....	6
Table 1.2 General characteristics of mass analysers commonly used for structural elucidation 1971 to 2015.	11
Table 1.3 Comparison of the relative computational chemistry approaches.	29
Table 1.4. Comparing the characteristics of CID associated with different types of mass analyser.	35
Table 2.1. Optimized geometries and relative energies for neutral and protonated species of dofetilide	44
Table 2.2 Comparison of bond length changes for neutral dofetilide and protonated species A-1 to A-6.	45
Table 2.3 Proposed structures for the product ions observed in the MSMS spectrum of dofetilide.	46
Table 2.4 Optimized geometries and relative energies for neutral and protonated species of four dofetilide analogues.	48
Table 2.5 Comparison of bond length changes for dofetilide analogues I to IV as a result of protonation to generate cations A-1 and A-6.	49
Table 2.6 Comparison of bond length changes for dofetilide analogues I to IV as a result of protonation to generate cations A-1 to A-6.	50
Table 2.7 Proposed structures for the product ions observed in the MSMS spectrum of the four dofetilide analogues I to IV.	51
Table 2.8 Accurate mass information for the product ions observed in the MSMS spectrum of the four dofetilide analogues I to IV.	51
Table 3.1 Comparison of bond length changes resulting from protonation of 1-methyl-2-pyrrolidinol at the sites specified in Figure 3.3.....	71
Table 3.2 The proposed product ion assignments for the ions in the CID spectrum of 1-methyl-2-pyrrolidinol	71
Table 3.3 The relative energies of the different protonated forms of ziprasidone calculated by using both AM1 and DFT.....	74
Table 3.4 Overall summary of the effectiveness of using calculated bond elongations to predict bond cleavages during CID fragmentation.....	75

Table 3.5 Changes in bond length in ziprasidone resulting from protonation of ziprasidone at the sites specified in Fig. 1, calculated using AM1 (Spartan'10).	76
Table 3.6 The proposed product ion assignments for the ions in the CID spectrum of ziprasidone.	77
Table 3.7 The proposed assignments of product ions resulting from carbon-carbon bond cleavage for trichlormethazide, reserpine, 5-(p-methyl)-phenylhydantoin and cortisone.	78
Table 3.8 Summary of over prediction of bond cleavage on the basis of proton-induced bond elongation.	81
Table 3.9 The bonds which were calculated to elongate by > 0.040Å after protonation at a site other than on one of the bonding atoms.	84
Table 3.10 Observations around relative abundance of product ions in the spectra of all fifteen compounds.	85
Table 4.1 Proposed structures for the product ions observed in the negative ion CID spectrum of dofetilide.	93
Table 4.2 Changes in bond length in of dofetilide resulting from deprotonation at the specified sites.	94
Table 4.3 Proposed structures for the product ions observed in the negative ion CID spectrum of sulpiride.	96
Table 4.4 Changes in bond length in of sulpiride resulting from deprotonation at the specified sites.	97
Table 4.5 Proposed structures for the product ions observed in the negative ion CID spectrum of reserpine.	99
Table 4.6 Changes in bond length in of reserpine resulting from deprotonation at the specified sites.	100
Table 4.7 Proposed structures for the product ions observed in the negative ion CID spectrum of reserpine.	102
Table 4.8 Changes in bond length in of sildenafil resulting from deprotonation at the specified sites.	103
Table 4.9 Changes in bond length in of 6-oxoheptanoic acid, aspirin, 1-palmitoyl lysophosphatidic acid and stearic acid resulting from deprotonation at the carboxylic acid or phosphate groups.	106

Table 6.1 The percentage abundance of product ions of desipramine at the stated collision energies.	123
Table 6.2 The percentage abundance of product ions of dofetilide at the stated collision energies.	123
Table 6.3 The percentage abundance of ions of doxazosin at the stated collision energies.	123
Table 6.4 The percentage abundance of ions of maraviroc at the stated collision energies.	124
Table 6.5 The percentage abundance of ions of amlodipine at the stated collision energies.	124
Table 6.6 The percentage abundance of ions of 1,1-dimethyl biguanidine at the stated collision energies.	125
Table 6.7. The percentage abundance of ions of sildenafil at the stated collision energies.	125
Table 6.8 The relative energies of maraviroc cations protonated at the initial ionisation site(s) compared to the cations formed by protonation at the dissociative sites yielding product ions at the collision energies stated.	128
Table 6.9 The relative energies of desipramine cations protonated at the initial ionisation site compared to the cations (s) formed by protonation at the dissociative site yielding product ions at the collision energies stated.	129
Table 6.10 The relative energies of doxazosin cations, protonated at the initial ionisation site compared to the structures formed by protonation at the dissociative site yielding product ions at the collision energies stated.	130
Table 6.11 The relative energies of amlodipine cations protonated at the initial ionisation site compared to the cations (s) formed by protonation at the dissociative site yielding product ions at the collision energies stated.	131
Table 6.12 The relative energies of sildenafil cations, protonated at the initial ionisation site(s), compared to the structures formed by protonation at the dissociative sites yielding product ions at the collision energies stated.	132
Table 6.13 The relative energies of 1,1-dimethylbiguanidine cations, protonated at the initial ionisation site(s), compared to the structures formed by protonation at the dissociative sites yielding product ions at the collision energies stated.	133

Table 6.14 The relative energies of dofetilide cations, protonated at the initial ionisation site(s), compared to the structures formed by protonation at the dissociative sites yielding product ions at the collision energies stated. 134

Table 6.15 The activation energies for the internal proton transfer from the starting and final cations of 1,1-dimethyl biguanidine, dofetilide, amlodipine and doxazosin. 136

Table 6.16 Physicochemical properties of the test compounds compared to the CE₅₀. 138

All Tables are compiled by the author, Patricia Wright, unless otherwise referenced

LIST OF ABBREVIATIONS

Abbreviation	Definition
AM1	Austin Model 1
APCI	Atmospheric pressure chemical ionisation
B3YLP	Becke, three-parameter, Lee-Yang-Parr
CID	Collision-induced Dissociation
DFT	Density Functional Theory
ESI	Electrospray ionisation
FTMS	Fourier-transform mass spectrometer
H-Bond	Hydrogen bond
IT	Ion trap
LDA	Local density approximation
MS	Mass spectrometry
MS/MS	Mass spectrometry/mass spectrometry (i.e. tandem mass spectrometry)
MP2	Møller–Plesset perturbation theory to second order
PM3	Parameterized Model number 3
TOF	Time-of-flight
QTOF	Quadrupole time-of-flight
[M+H] ⁺	Protonated molecular precursor ion

PUBLICATIONS AND PRESENTATIONS

Can computational chemistry be used to predict CID fragmentation of anions?

P.A. Wright, A. Alex and F. Pullen.

Accepted by *Rapid Communications in Mass Spectrometry* August 2015.

How useful is molecular modelling in combination with ion mobility mass spectrometry for 'small molecule' ion mobility collision cross sections?

C. Laphorn, F. Pullen, B. Z. Chowdhry, P.A. Wright, G. Perkins and Y. Heredia.

Analyst, 2015, Advance Article June 2015. DOI: 10.1039/C5AN00411J

Predicting collision-induced dissociation spectra: Semi-empirical calculations as a rapid and effective tool in software-aided mass spectral interpretation.

P.A. Wright, A. Alex and F. Pullen.

Rapid Communications in Mass Spectrometry **28**, 1127–1143 (2014).

Does not compute, or does it?

P. A. Wright. *Mass Matters* (British Mass Spectrometry Society) August 2014.

3D Thinking: Computational Aids for Bioanalysts.

P.A. Wright, A. Alex, and F. Pullen. *Bioanalysis* **5** (4), 395-398, 2013.

Understanding Collision-Induced Dissociation of Dofetilide: A Case Study in the Application of Density Functional Theory as an Aid to Mass Spectral Interpretation.

P.A. Wright, A. Alex, S. Harvey, T. Parsons, and F. Pullen.

Analyst **138** (22), 6869 – 6880, 2013.

Predicting Collision Induced Dissociation (CID) Spectra: Semi-empirical Calculations as a Rapid and Effective Tool in Software-aided Mass Spectral Interpretation.

P.A. Wright, A. Alex, and F. Pullen.

Rapid Communications in Mass Spectrometry **28**, 1127–1143 (2014).

Internal PhD seminar, University of Greenwich, July 3rd 2013:

'Understanding CID: A step towards effective software-aided mass spectral interpretation'.

Oral presentation BMSS Annual Conference, Eastbourne, 11th September 2013:

'Understanding CID: A step towards effective software-aided mass spectral interpretation'.

Chapter 1: INTRODUCTION

1.1. MASS SPECTROMETRY FOR SMALL MOLECULE ANALYSIS (LESS THAN 1000 DA)

1.1.1. Overview

The impact of mass spectrometry on the drug discovery and development process has changed significantly over the past forty years from a technique that was predominantly used in the drug development part of the process to generate information for drug registration purposes to now being an integral part of drug discovery, and as a tool to aid drug design at the earliest stages of the drug discovery process. Evolution of mass spectrometry instrumentation has gone hand-in-hand with the changing requirements within academia and industry. In fact it can be argued that improvements in technology have driven the changes, as the quality of data that can now be routinely obtained during early drug discovery would not be possible if we were still using magnetic sector mass spectrometers with probe sample introduction for structural identification..

A comprehensive review of mass spectrometry will not be made in this introduction as well-written reviews are available in the literature ^[1-4].

1.1.2. Ionisation sources

In the 1970s and early 1980s identifying a molecule in a complex mixture using mass spectrometry was a major undertaking. One reason for this was that the ionisation sources available on mass spectrometers were not readily amenable to being interfaced with HPLC. Gas chromatography-mass spectrometry (GC-MS, with electron ionisation) was the main technique used for mixtures, but polar compounds are not usually amenable to GC-MS, making the analysis of pharmaceutical compounds, in particular, difficult. Therefore, it was usual to either isolate the compound of interest, by HPLC, usually in microgram quantities due to the relative insensitivity of the instruments, or in certain cases suitable molecules could be derivatised prior to analysis by GC-MS. Isolation of the analyte was by no means trivial, particularly for analytes of biological origin which had to be isolated from an excess of biological matrix prior to derivatisation.

The development which had arguably the greatest impact on mass spectrometry becoming the widely applicable detector that it is today was the commercialisation of atmospheric pressure ionisation (API), in the forms of atmospheric pressure chemical ionisation (APCI) and electrospray (ESI)/ionspray (IS) or nebuliser-assisted electrospray. These techniques are compatible with a liquid inlet, allowing HPLC to be coupled to the mass spectrometer. In addition to facilitating the analysis of mixtures polar compounds, these atmospheric techniques offered an improvement in sensitivity.

APCI was first described in 1975 [5]. The significance of these sources is in the fact that the ionisation occurs at atmospheric pressure, and therefore heat transfer is efficient and electric field strengths are reduced compared to those under vacuum. High electric field strengths are to be avoided, such as occur in a vacuum, as these result in the combination of negative and positively charged ions to form neutral species [6]. Another advantage, in purely practical terms, of having the source at atmospheric pressure is that it removes the need to keep the source airtight. Any leak may make an evacuated source unusable, and so the practitioner often spent many a tedious hour leak-testing the seal in the source region. This usually involved spraying the joints with acetone in order to see if this caused a fluctuation in source pressure.

In APCI, the mobile phase (up to 2 mL/min) is nebulised into the source chamber, which is at atmospheric pressure. The source is heated to ensure rapid vaporisation. Ionisation is achieved by means of a needle to which a voltage is applied, sufficient to produce a corona discharge (i.e. a plasma of ions) around the needle point (Figure 1.1).

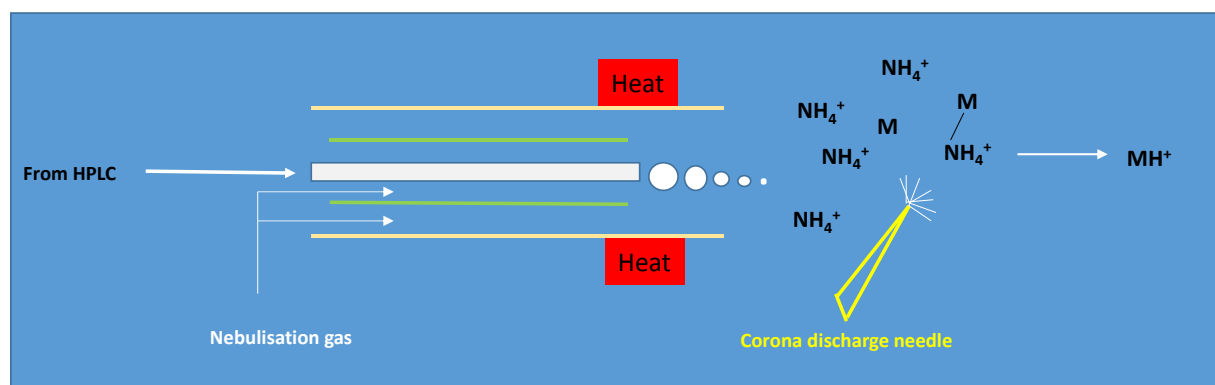


Figure 1.1 Schematic representation of atmospheric pressure ionisation (APCI).

The speed of vaporisation during APCI minimises thermal degradation, potentially

making it suitable for the analysis of polar and labile molecules. Intact glucuronides and sulphate conjugates of propofol were observed in human urine^[7]. There are some compounds which are not stable, however. For example, *N*-oxides are often unstable during APCI, with thermally-induced loss of oxygen being observed. This has a practical application in that this loss of oxygen can be used to distinguish between *N*-oxidation and hydroxylation at a carbon^[8].

For ESI to occur it is generally accepted that the analyte ions are preformed in solution. The analyte is introduced into the mass spectrometer in solution in a flowing liquid stream, usually an HPLC eluent. The eluent contains electrolyte in addition to the analyte, either from the presence of added buffers or modifiers, or the presence of impurities in the solvents, giving rise to a constant flow of ions into the mass spectrometer source. This flow enters the source via a metal capillary maintained at high potential, typically 2-5 kV (Fig 1.2a). The effect of this electric field at the capillary tip is to repel ions of the same charge. This causes a distortion of the eluent flow as it passes through the capillary tip to produce an elongated protrusion of liquid, known as the Taylor cone^[9]. Where the applied potential is positive, cations concentrate towards the tip of the cone in an effort to get as far as possible from the origin of the positive potential. This intensity of charge causes instability at the cone tip; eventually resulting in droplets cleaving off and being ejected into the ion source chamber. These droplets then travel towards the sampling cone, due to the applied field gradient between the capillary and the entrance to the vacuum region of the mass spectrometer. The solvent evaporates from the droplets as they move, causing them to shrink and increasing the repulsive forces within. Eventually the droplets become so unstable that they cleave apart to form smaller droplets in a process known as Coulombic explosion. The final stage of the process is the expulsion of the ions from solution into the gas phase. There are two main proposals on how this happens. In the charge residue model^[10], the Coulombic explosion process is repeated until each droplet contains only one charge. The remaining solvent evaporates leaving the ion in the gas phase. In the ion evaporation model^[11], it is proposed that ions are directly ejected from the droplets into gas phase as the electric field on the surface of the droplet reaches a level sufficient to allow the ions to overcome the surface tension. There is evidence for both mechanisms; however, it has been proposed that the ion evaporation model is more plausible for small ions, but the charge residue model is more applicable to

macromolecular ions^[12,13].

In the case of cations, the ions are usually formed in solution as the result of protonation at the most basic site in the molecule. In certain cases, it can be difficult to rationalise the product ions in the spectra by protonation on the most basic site. For example, spectra can be obtained for myoglobin at a pH (pH 10 adjusted with ammonia) where it is not ionised^[14]. In this case it is suggested that a proton transfer reaction, from the ammonium ion (NH_4^+) to myoglobin, occurs at the surface of the electrospray droplet. Zhou and Cook have proposed that protonation of caffeine, at neutral pH, is a result of proton transfer in the surface layer of the droplet^[15]. Also, it is debatable that the pH of the bulk solution is relevant, as discussed earlier, as the charge is not evenly distributed across the droplets generated during electrospray. It has been reported that the acidity at the surface of the droplet is 10³-10⁴ times greater than in the bulk solution^[16] and this may have a more significant effect on the ionisation state of the analyte, as it is only the ions at the surface which enter the gas phase. This may explain the finding that positive ion ESI response of certain pharmaceutical molecules may not be reduced, sometimes even enhanced, at high pH^[17-19].

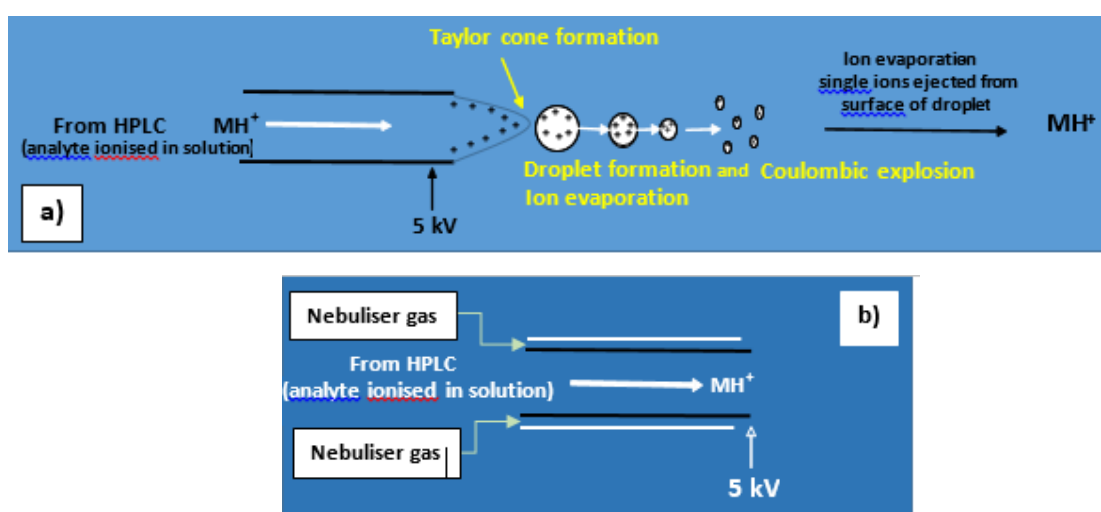


Figure 1.2 Schematic representation of a) electrospray with ion evaporation; b) capillary tip for nebuliser assisted electrospray (electrospray at high flow rates or ionspray).

It has been proposed in some publications that gas phase ionisation via ion-molecule reactions also plays a major role in ESI, for example by proton transfer from gaseous ammonium ions to analytes of higher proton affinity^[20]. However, many of the arguments in favour of gas phase ionisation may also be explained by proton

migration, which will be discussed in more detail later in the thesis.

True electrospray occurs at very low flow rates (1-10 $\mu\text{l}/\text{min}$) [21] and is therefore not compatible with HPLC at the higher flow rates commonly used for many identification studies. Therefore, the higher flow rate adaptation of electrospray, ionspray or pneumatically assisted electrospray, was developed (Figure 1.2b). With pneumatically assisted electrospray or ionspray, HPLC eluent flows through a stainless steel capillary maintained at high voltage. The combination of this voltage and nebulisation, with a high flow rate of nitrogen, results in the generation of a flow of charged droplets that then undergo ion evaporation. Currently, ionspray is the ionisation technique of choice for structural elucidation of small molecules due to its high sensitivity and lack of thermal degradation.

In ionspray, the ions are also preformed in solution and so it is only applicable to polar compounds or ionic samples. APCI, where the ions are formed in the gas phase, is suitable for apolar or weakly ionic analytes [6]. In terms of suitability for analysis of labile compounds, a comparison has been made of the analysis of 26 sulphates and glucuronides in rat urine, hepatocytes and microsomes. ionspray detected 22 of these conjugates but only 12 were detected by APCI [22].

The characteristics of the ionisation sources most commonly, and historically, used for structural elucidation of small molecules are summarised in Table 1.1. In addition to these ionisation sources there are a range of ambient ionisation sources that can be used to perform direct analysis via surface desorption. These include direct analysis in real time or DART [23], desorption electrospray ionisation mass spectrometry or DESI [24], matrix assisted laser desorption ionisation or MALDI [25] or paper spray [36]. These approaches ionise the molecule directly off the surface. They have been successfully applied to the analysis of many compounds [27,28]. MALDI and DESI are also used for the imaging of biological tissues. For example, the distribution of clozapine and its *N*-desmethyl metabolite were imaged in rat lung by DESI [29]. Similarly, whole rat slices have been imaged for pharmaceutical compounds and their metabolites [30]. The disadvantages of direct analysis are that, because there is no separation involved, analytes can be subject to ionisation suppression and sensitivity may be adversely affected.

Table 1.1 General characteristics of mass spectrometer ion sources commonly used for structural elucidation (1971 to 2015).

Source	Under vacuum?	Most common mode of sample introduction	Significant thermal degradation?	HPLC Flow Rate	Types of Analyte	Widespread use for structural elucidation	Comment
Electron Ionisation (EI)	Yes	Solid or liquid on probe; or GC	Yes	n/a	Polar; ionic; apolar; neutral	1970s to late 1980s	Can cause extensive fragmentation; potentially molecular ion not observed; libraries of spectra available
Chemical Ionisation (CI)	Yes	Solid or liquid on probe; or GC	Yes	n/a	Polar; ionic; apolar; neutral	1970s to late 1980s	Little fragmentation; molecular ion usually intact; spectra can be altered by changing reagent gas
Fast atom bombardment (FAB)	Yes	Solid or liquid on probe	Some	n/a	Polar; ionic; apolar; neutral	1980s	Not sensitive; little fragmentation; needs to be partially soluble in matrix
Thermospray (TSP)	Reduced pressure	HPLC	Some	0.5-1.5mL/min	Polar; ionic; apolar; neutral	1980s	Mixed mechanism of ionisation makes it suitable for a wide range of analytes
Atmospheric pressure ionisation (APCI)	Atmosphere	HPLC	Yes	0.2-2mL/min	Apolar; neutral	late 1980s to present	Little fragmentation; less subject to suppression by salts and matrix than ES
Electrospray (ES)	Atmosphere	HPLC	No	1-10 μ L/min	Polar; ionic	late 1980s to present	Little fragmentation; sensitive; subject to suppression by salts and matrix
Nano electrospray	Atmosphere	HPLC	No	nL/min	Polar; ionic	late 1990s to present	Little fragmentation; tolerant of salts and matrix
Ionspray (including Turboionspray)	Atmosphere	HPLC	No	0.01 to 1.5mL/min	Polar; ionic	late 1980s to present	Little fragmentation; sensitive; subject to suppression by salts and matrix
Paper spray	Atmosphere	Dried onto paper	No	n/a	Polar; ionic	Not yet widely used	Potentially useful for dried blood spot analysis

1.1.1. Mass Analysers

The mass analyser is the region of the mass spectrometer where the ions are sorted on the basis of their mass-to-charge ratio (m/z). It is the mass analyser that gives the mass spectrometer its characteristics of mass resolution, mass accuracy and mass range, so its design is crucial to the type and quality of the spectra obtained. In these doctoral studies, the mass analysers used were hyphenated quadrupoles, time-of-flight and Orbitrap™.

Quadrupole mass spectrometers were first developed in the 1950s^[31]. Today they are the most widely used mass analysers due to their stability and relatively low cost. As their name suggests, a quadrupole mass analyser consists of four rods. They are arranged in opposing pairs such that two opposing rods have a dc voltage applied to them and the other two rods have are supplied with an ac voltage. This results in an electric field between the rods that causes ions passing through this field to oscillate. For any specific combination of RF and DC voltage applied, only ions of a certain m/z value will follow a stable trajectory between these rods and reach the detector. Thus ions can be separated by varying the RF/DC voltage, RF only will transmit all ions. As well as stability and low cost, quadrupoles offer the advantage of tolerating higher pressures making them particularly suitable for interfacing with HPLC. Quadrupoles are low resolution instruments.

Ion traps were developed by the same person as first described quadrupoles, Wolfgang Paul, and are essentially the same technology. In ion traps, however, instead of the ions passing through the electric field the ions are trapped by it. For a 3 dimensional (3D) ion trap, rather than rods, the electric field is generated between a ring electrode and two end cap electrodes. The applied RF and DC can be selected to trap the ions in a stable trajectory. These voltages can be varied to make ions of particular m/z values unstable and cause them to be ejected from the trap towards the detector. 3D ion traps have a limited dynamic range as they have a finite capacity and can become 'full' due to the space charge effect^[32], limiting the number of ions they can hold. A recent development that overcomes this limitation is the linear ion trap^[33]. Instead of the 'electronic box' of the 3D trap, the linear ion trap consists of four parallel rods and two end caps. The ions are maintained along the axis of the quadrupole using a 2D radio frequency field. This gives this analyser a greater storage volume for ions

and hence a wider dynamic range. 2D traps exhibit greater sensitivity than 3D traps.

One major advantage of all ion traps is that a single ion can be isolated in the trap then induced to undergo multiple collision-induced dissociation events (MS^n , i.e. repeat fragmentation of product ions), giving extensive structural information. The fragmentation obtained, however, is over a limited mass range. Ion traps are subject to the 'one third rule', that is ratio between the precursor ion and the lowest fragment ion in the product ion spectrum is 0.3. For example if the product ion spectrum is obtained for an ion at m/z 600, the product ion spectrum will not be present below m/z 200, thus low mass structural information is not available^[34].

TOF (Time-of-flight instruments) utilise the fact that ions of the same energies, but different mass-to-charge ratios, will travel at different velocities after being accelerated out of an ion source through a fixed potential^[35]. Thus the ions reach the detector at different times depending on their m/z values. Therefore, measuring the time taken for the ion to reach the detector allows calculation of its m/z ion. TOF instruments are relatively low cost, robust but low resolution. A further development of TOF technology, the reflectron TOF^[36] has increased the applicability of TOF to metabolite identification. A reflectron TOF utilises an electrostatic mirror to reflect the ions towards the detector. This increases the length of the flight path and hence the length of time the ions are in flight. This increases the resolution of the TOF.

Fourier-transform ion cyclotron resonance mass spectrometry (FTICRMS or FTMS) involves monitoring ions orbiting in a magnetic field^[37]. In a constant magnetic field, the cyclotron (orbital) frequency of an ion is inversely proportional to its m/z ratio. These ions are excited with a pulsed RF voltage causing them to acquire an enlarged orbit and generate an image current via interaction with receiver plates (one of the three pairs of parallel plates arranged as a cube to trap the ions). These currents are time-dependent and can be deconvoluted using Fourier Transformation to produce a mass spectrum. FTMS instruments exhibit exquisitely high resolution but are more expensive than many other types of mass analysers. The OrbitrapTM is a particular type of FTMS^[38]. In the OrbitrapTM the ions are trapped about a central spindle electrode where they oscillate along the electrode with a frequency proportional to $(m/z)^{-1/2}$. These oscillations are translated into mass spectra via image currents and Fourier-transform calculations are described for FTMS. An OrbitrapTM gives excellent mass resolution (up to 150,000) and mass accuracy (<1 ppm).

Mass spectrometers can be constructed by combining two or more mass analysers. These may be of the same or different types. Mass spectrometers with multiple mass analysers are routinely applied to structural elucidation studies because of the flexibility they offer. The four types of instrument often used for this type of application are the triple quadrupole (quadrupole/quadrupole/quadrupole), Q-Trap (quadrupole/ion trap), the Q-TOF (quadrupole/time-of-flight) and the Orbitrap™ (linear ion trap/FTMS).

The quadrupole-TOF [39] is a hybrid of a quadrupole and a time-of-flight mass spectrometer. An example is the Waters Synapt Q-TOF shown in Figure 1.3. This instrument offers high mass resolution and MS² capability. It does not perform conventional precursor or constant neutral loss scans, but precursor-like data can be obtained by switching between two full scan acquisition methods, one of which has a high collision energy setting. Every other scan show ions derived from fragmentation [40]. The fragmentation is essentially that observed in equivalent conventional product ion scans, but these high energy full scans are not specific (the precursor ion is not isolated before fragmentation) and thus co-eluting material may contribute interfering ions. Extracting ion chromatograms for product ions observed in the high energy scans and comparing the unfragmented ions in the low energy scans will reveal potential precursor ions which may have given rise to these ions.

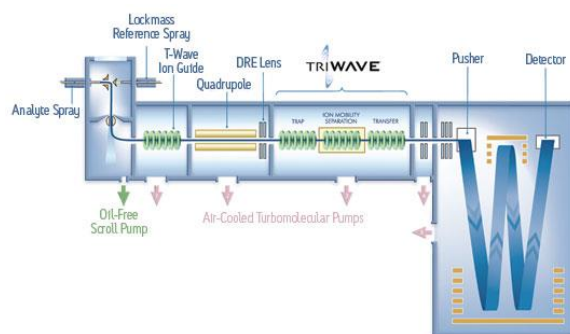


Figure 1.3 Schematic Waters Synapt™ marketed by Waters (copied from <http://www.Waters.com>).

The LTQ Orbitrap™ marketed by Thermo Fisher Scientific (Figure 1.4) consists of a linear trap hyphenated with an Orbitrap FTMS. Triple quadrupoles and quadrupole time-of-flight instruments give qualitatively very similar spectra^[41]. The Orbitrap may produce product ion (MS²) spectra exhibiting less fragmentation that observed for quadrupoles and quadrupole time-of-flight instruments. This is because the product ions formed in ion traps have less energy than those produced by CID and may not

go on to fragment further.

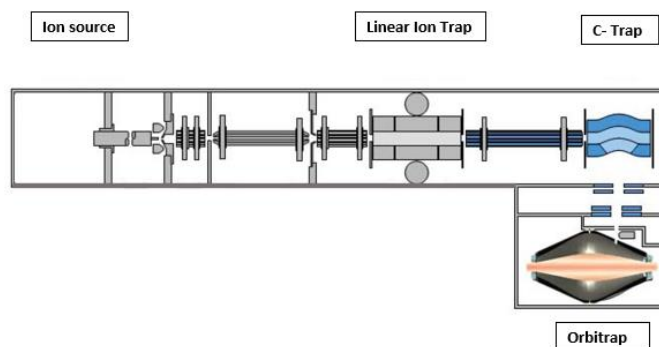


Figure 1.4 Schematic LTQ Orbitrap™ marketed by Thermo Fisher Scientific (adapted from <http://www.thermoscientific.com>).

Comparing hybrid instruments, the TOF and FTMS systems analyse ions in batches rather than separating each ion to obtain a spectrum. In a direct comparison of a quadrupole, a TOF and an FTMS, it was found that for the analyte fenbuconazole, greater full scan sensitivity is obtained on the TOF and FTMS [42]. The high resolution offered by the TOF and the FTMS significantly improves the signal-to-noise of the extracted ion chromatograms making it easier to locate drug-related material in a complex matrix, in addition to allowing the empirical formula to be determined for the product ions.

In a study the application of different mass analysers (triple quadrupole, hybrid linear ion trap triple quadrupole (Q-Trap), TOF and LTQ-Orbitrap) to drug discovery metabolite screening were compared using amitriptyline and verapamil as model compounds [43]. The microsomal metabolites of verapamil and amitriptyline were identified on a 'one injection per sample' basis. Only the TOF MS could be used to find all 28 amitriptyline and 69 verapamil metabolites, both expected and unexpected. The TOF instrument offered both sensitivity and high mass resolution facilitating finding components and assigning their spectra. The LTQ-Orbitrap also gives good mass accuracy but was less sensitive. The triple quadrupole and Q-Trap give the most fragmentation to facilitate structure assignment but are not high resolution instruments. The characteristics of mass analysers most commonly used for structural elucidation of low molecular weight samples are summarised in Table 1.2.

Table 1.2 General characteristics of mass analysers commonly used for structural elucidation 1971 to 2015.

Mass Analyser	Mass Resolution*	Mass Accuracy**	Mass Range	Tandem MS	Advantages	Disadvantages	Year first published	Popular for structural elucidation
Magnetic sector	100,000	5ppm	10,000	MS ²	High mass resolution	Expensive; limited sensitivity; not robust; high vacuum so difficult to interface with HPLC	1934	up to late 1980s
Quadrupole	4,000	100ppm	4,000	MS	Inexpensive; robust; recent instruments are fast scanning; tolerates higher pressures - facilitates interfacing with HPLC	Low mass resolution	1953	limited by resolution application for structural elucidation
Triple quadrupole	4,000	100ppm	4,000	MS ²	Inexpensive; robust; sensitive; newer designs are fast scanning; tolerates higher pressures - facilitates interfacing with HPLC	Low mass resolution	1978	late 1980s to present day
Ion trap	4,000	100ppm	4,000	MS ⁿ	Inexpensive; robust; sensitive;	Product ion mass range may be limited by 'one third rule'; low resolution	1953	1980s
TOF	8,000	100ppm	300,000	MS	Inexpensive; robust; sensitive; fast scanning	Low resolution ; Cannot perform constant neutral loss and precursor ion scans	1946	Limited by resolution application for structural elucidation
TOF Reflectron	15,000 (V geometry) 30,000 (W geometry)	10ppm (V) 1-5ppm (W)	10,000	MS ²	Inexpensive; robust; sensitive; fast scanning; high resolution	Cannot perform constant neutral loss and precursor ion scans	1973	late 1990s to present day
Quadrupole-TOF	15,000 (V geometry) 30,000 (W geometry)	10ppm	10,000	MS ²	High mass resolution; sensitive	Cannot perform constant neutral loss and precursor ion scans	1984	late 1990s to present
Triple quadrupole-TOF	40,000	2ppm	4,000	MS ⁿ	High mass resolution; fast scanning; stable	Expensive	2010	Late 2000s
Quadrupole-Trap	4,000	5ppm	4,000	MS ⁿ	Robust; sensitive; fast scanning	Low mass resolution; product ion mass range not limited	2002	mid 2000s to present day
FTMS	1,000,000	1-5ppm	10,000	MS ⁿ	Excellent resolution; good sensitivity	Expensive; limited sensitivity; less robust; not fast scanning	1974	mid 2000s to present day

*Mass resolution: the ability of the mass spectrometer to distinguish between ions of different mass-to-charge ratio. For example, if an ion at m/z 500 has a peak width at half height of 0.5 will have a resolution of 1000 ($500/0.5$). **Mass accuracy: a measure of the accuracy of mass determination. For example, if m/z 500 was measured to accuracy 0.05, the accuracy will be 500 ± 50 ppm

1.2. SOFTWARE TOOLS FOR ANALYTICAL SCIENTISTS

The section has been published: *3D Thinking: Computational Aids for Bioanalysts*. P.A. Wright, A. Alex, and F. Pullen. *Bioanalysis* 5 (4), 395-398, 2013.

1.2.1. Overview

Software that has been designed to help analysts understand three dimensional molecular structures take a variety of approaches. These include correlating properties, applying 'rules', referring to databases and applying quantum mechanical calculations.

Quantitative structure-property relationship (QSPR) or quantitative structural activity relationship (QSAR) approaches establish relationships between molecular structure and their properties by examining a 'training' set of molecules for which experimentally determined values are available. An example of a structure-property relationship is solubility which has been found to decrease with increasing molecular weight across a homologous series [44,45]. Other properties that can be predicted by QSPR include cLogP, polar surface area and pKa. Appropriate descriptors have not yet been determined which allow the modelling of certain molecular behaviours. For example, Caetano et al. calculated 429 molecular descriptors for 170 molecules and used these to look for correlations with ESI and APCI response [46]. Six different chemometrical tools were tried but the authors were unable to use molecular descriptors to predict which ionisation technique would give the greatest sensitivity.

Expressing which part(s) or property of the molecule contribute to an observed physicochemical property in terms which enable mathematical correlation to be undertaken by the software, are achieved by cleaving down the molecule into a series of 'descriptors'. Descriptors are numerical values representing chemical information [47].

The term QSPR is used where the descriptor relationship is to a physicochemical property whereas QSAR is applied when the descriptor is related to a biological activity. These structure (descriptor)/property relationships can be extrapolated to molecules outside the training set to determine the properties for molecules for which experimental data is not available.

Extrapolation beyond the training data set requires an appropriate mathematical tool. These may be statistical regression methods such as multilinear regression or

multivariate analysis (e.g. partial least squares) or non-linear tools such as decision trees and neural networks may also be used [48]. The applicability of the QSPR will depend on the mathematical approach adopted in addition to the size and type of training set [49].

QSPR-based software has the advantage that it is computationally economical and results are obtained rapidly. The quality of the prediction of the properties will depend on the structure of the molecule of interest being within the chemical space of the molecules in the training set. Therefore the predictions are likely to be less valid for molecules that exhibit novel chemistry. For commercially available software, the nature of the training set is usually unknown to the customer, so it can be difficult to judge if the predictions will be valid for a particular series of compounds. If possible, the software should be validated by obtaining chemically determined values for some of the compounds of interest and determining how close the predicted values are to the experimental values.

There are many QSPR software packages available; for example ACD/Labs [50], ADMET predictor [51], ChemSilico [52], Pipeline pilot [53] and SPARC [54] will generate cLogP, aqueous solubility and pKa values. Each of these packages may predict different values for the properties of the same compound. For example, pKa's of over six hundred compounds calculated by six different packages gave MAE's (mean arithmetical errors) of 0.32 to 1.17 depending on the software used [91]. Therefore, it is worth validating an alternative software package if the first predictions do not hold for a particular compound series.

Accurately predicting physicochemical properties where a numerical value is generated is a challenge, but stepping beyond this to predicting what happens to a molecule in a complex physiological environment increases the demands on the prediction tool still further. There are several methodologies for the *in silico* prediction which highlights sites on a molecule that are vulnerable to metabolism. Some of these are QSAR-based, whilst others are protein-pharmacophore (three-dimensional-QSAR) models or predictive databases.

Protein-pharmacophore modelling predicts, from three dimension structure of a known pharmacophore, their interaction with the protein (enzyme). This assumes the mode of protein binding is unique, which of course may not be the case [55-57]. These models are further limited by the active site of the enzyme being well

modelled, in practice restricting the application to cytochrome P450 phase I and UDP-glucuronosyl transferases, which are well characterised. An example of a commercially available metabolite prediction package is Metasite. Metasite considers molecular interaction fields (areas of potential molecular interactions taking into account electrostatic, hydrogen-bonding, hydrophobic and van der Waals interactions) for both ligand and binding site, particularly in terms of protein-ligand distance ^[58]. The molecular interaction fields are calculated using GRID, a program for QSAR design to generate a series of descriptors ^[59]. In addition Metasite uses molecular orbital calculations (Gaussian, B3LYP 6-31G**, AM1) to determine the probability of a metabolic reaction occurring at a certain atom.

An example of the predictive database approach is that taken by the software Meteor (Lhasa). Meteor contains a database of mammalian reactions to which it then applies reasoning rules to predict if the molecule is likely to undergo any of the data based reactions. These rules are sophisticated, taking into account probability, plausibility and prioritises competing reactions, taking into account the physico-chemical properties of the molecules. Database predictions have the advantage that they are not limited to enzymes for which the binding site is well characterised. Thus Meteor covers both phase I (including non-P450) and phase II metabolism predictions.

In practice, the author has found that both Meteor and Metasite over-predict the number and type of metabolites formed (not published). They are most usefully applied to confirm the plausibility of the experimentally detected metabolites, rather than to replace the metabolism experiment.

Software is available that is designed to predict chromatographic retention times. Commercial packages include DryLab (Molnar-Institute for Applied Chromatography, Berlin, Germany ^[60] and ChromSword (Riga, Latvia) ^[61]. DryLab uses the linear solvent strength model ^[62] and experimentally determined retention times to predict retention times for structurally similar compounds. Both ChromSword and DryLab combine using the physico-chemical properties of the molecules with a database of sorbent/eluent properties to predict chromatographic retention. Similarly, ChromGenius ^[63] is used to calculate the physicochemical properties of the analyte and uses these to predict retention time in conjunction with experimentally determined information relating to structurally similar compounds in

their database. The user can add their own compounds to the database to increase its applicability to their own chemical space. Although very useful, there is still a significant degree of error in retention time predictions. In a recent publication, it was reported that ChromGenius predicted the correct elution order for 68% of 118 compounds for which the retention times were calculated [64].

1.1.1. Software aids for the mass spectrometrist

Various commercially available software packages aid with interpretation of MS/MS spectra. These packages tend to be fragment database and/or fragmentation rule based approaches, although the exact nature of the algorithms underlying these programmes has not been disclosed for commercial reasons.

Both database and rule-based approaches have major limitations:

- Minor molecular structural changes can have a major effect on both the ionisation and fragmentation of a molecule, so the assumption that extrapolations in fragmentation behaviour can be made between similar structures may not be valid.
- Unlike EI, the more commonly used ionisation techniques for small pharmaceutical-like compounds, ESI and APCI produce CID spectra that are highly dependent on both the instrumentation and settings used. Thus making it difficult to widely apply CID spectral libraries.

Although, the exact nature of the rules used in these commercial programmes is not published, rules established for EI fragmentation are well known and accepted as valid. Fragmentation rules have been established for certain compound series. Sulphonamides have been reported to show common losses [65,66]; Holman et al. [67] have reported characteristic losses, loss of the nitrogen-containing group, when fragmenting dialkyl tertiary amines. In addition, alkyl sulphoxides have been shown to lose the substituent on the sulphur as a radical under CID conditions [68]. However, both the experience of the author and literature searches have failed to establish any broadly applicable rules for CID-induced fragmentation. As some of these software packages have been found to propose fragmentation behaviour such as cleavage across aromatic rings that would require high energy conditions, it is suspected that these rules are, at least partly, based on EI behaviour. In addition,

rules may not be exclusive and one rule may affect another ^[69].

1.1.1.1. Mass Frontier

Mass Frontier is a spectral interpretation and management software package marketed by Thermo Scientific ^[70]. It is a sophisticated programme that combines two approaches to assign product ions: comparison with their database (from the literature and in-house database) and applying general fragmentation/rearrangement rules. The Mass frontier database is very large, containing over 30,000 fragmentation schemes.

1.1.1.2. MS Fragmenter

MS Fragmenter, ACDLabs ^[71], predicts mass spectral fragments from the imported precursor structure by applying rules of fragmentation. MS Fragmenter contains different rule sets for different ionisation techniques and so can be applied to EI data in addition to the soft ionisation techniques of ESI, APCI and CI. The results are displayed as a fragmentation tree, showing precursor-product relationships. As MS Fragmenter is purely rule based, unusual fragmentation routes and rearrangements may be missed.

1.1.1.3. Mass Spec Calculator

This is an arithmetical tool that cleaves imported molecular structures and generates masses for the fragments. It is useful as an aid to manual spectral interpretation, as it is faster than using a calculator for determining the mass of the fragments ^[72] but could not be considered as an intelligent prediction tool.

1.1.1.4. Fragment iDentificator (FiD)

Fragment iDentificator is a programme developed at the University of Helsinki ^[73]. This takes an alternative approach to explaining the fragmentation. The identification of the fragments occurs in two stages. Firstly, all the possible fragments that correspond to the accurate mass of the observed fragments are generated. These are then ranked in order of how likely these fragments are to be cleaved from the precursor molecule. This is done on the basis that weak bonds are likely to cleave first. The strength of the bond is approximated (not calculated) with

the standard covalent bond energy. FiD works for both single stage and multistage fragmentation, with single stage fragmentation giving the highest accuracies of prediction (up to 90%). It is computationally complex and generating the fragmentation data can take several hours for a compound of molecular weight of 300 Da.

1.1.1.5. EPIC (*Elucidation of product ion connectivity*)

This programme was developed in-house by Merck [74]. It is a 'systemic bond dissociation method'. Bond dissociation methods cleave all possible bonds in the molecule and compare the accurate masses of the resulting fragments with those of the CID products. These packages do not consider chemical structure and its associated properties and do require databases.

EPIC is analogous to FiD, however, in that it has the capacity for the user to set its own limits on bond cleavage. EPIC differs from FiD in that, rather than using bond energy to indicate probability of cleavage, weightings as to likelihood of cleavage are assigned by the user, utilising the user's knowledge and experience of their molecules.

1.1.1.6. MetFrag

MetFrag is another systemic bond dissociation method [75]. Initially all bonds are broken to generate a series of fragments. In addition the structure is processed by 'rules' to generate neutral loss (e.g. loss of water, ammonia, hydrogen cyanide) driven rearrangements that cannot be accounted for by straightforward bond cleavage. The fragments are then ranked in order of probability in terms of bond cleavage based on literature reported bond dissociation energies (BDEs). However, BDEs vary with increasing size.

1.1.1.7. Mass Bank

MassBank is a public database of mass spectra of compounds of molecular weight less than 3000 Da [76]. It contains 9276 electrospray ionization (ESI)-MSⁿ spectra and 3045 ESI-MS² data of 679 synthetic drugs contributed by 16 research groups (quoted on January 2010). ESI-MS² data were analysed under non-standardised, independent experimental conditions.

1.1.1.8. Metabolite Specific Software

Mass spectrometer manufacturers supply software to assist in the finding and identification of drug metabolites. Observing metabolites against a background derived from a complex biological matrix is challenging. It is possible to look for expected metabolites by applying common routes of metabolism to the parent molecule and generating accurate mass for the predicted metabolic products. Information is available on even unexpected metabolites, however, in that they have structural characteristics in common with the parent molecule from which they are derived. These characteristics may include isotope patterns and the mass defect window (i.e. using a mass filter to visualise compounds that have accurate masses that differ from the integral mass by similar values to the parent compound). Software from the major manufacturers include MetWorks^[77] from ThermoScientific, MetabolitePilot^[78] and LightSight^[79] from ABSciex, Bruker's MetaboliteTools^[80] and Metabolyx^[81] from Waters.

1.3. QUANTUM MECHANICAL APPROACHES

Quantum mechanics describes the behaviour of matter at the molecular, atomic and subatomic level and its interactions with energy. Software based on quantum mechanics can be used to calculate bond lengths and the most energetically favourable site of protonation. Thus it has practical applications in predicting pKa's, lipophilicity, modelling chromatographic behaviour and explaining mass spectra by determining the site of protonation and predicting bond cleavages. These software programmes undertake predictions based on the properties of the molecule itself. This offers a theoretical advantage over the QSPR and database approaches in that the prediction is tailored to the molecule of interest and based on chemical assumptions which may or not be valid.

One of the most widely applied quantum mechanical tools is Density Functional Theory (DFT)^[82] which is used to determine the electronic structure of molecules. DFT is valid for molecules in their isolated state, free from the influence of their environment, and so is ideal for use in modelling molecules in the gas phase and for determining the behaviour of molecules and ions in the vacuum of a mass spectrometer.

Software packages (e.g. Jaguar^[83] and COSMO-RS^[84]) utilise DFT to calculate properties of molecules in solution such as pKa and lipophilicity. It has been reported that these pKa and lipophilicity predictions are inferior to the QSPR approaches. Laio and Nicklaus compared nine programmes predicting pKa and found that the quantum chemistry based programme Jaguar gave only a 0.58 (r^2) correlation with experimentally determined values in comparison with r^2 values of 0.76 to 0.94 for the eight programmes based on empirical methods^[85]. The quality of prediction may also be dependent on functional group and geometry optimisation method, with the quality of pKa prediction for heterocyclic compounds showing a greater dependence on the optimisation method than for amines or carboxylic acids. If solvation considerations* are built into the DFT model, however, the quantum mechanical predictions of pKa improve relative to those of QSPR packages. Bryantsev et al.^[86] reported mean absolute error (MAE) of 0.1 for the pKa's of ten aliphatic amines calculated by DFT (with the Poisson–Boltzmann continuum solvent*) compared with MAEs of 0.3 to 1.2 for six different QSPR software packages^[44]. These studies are not directly comparable, however, as the QSPR packages were evaluated with 654 chemically diverse compounds whereas the structures in the DFT investigation the compounds were closely related.

DFT has been used to model and/or predict chromatographic retention (GC and RP-HPLC) in several ways; by modelling the stationary phase^[87] and modelling how the molecule interacts with column^[88]. Szalaniec et al.^[89,90] have reported that introducing 3D descriptors (molecular conformation calculated by DFT) increases the accuracy of the prediction of HPLC retention and separation.

(*The Poisson–Boltzmann equation is a differential equation that describes electrostatic interactions between molecules in ionic solutions. Continuum solvation considers the solvent to be a continuous medium instead of distinct molecules for the purpose of undertaking modelling calculations).

DFT has been used to great effect to rationalise fragmentation based on the thermodynamic effects that protonation has on the molecule^[91,92]. This DFT approach has been used to calculate the thermodynamically most stable protonated species based on the three dimensional structure, and this information has been useful in predicting the potential cleavage sites of those different molecular ions. This approach has been utilised by the authors in previous studies with the

pharmaceutical compounds fluconazole and maraviroc, to highlight that the molecular ion appears to be a mixture of molecular species which are protonated on a number of different basic sites across the molecule [91,92]. These same publications also reported that protonation may affect bond length and that bond lengthening, hence weakening, correlated with the bonds, which were observed to cleave in the MS/MS spectra.

So why are quantum based methods not used more widely? There are several reasons. Often, analysts are unaware of what these programmes can do for them and, if they have heard of them, feel that their use is beyond their expertise as quantum mechanics must be complex and can only be understood by a specialist. The word 'quantum' immediately brings images of such scientific giants as Erwin Schrodinger and Niels Bohr to mind, and yet we apply quantum mechanics on a daily basis; most of us find the operation of a DVD player (which based on quantum mechanics) straightforward because it is designed by experts to be operated by all. Similarly, software programmers and computational chemists are looking to design quantum mechanics packages tailored to specific applications such that they can be easily used by scientists in many fields, the 3D modelling calculations being essentially invisible to the user unless they wish otherwise. The other limitation of quantum methods is that they are computationally 'expensive'. Calculations can take from several minutes to several hours and require a high specification computer (although nothing that cannot be bought at a reasonable cost on the high street these days). Again work is under way to minimise the type and the number of calculations needed, which will speed up the time to generate the predictions. Relatively fast packages are already out there; users of Metasite may not realise they are running quantum calculations when they generate their metabolite predictions. These predictions take only minutes because the calculations are not completely *ab initio*, some quantum values are approximated.

The author believes that *in silico* predictions of molecular properties and activities will never completely replace experimental determinations. However, the confidence in predictions for many classes of compounds will be increased using quantum mechanical approaches in two ways; a) by the development of software that makes its predictions tailored to the molecule utilising quantum chemistry software, these 3D conformational calculations occurring in the background and

requiring no user intervention, and b) the development of rule sets describing molecular behaviour with a broader validity, thanks to a deeper understanding molecular properties arising from off-line molecular modelling using quantum mechanical approaches.

It is the aim of the research presented in this thesis to determine how DFT can contribute to a deeper understanding of mass spectral ionisation and MS/MS fragmentation based on the three dimensional consideration of the molecule and ion and how this understanding may potentially be used to improve software tools to aid the mass spectrometrists.

1.4. INTRODUCTION TO COMPUTATIONAL CHEMISTRY

Computational chemistry methods may be divided into two categories based on the branch of physics they utilise ^[93–95]:

- Molecular mechanics (field force methods) where atoms (or groups of atoms) are treated as balls and bonds as springs ^[96] i.e. a classical mechanically connected system. It is used to calculate the energy of the molecule by adjusting bond lengths and angles to achieve an energy minimum. Molecular mechanics considers bond stretching, bending, and torsion in addition to van der Waals and electrostatic forces. It can be applied to calculate dipole moments, entropies, enthalpies of formation and strain energies ^[97]. It is not applicable to bond cleaving. Parameters, also known as force fields in this context, are set using training sets of data tailored to deliver best fit for specific molecules or bond types. Examples of programmes available are MM2 which is applied to large organic systems and AMBER which is used for macromolecules. Molecular mechanics is the basis of docking software, where the interaction of binding sites of macromolecules with low molecular weight compounds are modelled, often to aid drug discovery ^[98]. Generally speaking molecular mechanics considers processes in the macroscopic range, i.e. pico seconds to micro seconds and nano meters to micro meters. It is relative fast, but of lower accuracy.
- Quantum mechanics considers systems at the atomic and sub atomic level. It considers processes in the microscopic range i.e. nanoseconds to pico

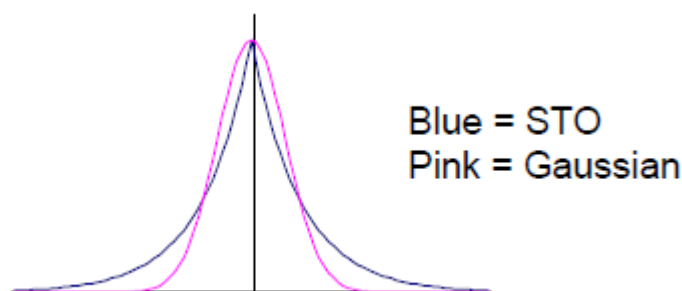
seconds and angstroms to nanometres. Quantum mechanical methods are accurate, but slow, which limits the size of the system to which it can be applied. Quantum mechanics differs significantly from classical mechanics and effectively describes a different, and often surprising, world to the one we observe on a daily basis. It relates to the following properties of particles. Matter has both wave and particle-like properties, but the wave nature is only exhibited significantly for small species and light ^[99]; at the atomic and sub atomic level energy is not continuous but is absorbed and emitted in packets known as quanta; the movement of particles is random; both the position and momentum of a particle are not known at the same time, the Heisenberg Uncertainty Principle ^[100,101]

Quantum mechanical computational methods may be further categorised into molecular orbital calculations, both *ab initio* and semi empirical, and electron density determinations, Density Functional Theory (DFT).

1.4.1. Molecular orbital calculations

In molecular orbital theory the molecule is considered to have a set of molecular orbitals, the weighted sum of its atomic orbitals, in which the electrons are not assigned to bonds but could be anywhere around the molecule. In these molecular orbitals, the movement of the electrons is influenced by the nuclei ^[102–107].

The atomic orbitals used in the summation, are represented mathematically as wavefunction (ψ ; see also the Schrodinger equation later in this chapter). Slater-type orbitals (STO) are functions used to compute ψ ^[157]. STOs give a good approximation of ψ for a limited number of electrons but, if several electrons are present, STOs are mathematically too demanding to be applied routinely. Therefore Gaussian functions (GTOs) are used as the next best approximation of the atomic orbitals ^[109]. The relative areas of integration for both orbitals are shown below.



Mathematically GTOs are easier to calculate as the product of more than one Gaussian is also represented as a Gaussian and thus they can be integrated more easily for electrons at different centres enabling more rapid coverage of the molecule. Typically it takes 3 to 6 GTOs to approximate an STO. However, even GTOs are computationally too expensive for large molecules (more than 30 atoms) and molecular mechanics based systems or semi empirical methods (discussed later) are applied instead.

Molecular orbital calculations fall into two categories; *ab initio* and semi-empirical. *Ab initio* calculations are made from 'first principles', that is minimal assumptions are made in the solution of the Schrodinger equation ^[110]:

$$H \psi = E \psi$$

Where H is the Hamiltonian operator, which is representative of the kinetic energy, interaction with external potential and electron-electron interactions, and E is the proportionality constant, which is the energy state of ψ in the stationary state. The wavefunction is denoted by ψ and pertains to the probability of finding the particle in a given area and also the probability of it having a certain momentum or energy ^[111]. Therefore, the Schrodinger equation determines the probability of events in a dynamic system. This seemingly simple equation is the key contribution to the field of quantum mechanics. It predicts that the calculated parameters, (for example energy), may be quantised. It also predicts the phenomenon known as 'quantum tunnelling' as it confirms that there is a small probability that a particle will go through an energy barrier for which it has insufficient energy to get over. Heisenberg's Uncertainty Principle also explains tunnelling in that if the location of the particle is unknown there is a chance it will be on the wrong side of the energy barrier. Quantum tunnelling will be revisited in the results chapters of this thesis, as it is integral to the interpretation of the data obtained during this research.

In practice, the Schrodinger equation can only be completely solved for hydrogen. The computational requirements of solving the equation for any molecule larger are too vast. Therefore, for all other molecules, assumptions are made in solving the equation. Different approaches make different assumptions and exhibit different limitations and errors. There are two main approaches to solving the Schrodinger equation: wavefunction based approaches, such as the *ab initio* methods of Hartree-Fock and MP2, and those based on electron density.

The most widely used *ab initio* methods use the Hartree-Fock approach to solving the Schrodinger equation for ground state wave function and ground state energy^[112,113]. Hartree-Fock assumes the electrons move as an average electron cloud, experiencing the effects of all the other electrons combined, leading to an over estimation of the electron-electron repulsion. It also assumes that the electrons act independently of the nuclei, the position of the nuclei being fixed (Born-Oppenheimer approximation^[114]). Hartree-Fock only considers occupied orbitals. Initially, it was applied to atoms but was further advanced by Pople to describe molecules^[115].

In order to obtain an improved treatment of complex systems, Moller-Plesset perturbation theory^[116] (MP) may be applied. It is a more accurate model than Hartree-Fock because it does not assume the electrons are independent but incorporates an electron correlation factor. It does this by varying the electron-electron interactions by mixing excited state determinants with ground state determinants. Effectively it considers that electrons may be promoted into virtual unoccupied orbitals, reducing electron-electron interactions. A large basis set, such as 6-31G or 6-311G**, is required to account for sufficient orbitals. The most commonly used perturbation theory method is MP2^[117], which considers the excitation of two electrons. As MP2 is more complex than Hartree-Fock, the calculations take longer.

1.4.2. Semi-empirical calculations

Semi empirical methods were championed by Dewar^[118,119] in the 1950s to 1970s, when computers were still severely limited by processor speed and memory, creating a real need for an approach which would allow computational chemistry calculations to be undertaken in realistic time scales, less than the days and weeks

that *ab initio* methods were taking. They are based on Hartree-Fock but calculations are not made from first principles; certain parameters are omitted or approximated using experimental data such as ionisation energies or dipole moments. The parameters can be adjusted to improve agreement with experimental data and give best fit for molecular classes being studied. Core electrons are not considered as they generally do not change during reactions and only minimal valence electrons are included. Semi empirical methods use Slater functions in which repulsion is parameterised more accurately than using Gaussian functions

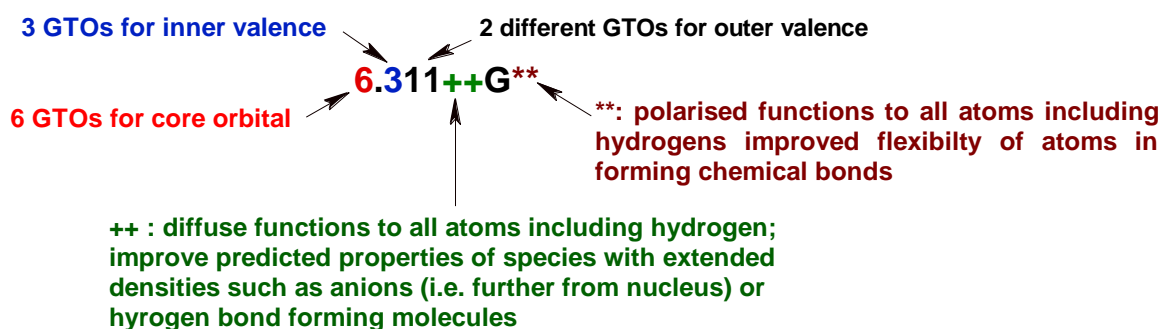
Semi-empirical methods are used to calculate heats of formation, geometry, dipole moment and ionisation potential ^[120]. They give similar results to DFT for calculating bond dissociation energies but they tend to over-estimate ionisation potentials ^[121,122]. Semi empirical approaches are better for hydrogen bonding, four member rings and determining activation energies than *ab initio* methods. They are particularly useful for large molecules where *ab initio* calculations take too long. However, the increased speed of calculation by semi-empirical methods is at the expense of accuracy, especially for energetics such as reaction rates. Semi-empirical methods tend to be used for anions as they are more effective than *ab initio* methods. They give poor results for halogenated compounds. They are often used to minimise surface energy before further optimisation using *ab initio* calculations.

Two of the most popular semi empirical methods are Austin Model 1, AM1 ^[123] and PM3. PM3 is a modified version of AM1. AM1 and PM3 differ in that AM1 is parameterised based on a small number of atomic properties whereas PM3 is based on a large number of molecular data ^[124]. Both methods contain modified expressions to deal with nuclear repulsion but deal with this repulsion in different ways. PM3 is better at thermochemical predictions than AM1. PM3 overestimates hydrogen-hydrogen interactions which lead to poor predictions of both intermolecular and intramolecular interactions resulting in inadequate modelling of conformations of flexible molecules (the predicted structures tend to be too condensed). AM1 over estimates electron repulsion and so leads to more open structures, which tend to be more accurate than the more compact structures predicted by PM3. Both AM1 and PM3 tend to overestimate basicity. AM1 performs well in calculating bond lengths, being in good agreement with

experimental data, however relative energies of molecules are calculated more accurately by DFT [125]. AM1 has been shown to be unreliable for calculating proton affinities [126].

1.4.3. Basis sets

A basis set is a set of wave functions which are used to describe an atomic orbital. Molecular orbitals are described by combining the atomic orbitals in a linear fashion (LCAO). Minimal basis sets use one basis set for each atomic orbital. More commonly used as they give more accurate results are split basis sets (also known as Pople basis sets) [127]. Details of a commonly used basis set, 6.311++* are shown below. The higher the basis set the greater accuracy of results but the longer the calculation takes. For example, the CPU time for the minimal basis set STO-3G is 500 times less than that of 6.311++G**.



1.4.4. Density Functional Theory (DFT)

The development of DFT is considered one of the greatest advances in computational chemistry. Two of the ten most cited papers of all time are concerned with DFT [128]. DFT has its origins in the Hohenberg-Kohn paradigm which states that the electron density of a molecule is functionally* related to the Hamiltonian operator [129] (*the word functional describes the transformation of a number into a property, in this case energy). Effectively this means that electron density uniquely describes the position and charge of the nuclei, determining the Hamiltonian operator and making the calculation of ψ unnecessary. The Kohn-Sham formulation improves the accuracy of DFT by including exchange and correlation effects to overcome the issues caused by interacting electrons. It does this by mapping the electrons into a theoretical model where they do not interact [130]. Hohenberg-Kohn theorems use

approximations that mean that only a small part of the Schrödinger equation is unknown, thus there are no large errors. The Kohn-Sham approach uses the potential energies of attraction and repulsion for the electrons, together with the kinetic energies of these electrons to calculate the energy of the system. In a similar way to Hartree-Fock, it considers non-interacting electrons.

The limitation of only considering non interacting electrons in the Kohn-Sham model is that the exact functionals for exchange and correlation are not known. Therefore, they need to be approximated. The simplest approach for approximation is local-density approximation (LDA). LDA considers the electron density at each individual point in space assuming the electrons to be a homogeneous electron cloud [130]. This is not a realistic model and can be improved by including generalised gradient approximations (GGA) which introduce a model for the gradient of electron density, reflecting better the uneven distribution of electron density across the molecule. The most popular approach currently applied is B3LYP, a hybrid functional which combines GGA with Hartree-Fock exchange [131,132]. Hybrid functionals are more accurate in the determination of energies than GGA on its own; the estimated error on energy predictions by B3LYP being 2-3 kcal mol⁻¹ [133]. There are other hybrid gradient density functionals, but they produce minimal differences in geometry optimisation such that the functional used does not significantly affect the geometry values calculated [134].

DFT is empirical but may be considered *ab initio* in that the user inputs the structure and the software predicts the properties with further user intervention [82]. DFT is computationally less demanding than MP2, requiring the calculation of the Schrödinger wavefunction (ψ) coordinates of the x, y and z spin states of all electrons i.e. only three variables need be calculated as opposed to multi-variables required for Hartree-Fock and MP2 (the wavefunction of an N electron system being dependent on 3N variables). DFT is comparable to MP2 in terms of accuracy (to within 0.5-1.0 kcal mol⁻¹) but is inferior to MP2 for calculating energy differences in which bonds are not made or broken, such as H-bonds and conformation energies [135-137].

Geometries predicted by DFT agree closely with experimental X-ray diffraction data [138]. DFT performs well for modelling cations because 99% of electrons are in the ranged defined by the Gaussian orbital model used in DFT. In anions, however,

the electrons may have an infinite range and so may not be within the scope of the Gaussian function ^[139]. Thus DFT may be poor for modelling anions, although using a basis set with a diffuse function may improve the accuracy. Semi-empirical calculations may provide more accurate data for anions as Slater orbitals cover a greater area. In addition, DFT does not model well for weak interactions such as van der Waals or hydrogen bonding ^[140], although recently developed dispersion correction functionals go some way to improve modelling dispersive interactions ^[141].

DFT models molecules in the gas phase. The effects of solvation may be added using approaches such as the continuum solvation model (CSM) ^[142]. This was developed by Klamt ^[143]. CSM considers the solvent as a continuum characterised by macroscopic properties such as dielectric constant. There are three stages to this model: charges on the molecule are turned off before inserting the molecule into a solvent with infinite dielectric constant i.e. a perfect conductor; the charge is then turned on, the calculation being done by DFT; finally, the result is corrected for the properties of the actual solvent. CSM offers the advantage that lengthy quantum mechanical calculations are done only one and then can be adjusted for any solvent.

The features of these different computational approaches are summarised in Table 1.3 and Figure 1.5.

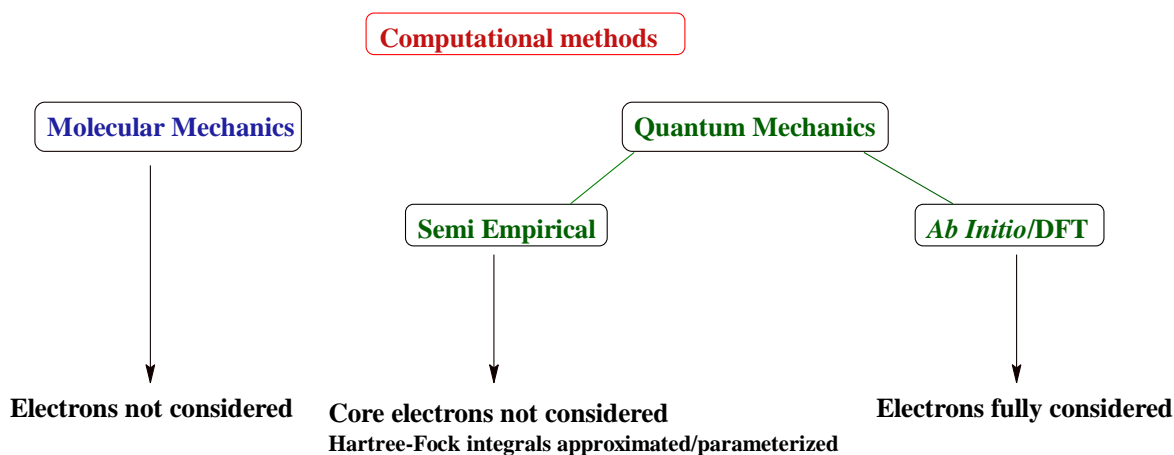


Figure 1.5 Overview of differences between computational methods.

Table 1.3 Comparison of the relative computational chemistry approaches.

Approach	Theory	Advantages	Disadvantages	Size of molecules to which applied	Applications	Examples of programmes
Molecular Mechanics	Classical physics Atoms (or groups of atoms) are treated as balls and bonds as springs	Computational economical Suitable for macromolecules	Not suitable for bond breaking Requires <i>ab initio</i> or experimental data; relevant training required for accurate predictions Does not determine electronic properties	Large systems (thousands of molecules)	Protein docking Calculate dipole moments, entropies, enthalpies of formation and strain energies	MM2, AMBER
<i>Ab initio</i> molecular orbital	Quantum physics (Schrodinger equation) Calculates molecular orbitals by summing the atomic orbitals	No additional data/parameters required High accuracy	Computationally expensive	Small , tens of atoms	Calculates transition and excited states Determination of electronic properties	MP2, Hartree-Fock
Semi-empirical molecular orbital	Quantum physics (Schrodinger equation) Uses assumptions and experimental data	Computationally faster than <i>ab initio</i> and DFT Better than <i>ab initio</i> for anions	Requires <i>ab initio</i> or experimental data; relevant training required for accurate predictions Poor for halogens, reaction rates and energetics, H-bond geometries, hybridization (e.g nitrogen in amides and heterocyclic aromatic rings)	Medium , hundreds of atoms	Calculates transition and excited states Determination of electronic properties ((dipole moments, electrostatic potential, HOMO/LOMO energies) and geometry	AM1, PM3
Density Functional Theory	Quantum physics (Schrodinger equation) Calculates electron density Makes approximations	Faster than <i>ab initio</i> Potentially high accuracy Electron density can be confirmed by X-ray diffraction	Variable accuracy Poor for H-bonds and π - π interactions Poor for anions	Medium, hundreds of atoms	Determination of electronic properties	Spartan, Jaguar, Gaussain

1.5. THERMODYNAMICS AND KINETICS OF IONS DURING ESI AND CID (COLLISION-INDUCED DISSOCIATION)

1.5.1. ESI and ion transmission

ESI produces protonated molecules in positive ion mode and deprotonated molecules in negative ion mode as described earlier in the introduction. Rarely, however, compounds with low oxidation potentials may undergo electrochemical oxidation in the electrospray capillary to give radical cations as the molecular species, for example tetra(aryl) benzidine derivatives^[144]. When considering the internal energy of ions, the term 'internal energy' is often used interchangeably with 'temperature'. This is because the temperature of the molecule describes the molecule's average internal energy (E_{int}) according to the equation below^[145,146]:

$$E_{\text{int}} = C(T, \nu)skT$$

where T = absolute temperature, $C(T, \nu)$ = temperature and vibrational frequency dependent factor, s = number of oscillators, k = Boltzmann constant.

Indeed, it has been shown that ions formed in an electrospray source do exhibit a thermal 'Boltzmann' distribution^[147,148].

Ions produced by electrospray are generally of lower internal energy and less prone to in-source fragmentation than those formed by other ionisation methods. Where in-source fragmentation does occur, rearrangements are favoured. The internal energy of molecular ions is a combination of the initial thermal energy of the molecule and the energy changes resulting from ionisation. The initial energy is dependent on the degrees of freedom and vibrational frequencies, as in the equation above, therefore is proportional to molecular weight. Molecules above 1000 Da may have thermal energy in excess of that added by ionisation^[145], whereas the mean thermal energy of a molecule of mass 200 Da is approximately 1 eV. Most of the internal energy of an ion below m/z 500 is derived from ionisation^[145].

The internal energy of ions in an ESI source has been reported to increase linearly with orifice voltage in the range 10-50 eV, independent of compound class^[149,150]. This increase in internal energy can result in fragmentation; 'in-source-CID'. However, this

increase in internal energy in the source is not maintained until the ions reach the collision cell as orifice voltage does not have a significant effect on fragmentation in a quadrupole collision cell^[151]; varying the orifice voltage from 5 to 75 V has been reported to have less than 1 eV effect on the collision energy required to induce fragmentation^[152]. Energy is lost before the ions reach the collision cell, for example during supersonic expansion through the sampling orifice. Ion internal energy is also dependent on capillary voltage, with increases of up to 16 eV per ion being reported by increasing this voltage. Thus, in-source fragmentation increases linearly with capillary voltage^[153].

Source temperature also influences the internal energy of the ions. The internal energy increases with temperature^[150], however, this does not necessarily increase in-source fragmentation as desolvation may not be complete at lower temperatures, solvated molecule being less likely to fragment.

Typically, the residence time in an ion source is of the order of 1 μ s before passing through the orifice^[145]. Only 1 in 10^3 to 10^5 ESI ions are sampled into the mass spectrometer (0.1 to 0.001% transmission)^[154]. These losses are due to dispersion of the plume of ions as a result of charge repulsion, causing the area of ions at the interface to be significantly larger than the sampling orifice. Increasing the orifice potential increase transmission but sensitivity may be offset by in-source fragmentation reducing the number of molecules available for transmission. Increasing the proximity of the capillary to the orifice increases transmission by decreasing the opportunity for ion dispersion. Having the capillary close to the orifice, however, is only feasible at very low flow rates to avoid solvent break-through into the vacuum region.

The flow of gaseous ions through the orifice results in adiabatic* expansion leading to formation of a supersonic jet. Supersonic expansion results from a gas flow passing through a small opening into a low pressure region^[155,156]. The axial velocity of the gas increases relative to the radial velocity and the ions are cooled by conversion of some of the internal energy into kinetic energy. At this stage the ions may not be fully desolvated and clustering is possible.

*Adiabatic expansion occurs when a gas in an insulated container expands into a vacuum. There is no pressure for the expanding gas to push against so the work done by the system is zero. The temperature of the system is constant, entropy is proportional to volume, and therefore adiabatic expansion results in an increase in

entropy.

1.5.2. CID

The collision cells in the ThermoScientific LTQ Orbitrap and the Waters Q-TOF used for the experiments in this thesis are the linear ion trap and an rf-only hexapole collision cells, respectively. The LTQ Orbitrap and the Q-TOF generate product ion spectra by performing tandem mass spectrometry in time and space respectively. For an ion trap, isolation of precursor ions and their subsequent fragmentation are separated in time; the ions are trapped in pseudo potential wells, the well depth being inversely proportional to m/z ^[157]. A small 'tickle' potential is applied which corresponds to the secular frequency of the ions (i.e. the frequency at which ions of a particular m/z are in synchronised orbit). This leads to on-resonance excitation wherein the increase in oscillation amplitude of the ions (without exceeding the potential well depth) and the resulting kinetic energy increase promote fragmentation via ion-molecule collisions. In the LTQ, the precursor ion is selected in a quadrupole, then transferred to a linear ion trap for fragmentation and the product ions transferred to the Orbitrap mass analyser; hence tandem mass spectrometry in space.

In both cases, CID is the result of collisions between ions and target gas molecules which have been introduced into the collision cell activating the ion sufficiently to initiate bond cleavage. The maximum increase in internal energy is given by the equation below for inelastic collisions:

$$E_{\text{int}} = E_{\text{coll}} (M1/M1+M2)$$

where E_{int} = internal energy, E_{coll} = collision energy, $M2$ = mass of precursor ion, $M1$ = mass of collision gas.

An approach for comparing fragmentation of ions between molecules and instruments widely applied in the literature is the survival yield (SY) method ^[158,159]:

$$\text{SY} = \frac{(\text{intensity of precursor ion} \times 100) \%}{(\text{intensity of precursor ion} + \text{intensity of all product ions})}$$

Therefore, SY is percentage of ions with energy equal to or exceeding the critical energy (E_0), which is the minimum energy required for fragmentation i.e. the energy

required to cleave the weakest bond. Gabelica et al. have used AM1 computational methods to calculate the critical energies of several benzyl pyridium ions and found them to agree well with the observed survival yields^[155].

Ions with energies of E_0 or greater may not fragment if the rate of decomposition is more than the collision cell residence time. Under these circumstances, fragmentation may be induced by putting in additional internal energy to increase the reaction rate. This is additional energy known as the 'kinetic shift' and the resulting internal energy is termed E_{app} .

Plotting SY against collision energy gives a sigmoidal curve known as a breakdown graph. The appearance of the breakdown graph is instrument dependent because it depends on the residence time ('t') in the collision cell. For a fixed 't', the breakdown graph is characteristic of the molecule and can vary markedly even between molecules with only minor structural differences^[159]. For example Kertesz et al.^[160] studied the fragmentation of six isomers of (dimethylamino) benzoic acid. They found that differences in electron withdrawing and electron donating resonance effects between the *ortho*, *meta* and *para* positions resulted in differences between their breakdown graphs. An increase in electron donation increases CE_{50} whereas increasing electron withdrawing reduced the CE_{50} .

The voltage at which SY is 50% is commonly referred to as CV_{50} or CE_{50} ^[160] and is a property of the structure of the ion. A plot of CE_{50} against m/z for closely related compounds^[161] such as a series of poly(ethylene glycols), poly(tetrahydrofuran) and peptides, is linear. Thus it may be possible to predict CE_{50} for compounds in a homologous series. At collision energies 10-20% less than CE_{50} , there is usually no fragmentation. At collision energies 10-20% above CE_{50} , most of the precursor ion is fragmented^[161].

CID has both thermodynamic and kinetic components; that is the molecule must have both sufficient energy and sufficient time to fragment in the collision cell. CID may be considered a two-step process, ion activation followed by decomposition. It has been proposed that it is the rate of decomposition and the time scale of the experiment which determine the ratio of precursor to product ion intensity^[145,162]. Typical time scales for experiments in the different mass spectrometer types are shown in Table 1.4.

'Rapid' heating of ions occurs when the rate of activation of ions is greater than

the decomposition rate. This is typical of systems where high (keV) collision energies are applied, such as sector instruments. 'Slow' heating is when the activation rate is less than the decomposition rate. Slow heating allows multiple collisions (and hence energy transfers) to occur during the excitation period. The ions may dissociate or isomerise between collision^[163]. Slow heating occurs within multipole collision cells and quadrupole ion traps.

The rate of decomposition of an ion depends on^[160]:

- Internal energy of the molecule
- Activation energy for product ion formation; the lower the activation barrier the faster the rate.
- Vibrational degree of freedom; the larger the molecule the less kinetic shift is required to initiate fragmentation.^[145]
- Entropy of the transition state ΔS^* ; decreasing entropy results in a decreased distribution of energies and a lower reaction rate.

The internal energy of the molecule is largely dependent on the voltage applied to the collision cell, whereas the activation energy, degrees of freedom and transition state entropy are functions of the molecular structure.

The decomposition rate constant is directly proportional to SY as described below put in context of the Arrhenius equation:

$$SY = e^{-kt}$$

where k = decomposition rate constant, t = collision cell reaction time, $k = (\ln(SY))/t$
' t ' is constant for a given collision cell, therefore $k \propto SY$ and hence $k \propto$ collision energy.

There are two proposed main models of fragmentation:

1. Direct inelastic collision
2. Via a long-lived ion-gas complex with the internal energy spread across the whole complex; fragmentation occurring on dissociation of the complex^[148].

Using the transition state model^[145], for direct bond cleavage the transition state is termed 'loose' and is geometrically close to the product, making it a 'late' transition

state. The bond to be cleaved is stretched and vibrational energy may be decreased or converted into internal rotation. In the case of rearrangements, the transition state is 'tight', geometrically close to the precursor ion and described as an 'early' transition state. Rearrangements usually proceed via a cyclic structure where some rotations become frozen and are converted to vibrations.

Mass Analyser	CID energy	Average number collisions	Activation time	Instrument residence time	Efficiency
Sector, TOF/TOF	1-10 keV	1-5	1-10 ms	10-100 ms	<10%
Quadrupole and quadrupole hybrids	1-200 eV	10-100	0.5-1 ms	0.1-1 ms	5-50%
Quadrupole ion traps, FT-ICR	1-20 eV	100's	10-100 ms	10 ms-1 s	50-100%

Table 1.4 Comparing the characteristics of CID associated with different types of mass analyser^[163].

Direct bond cleavage occurs at higher collision energies than molecular rearrangements, because rearrangements involve bond formation in addition to bond cleavage. Therefore, collision energies may be manipulated to alter the type of fragmentation in addition to the abundance of ions. The long activation time in ion traps favours rearrangement over direct bond cleavage^[164].

Mass spectrometers may utilise high energy CID with energies applied in the keV range (sectors or TOFs) or low energy CID (quadrupoles and quadrupole ion traps) which apply energies in the eV range (see Table 1.4). Ion excitation is mainly electronic at high collision energies but there is some vibrational and rotational contribution^[165]. At these energies ions frequently only need to undergo single collisions to fragment. High collision energies (keV) are not generally applied to quadrupole cells as at these energies the residence time is too short to allow decomposition^[166]. Collision energy changes have a significant effect on fragmentation in low energy CID but little effect in high energy CID, where there is potential for all routes of fragmentation, independent of collision gas and pressure^[154,167].

Chapter 2: UNDERSTANDING COLLISION-INDUCED DISSOCIATION OF DOFETILIDE: A CASE STUDY IN THE APPLICATION OF DENSITY FUNCTIONAL THEORY AS AN AID TO MASS SPECTRAL INTERPRETATION

Published: *Analyst* **138** (22), 6869 – 6880, 2013. Wright, P.A., Alex A., Harvey, S., Parsons, T. and Pullen, F.S.

2.1. INTRODUCTION

The ability to predict the MS/MS fragmentation of non-peptidic molecules would be a significant aid to the mass spectrometrists in terms of reducing spectral interpretation time, introducing consistency and in assisting less experienced practitioners in the art of spectral interpretation. Attempts have been made to establish rules by which the number of possible options for fragmentation can be limited based on prior knowledge of the compound class or structural motifs. Commercial prediction programs, such as ACDLabs Mass Fragmenter, ThermoScientific's Mass Frontier and Waters MassFragment, have reported a number of successes in this arena, but all of these approaches tend to predict more fragmentation *in silico* than is actually observed in the experimental data [168,169]. Many of the proposed fragment ions, using these approaches, may be considered to be chemically unlikely by an experienced mass spectrometrists, but not necessarily by the new practitioner. The reasons for this limit in the effectiveness of these commercial packages are that approaches may be mainly arithmetical, cleaving all possible bonds and calculating fragment masses (bond disconnection approach), whilst others apply 'rules' and/or extrapolation from databases for their predictions, making assumptions which may not be valid for the molecule of interest. Potentially, predictions made by these software packages may be improved by tailoring the predictions to each individual molecule by modelling the properties of the molecule itself. Considering each molecule at a quantum level and identifying what structural changes may lead to bond cleavage. It may then be possible to use this quantum information as a descriptor (numerical data which is used to represent chemical information in computational modelling). Quantum chemical descriptors have been applied successfully in analytical chemistry and the determination of physicochemical properties : 3D descriptors (molecular conformation calculated by DFT) have been reported to increase the accuracy of the prediction of

HPLC retention and separation ^[170]; descriptors have been identified for the protonation process;^[171] the *in silico* prediction of pKa's of guanidine containing compounds has been improved by using calculated bond length as a descriptor as there was a correlation between bond lengths and the pKa ^[172].

In practice, rather than identifying descriptors, thermodynamics has been used to understand and explain mass spectral fragmentation routes. This commonly involves generating potential energy diagrams which show the energies of the precursor molecular ion, all transition states and the final product ion. Originally experimentally determined values, such as heats of formation and kinetic energy release measurements, which were made on double focussing magnetic sector mass spectrometers, were used to generate these potential energy profiles ^[173,174]. With the advances in both computer technology and computational chemistry tools, theoretical energies for energy minimised structures can be readily determined and applied to rationalise spectra ^[175–178]. One of the most widely used computational approaches is Density Functional Theory (DFT) ^[94]; a quantum chemistry method for calculating molecular properties based on electron density. These detailed energy studies are highly informative but require significant computer and operator time, and indeed expert knowledge, to generate thermodynamically feasible fragmentation routes. Thus this approach is not widely undertaken on a routine basis, particularly in industrial laboratories where time-constraints limit the resource available for fully rationalising spectra.

In the work presented in this thesis, a different approach to applying DFT to rationalize mass spectral fragmentation has been taken. DFT has been used to calculate the thermodynamically most stable protonated species based on the three dimensional structure and to determine the effect that protonation has on the electronic properties and 3D shape of the molecule; specifically the effect of protonation on bond length. In general, with a few exceptions ^[179], lengthening a bond will cause it to weaken and render it more susceptible to cleavage ^[180,181]. This approach has been used to rationalise the cleavage sites of the different potential protonated molecules ions of fluconazole and maraviroc ^[92,182].

The effect of protonation on bond lengths has been studied using *ab initio* and DFT quantum methods. Alcami et al. have shown that protonation may be followed by cleavage of adjacent bonds if the basic atom is sufficiently electronegative, citing

alcohols or fluoroalkanes as examples ^[183–185]. The presence of the proton on the electronegative centre pulls the bonding electrons toward the charged centre, reducing the electron density in the bonding region. Cleavage can occur if there is sufficient difference in electronegativity between the basic centre and the atom bonded to it. The reverse is true if the basic centre is less electronegative than the atom to which it is bonded; the electron density in the bonding region increases as electrons are pushed toward it. This does not explain cleavage of non-polarised bonds, but a study of the fragmentation of cyclic sulphur compounds suggest that cleavage of sulphur-sulphur bonds was driven by the stability of the product ion formed ^[186].

Several groups have reported that molecular ions appear not to be a single species, but a mixture of molecular ions which are protonated on a number of different basic sites across the molecule ^[187,188]. For example, it has been proposed that the ions were generated by protonation at the most basic site in solution but then the proton moved to a less thermodynamically favourable site(s) in the gas phase. In separate studies, it has been reported that two isobaric ions observed within the same spectra could only be explained if they correspond to precursor ions protonated on different atoms, giving rise to different product ions. The publication by Kaufmann provided experimental evidence, including the effect of differing cone voltages on sampling of the isobaric molecular ions, that a mixture of singly charged species was formed in the source. Komaromi et al. observed that *N*-acetyl-*O*-methoxy (*N*-acetyl-*O*-Me) proline exhibits two distinct fragmentation pathways indicative of the coexistence of several protonated forms ^[189]. These observations were supported by both DFT and *ab initio* calculations.

Fragmentation pathways are often dictated by the site of ionisation; this is termed 'charge-directed fragmentation'. Charge-directed fragmentation has been widely reported for peptides ^[190], but has also been reported for small molecules such as aromatic sulphoxides ^[68] and low molecular weight aromatics ^[191]. Therefore, knowledge of the protonation site may significantly assist spectral interpretation. As discussed previously, it cannot be assumed that protonation at the most basic nitrogen predominates, as there are a number of examples where the mass spectral fragmentation can only be explained by protonation at less basic sites, possibly as a result of proton migration or steric hindrance ^[192,193]. Therefore, an understanding of the site(s) of protonation is essential to developing tools to aid mass spectral

interpretation.

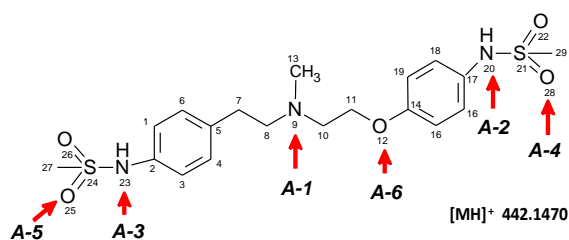


Figure 2.1 Structure of dofetilide highlighting the possible protonation sites, labelled in order of DFT calculated probability of protonation.

In this study, DFT was used to model dofetilide, and four methylated analogues (Figure 2.2), to determine the nature of bond length changes resulting from protonation at all potential basic sites within the molecule. The *in silico* data were compared to the ions observed in the mass spectra obtained experimentally, and the effect of the introduction of the extra methyl groups on fragmentation pathway was also considered. Thermodynamic, kinetic and conformational aspects of the protonation and CID fragmentation will be discussed, particularly in terms of the potential for proton migration leading to charge-directed fragmentation. The aim is to both gain further understanding of the processes involved in CID and also to determine if protonation-induced bond lengthening has the potential to be used as a descriptor, highlighting potential bond cleavages, and, therefore, be used in the future in mass spectral interpretive software.

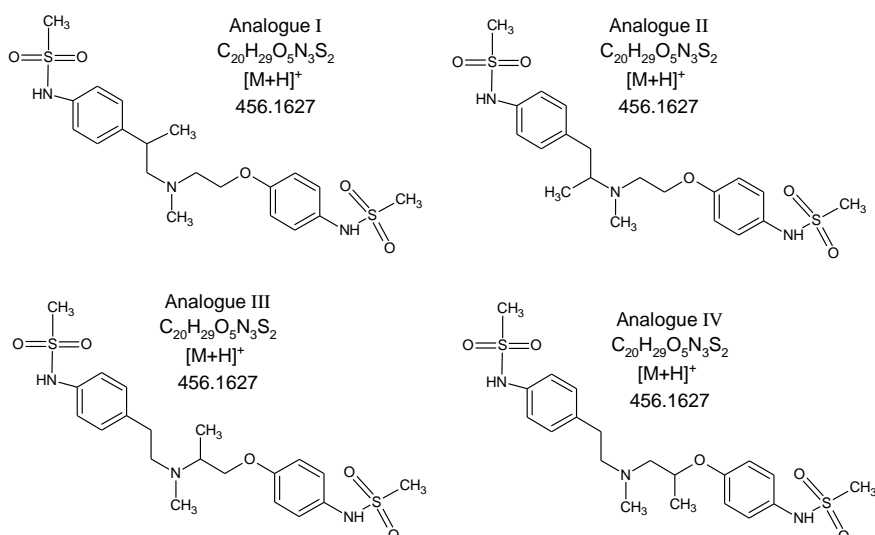


Figure 2.2 The structures of the four methylated analogues of dofetilide.

2.2. EXPERIMENTAL

2.2.1. Chemicals

All compounds used in this investigation were synthesized by Pfizer Global Research and Development and were used without further purification. Methanol >99.9 % and HPLC grade water were purchased from Sigma Aldrich. Formic Acid 99 % was purchased from Acros Organics.

2.2.2. High resolution MS/MS

All the mass spectrometric measurements were performed on an LTQ Orbitrap XL instrument (ThermoFisher Scientific, San Jose, CA, USA) equipped with the heated ESI Probe operated in positive ion mode.

The ESI (positive ion) parameters for all compounds studied were; source voltage 5 kV, entrance capillary voltage 35 V, entrance capillary temperature 275°C, Nitrogen sheath gas flow rate 8 a.u. The solutions of dofetilide and its analogues were prepared to 1 mg/mL in methanol, were introduced into the ESI source by loop injection using 0.1 % formic acid in water as the mobile phase.

For all compounds studied, a full MS scan was performed in the FTMS between m/z 50-2000 at 60,000 resolution. MS/MS of the predefined molecular ion was then performed in the linear ion trap by Collision Induced Dissociation (CID); the product ions formed were detected in the FTMS at a resolution of 30,000. The MS/MS parameters were; isolation width 2, normalized collision energy 35%, collision gas; Nitrogen. Wideband activation was not used. Data was analysed using the Excalibur 2.0 software package (ThermoFisher Scientific, San Jose, CA, USA).

2.2.3. Computational calculations

Gas Phase Basicity, 3D structure and bond length calculations were performed using DFT calculations at the B3LYP level using the 6-31G** basis set in Jaguar (Schrödinger, New York, USA). The optimized geometry for the neutral molecule was calculated, basic sites were then protonated and the relating minimum global energy geometry determined for each. No symmetry constraints were imposed in the optimizations. Calculations were undertaken on neutral molecules and on the cations formed from these molecules by protonation on the heteroatoms. Only the heteroatoms were considered as protonation sites in this study as carbon-carbon

cleavage was not observed for these compounds.

2.3. RESULTS AND DISCUSSION

Our results indicate that charge-directed fragmentation, potentially requiring gas phase proton migration (potentially within the collision cell) to less thermodynamically favourable site(s), may be explained thermodynamically using DFT calculations to calculate bond lengths changes. In the discussion of the fragmentation of dofetilide and its analogues, four aspects of the ionisation and fragmentation process will be considered; ionisation, proton migration/tunnelling post ionisation, thermodynamics of fragmentation and, finally, product ion stability.

2.3.1. Ionisation

The first stage in understanding the CID process, and how best to apply DFT, is to consider the significance of the site of ionisation. It is generally accepted that in the ESI process, the analyte ions are pre formed in solution and these ions are directly transferred into the gas phase. In the case of cations, the ions are usually formed in solution as the result of protonation at the most basic site in the molecule, as reflected by the pKa's. However, the molecular ion observed in mass spectra has been reported to correspond to a mixed protonated population, with the proton not necessarily present on the atom with the highest pKa^[92,194]. As it is unlikely that multiple protonated species are formed in solution prior to electrospray, either chemical ionisation type (ion-molecule charge transfer) reactions occur in the gas phase or the protonation is at a single site in solution but the proton subsequently moves within the molecular ion. It is important to understand which of these ionisation processes predominates because it impacts on what DFT calculations are required and how the data is assessed. If the proton migrates, then protonation at all positions needs to be considered, irrespective of thermodynamic feasibility (this is discussed in detail later). If protonation is occurring in the gas phase, that is the proton is attached directly to atom and stays there, then only the thermodynamically feasible protonation sites need be modelled.

A comprehensive literature search revealed a number of publications that favour the gas phase electrospray ionisation theory, in many cases direct gas phase ionisation, because it is difficult to rationalise the product ions in the MS/MS spectra

of certain compounds by protonation only on the most basic site in solution. For example, it has been proposed that gas phase ionisation via ion-molecule reactions plays a major role in ESI, by proton transfer from gaseous ammonium ions to analytes of higher proton affinity [20]. However, alternative explanations may account for the lack of correlation between ionisation state in solution and that observed in the mass spectrum.

Kamel et al. have reported that the ESI sensitivity of a series of purine and pyrimidine base antiviral agents was independent of the mobile phase pH [18] and considered this as an indication that the ionisation state in aqueous solution is not a major influence on ESI of these molecules. However, the charge is not evenly distributed across the droplets generated during the ESI process; the ions are concentrated at the surface. It has been reported that the acidity at the surface of the droplet is 10³-10⁴ greater than in the bulk solution [24]. This has a significant effect on the ionisation state of the analyte as it is only the ions at the surface which enter the gas phase. Therefore, it is debatable if the pH of the bulk solution is relevant. This may explain the observation that positive ion ESI response of these antiviral agents and certain other basic pharmaceutical molecules may not be reduced, and sometimes even enhanced, at high pH [17,19,195].

In another example, spectra were obtained for myoglobin at a pH (pH 10 adjusted with ammonia) at which it is not ionised in solution [196]. In this case it is suggested that a proton transfer reaction, from NH₄⁺ to myoglobin, occurs at the surface of the electrospray droplet rather than as a result of protonation in the gas phase. Zhou and Cook have also offered this explanation for protonation of caffeine at neutral pH [15].

Tian and Kass in 2009 made the interesting observation that the protonated species changes with the infusion solvent [197]. *p*-Aminobenzoic acid was found to be *N*-protonated in acetonitrile/water but *O*-protonated in methanol/water. This is suggestive of ion-molecule charge transfer reactions in the gas phase, but an alternative explanation that charge transfer is occurring on the surface of the droplet may also apply.

In contrast to Kamel's observation that electrospray response was independent of pH [195], Ehrmann et al. have shown that that ESI response is dependent on the pK_b of the analytes and not their gas phase proton affinities [198], the compounds in this study having greater proton affinities than the methanol in the mobile phase. This

suggests that gas phase ionisation does not contribute significantly during the ESI process. Additional evidence for ionisation occurring mainly in solution comes from the observations relating to ionisation suppression. In ESI, ionisation suppression is reported to result from changes in droplet properties which prevent ions reaching the gas phase. The changes to the ESI droplets which have been proposed to lead to ionisation suppression include increased viscosity and surface tension which restrict the transfer of the analyte to the gas phase [6,199]. A significant increase in conductivity of the liquid in the droplets has been measured during suppression indicating a rise in electrolyte levels, affecting surface tension [200]. Non-volatile suppressants may cause co-precipitation of the analyte and/or prevent the droplets from reaching the size required for Coulombic explosion [201]. The gas phase process APCI is less prone to ionisation suppression than ESI [202] further confirming that suppression is due to ions failing to reach the gas phase and hence that ionisation had occurred in solution.

Thus, the weight of literature evidence suggests that electrospray ionisation predominantly occurs in solution and that many of the reports of gas phase ionisation may also be explained by other mechanisms including proton migration. Therefore, all the potential protonation sites of dofetilide needed to be modelled in this study, as the potential for proton migration means that the proton may be located on any heteroatom and it cannot be assumed that protonation is restricted to the most thermodynamically likely sites (i.e. those with sufficient gas phase basicity).

The six possible sites of protonation on heteroatoms in dofetilide are shown in Figure 2.1. DFT energy calculations for all six potential cations were performed to rank the probability of protonation occurring at each of these sites. From the DFT calculations the most thermodynamically favoured protonation site in the gas phase is calculated to be the tertiary nitrogen (N9), producing the cation A-1 (Table 2.1). This rank order for gas phase basicities (based on the DFT calculated energies of each protonated species) mirrors those in solution, the experimentally determined pKa's for N9, N20 and N23 being 9.6, 9.0 and 8.0 respectively [203]. Both the DFT predicted basicities (Table 2.1) and the calculated pKa's (Marvin, Chemaxon, Hungary), for the four analogues also follow the same pattern; pKa's for N9, N20 and N23 calculated to be 10.8, 10.1 and 9.0 respectively for all four analogues. Therefore, based on these pKa's, protonation in solution will occur predominantly at N-9 to form cation A-1, and, therefore, it is as cation A-1 that the analyte ions will enter the gas phase.

Table 2.1 Optimized geometries and relative energies for neutral and protonated species of dofetilide (1 Hartree unit is 627.503 kcal mol⁻¹).

Energy neutral molecule (Hartree)	Cation	Energy cation (Hartree)	Energy difference between Cation A-1 and Cations A-2 to A-6 (kcal mol ⁻¹)
-2076.926601	A-1	-2077.307630	n/a
	A-2	-2077.279472	17.7
	A-3	-2077.272230	22.2
	A-4	-2077.265933	26.2
	A-5	-2077.260337	29.7
	A-6	-2077.252497	34.6

As will be discussed later, the product ions in the CID spectra cannot all be attributed to protonation at N-9; at least two other protonated forms of dofetilide (A-6 and A-3) are proposed to be generated as a result of proton migration, which also contribute to the observed product ion spectrum.

2.3.2. Thermodynamics of Fragmentation

Key changes in bond lengths induced by protonation of dofetilide at the six possible protonation sites are shown in Table 2.1. The greatest changes in bond length occurred in the bonds closest to the site of protonation. This is consistent with literature reports that protonation causes the greatest perturbation to electron density immediately around the protonation site [204]. For example, for cation A-1, the bonds of the tertiary nitrogen N9, which was proposed as the thermodynamically most likely ionisation site, elongated or contracted by - 0.051 Å to +0.063 Å, whereas the N-S bonds of the sulphonamide groups at either end of the molecule elongated/contracted by much less (- 0.01 Å to +0.008 Å).

The MS/MS spectrum of dofetilide is shown in Figure 2.3, and Table 2.3 shows the proposed ion formulae and structures of product ions observed at a relative intensity of above 10%. The spectrum showed two major ions present in greater than 90% relative intensity. The more intense of these two ions was observed at

m/z 255.1166 which is consistent with a molecular formula of $C_{12}H_{19}O_2N_2S$ formed by cleaving O12-C11 bond. The second most abundant product ion (94%) was observed at m/z 198.0586 corresponding to molecular formula $C_9H_{12}O_2NS$, formed by cleavage of the C8-N9 bond. The lower abundance cation at m/z 245.0959 was formed from by cleaving C8-N9. The minor ion at m/z 179.1180 resulted from cleaving three bonds (N23-S24, O12-C14, N9-C13).

Table 2.2 Comparison of bond length changes for neutral dofetilide and protonated species A-1 to A-6. Refer to Figure 2.1 for atom numbering. Significant bond elongations (>0.045 Å), which contribute to observed bond cleavage, are highlighted.

Bond	Bond length changes (Å)						Bond observed to cleave in MS/MS spectrum?
	Cation A-1	Cation A-2	Cation A-3	Cation A-4	Cation A-5	Cation A-6	
	(N9)	(N20)	(N23)	(O28)	(O25)	(O12)	
N9-C8	+0.063	+0.002	-0.009	+0.03	-0.001	+0.009	Yes
N9-C10	-0.051	-0.004	-0.003	0.000	-0.003	-0.005	No
N9-C13	+0.047	+0.004	+0.002	+0.004	+0.002	+0.007	Yes
N23-S24	+0.034	+0.003	+0.327	+0.002	-0.066	0.000	Yes
O12-C14	+0.025	-0.028	+0.005	-0.018	+0.009	+0.098	Yes
O12-C11	-0.021	+0.02	-0.006	+0.017	-0.006	+0.123	Yes
N20-S21	+0.004	+0.335	0.000	-0.071	0.000	+0.032	No
N23-C2	-0.008	-0.002	+0.033	-0.005	+0.033	-0.009	No
C17-N20	-0.011	+0.019	-0.001	+0.022	-0.003	+0.032	No

Figure 2.3 MS/MS (CID) spectrum of protonated dofetilide.

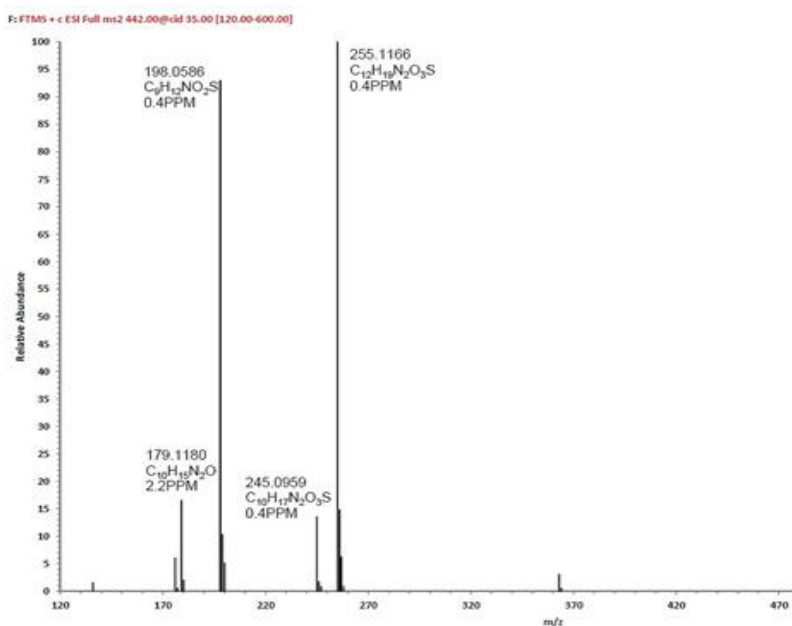


Table 2.3 Proposed structures for the product ions observed in the MS/MS spectrum of protonated dofetilide.

Relative intensity (%)	Experimental m/z	Proposed ion formula and calculated accurate mass	Error (ppm)	Proposed structure(s) of product ion	Bond breaking
100	255.1166	$C_{12}H_{19}O_2N_2S$ 255.1167	0.4		O12-C11
13	245.0959	$C_{10}H_{17}N_2O_3S$ 245.0960	0.4		N9-C8
94	198.0586	$C_9H_{12}O_2NS$ 198.0589	1.5		N9-C8
17	179.1180	$C_{10}H_{15}ON_2$ 179.1184	2.2		N23-S24 O12-C14 N9-C13

Comparing the product ion assignments of dofetilide (Table 2.3) with the DFT calculations of the effect of protonation on bond length (Table 2.2), it may be seen that

all the bonds cleaved during CID fragmentation were lengthened, and hence weakened, by protonation at N9 or O12, (cations A-1 and A-6). All the bonds which were observed to cleave lengthened by greater than 0.025 Å. Although previous work^[91] had not established a minimum bond lengthening, it appears for dofetilide the bond lengthening had to be significant, in this case greater than 0.025 Å, before the cleaving of the bond is observed.

Formation of the precursor ion A-1 is expected as N9 is the thermodynamically most likely site for protonation. However, O12 (giving rise to A-6) is thermodynamically unlikely to be protonated either in the gas phase or in solution. Moreover, the observation that m/z 255, derived from A-6, and m/z 198, derived from A-1, are both present in the spectrum at greater than 90% suggests that precursors A-1 and A-6 are formed to a similar extent. As discussed in the next section, it is proposed that proton migration accounts for the formation of the thermodynamically unlikely cation A-6.

The product ion spectra of the four dofetilide analogues are shown in Figure 2.4. DFT predicted the protonation site stability (Table 2.4) and bond length changes (Tables 2.5 and 2.6) resulting from protonation, and these were compared to those observed for dofetilide. The MS/MS fragmentation was very similar for dofetilide and all four analogues, with all products ions resulting from protonation at N9 or O12. The proposed product ions present at greater than 10% are shown in Table 2.7, with accurate mass data in Table 2.8. The bond cleavages O12-C11 and N9-C8 which gave rise to the major ions in the dofetilide spectrum were also observed for all analogues.

Table 2.4 Optimized geometries and relative energies for neutral and protonated species of four dofetilide analogues (1 Hartree unit is 627.503 kcal mol⁻¹).

Dofetilide Analogue I neutral energy = -2116.237705 Hartree		Dofetilide Analogue II neutral energy = -2116.23430 Hartree		Dofetilide Analogue III neutral energy = -2116.243764 Hartree		Dofetilide Analogue IV neutral energy = -2216.246530 Hartree		
Cation	Cation energy (Hartree)	Energy difference between Cation A-1 and Cations A-2 to A-6 (kcal mol ⁻¹)	Energy cation (Hartree)	Energy difference between Cation A-1 and Cations A-2 to A-6 (kcal mol ⁻¹)	Energy cation (Hartree)	Energy difference between Cation A-1 and Cations A-2 to A-6 (kcal mol ⁻¹)	Energy cation (Hartree)	Energy difference between Cation A-1 and Cations A-2 to A-6 (kcal mol ⁻¹)
A-1	-2116.61896	n/a	-2116.62600	n/a	-2116.62825	n/a	-2116.62912	n/a
A-2	-2116.59049	-17.86	-2166.59109	-21.90	-2116.59460	-21.11	-2116.59913	-18.63
A-3	-2116.58443	-21.67	-2116.58349	-26.67	-2166.58879	-24.76	-2116.59120	-23.79
A-4	-2116.57804	-25.68	-2116.57903	-29.47	-2116.58109	-29.59	-2116.58370	-28.50
A-5	-2116.57174	-29.63	-2116.57061	-34.76	-2116.57599	-32.79	-2116.57975	-30.98
A-6	-2166.56592	-33.28	-2116.56708	-36.97	-2166.56827	-37.64	-2116.57776	-32.22

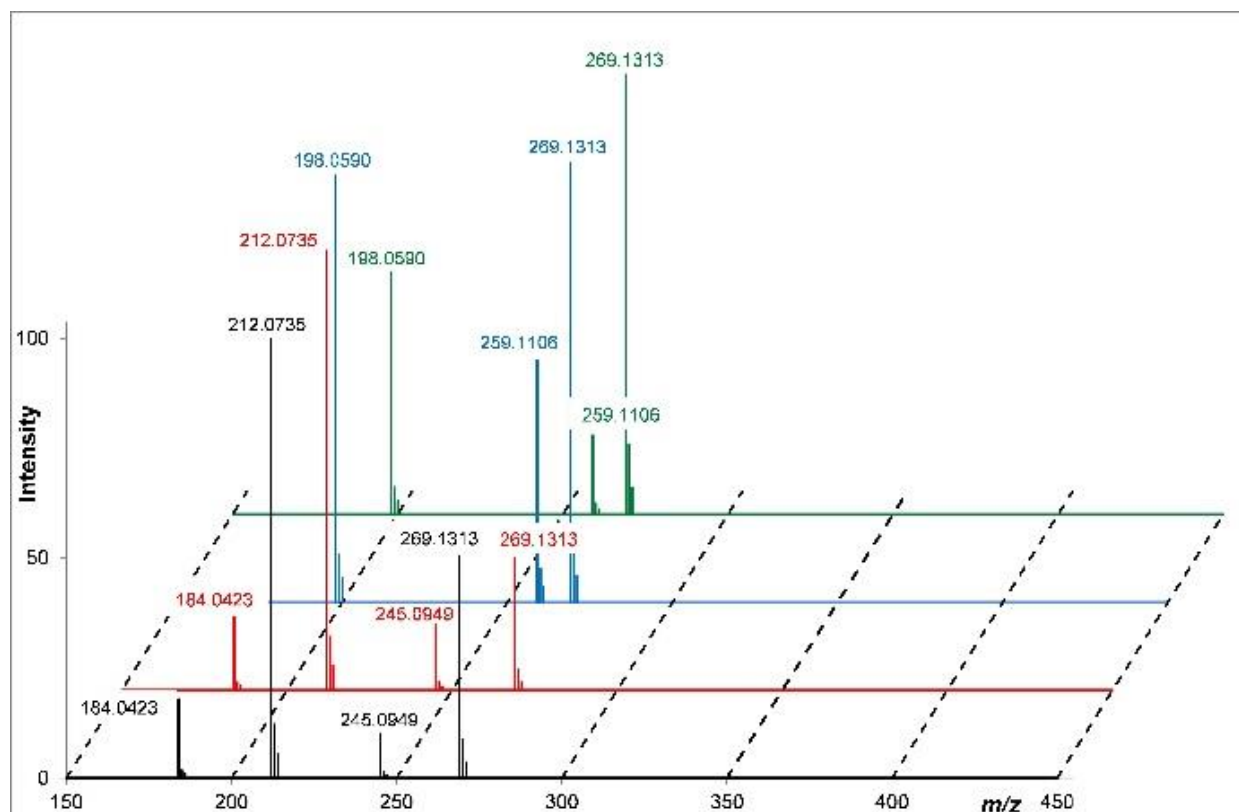


Figure 2.4 MS/MS (CID) spectra of protonated dofetilide analogues I to IV recreated in 2- dimensions.

Table 2.5 Comparison of bond length changes for protonated dofetilide analogues I to IV as a result of protonation to generate cations A-1 and A-6. A full table of data for all six cations is available in Table 2.6. Significant bond elongations (>0.045 Å), which contribute to observed bond cleavage, are highlighted.

Bond	Dofetilide analogue I			Dofetilide analogue II			Dofetilide analogue III			Dofetilide analogue IV		
	Bond length changes (?)		Bond observed to cleave in MS/MS spectrum?	Bond length changes (?)		Bond observed to cleave in MS/MS spectrum?	Bond length changes (?)		Bond observed to cleave in MS/MS spectrum?	Bond length changes (?)		Bond observed to cleave in MS/MS spectrum?
	Cation A-1 (N9)	Cation A-6 (O12)		Cation A-1 (N9)	Cation A-6 (O12)		Cation A-1 (N9)	Cation A-6 (O12)		Cation A-1 (N9)	Cation A-6 (O12)	
N9-C8	+0.082	+0.014	Yes	+0.081	+0.018	Yes	+0.066	+0.010	Yes	+0.064	+0.008	Yes
N9-C10	+0.055	-0.009	Yes	+0.066	+0.006	Yes	+0.064	-0.007	No	+0.052	-0.002	No
N9-C13	+0.052	+0.008	No	+0.055	+0.015	No	+0.044	-0.003	No	+0.044	-0.014	No
N23-S24	+0.009	+0.001	No	+0.033	-0.007	No	+0.032	+0.001	No	+0.035	+0.004	No
O12-C14	+0.029	+0.099	No	+0.022	+0.086	No	+0.024	+0.093	No	+0.023	+0.089	No
O12-C11	-0.024	+0.134	Yes	-0.013	+0.134	Yes	-0.023	+0.151	Yes	-0.023	+0.153	Yes
N20-S21	+0.020	+0.019	No	+0.023	+0.023	No	+0.005	+0.035	No	+0.002	+0.032	No
N23-C2	-0.016	-0.010	No	-0.006	-0.013	No	-0.012	-0.012	No	-0.010	-0.008	No
C17-N20	-0.017	-0.044	No	-0.022	-0.039	No	-0.012	-0.031	No	-0.010	-0.033	No

Table 2.6 Comparison of bond length changes for dofetilide analogues I to IV as a result of protonation to generate cations A-1 to A-6.

Bond	Dofetilide analogue I							Dofetilide analogue II						Dofetilide analogue III						Dofetilide analogue IV								
	Bond length changes (?)						Bond observed to cleave in MS/MS spectrum?	Bond length changes (?)						Bond observed to cleave in MS/MS spectrum?	Bond length changes (?)						Bond observed to cleave in MS/MS spectrum?							
	Cation A-1 (N9)	Cation A-2 (N20)	Cation A-3 (N23)	Cation A-4 (S21)	Cation A-5 (O25)	Cation A-6 (O12)		Cation A-1 (N9)	Cation A-2 (N20)	Cation A-3 (N23)	Cation A-4 (S21)	Cation A-5 (O25)	Cation A-6 (O12)		Cation A-1 (N9)	Cation A-2 (N20)	Cation A-3 (N23)	Cation A-4 (S21)	Cation A-5 (O25)	Cation A-6 (O12)		Cation A-1 (N9)	Cation A-2 (N20)	Cation A-3 (N23)	Cation A-4 (S21)	Cation A-5 (O25)	Cation A-6 (O12)	
N9-C8	+0.082	+0.004	-0.015	+0.007	-0.015	+0.014	Yes	+0.081	+0.017	+0.002	+0.004	+0.004	+0.018	Yes	+0.066	+0.006	-0.011	+0.005	-0.008	+0.010	Yes	+0.064	+0.004	-0.009	+0.002	-0.007	+0.008	Yes
N9-C10	+0.055	-0.005	+0.003	+0.005	+0.002	-0.009	Yes	+0.066	+0.017	+0.015	-0.018	+0.015	+0.006	Yes	+0.064	-0.004	+0.002	-0.003	+0.002	-0.007	No	+0.052	-0.009	+0.002	-0.007	+0.002	-0.002	No
N9-C13	+0.052	+0.001	+0.002	+0.004	0.000	+0.008	No	+0.055	+0.015	+0.011	+0.088	+0.010	+0.015	No	+0.044	+0.002	-0.001	+0.002	+0.001	-0.003	No	+0.044	-0.002	-0.001	-0.004	-0.059	-0.014	No
N23-S24	+0.009	+0.003	+0.083	-0.066	-0.091	+0.001	No	+0.033	-0.005	+0.318	-0.003	-0.072	-0.007	No	+0.032	+0.002	+0.325	+0.002	-0.065	+0.001	No	+0.035	+0.004	+0.326	+0.002	-0.065	+0.004	No
O12-C14	+0.029	-0.026	+0.008	-0.022	+0.006	+0.099	No	+0.022	-0.033	+0.002	-0.029	-0.001	+0.086	No	+0.024	-0.029	+0.006	-0.024	+0.005	+0.093	No	+0.023	-0.030	+0.005	-0.026	+0.004	+0.089	No
O12-C11	-0.024	+0.026	-0.008	+0.016	-0.006	+0.134	Yes	-0.013	+0.024	-0.010	+0.019	-0.009	+0.134	Yes	-0.023	+0.020	-0.005	+0.017	-0.004	+0.151	Yes	-0.023	+0.022	-0.006	+0.020	+0.001	+0.153	Yes
N20-S21	+0.020	+0.324	+0.006	-0.084	+0.002	+0.019	No	+0.023	+0.090	-0.015	-0.086	-0.016	+0.023	No	+0.005	+0.337	+0.002	-0.064	+0.003	+0.035	No	+0.002	+0.339	-0.001	-0.069	-0.001	+0.032	No
N23-C2	-0.016	-0.003	+0.025	-0.006	+0.027	-0.010	No	-0.006	-0.005	+0.030	-0.022	+0.040	-0.013	No	-0.012	+0.002	+0.033	-0.004	+0.037	-0.012	No	-0.010	-0.003	+0.033	-0.003	+0.034	-0.008	No
C17-N20	-0.017	+0.005	-0.003	+0.009	-0.001	-0.044	No	-0.022	+0.008	+0.006	+0.014	-0.015	-0.039	No	-0.012	+0.018	-0.003	+0.019	-0.002	-0.031	No	-0.010	+0.016	-0.002	+0.028	-0.001	-0.033	No

Table 2.7 Proposed structures for the product ions observed in the MS/MS spectrum of the four protonated dofetilide analogues I to IV (n/a = cleavage not observed).

Bond cleaved	Analogue I			Analogue II			Analogue III			Analogue IV		
	Relative intensity (%)	Nominal <i>m/z</i>	Proposed structure of ion	Relative intensity (%)	Nominal <i>m/z</i>	Proposed structure of ion	Relative intensity (%)	Nominal <i>m/z</i>	Proposed structure of ion	Relative intensity (%)	Nominal <i>m/z</i>	Proposed structure of ion
O12-C11	55	269		30	269		100	269		100	269	
N9-C8	10	245		15	245		55	259		18	259	
N9-C8	100	212		100	212		97	198		55	198	
N9-C10	18	184		18	184		n/a	n/a	n/a	n/a	n/a	n/a

Table 2.8 Accurate mass information for the product ions observed in the MS/MS spectrum of the four protonated dofetilide analogues I to IV (n/a = cleavage not observed).

Bond cleaved	Analogue I			Relative intensity (%)	Analogue II			Experimental <i>m/z</i>	Analogue III			Analogue IV		
	Experimental <i>m/z</i>	Proposed ion formula and calculated accurate mass	Error (ppm)		Experimental <i>m/z</i>	Proposed ion formula and calculated accurate mass	Error (ppm)		Experimental <i>m/z</i>	Proposed ion formula and calculated accurate mass	Error (ppm)	Experimental <i>m/z</i>	Proposed ion formula and calculated accurate mass	Error (ppm)
O12-C11	269.1313	C ₁₃ H ₂₁ O ₂ N ₂ S 269.1324	1.8	30	269.1313	C ₁₃ H ₂₁ O ₂ N ₂ S 269.1324	2.1	269.1313	C ₁₃ H ₂₁ O ₂ N ₂ S 269.1324	2.0	269.1313	C ₁₃ H ₂₁ O ₂ N ₂ S 269.1324	2.0	
N9-C8	245.095	C ₁₀ H ₁₇ O ₃ N ₂ S 245.0956	1.9	15	245.0949	C ₁₀ H ₁₇ O ₃ N ₂ S 245.0956	2.4	259.1106	C ₁₁ H ₁₉ O ₃ N ₂ S 259.1116	1.9	259.1106	C ₁₁ H ₁₉ O ₃ N ₂ S 259.1116	1.7	
N9-C8	212.0735	C ₁₀ H ₁₄ O ₂ NS 212.0745	2	100	212.0735	C ₁₀ H ₁₄ O ₂ NS 212.0745	2.4	198.059	C ₉ H ₁₂ O ₂ NS 198.0589	2.2	198.059	C ₉ H ₁₂ O ₂ NS 198.0589	2.2	
N9-C10	184.0423	C ₈ H ₁₀ O ₂ NS 184.043226	2.1	18	184.0423	C ₈ H ₁₀ O ₂ NS 184.043226	2.4	n/a	n/a	n/a	n/a	n/a	n/a	

There was a difference observed between dofetilide and analogues I and II with respect to the relative abundance of the two major product ions in their respective spectra. The ions generated by cleavage N9-C8 (*m/z* 198 and *m/z* 212) were base peaks in the spectra of I and II, respectively, but the ion at *m/z* 269 formed by cleaving

O12-C11 was present at lower abundance (55% and 30%) in these analogues than the equivalent ion observed in the dofetilide or analogue III or IV spectra (where it was greater than 90%). For the analogues I and II, the bond elongation of N9-C8 was 30% greater than that calculated for dofetilide and analogues III and IV, which may explain why this bond cleavage predominates over that of O12-C11 in the spectra. Therefore, for dofetilide and these four closely related analogues, DFT correctly identifies the bonds that will cleave to produce the two major ions in the product ion spectrum and also which of the two will be the most intense ion on the basis that it is the bond which lengthens to the greatest extent.

2.3.3. Proton migration/tunnelling

Protonation migration has been widely reported in mass spectrometry. Where the proton movement results from the system passing through energy barriers rather than going over them, the process is known as proton tunnelling [205]. Proton tunnelling transfer times are in the nano second range [206] and so are well within the transit times of ions passing through the mass spectrometer, typically 50 milliseconds [38].

Proton migration to a thermodynamically less favourable site has been observed to be necessary before fragmentation occurs. The classic example of this behaviour is exhibited by peptides and proteins, and arises from the observation that loss of ammonia from amides requires protonation on the nitrogen even though the oxygen is both the most energetically favoured protonation site and the observed initial protonation site [62,207,208]. Proton migration has also been observed in non-peptidic molecules. The mass spectrum of penicillin shows cleavage of the β -lactam bond after transfer of the proton from the carbonyl to the lactam nitrogen [209]. Proton migration has not only been observed for amides; dibenzyl ether [192], the pharmaceutical compound maraviroc,^[91] dialkylphosphoric acid esters [210] and thiourea/urea compounds^[211] have all been reported to exhibit proton migration in their mass spectra. It has also been observed for fatty acids where long range proton migration was cited as evidence for the cleavage of stable carbon-carbon bonds to form two less stable radical products ions [212]. It has been calculated using computational chemistry that short-range proton migration is energetically unfavourable as the model assumed that the proton migration was via an internal hydrogen bond and the strain would be too great to allow hydrogen bond formation between proximate atoms^[213]. It has been

proposed in this case that interaction with another molecule may act to facilitate short-range proton migration; for example the migration of a proton from an alcoholic oxygen to the carbon alpha to the oxygen is mediated via water or ammonia, both of which have a higher proton affinity than the alcoholic oxygen [39]. Protonated *N*-benzyl lactams dissociate via amide (C-N) cleavage, to give a minor product ion, and also by C^α-C^β (relative to the amide nitrogen) cleavage, to give the major product ion. It has been proposed that fragmentation occurs after migration from the carbonyl oxygen (the thermodynamically favourable site) to the dissociative site either directly in the case of C^β or stepwise to the amide nitrogen^[215].

Crucially, whatever the migration distance, it has been reported that fragmentation occurs at the atoms bearing the positive charge^[216] and that this may involve migration of the proton to the 'dissociative site'^[217], which triggers charge directed fragmentation. Therefore, it is proposed that it is proton migration to a dissociative site in dofetilide, O12 (cation A-6), which initiates the fragmentation to generate product ion *m/z* 255.

Additional evidence for proton migration being the origin of A-6, rather than direct protonation of O12 in the gas phase, lies in the calculated stabilities of the possible protonated species. The DFT calculated energy difference between A-1 and the next most thermodynamically stable site, N20 (cation A-20), is 17.7 kcal mol⁻¹ (Table 2.1). As an energy value this, in itself, does not seem excessive, but if this value is translated to a molecular level, a 17.7 kcal mol⁻¹ energy difference equates to a massive excess of A-1 ions over A-2 ions (greater than 2,000,000 A-1 ions for every A-2 ion, Equation S-1, page 48). This molecular ratio was estimated using the standard Gibbs free energy equation^[218].

Thus, considering gas phase protonation only, there would be a vast excess of A-1 to all other cations. In particular, if gas phase protonation only was occurring, the relatively high energy difference of 34.6 kcal mol⁻¹ (Table 2.1) between A-1 and A-6 means that protonation to form A-6 in the gas phase is statistically extremely unlikely to occur. Yet, both the DFT bond length calculations and the observed fragmentation suggests that protonation of dofetilide to give A-6 occurred to a sufficient extent to give a product ion that is the base peak in the spectrum. A more plausible explanation for the formation of A-6 is via proton migration (or tunnelling) from the most basic site N9.

Equation S-1

Calculation of the excess of A-1 over A-2 due to energy difference of 17.7 kcal mol⁻¹:

$$\Delta G = -RT \ln K$$

where ΔG is the change in free energy, R is the universal gas constant (0.00199 kcal mol⁻¹ K), T is temperature and K is the equilibrium constant.

K is a reflection of the probability of the molecules present in any particular form, so the equation may be written for ions A-1 and A-2 as:

$$\Delta G = -RT \ln([A-2]/[A-1])$$

Therefore, for ions A-1 and A-2:

$$17.7 \text{ kcal mol}^{-1} = - (0.00199 \text{ kcal K}^{-1} \text{ mol}^{-1} \times 293\text{K}) \ln(A-2/A-1), \text{ or}$$

$$\ln([A-2]/[A-1]) = 17.7 \text{ kcal mol}^{-1} / -(0.00199 \text{ kcal K}^{-1} \text{ mol}^{-1} \times 293 \text{ K})$$

$$([A-2]/[A-1]) = e^{17.7 \text{ kcal mol}^{-1} / -(0.00199 \text{ kcal K}^{-1} \text{ mol}^{-1} \times 293\text{K})} \text{ or}$$

$$([A-2]/[A-1]) = 6.6e^{-14}, \text{ an excess of A-1 over A-2 greater than } 1.5e^{13}$$

Equation S-2

Calculation of the internal energy gain to form the excited dofetilide cation.

The transfer of energy from kinetic to internal energy (E_{int}) on collision between the analyte ion and the collision gas (in this case nitrogen) is given by the equation [219,220].

$$E_{int} = E_{coll} (M1/M1+M2)$$

$$M1 = \text{mass of collision gas} \quad M2 = \text{mass of analyte} \quad E_{coll} = \text{collision energy}$$

Therefore for dofetilide (m/z 442) in this study:

$$E_{int} = *10\text{eV} (28/442+28) = 0.5 \text{ eV} = 11 \text{ kcal mol}^{-1}$$

*Estimated after discussions with ThermoScientific.

Average number of collision within an ion trap is reported as 100 or 2.6 within a quadrupole filter [221,222].

Therefore, total energy gain for the dofetilide significantly exceeds the 34.6 kcal mol⁻¹ (Table S-1) required to form A-6.

The proton may gain the energy required for migration to occur from the ion-molecule collisions in the collision cell of the mass spectrometer. These ion-molecule reactions are only likely to occur in the collision cell region, as the rest of the mass spectrometer is at a significantly lower pressure. Collisions of dofetilide ions with the

target gas result in the transfer of energy from kinetic to internal. This internal energy excites the ion into a higher energy state, typically each collision resulting in a gain of 0.5-3 eV^[223], with 2.6 to 10 collisions being the average for an ion of m/z 400 passing through a quadrupole collision cell^[220-222,224]. This represents an increase in the internal energy of the ion in excess of the 34.6 kcal mol⁻¹ required to protonate O12, forming the ion A-6 (calculated for dofetilide using Equation S-2).

The question then arises as to why the proton migrates to O12 and not to any of the other basic centre(s)? For example, if the proton had migrated to N20, the second most thermodynamically likely site in the terminal sulphonamide group, the bond lengthening predicted (+0.335 Å) would have resulted in sulphonamide bond cleavage, which is not observed in the spectra. It is proposed that there is a kinetic reason for the migration to O12 in preference to any other basic site. The atom O12 is the nearest to the original location of the proton at N9, and is considerably nearer than N20. It is proposed, therefore, that when the proton migrates from N9 it reaches O12 first and the resulting bond elongation induces cleavage, which causes fragmentation to occur before the proton can travel further. A similar argument exists against significant proton migration to N23 to form A-3, the third most likely site of protonation, as a major ion; protons will reach O12 before those travelling in the opposite direction will arrive at N23.

The proposed routes of formation of the dofetilide product ions are shown in Figure 2.5. The DFT calculations (Table 2.2) confirmed that the bond lengthening which precedes formation of both m/z 198 and m/z 245 arises from protonation at N9, the most basic site in solution. The ion m/z 198 itself no longer contains N9 and so the proton would need to be transferred to C8 during bond cleavage. The proton may remain on C8 or possibly migrate along the molecule to the thermodynamically most likely site for this cation, N23 (A-3).

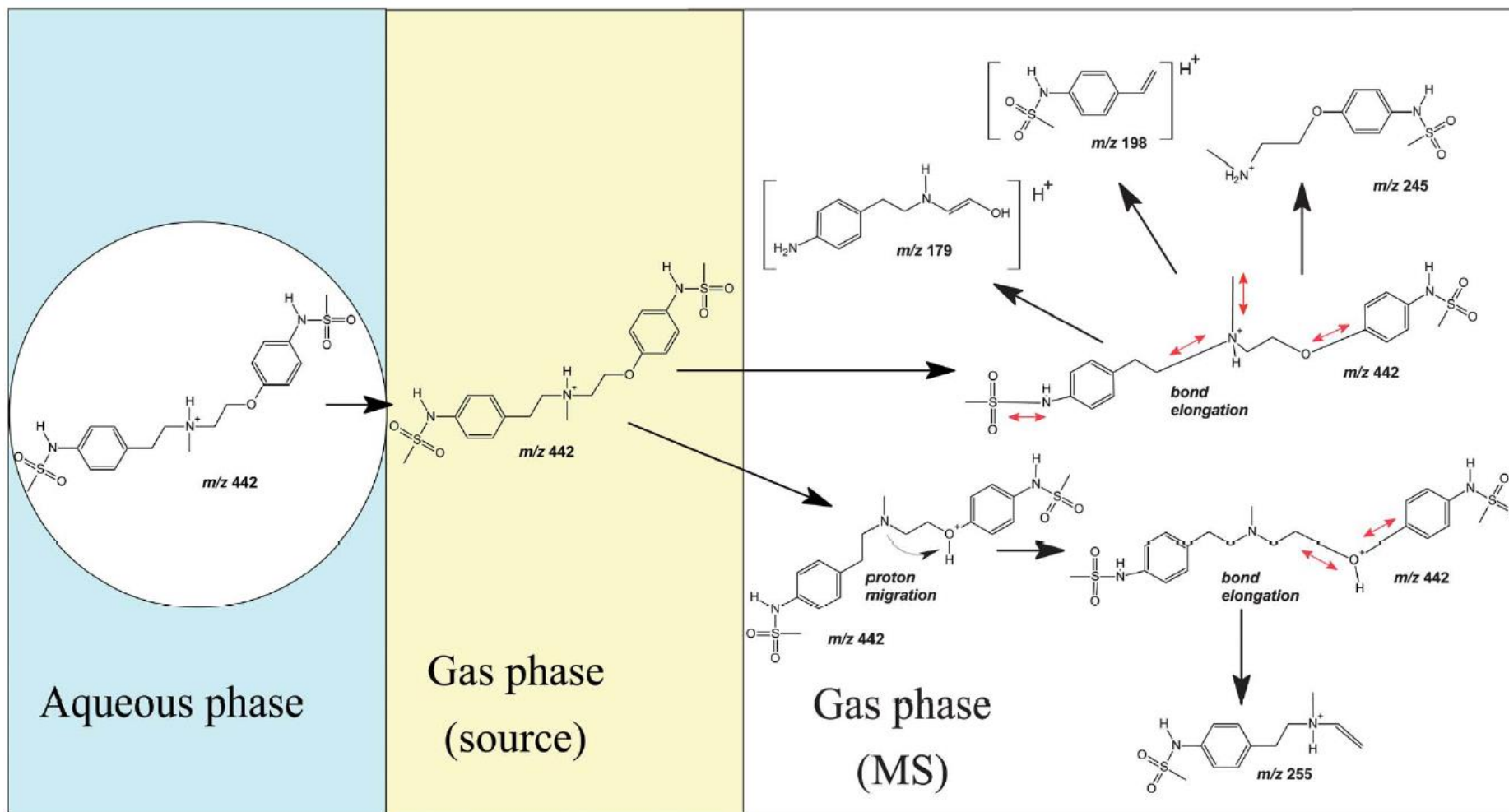


Figure 2.5. Proposed scheme for the formation of the product ions of dofetilide.

2.3.4. Stability of product ions

In dofetilide, the ion at m/z 179 resulted from the cleavage of bonds N23-S24, N9-C13 and O12. This ion was minor in the spectrum, at least in part because the cleavage of multiple bonds is energetically less favourable than the cleavage of a single bond, even though the cleavage of each of the individual bonds is thermodynamically favoured. The impetus for the cleavage of multiple bonds is usually the formation of a particularly stable product ion ^[225,226] or formation of a product ion via a low energy transition state ^[227]. Therefore it may be that it is the stability of m/z 179 which drives its formation.

The fragmentation of analogues I, II, III and IV differed from that of dofetilide itself in that the three bonds N9-C13, N23-S24 and O12-C14 were not observed to cleave to form a product ion analogous to m/z 179. DFT calculated that all these bonds were elongated by protonation at the most thermodynamically likely site (Table 2.7) and so may be expected to cleave. It may be that these bonds were not observed to cleave because the product ion formed by this multi bond cleavage would not be sufficiently energetically favourable. It has been reported that the stability of the product ion can have a greater influence than bond weakening in the fragmentation process ^[91], particularly where the product ion resulted from a rearrangement.

An additional cleavage of N9-C10 was only observed in the spectra of the analogues I and II. This bond cleavage gives rise to the ion at m/z 184, which is proposed to be an oxirane, as shown in Figure 2.6. Oxiranes are particularly stable compared to their linear counterparts ^[228]. Formation of the oxirane is analogous to the formation of the tropylium ion, in that molecules are stabilized by incorporation of the charged methyl group into a cyclized structure. This cleavage is also thermodynamically favourable in that bond N9-C10 is calculated to elongate significantly in these two analogues (Table 2.6) as a result of protonation at N9. Thus cleavage of this bond may be driven by both bond elongation and formation of a particularly energetically stable product ion.

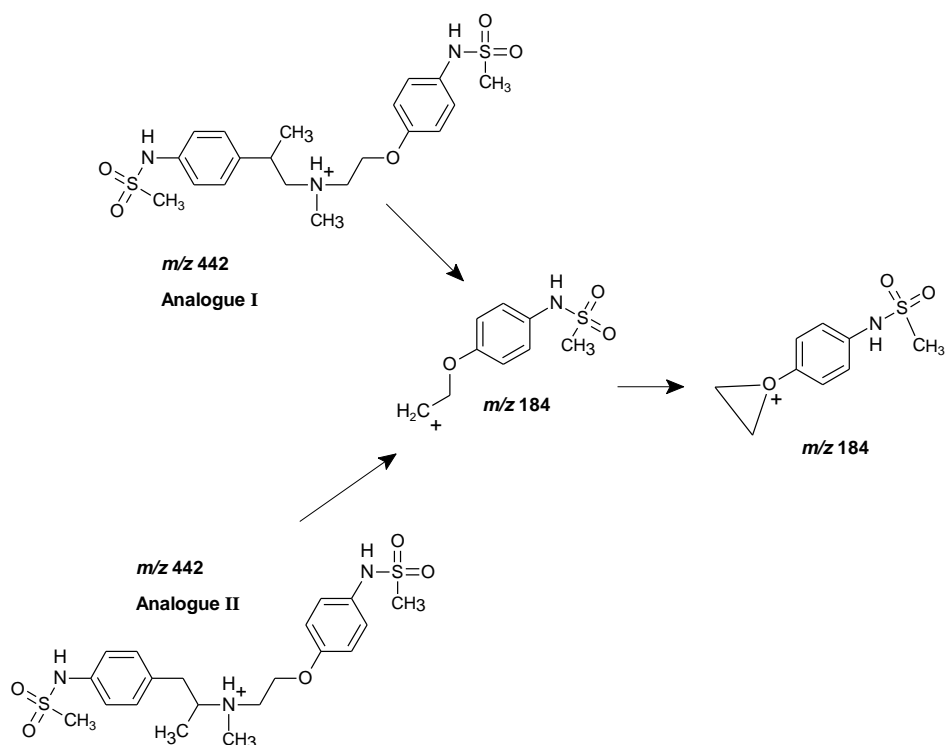


Figure 2.6 Proposed formation of the product ion m/z 184 (resulting from cleavage of N9-C10) observed in the spectra of analogues I and II.

This N9-C10 cleavage was not observed for dofetilide and analogues III and IV. In the case of dofetilide this is consistent with the DFT prediction that this bond either contracts or remains unchanged after protonation at all possible sites. However, bond N9-C10 in analogues III and IV did elongate significantly after protonation but did not appear to cleave. There are two possibilities for this observation: This may be a kinetic effect resulting from steric hindrance by the additional methyl groups or, alternatively, the presence of the methyl group on C10 or C11 which reduces the propensity to form the highly stable oxirane product ion.

There have been reports of steric hindrance of gas phase protonation during chemical ionisation. For example, steric hindrance had been seen for protonation under CI condition for low molecular weight alkyl compounds ^[229,230], and also for maleates and succinates ^[231]. Steric effects have also been proposed for ESI; the MS/MS spectrum of crizotinib following electrospray ionisation differs significantly from those of its N-alkyl analogues ^[193]. It was suggested that the difference in the spectra was due to the presence of alkyl groups on the piperidine nitrogen on the analogue

structures, which would sterically hinder the direct protonation of the piperidine nitrogen, hence shifting the ionisation site to the pyridine nitrogen. However, there is an alternative explanation for these observations, that being the possibility of proton migration to a site that initiated charge-directed cleavage, but this was not considered in that manuscript.

If ionisation occurs predominantly in the solution, as the weight of evidence suggests, followed by the proton migrating around the molecule in the gas phase, then steric hindrance of protonation during ESI is not the explanation for the additional methyl preventing the thermodynamically favoured N9-C10 cleavage. Therefore it is proposed that the presence of the methyl on C10 or C11 in analogues III and IV results in the formation of a less energetically favourable product ion than the oxirane cation observed for analogues I and II. This supported by the 3-dimensional conformations of dofetilide and its methyl analogues generated in Jaguar in that cleavage of N9-C10 in dofetilide and analogues I and II causes C10 to snap back to bond to O12 forming the oxirane. When there is a methyl on C10 or C11 spontaneous cyclizing is not observed.

In dofetilide itself, the ion at m/z 255 was postulated to be formed as a result of proton migration to O12. It is also possible that the impetus for formation of m/z 255 is derived from formation of particularly stable product ion. However, the 3D models of parent dofetilide and its product ion at m/z 255, shown in Figures 2.7 and 2.8, respectively show that m/z 255 is not a planar product (also conjugation has not been extended and rearrangement is not feasible) so this product ion is not an obviously conformationally more stable product than the starting ion. This supports the proposal that it is proton migration that initiates the cleavage.

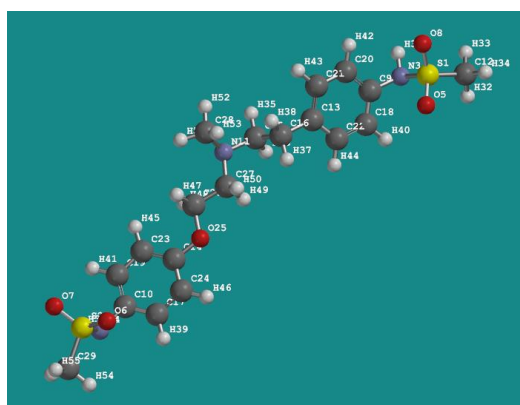


Figure 2.7 AM1 modelled configuration of dofetilide protonated at most basic centre.

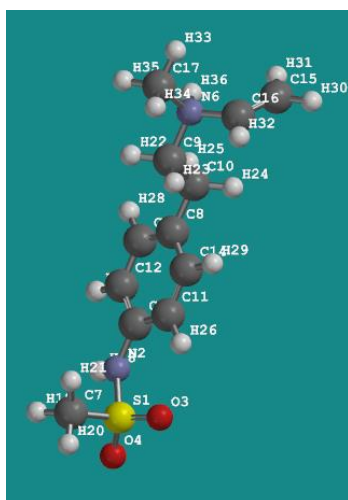


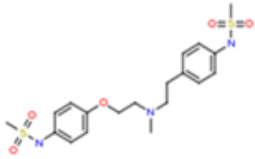
Figure 2.8 AM1 modelled configuration of dofelilide product ion at m/z 255 protonated at most basic centre.

2.3.5. Mass Fragment Prediction of Dofetilide Product Ions

Waters MassFragment is a predictive software package forming part of their MassLynx software suite. It compares an acquired spectrum with potential structures for the product ions generated based on systemic bond disconnection of the precursor ion [232]. In order to compare the DFT calculations of bond lengths with those from commercially available mass spectral interpretation packages, the fragmentation of dofelilide was predicted using Waters MassFragment (version 3; with MassLynx 4.1). The MassFragment report for the assignment of the ions in the accurate CID mass spectrum of dofelilide (Figure 2.9) predicts twenty product ions, excluding isotope peaks, for the accurate mass data (mass resolution 15,000 FWHM). On the basis of the nominal mass spectra, over one hundred ions were predicted. As only four fragment ions were actually observed, there is a highly significant degree of over prediction by the MassFragment software. This would be particularly problematic for users of low resolution mass spectrometers as there would be an excessive number of predictions to consider.

Report

Input:

	ID (job)	72
	Mass (Da)	441.1392
	Formula	C ₁₉ H ₂₇ N ₃ O ₅ S ₂
	DBE	8

Experiment:

Product ion(s) (Da)	103.0535 118.0643 119.0717 120.0799 121.0782 176.1295 179.1167 198.0570 199.0598 200.0542 245.0935 255.1143 256.1180 257.0967 442.1426 443.1450 444.1410 91.0537 92.0605 93.0638 +/- 0.1 in positive mode, structure filter off
DBE	-10 to 50
Electron count	both
Maximum H deficit	6
Fragment number of bonds	4
Scoring	aromatic: 6, multiple: 4, ring: 2, phenyl: 8, other: 1 H-deficit: 0, hetero modifier: 0.5, max score: 16
Order:	mass
Plot:	show <input checked="" type="radio"/> hide <input type="radio"/>
Files:	CSV

Figure 2.9 Screen shot of Waters MassFragment (version 3; with MassLynx 4.1) report on the accurate mass spectrum of dofetilide acquired on a Waters Q-TOF Ultima at a resolution of 15,000 FWHM.

Using the DFT calculated bond lengths, with the criterion that bond elongations equal to or greater than 0.025 Å of bonds connected to a protonated atom may lead to bond cleavage, the bond elongations reported in Table 2.2 predicted five product ions would be formed. Four of these predictions corresponded to the observed four product ions. Thus, only one fragmentation was predicted but did not occur. Therefore, in this example, applying bond elongation considerations effectively acts as a filter, eliminating the reporting of thermodynamically unlikely fragmentations. An additional advantage is that this approach depends entirely on the calculated geometry of the molecules and so is independent of the resolution of the mass spectrometer by which the spectra were obtained. Therefore, this approach is particularly effective in reducing the number of potential product ions incorrectly predicted for low resolution spectra.

2.4. Conclusions

Modelling bond length changes was successful in determining which bonds cleaved to form the product ions of dofetilide and its four methylated analogues. It was particularly reassuring as to the effectiveness of this approach that false negatives were not produced; all the bonds which cleaved were predicted to elongate significantly as a result of protonation; none of the cleavages observed were of bonds which were calculated to contract or remain the same. Our results also show that not all bonds which elongate cleave; conformational and ion stability considerations are additional contributors to MS/MS fragmentation behaviour. The effect of introducing additional methyl groups into the dofetilide template suggests that steric and kinetic factors may also influence fragmentation.

This case study illustrated the potential for quantum chemistry calculations to be used predictively as an aid for the interpretation of mass spectra, as they highlight the centres around which charge-directed cleavage is likely to occur, i.e. the sites at which protonation has the greatest effect on bond lengthening. This approach is computationally economical in that only bond length changes need to be calculated; calculation of the gas phase basicities of dofetilide and its analogues was not required to successfully identify sites of bond cleavage as proton migration from the initial site(s) of ionisation to the site where dissociation occurs is proposed.

In addition, this approach limits the number of predicted possible product ions to only those which are thermodynamically likely in terms of bond elongation. In particular, quantum chemistry methods, such as DFT, may be applied to improve software packages designed to assist with the assignment of product ions, by both contributing to a greater understanding of the 'rules' of CID fragmentation and also offering the possibility of incorporating quantum descriptors, such as bond lengths, into interpretational software.

It may also offer the potential for prediction of product ions which can be used to detect related structures, such as drug metabolites, in complex mixtures.

Chapter 3: PREDICTING COLLISION INDUCED DISSOCIATION (CID) SPECTRA: SEMI-EMPIRICAL CALCULATIONS AS A RAPID AND EFFECTIVE TOOL IN SOFTWARE-AIDED MASS SPECTRAL INTERPRETATION

Published: *Rapid Communications in Mass Spectrometry* **28**, 1127–1143 (2014).
Wright, P.A., Alex, A. and Pullen, F.S.

3.1. INTRODUCTION

Mass spectrometry is not an established rule-based discipline in that the mass spectrometric behaviour of compounds, both in terms of quantitative sensitivity and the qualitative fragmentation, is difficult to predict even by practitioners with many years' experience. This makes interpretation of CID product ion spectra time-consuming, potentially rate-limiting, and sometimes subjective. In addition, novice users can find mass spectral interpretation challenging.

There are commercial software packages available to aid spectral interpretation but in general these have the limitation that they over-predict the number of product ions formed. For example, four major (>5%) product ions were observed in the product ion spectrum of dofetilide, but the Waters Mass Fragment software predicted a possible twenty product ions on the basis of the accurate mass data and over a hundred product ions for the nominal mass values.^[233] The reason for this over-prediction is that many of the software packages do not take into account the specific chemical structure of a given compound, so that they may predict product ion structures which are not chemically feasible. This is because the predictions are made on the basis of applying rules which are often based on electron ionisation fragmentation rather than CID and extrapolated from databases, or by the use of a 'systemic bond dissociation approach in which all possible bonds in the molecule are cleaved and the mass of the remaining substructure calculated. Although the predictions made by these commercial software packages are generally useful, the method described in this thesis for predicting fragmentation by calculation of bond elongation is able to narrow down the number of possible choices significantly and therefore enables much faster and more efficient interpretation of spectra.

Examples of commercially available packages include Mass Frontier (Thermo Scientific)^[70] which combines comparison with their database (containing over 30,000

fragmentation schemes from the literature and in-house data) with applying general fragmentation/rearrangement rules. Another package, MS Fragmenter (ACDLabs),^[71] predicts mass spectral fragments from the imported parent structure by applying rules of fragmentation. Fragment iDentificator (FiD)^[73] takes an alternative approach of generating all the possible fragments that correspond to the accurate mass of the observed ions and then ranking in order of how likely these fragments are to be cleaved. EPIC (Elucidation of Product Ion Connectivity)^[74] and MetFrag^[75] are both 'systemic bond dissociation' methods.

All these programmes do assist with mass spectral interpretation via different approaches, but common to them all is the limitation that predictions are made on the basis of assumptions or extrapolations which may not be valid. This results in the prediction of a large number of product ions which are not, in practice, observed in the mass spectra. For software to be truly effective it needs to make predictions based mainly on the properties of the molecule itself without recourse to assumptions. Quantum chemistry offers the potential to improve the accuracy of *in silico* product ion predictions as it describes the behaviour of matter at the molecular, atomic and sub-atomic level. Quantum based computational chemistry has been applied in mass spectrometry^[183] for many years, often used to calculate the energies of the precursor ions, the product ions and any intermediates as a way of determining both the most likely routes of product ion formation and which product ions are the most energetically favourable. The approach described herein differs from the majority of these previous studies reported in the literature regarding application of computational chemistry to mass spectrometry, in that it focuses on bond length changes as a result of ionisation to identify the bonds which are likely to cleave.

One of the most widely applied quantum chemistry approaches is Density Functional Theory (DFT)^[82] which is used to calculate the electronic structure of a given molecule. DFT models molecules in the gas phase and so is very well suited for determining the behaviour of ions within a mass spectrometer. Molecular geometries predicted by DFT are known to be accurate as they agree closely with experimental X-ray diffraction data.^[138] DFT has been used to great effect to rationalise fragmentation based on the thermodynamic effects that protonation has on the molecule,^[91,92] by calculating the thermodynamically most stable protonated species based on the global minimum energy of the three dimensional structure. This

information has been useful in predicting the potential cleavage sites of those different molecular ions. DFT is not routinely used to explain CID product ion mass spectra; however, because the amount of computational resource both in terms of time and computer specification, as well as computational chemistry expertise required, limits its accessibility to the mass spectrometrist. The time taken to calculate the geometry of a single, drug-like molecule can take anything from minutes to days depending on the size and molecular flexibility of the molecule.

Calculating low-energy geometries and electronic structures with semi-empirical methods is considerably faster than with DFT, and can be undertaken on any desktop PC of reasonable specification using widely available commercial and academic software. Semi-empirical methods were championed by Dewar ^[118,119] in the 1950s to 1970s, when computers were still severely limited by processor speed and memory creating a real need for an approach which would allow computational chemistry calculations to be undertaken in realistic time scales.

Semi-empirical methods are used to calculate heats of formation, geometry, dipole moment and ionisation energy as well as chemical reactivity.^[120] They give similar results to DFT for calculating bond dissociation energies, but they tend to overestimate ionisation energies.^[121,122] Semi empirical methods are particularly useful for large molecules where DFT calculations take too long. However, the increased speed of calculation afforded with semi-empirical methods is offset by a lower accuracy compared to DFT.

One of the most popular semi-empirical methods is Austin Model 1, AM1.^[123] AM1 performs well in calculating bond lengths, being in good agreement with experimental data (approximately 5% error) ^[234]. However, relative energies of molecules are calculated more accurately by DFT^[125]. AM1 tends to overestimate basicity, having been shown to be somewhat less reliable for calculating proton affinities.^[20,21] DFT also generates more accurate heats of formation than AM1.^[133]

The work presented in chapter 2 and also presented in previous publications has used DFT to study the pharmaceutical compounds fluconazole, maraviroc and dofetilide, to rationalise CID product ion spectra in terms of bond weakening resulting from conformational changes. ^[91,92,233] In general, with a few exceptions,^[179] lengthening a bond will cause it to weaken and render it more susceptible to cleavage.^[180,181] Protonation-induced elongation of bonds did correlate with the bonds

which were actually found to cleave as observed from the product ions in the MS/MS process.

In order to further test the hypothesis that bond cleavage during CID may be predicted by quantum based computational chemistry, on the basis that bonds which are calculated to elongate significantly as a result of conformational changes induced by protonation cleave preferentially during the CID process, fifteen pharmaceutical-type molecules in the mass range 101 to 608 Da were modelled. Major bond elongations were highlighted to flag potential bond cleavages. The CID mass spectra were then subsequently obtained experimentally, and interpreted to establish if the predicted bond cleavages had been observed in the CID MS/MS experiment. This represented a 'blind trial' of using bond elongation as a descriptor to predict bond cleavage.

Bond length calculations were undertaken both using DFT (basis set 6.31G**) and AM1. The parameterised approach of AM1 is generally accepted to give good approximations for molecular geometry,^[125] so has the potential to give sufficiently accurate estimates of bond elongation for this application, especially as the absolute values are not required. AM1 calculations run in seconds rather than the hours required for DFT; for example geometry optimisation of indole takes 5 seconds by AM1 but more than 1.5 hours by DFT (B3LYP 6.31G).^[236] If AM1 were found to give adequate estimates of bond lengths, this would extend the potential for this application of quantum computational chemistry to mass spectral interpretation as both the speed and lack of requirement for specialist computational resource, offering the possibility of routine desktop use by non-expert users.

3.2. EXPERIMENTAL

3.2.1. Chemicals

HPLC grade methanol and acetonitrile were supplied by Rathburn (Walkerburn, UK). HPLC grade water was obtained from VWR International Ltd (West Chester, PA, USA). Formic acid (99%+) was supplied by Biosolve (Valkenswaard, The Netherlands).

CEN025-014 was donated by Cyclofluidic (Welwyn Garden City, Hertfordshire, UK). Sildenafil, doxazosin, ziprasidone and dofetilide were donated by Pfizer Ltd.

(Sandwich, Kent, UK). All other compounds were obtained from Sigma-Aldrich (Poole, Dorset, UK). The structures of all fifteen authentic standard compounds are shown in Figure 3.1.

All compounds were prepared at 1mg/mL in acetonitrile/water (between 10 and 100% acetonitrile depending on the compound solubility), then diluted with 50/50 (v/v) methanol/water 0.1% formic acid to give a final concentration of 20 μ g/mL.

3.2.2. LC/MS

Data was acquired on a Waters Synapt G1 Q-TOF (quadrupole-time-of-flight) mass spectrometer (Waters Corporation, Manchester, UK) in ESI positive ion and V mode (resolution 15,000 FWHM), calibrated with sodium formate. Leucine enkephalin (MH⁺ 556.277) was infused at 5 μ l/minute as the reference lock mass. Sample (10 μ L; 20 μ g/mL) was introduced via flow injection (0.5 mL/min 50/50 methanol/water 1% formic acid; no HPLC column). Methanol was chosen as the modifier as it has a lower proton affinity than the other common modifier, acetonitrile, potentially enhancing protonation of the analyte.

The following instrumental conditions were applied: capillary voltage 5 kV; corona discharge 5 kV; extraction cone voltage 5 V; sampling cone 35 V; transfer collision energy 5 eV; cone gas 150 L/h; desolvation gas 1800 L/h; source temperature 100°C; desolvation temperature 500°C; trap collision energy 25 to 35 eV (set on a compound by compound basis to obtain product ions spread across the mass range). The collision gas was argon.

The data acquisition settings are as follows: scan range *m/z* 50 to 700; scan rate 1s, data centroid.

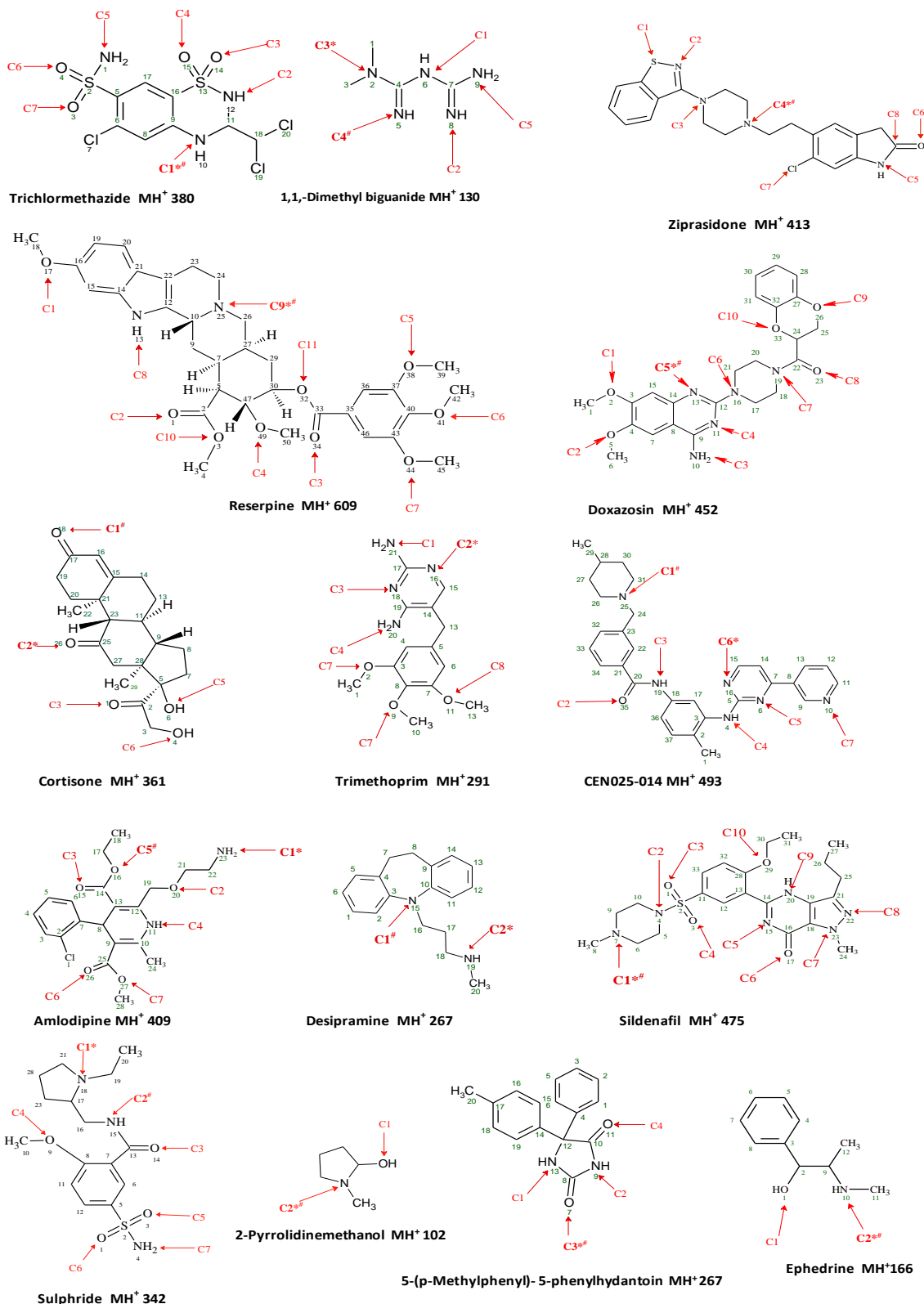


Figure 3.1 The structures of the fifteen compounds analysed in this study. The structures are annotated to flag the most basic centre(s) in the gas* and liquid# phases. The potential sites of protonation modelled are labelled as cations C1-C10.

3.2.3. Computational modelling

All quantum mechanical calculations were undertaken using Spartan'10 (Wavefunction, Inc., California, USA). Structures were drawn in ACD Labs Chems sketch (freeware), saved as skc files and then opened in Spartan. The starting geometries were obtained using molecular mechanics MMFF minimum energy geometry optimisation.

All compounds were geometry optimised after protonation at all heteroatoms using both DFT 6.31G** and AM1 with the following preferences: maximum ligand distance 2.00Å; polar area range 1000 kJ mol⁻¹; accessible area radius 1.000; 'converge' was selected.

All calculations were undertaken with the explicit hydrogens on the molecule. All calculations were undertaken locally on a desktop computer of specification Intel® i7-3370k CPU @ 3.50Hz, 16GB RAM, 64bit.

Certain structures were shown to form internal hydrogen bonds when modelled using an initial maximum ligand distance of 3.60Å, the default setting. Internal hydrogen bonding appeared to distort the bond lengths locally and lead to erroneous bond calculations. Therefore, hydrogen bonding was eliminated from the model by reducing the maximum ligand distance to 2.00Å for all calculations.

3.2.4. Assignment of product ions

Product ions of greater than approximately 8% of the most abundant product ion were structurally assigned. All percentages in the assignment Tables are relative to the most abundant product ion (this may not be the base peak where there is a considerable amount of unfragmented precursor ion).

Previous investigations into the fragmentation of dofetilide and four of its analogues^[233] indicated that only bonds which elongated significantly as a result of protonation on a heteroatom at the site of cleavage were observed to cleave. Therefore, only bond elongations of >0.40 Å which result from protonation on one of the atoms to which the bond was connected, would be considered as predictive of bond cleavage in this study.

3.3. RESULTS AND DISCUSSION

3.3.1. Comparison of AM1 and DFT for calculating bond length changes

Changes in bond length of the fifteen compounds (Figure 3.1) resulting from protonation on all heteroatoms were calculated individually using both AM1 and DFT (6-31G** basis set). This represents the calculation of 4147 bond length changes by each computational method. Using all these data points (bond elongation, contraction and unchanged) there was a correlation of 0.87 ($R^2 = 0.76$) observed between these two methods (using the 'Correl' function in Microsoft Excel 2013). Therefore, there is a statistically significant correlation between the two calculation methods. This correlation is even greater if only the significant bond length increases ($>0.040\text{\AA}$; $n=123$) were compared. The correlation then improved to 0.96 ($R^2 = 0.88$), as shown in Figure 3.2. Most importantly, the predictions made as to which bonds are likely to break would be the same based on data generated by either method for all fifteen compounds. Considering one of the compounds as an example, that being 1-methyl-2-pyrrolidinol (Table 3.1), the same bonds were calculated to elongate by $> 0.040\text{\AA}$ by both computational methods and these were also the bonds which were observed to cleave experimentally during CID (spectrum shown in Figure 3.3 and product ion assignments in Table 3.2). It is notable that considering the data in Table 3.2 the product ions were formed from two different precursor ions, cations 1 and 2, and were not derived from a single molecular species.

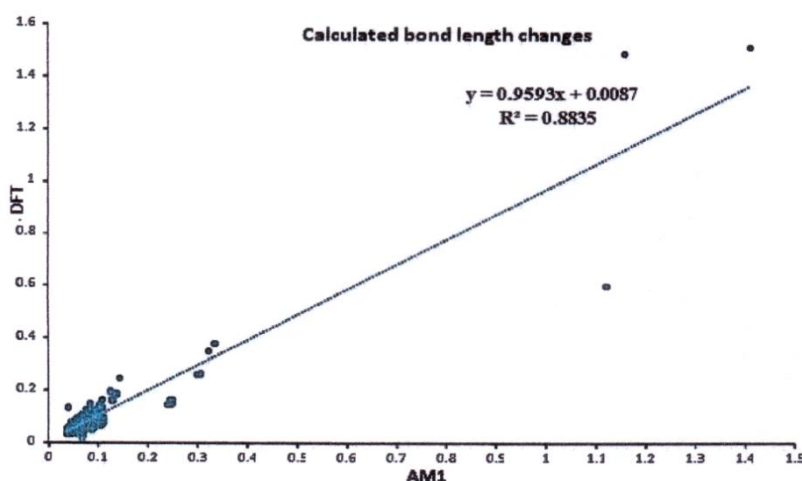
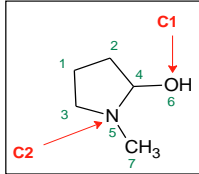


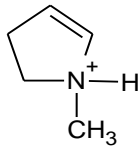
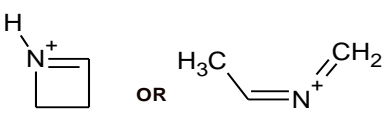
Figure 3.2 Comparison of bond elongations ($>0.039\text{\AA}$; $n=123$) calculated by both AM1 and DFT using Spartan'10.

Table 3.1. Comparison of bond length changes resulting from protonation of 1-methyl-2-pyrrolidinol at the sites specified in Figure 3.3, calculated using both DFT and AM1 (Spartan'10). Bond elongation calculated to be greater than 0.040 Å as a result of protonation on one of the bonding atoms are highlighted in the Table.



Bond	Bond length change (Å)				Bond observed to cleave in MS/MS spectrum	Cleavage predicted on basis of bond lengthening ?
	AM1		DFT 6.31G**			
	Cation C1 (O1)	Cation C2 (N5)	Cation C1 (O1)	Cation C2 (N5)		
C1,C2	+0.013	-0.002	-0.003	-0.014	No	No
C1,C3	+0.007	-0.007	+0.004	-0.015	No	No
N5,C3	+0.02	+0.039	+0.027	+0.049	Yes	Yes
N5,C7	+0.002	+0.039	+0.016	+0.044	Yes	Yes
C4,N5	-0.157	+0.083	-0.162	+0.15	Yes	Yes
C4,O6	+1.413	-0.031	+1.514	-0.066	Yes	Yes
C2,C4	-0.045	-0.011	-0.051	+0.002	No	No

Table 3.2 The proposed product ion assignments for the ions in the CID spectrum of protonated 1-methyl-2-pyrrolidinol.

Relative intensity (%)	Experimental <i>m/z</i>	Proposed ion formula and calculated accurate mass	Error (ppm)	Proposed structure(s) of ion	Bond(s) cleaved
100	84.0817	C ₅ H ₁₀ N 84.0813	4.8		C4,O6
20	56.0506	C ₃ H ₆ N 56.0500	10.0		N5, C7 and/or N5,C3 and/or N5,C4 and/or C2,C4 and/or C1,C2 and/or C1,C3

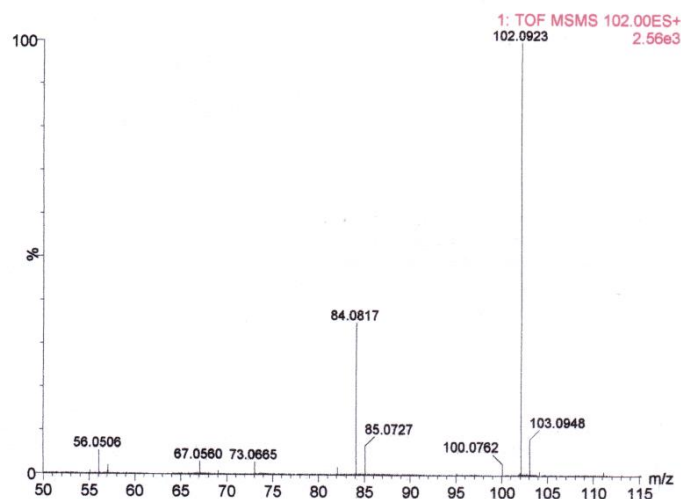


Figure 3.3 CID product ion spectrum of protonated 1-methyl-2-pyrrolidinol ($[MH]^+$ 102).

AM1 is far less demanding than DFT, both in terms of speed of calculation and computational resource required. AM1 calculations typically took less than 30 seconds, whereas the DFT calculations took between 15 minutes and 9 hours. This means these calculations may be undertaken routinely by the mass spectrometrists as an aid to mass spectral interpretation without recourse to specialist computational resource. The speed of calculations also offers the potential for bond length calculations to be incorporated into commercial mass spectral interpretation software packages to improve the accuracy of the predictions.

Therefore, on the basis of the calculated bond lengths for these fifteen compounds, AM1 has been shown to be fit-for-purpose and only AM1 calculated bond length changes will be reported and discussed further in this chapter of the thesis.

3.3.2. Comparison of AM1 and DFT for calculating relative gas phase basicities

The relative gas phase basicities were determined by calculating the global energy minimum for each protonated form for all the molecules considered in this chapter, with the ion of the lowest energy being the most basic. The energies did not always give the same order for gas phase basicities when calculated by AM1 and DFT. An example is shown for ziprasidone in Table 3.3. The difference in basicity order may result from the higher degree of error associated with the energies determined by AM1; AM1 tends to only be accurate to 3-4 kcalmol⁻¹ [133]. Therefore, for ions with energy

minima which differ by smaller values, the order calculated by AM1 is less reliable than that calculated by DFT. Therefore, in any further discussions in this chapter, only the DFT calculated relative energies (not bond lengths) will be referred to.

In this study, the relative gas phase basicities were calculated to elucidate the mechanism of bond cleavage in terms of the possibility of proton migration occurring subsequent to ionisation. Calculation of gas phase basicities was not required for the prediction of bond cleavages as proton migration to the 'dissociative site'^[192] appears to initiate cleavage^[233] and so knowledge of the initial site of ionisation was not required. Bond length elongations were the only parameter required to predict bond cleavages for these fifteen compounds and therefore in practice, only AM1 calculations are required for predicting and rationalising bond cleavage.

3.3.3. Prediction of bond cleavage on basis of calculated bond elongations

For the fifteen compounds considered in this study 98 distinct bonds were observed to cleave to form the product ions observed in the CID product ion spectra. Of these, 98 experimentally observed bond cleavages, 82 bond cleavages were correctly predicted on the basis of bond elongation calculations alone. This represents an overall success rate of 84%. Only the carbon-carbon bond cleavages were not predicted (n=16). As mentioned above, this may be due to the thermodynamic factors and product stability, which is currently not considered in this approach. If polarised bonds only are considered, the success rate for predicting bond cleavage at a heteroatom is 100% (n=82). Table 3.4 summarises the results of this 'blind trial'.

The results obtained for ziprasidone (spectrum shown in Figure 3.4; bond length changes in Table 3.5 and product ion assignments in Table 3.6) are typical for all fifteen compounds. Of the 10 bonds which were observed to break, 9 were correctly predicted. The bond which was not predicted to break was a carbon-carbon bond (C2-C28). Initial modelling was performed on cations C1 to C7. The carbocation C8 (Figure 3.5) was modelled in retrospect in order to try to rationalise cleavage of C2-C28. Addition of a proton across double bond in the carbonyl group to centre the charge on C2 did result in a significant elongation of the C2-C28 bond. This was also the case for the other compounds which underwent carbon-carbon bond cleavage (cortisone, 5-(*p*-methyl)-phenylhydantoin, reserpine, trichlormethazine and ziprasidone);

modelling the appropriate carbocations rather than locating the proton on a heteroatoms did not predict the bond cleavage.

Table 3.3 The relative energies of the different protonated forms of ziprasidone calculated by using both AM1 and DFT. The energy values are normalised to the most stable cation.

<i>E (kcal mol⁻¹)</i>		<i>Energy Difference between most stable cation and others (kcal mol⁻¹)</i>	<i>E (Kcal/mol⁻¹)</i>		<i>Energy Difference between most stable cation and others (kcal mol⁻¹)</i>
AM1			DFT 6.31G**		
60.7	Neutral	n/a	-1233397	Neutral	n/a
204.3	Cation 3	0	-1233643	Cation 4	0
204.3	Cation 4	0	-1233639	Cation 2	4
205.4	Cation 2	1	-1233634	Cation 3	9
223.5	Cation 1	19	-1233605	Cation 6	26
228.2	Cation 6	24	-1233608	Cation 8	36
228.9	Cation 8	25	-1233602	Cation 1	39
229.8	Cation 5	25	-1233602	Cation 5	41
267.2	Cation 7	63	-1233565	Cation 7	78

It may be that bond weakening (via lengthening) around heteroatoms results from an increase in polarity of the bond by the addition of proton to the most electronegative atom. This is consistent with the bond activation rule (BAR) proposed by Alcamí;^[183–185] the presence of the proton on the electronegative centre pulls the bonding electrons toward the charged centre, reducing the electron density in the bonding region, with cleavage occurring if there is sufficient difference in electronegativity between the basic centre and the atom bonded to it.

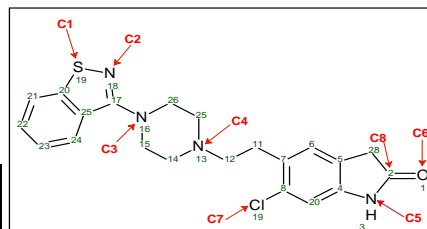
Table 3.4 Overall summary of the effectiveness of using calculated bond elongations to predict bond cleavages during CID fragmentation.

Compound	Number of bond cleavages		Percentage accuracy of prediction	Type of bond cleavage not correctly predicted
	Correctly predicted	Observed to cleave but <u>not</u> predicted by bond elongation		
1-Methyl-2-pyrrolidinol	4	0	100%	n/a
Sulphide	3	0	100%	n/a
Ziprasidone	10	1	91%	C-C bond
Ephredine	3	0	100%	n/a
Doxazosin	9	0	100%	n/a
CEN024-014	3	0	100%	n/a
Trichlormethazide	10	1	90%	C-C bond
Reserpine	10	4	71%	C-C bond
5-(p-Methylphenyl)-5-phenylhydantoin	2	4	33%	C-C bond
1,1-Dimethyl biguanide	5	0	100%	n/a
Amlodipine	8	0	100%	n/a
Cortisone	2	6	25%	C-C bond
Desipramine	3	0	100%	n/a
Sildenafil	4	0	100%	n/a
Trimethaprim	6	0	100%	n/a
Total	82	16	84%	n/a

The product ions of ziprasidone were formed from seven different precursor ions, cations 1 to 7, and were not derived from a single molecular species. This was observed to be true of all fifteen compounds in that their product ions were all derived from several protonated precursors, and further exemplified by the data for 1-methyl-2-pyrrolidinol shown in Table 3.2. This is consistent with previous studies which highlighted that the molecular ion appears to be a mixture of protonated species which are protonated on a number of different basic sites across the molecule.^[91,92,233] Other research groups have also reported that molecular ions appear to be a mixture of molecular ions protonated at different positions. Two isobaric ions observed in an MS/MS spectrum could only be assigned if they are derived from precursor ions protonated at different sites, giving rise to different product ions.^[188] Kaufmann reported that a mixture of singly charged species of difloxacin was formed in the source.^[194] Komaromi et al. observed that N-acetyl-O-methoxyproline exhibits two distinct fragmentation pathways indicative of the coexistence of several protonated forms.^[189]

Komaromi used appropriate DFT calculations to support these observations.

Table 3.5 Changes in bond length in ziprasidone resulting from protonation of ziprasidone at the sites specified in Fig. 1, calculated using AM1 (Spartan'10). Bond elongations calculated to be greater than 0.040 Å as a result of protonation on one of the bonding atoms are highlighted in the Table.



Bond length changes (Å)									Bond observed to cleave in MS/MS spectrum	Cleavage predicted on basis of bond lengthening?
Bond	Cation C1 (S19)	Cation C2 (N18)	Cation C3 (N16)	Cation C4 (N13)	Cation C5 (N3)	Cation C6 (O1)	Cation C7 (C19)	Cation C8 (C2)		
O1,C2	-0.002	-0.002	-0.002	-0.004	-0.023	+0.105	-0.070	+0.097	No	Yes
C2,N3	+0.004	+0.004	+0.005	+0.009	+0.143	-0.064	+0.015	-0.06	Yes	Yes
N3,C4	-0.004	-0.004	-0.005	-0.010	+0.060	+0.03	-0.014	+0.032	No	Yes
C2,C28	0.000	0.000	-0.099	-0.041	-0.026	-0.009	0.000	-0.005	Yes	No
C28,C5	0.000	0.000	0.000	0.000	-0.005	+0.004	+0.002	+0.003	No	No
C8,C19	+0.002	0.000	+0.003	+0.003	-0.013	-0.013	+0.070	-0.013	Yes	Yes
C11,C12	0.000	+0.001	0.000	-0.002	0.000	+0.005	-0.002	0.000	n/a	n/a
C12,N13	+0.002	0.000	0.000	+0.040	+0.005	-0.006	+0.005	0.005	Yes	Yes
N13,C14	-0.002	-0.005	+0.002	+0.040	-0.005	-0.001	-0.003	-0.005	Yes	Yes
C14,C15	-0.001	+0.002	-0.002	+0.001	+0.002	+0.001	0.000	+0.002	n/a	n/a
C15,N16	+0.005	+0.002	+0.048	-0.003	+0.001	+0.004	+0.004	-0.004	Yes	Yes
N16,C26	-0.003	+0.003	+0.045	-0.006	+0.004	+0.003	0.000	+0.004	Yes	Yes
C25,N13	-0.005	-0.004	-0.002	+0.042	+0.002	0.000	-0.005	-0.024	Yes	Yes
N16,C17	-0.073	-0.059	-0.004	+0.011	+0.001	0.000	+0.004	0.000	n/a	n/a
C17,N18	+0.025	+0.048	+0.005	+0.003	0.000	+0.001	+0.001	+0.002	Yes	Yes
N18,S19	-0.019	+0.017	+0.037	-0.015	-0.005	-0.005	+0.002	-0.005	n/a	n/a
S19,C20	+0.046	-0.010	-0.032	0.000	-0.001	-0.001	+0.003	-0.003	Yes	Yes
C17,C25	+0.035	-0.009	-0.019	-0.013	-0.006	-0.003	-0.001	-0.001	n/a	n/a

Table 3.6 The proposed product ion assignments for the ions in the CID spectrum of protonated ziprasidone.

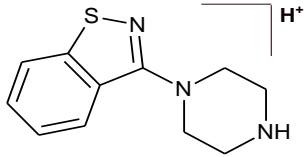
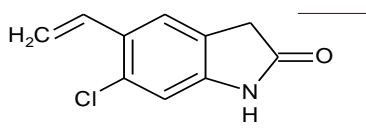
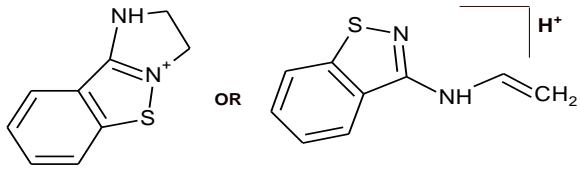
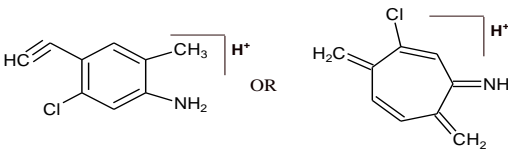
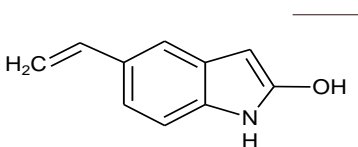
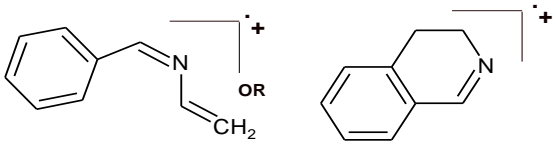
Relative intensity (%)	Experimental <i>m/z</i>	Proposed ion formula and calculated accurate mass	Error (ppm)	Proposed structure(s) of ion	Bond(s) cleaved
5%	220.0924	C ₁₁ H ₁₄ N ₃ S 220.0908	7		N13,C12
100%	194.0331	C ₁₀ H ₉ ClNO 194.0373	22		N13,C12
23%	177.0487	C ₉ H ₉ N ₂ S 177.0486	<1		N13,C25 N13,C14 N16,C15 N16,C26
20%	166.0427	C ₉ H ₉ ClN 166.0424	2		N13,C12 C2,C28 C2,N3
25%	159.0678	C ₁₀ H ₉ NO 159.0684	4		N13,C12 C8,C19
8%	131.0738	C ₉ H ₉ N 131.0735	2		S19,C20 N18,C17 N16,C25 N16,C13 N13,C14 N13,C25

Table 3.7 The proposed assignments of product ions resulting from carbon-carbon bond cleavage for protonated trichlormethazide, reserpine, 5-(*p*-methyl)-phenylhydantoin and cortisone.

Relative intensity	Experimental <i>m/z</i>	Proposed ion formula and calculated accurate mass	Error (ppm)	Proposed structure(s) of ion	Bond(s) cleaved	
40%	448.1190	C ₂₃ H ₃₀ NO ₈ 448.1971	4		C10,C12 C24,C23	 Reserpine
10%	336.1573	C ₁₈ H ₂₄ O ₆ 336.1600	8		C47,C5 C5,C7 C26,N25 C9,C10	
20%	236.1268	C ₁₃ H ₁₈ NO ₃ 236.1287	8		C22,C21 N13,C14 O32,C33	
50%	174.0933	C ₁₁ H ₁₁ NO 174.0919	8		C10,C12 C24,C23	
8%	239.1200	C ₁₅ H ₁₅ N ₂ O 239.1184	7		N13,C8 C8,N9	 5-(<i>p</i>-methyl)-phenylhydantoin
100%	196.1108	C ₁₄ H ₁₄ N 196.1126	10		C12,C10 N13,C8	
8%	104.0505	C ₇ H ₆ N 104.0500	5		C12,C14 C12,C10 N13,C8	
10%	183.9639	C ₄ H ₆ Cl ₂ N ₂ S 183.9629	5		S13,O15 S13,O14 C16,C17 C9,C8	 Trichlormethazide
15%	258.1617	C ₁₇ H ₂₂ O ₂ 258.1620	1		C7,C5 C28,C5	 Cortisone
10%	241.1597	C ₁₇ H ₂₁ O 241.1592	2		C7,C8 C28,C5 C2,O1	
100%	163.1119	C ₁₁ H ₁₅ O 163.1123	2		C23,C25 C9,C8 C5,C28	
30%	145.1022	C ₁₁ H ₁₃ 145.1017	3		C23,C25 C9,C11 C17,O18	
25%	121.0660	C ₈ H ₉ O 121.0653	5		C23,C21 C13,C14	
30%	105.0708	C ₈ H ₉ 105.0708	4		C23,C21 C14,C13 C17,O18	
15%	93.0700	C ₇ H ₉ 93.0704	5		C23,C21 C14,C13 C17,O18	

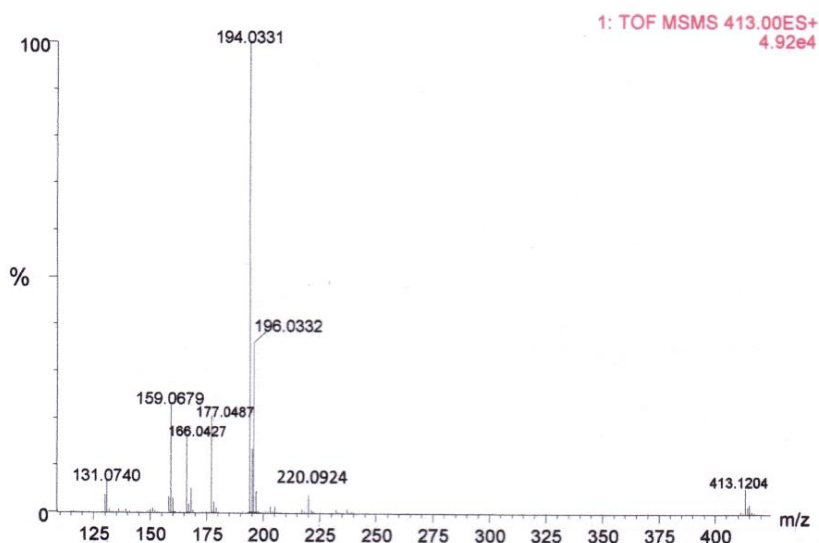


Figure 3.4 CID product ion spectrum of protonated ziprasidone ($[MH]^+$ 413).

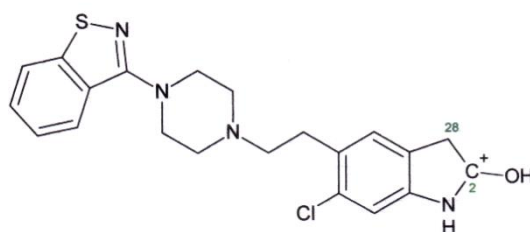


Figure 3.5 Structure of ziprasidone carbocation modelled by AM1 for which delta bond length data are reported in Table 3.5.

As the carbon-carbon bonds are not (or are less) polarised, addition of the proton may have a limited effect. In particular, there is less 'incentive' for the proton to remain associated with a particular carbon within an unpolarised bond and it may migrate along the molecular backbone, possibly via hydride shifts. Therefore, formation of a carbocation has less effect on the polarity of an individual carbon-carbon bond. There carbon-carbon bond cleavage may occur via an alternative mechanism to protonation-induced bond weakening.

A study of the fragmentation of sulphur-sulphur-bond-containing heterocycles suggests that cleavage of sulphur-sulphur bonds was driven by the stability of the product ion formed.^[186] Carbon-carbon bond cleavage may be analogous to this, especially as all the product ions formed via carbon-carbon bond cleavage in this

investigation (i.e. for cortisone, 5-(*p*-methyl)-phenylhydantoin and ziprasidone) showed increased conjugation and/or increase in planar geometry relative to the precursor ions. These proposed product ions are shown in Table 3.6 for ziprasidone and Table 3.7 for the other compounds.

This bond elongation approach over-predicted bond cleavage by 33% (32 bonds were predicted to break but were not observed to do so). This is a significantly improved over-prediction rate compared with many commercial packages. In one example, Waters Mass Fragment was observed to over predict by 400% based on accurate mass data and over 2000% for nominal mass data^[233]. Basing fragmentation predictions on bond lengthening has the advantage that it is entirely *in silico*, based on the inherent properties of the molecule itself and will give the same predictions for nominal mass data as for accurate mass data. From the summary shown in Table 3.8 it appears that there were certain classes of bond which were prone to over-prediction: Over half (56%; n=18) of the bonds incorrectly predicted to cleave were to an atom on which one or more of the other bonds was observed to cleave. The bonds which did cleave were elongated to a significantly greater extent (30-600%) than the bonds to the same atom which did not cleave in eight out of the eighteen cases (i.e. 25% of the total over-predicted cleavages). This suggests that cleavage of multiple bonds to the same atom was not favoured. Also, there was a tendency for the most extended bond to cleave in preference, but there were sufficient exceptions that this may not be considered as a 'rule'.

Protonation of nitrogens (n=6; or 19% of the incorrectly predicted bond cleavages) within a conjugated system was predicted to initiate cleavage, but did not do so. This may be due to stabilisation by delocalisation of the charge across the conjugated system, resulting in the charge not being associated with a single centre. Because the charge is delocalised, the proton will have less effect on the polarity, and hence the strength, of any single bond.

Although some sulphonamide cleavage was observed, there was a tendency to over predict the cleavage of all the bonds within sulphonamide groups (n=4 or 13%). This may be because sulphonamide bonds are flexible^[237] and able to absorb conformational change, and are also able to delocalise the charge across the sulphonamide group such that it is not strongly associated with any single atom.

Table 3.8 Summary of over-prediction of bond cleavage on the basis of proton-induced bond elongation.

Compound	Number of bonds predicted to cleave but did not cleave (i.e. over-predicted)	Type of bond over predicted
1-Methyl-2-pyrrolidinol	0	n/a
Sulphuride	5	Centred around sulphur (n=4) ; N18-C21: other bond to N18 broke in preference (i.e. N18,C19)(n=1)
Ziprasidone	1	N3-C4: other bond to N3 broke in preference (i.e. N3-C2 elongates twice as much)(n=1)
Ephredine	0	n/a
Doxazosin	3	C-O (aliphatic; n=3): other bond to same oxygen breaks in preference
CEN024-014	4	C26-N25 and C31-N25: other bond to N25 broke in preference (C24-N25)(n=2) C18-N19: other bond to N19 broke in preference (C20-N19 elongates twice as much) (n=1) C5-N4: other bond to N4 broke in preference (C3-N4 elongates half as much)(n=1)
Trichlormethazide	0	n/a
Reserpine	6	N25-C10: other bond to N25 broke in preference (C24-N25)(n=2); C-O (aliphatic; n=6), other bond to same oxygen broke in preference
5-(p-Methylphenyl)-5-phenylhydantoin	2	N13-C12 other bond to N13 broke in preference (C8-N13 elongates by 50% more) (n=1)
1,1-Dimethyl biguanide	1	C4-N5 other bond to C4 broke in preference (C4-N2 elongates by 30% more much) (n=1)
Amlodipine	0	n/a
Cortisone	0	n/a
Desipramine	2	N15 to aromatic carbons (n=2); two bonds need be broken to generate leaving group
Sildenafil	8	N4-C5 other bond to O29 broke in preference (N4-S2 elongates by 600% more) (n=1); C28-O29 other bond to O29 broke in preference (C30-O29 elongates by 100% more) (n=1); Bonds to N23 (n=3)* ; Bonds to N20 (n=2)* ; N14,C14 (n=1)* *All in extended conjugated systems
Trimethaprim	0	n/a

3.3.4. Prediction of product ion intensity

A summary of factors which may influence product ion abundance is shown in Table 3.9. There appears to be no correlation between the basicity in water of the molecule (pKa) and formation of the major product ion. For only 5 of the 15 compounds the major product ion was formed by protonation at the most basic centre in solution. For five compounds none of the product ions resulted from protonation at the most basic centre in water. For all of these five compounds, however, the most basic atom

in the gas phase was part of a conjugated system which could delocalise the charge. This both stabilises the precursor ion, hence reducing the propensity for fragmentation, and also means that the charge is not associated with any particular bond. The results of this study to date indicate that the charge has to be centred on one of the atoms in the bond to initiate cleavage.

Potentially, the number of bonds cleaved to form an ion may reflect in its relative abundance, in that more energy is required to cleave multiple bonds. However, the data in Table 3.9 shows that the intensity of the product ions does not appear to depend on the number of bonds broken during its formation. For only six out of the fifteen compounds the major product ion was formed by single bond cleavage; the other nine resulted from multiple bond cleavage.

Overall, no correlation was observed between the extent of bond lengthening and the intensity of the product ion. In a previous study (chapter 2) using bond length changes to predict the CID fragmentation of dofetilide, there was a quantitative relationship between the extent of bond elongation and product ion intensity.^[233] However, this larger study shows that although product ion intensity may be predictable on the basis of bond lengthening for certain compounds, it is not valid to apply this approach indiscriminately. Other research groups have successfully applied DFT to predict ion intensity for peptides^[238] and quinazolines^[239] on the by calculating transition energy profiles for formation of their product ions. Thus it appears that bond weakening may dictate which polarised bonds break, but it may be the relative product ion stability which determines the relative intensity of the product ions formed as a result of these bonds cleavages.

There was no obvious correlation between the pKa of the molecule and the appearance of spectra in terms of the number and abundance of the ions. For example, trichlormethazide, which has no basic centre, produces six product ions four of which are major (greater than 30%). Amlodipine contains a nitrogen with a pKa of 9.5 and gives a product ion spectrum containing eight ions, four of which are major. Similarly, there was no correlation with the gas phase basicities of the protonation sites and the type or intensity of product ion.

3.3.5. Proton migration

To rationalise the formation of certain product ions, proton migration to a thermodynamically less favourable site has been proposed. For example, the loss of ammonia from peptidic amides required protonation on the nitrogen even though the oxygen is both the most energetically favoured protonation site and the observed initial protonation site.^[62,207,208] Penicillin shows cleavage of the β -lactam bond after transfer of the proton from the carbonyl to the lactam nitrogen.^[209,240] In addition dibenzyl ethers,^[192] the pharmaceutical compound maraviroc,^[91] dialkylphosphoric acid esters^[210] and thiourea/urea compounds^[211] have all been reported to exhibit product ions in their mass spectra generated following proton migration from the most thermodynamically likely site. It has been proposed that the energy for proton migration is obtained by the transfer of kinetic to internal energy during ion molecule collisions,^[21] probably in the collision cell during CID.

The results from this larger scale study support the hypothesis that proton migration from the initial site of ionisation to the 'dissociative' site may be required to initiate fragmentation:^[1,27]

As expected, the greatest effect in terms of conformational change, and hence bond length changes, occurred in the immediate area around the protonation site. In a few cases, however, protonation did result in significant bond elongation remote from the protonation site (Table 3.9). None of these bond length changes gave rise to the product ions observed in the CID spectra, reinforcing the premise that the proton is needed to be adjacent to the site of cleavage for fragmentation to occur.

The spectra of four compounds (doxazosin, reserpine, 1,1-dimethyl biguanide and sildenafil) did not contain any product ions derived from precursors protonated at the most basic site (Table 3.10). As all spectra were obtained via ESI, the original ionisation site is likely to be the centre with the highest pKa. A review of the literature showed examples of gas phase protonation during ESI, in many cases direct gas phase ionisation is proposed because it is difficult to rationalise the product ions in the spectra of certain compounds by protonation on the most basic site in solution. For example, it has been proposed in that gas phase ionisation via ion-molecule reactions plays a major role in ESI, for example by proton transfer from gaseous ammonium ions to analytes of higher proton affinity.^[45] However, for all of these four compounds the most basic site is the same in both solution and gas phase, therefore direct gas

phase ionisation at the less basic, dissociative site is thermodynamically unlikely. Thus, the proton needs to move from the site of greatest basicity (i.e. the initial ionisation site) to the dissociative site to initiate fragmentation. This raises the possibility that some cases of charge-remote fragmentation^[46] reported in the literature may, in fact, represent proton migration followed by charge-directed fragmentation.

Table 3.9 The bonds which were calculated to elongate by > 0.040 Å after protonation at a site other than on one of the bonding atoms.

Compound	Bond	Calculated increase in bond length (?)	Site of protonation causing bond length increase	Observed to cleave during CID?
Sulphride	S2,N4	0.335	N7	No
	S2,C5	0.040	O14	No
	C13,O14	0.103	O9	No
Doxazosin	C12,N16	0.052	O23	No
Trichlormethazide	S2,C5	0.070	N10	No
	S2,C5	0.049	N12	No
	S2,C5	0.490	O14	No
	S2,C5	0.815	O15	No
Reserpine	O1,C2	0.880	O49	No
Sildenafil	S2,N4	0.043	N7	No
	C10,N4	0.057	O29	No
	S2,C11	0.092	O29	No
	S2,N4	0.078	O29	No
	N4,C5	0.067	O29	No

Table 3.10 Observations around relative abundance of product ions in the spectra of all fifteen compounds. The pKa was calculated using Marvin (ChemAxon, Budapest, Hungary) and the gas phase basicities refer to the relative stabilities (global energy minima) of the protonated species.

Compound	Major ion due to single bond cleavage?	Major ion protonated at most basic centre (aqueous)?	pKa of most basic site (aqueous)?	Most basic sites same in gas phase and solution	At least one product ion due to protonation at most basic site?	Appearance of spectra
1-Methyl-2-pyrrolidinol	Yes	No	8.6	Yes	Yes	One major ion; two ions in total
Sulphride	Yes	Yes	8.4	Yes	Yes	Two major ions; four ions in total
Ziprasidone	Yes	Yes	7.1	Yes	Yes	One major ion; four ions in total
Ephredine	Yes	No	9.5	Yes	Yes	One major ion; three ions in total
Doxazosin	No	No	7.1	Yes	No	Three major ions; five ions in total
CEN024-014	Yes	Yes	8.4	No	Yes	One major ion; four ions in total
Trichlormethazide	No	Yes	-4.1	No	Yes	Four major ion; six ions in total
Reserpine	Yes	No	7.3	Yes	Yes	Four major ion; eight ions in total
5-(p-Methylphenyl)-5-phenylhydantoin	No	No	-9.0	Yes	No	Only one major ion
1,1-Dimethyl biguanide	No	No	12.6	Yes	No	Multiple major ions: many basic centres?
Amlodipine	No	No	9.5	Yes	Yes	Four major ions; eight ions in total
Cortisone	No	No	-3.2	Yes	Yes	Two major ions; seven ions in total
Desipramine	No	Yes	10	No	Yes	Two major ions; four ions in total
Sildenafil	No	No	6.0	Yes	No	Three major ions; five ions in total
Trimethaprim	No	No	7.2	Yes	No	Seven major ions; nine ions in total

3.4. CONCLUSIONS

The study discussed in this chapter, (15 compounds, 98 observed bond cleavages and over 8000 bond length calculations) has confirmed that significant bond elongation ($>0.040 \text{ \AA}$) may be used as a descriptor for cleavage of polarised bonds during CID by flagging which bonds have been weakened as a result of structural changes due to protonation. This approach achieved 100% success rate in the prediction of polarised bond cleavage. Moreover, it has been shown that the semi-empirical computational approach AM1 can be used for calculating these bond length changes as it gives very similar results to those obtained by DFT. Most studies to date applying computational chemistry to mass spectral data have used DFT, which is computationally demanding both in terms of calculation time and computing power required. This has limited the spread of the application by mass spectrometrists of computational chemistry to the prediction or rationalisation of mass spectral fragmentation. The evidence that AM1 can be used to predict bond cleavage opens up this approach to many more scientists. AM1 calculations may take only seconds and be undertaken on a standard computer, rather than an extremely high specification server which is often used for DFT calculations. The speed of the AM1 calculations also offers the potential for their incorporation into commercial software to improve the 'chemical sense' of these packages and reduce the over-prediction of product ions. Over-prediction of bond cleavage was only 34% in this study, a massive improvement over the over-prediction of product ion formation by many commercial spectral interpretation software packages.

The behaviour of these fifteen compounds is consistent with the model of CID fragmentation that has been proposed in previous publications:

- Protonation caused conformational changes in the structure, which had an effect on bond lengths within the ion. These were able to be accurately calculated using quantum chemistry based computational software.
- Weakening of bonds is indicated by lengthening of bonds and significant bond length increases ($>0.040 \text{ \AA}$) weakens the bond to such an extent that it was preferentially broken during CID.
- The proton had to be located on one of the atoms (the most electronegative) involved in the bond for cleavage to occur; bond elongation remote from the protonation site did not lead to bond cleavage.

- Protonation at the most basic sites (liquid and gas phase) did not necessarily lead to bond cleavage. Therefore, for some compounds, the proton appears to have migrated from the primary site of protonation during ionisation to a thermodynamically less stable site to initiate cleavage.
- As the proton may migrate from the protonation site during ionisation, calculation of basicity (gas and liquid phase) was unnecessary for fragmentation predictions; the only bond length changes need be calculated. It is the protonation site which has the greatest effect on adjacent bond lengths rather than the centre at which ionisation occurs.
- No single protonated molecular species can rationalise the product ion spectrum. In many cases the product ions appear to be formed from a mixture of singly charged protonated precursors.

Unpolarised, carbon-carbon bond cleavage apparently cannot be predicted on the basis of bond length changes. It is, therefore, proposed that C-C bond cleavage is at least partly driven by the thermodynamic stability of the resulting product ions rather than bond lengths changes during protonation. Also, product ion intensity did not correlate with the extent of bond elongation and thus could not be predicted by bond elongation alone. For both unpolarised bond cleavage, and product ion intensity, calculation of product ion stability may be required to further rationalise the spectral data. Relative stability of ions and fragmentation products can be predicted in principle using both DFT and AM1. Fortunately, cleavage of non-polar bonds is less common than the cleavage of polarised bonds and product ion intensity, although very useful in comparing spectra with library data, is not critical in interpreting mass spectra. Therefore, both these limitations of the bond lengthening approach do not significantly restrict the application of AM1 as a tool to the interpretation of CID mass spectra.

Chapter 4: THE USE OF AM1 FOR PREDICTING NEGATIVE ION CID FRAGMENTATION

4.1. INTRODUCTION

Negative ion fragmentation mechanisms have been less studied than those of positive ion. However, similarities have been reported for anion and cation fragmentation which may suggest that conformational changes as a result of ionisation predict bond cleavage in anions in an analogous manner to that observed for cations. For example, John Bowie of Adelaide University, one of the leaders in the field of negative ion mass spectrometry, has identified three mechanisms for fragmentation of cations formed by deprotonation^[242,243]: (1) formation of an ion-molecule complex which dissociates via loss of a neutral molecule; (2) homolytic cleavage forming radicals; (3) rearrangements. These are all mechanisms also reported for positive ion fragmentation, although homolytic cleavage is less common for CID of protonated molecules which favour heterolytic cleavage.

Other similarities of even-electron anion CID fragmentation with that of cation include the following. Proton transfer/migration has been observed. The proton abstracted from the oxygen of organic sulphate ester anions has been shown (via deuterium labelling experiments) to originate from a proximal carbon and potentially via migration from more distant carbons as well ^[244,245]. Similarly, fragmentation of anions of peptides containing serine is proposed to involve proton transfer from the C-terminal carboxylic acid ^[246]. Also, negative ion CID studies of a range of thiazidic diuretics were consistent with long-distance proton transfer leading to loss of neutral species ^[247]. Phenyl urea based herbicides have been reported to undergo 1,3 proton shifts prior to negative ion CID fragmentation^[248]. Mobile protons have also been proposed to involve in the fragmentation of oligosaccharide anions^[249].

There is evidence that fragmentation may be charge-driven; estradiol fragmentation is proposed to be initiated by a charge-driven rearrangement ^[250]. Similar proposals have been made for fatty acids ^[212] and diacyl glycerophosphatidyl acids ^[251]. Some compounds, including some nonsteroidal anti-inflammatories, give the same fragment ions in positive and negative ion, differing in mass by the equivalent of two electrons^[252].

Homolytic carbon-carbon bond cleavage in hydroxycarboxylic acids was observed for the acids containing phenyl substituents, the phenyl group acting to stabilise the

products [253].

In order to evaluate the ability of AM1 to predict bond cleavage in negative ion CID, seven molecules in the mass range 340 to 608 Da were modelled with respect to bond length changes arising from deprotonation. Major bond elongations were highlighted to flag potential bond cleavages. The CID mass spectra were then interpreted to establish if the predicted bond cleavages had actually occurred.

CID spectra for the following compounds were obtained for the following compounds: Sulpiride, reserpine, sildenafil and dofetilide (Pfizer Ltd., Sandwich, Kent, UK). These compounds were chosen because their cations were modelled in previous studies and it was found that AM1 calculated bond length elongations did predict for CID fragmentation. Modelling their corresponding anions enables direct comparison of results obtained in these previous studies. In addition, the carboxylic acids and phosphate 6-oxoheptanoic acid, aspirin, stearic acid and 1-palmitoyl lysophosphatidic acid were also selected for AM1 modelling because they contained acidic groups at which deprotonation may occur. Major bond elongations were highlighted to flag potential bond cleavages. The CID mass spectra were then interpreted to establish if the predicted bond cleavages had actually occurred.

The anions were modelled using AM1 only for two reasons:

- AM1 proved to be successful in our studies to date in modelling bond length changes in cations. AM1 has more utility than DFT for this application in that the speed and computing resource needed for AM1 calculation offer the potential for routine application by mass spectrometrists rather than by computational chemists. Therefore, AM1 is likely to be the computational approach of choice for making this predictive approach widely applicable in mass spectral interpretation.
- *In silico* modelling of anions is more challenging than modelling cations or neutral species for several reasons: In anions, the extra electron is usually weakly bound and may have an infinite range (the electron range expands in space due to repulsion) and thus may not be within the area defined by the Gaussian function [139]. DFT which uses GTOs (Gaussian Type Orbitals) may be poor for modelling anions. AM1 uses Slater orbitals which have an extended range compared to GTOs and, therefore, AM1 models anions more accurately.

In addition, in an anion a valence electron in the asymptotic region of the orbital (i.e. is far from the nucleus, having a large 'r' value) experiences no net Coulombic attraction to the nucleus, whereas in cations and neutral molecules the electrons do experience attraction. DFT contains terms which assume a positive attraction for the valence electrons which is not a viable assumption in the case of anions, resulting in DFT over-estimating electron affinity and anion stability^[254]. This is not a problem with AM1 as it is parameterised to reflect the system it is modelling.

4.2. EXPERIMENTAL

4.2.1. Chemicals

As described in section 3.2.1.

4.2.2. LC/MS

Data were acquired using a Waters Synapt G1 Q-TOF mass spectrometer (Waters Corporation, Manchester, UK) in negative ion V mode (resolution 15,000 FWHM), calibrated with sodium formate. Leucine enkephalin ($[M-H]^-$ 554.2615) was infused at 5 μ L/minute as the reference lock mass. Sample (10 μ L; 20 μ g/mL) was introduced via flow injection (0.5 mL/min, 50/50 acetonitrile/water; no HPLC column). Acetonitrile was chosen as the modifier as it has a higher proton affinity than the other common modifier, methanol, potentially enhancing deprotonation of the analyte. Acid was not added to the mobile phase as it may suppress ionisation.

The following instrumental conditions were applied: extraction cone: -5 V; sampling cone -35 V (unless specified otherwise in the Results and Discussion); transfer collision energy 5 eV; cone gas: 150 L/h; desolvation gas nitrogen 1800 L/h; source temperature 100°C; desolvation temperature 500°C; trap collision energy 35 eV (unless specified otherwise in the Results and Discussion).

The ESCi (combined APCI and ESI source supplied by Waters Limited) source was fitted, and both ESI and APCI spectra were obtained (alternate scans) on the same sample. Only the ESI data will be discussed in this chapter. The capillary voltage and corona discharge voltage were both set to -5 kV. The data acquisition settings are as follows: scan range 50 to 700; scan rate 1 s, data are centroided.

4.2.3. LC/MS Computational modelling

All AM1 calculations were undertaken using Spartan'10 (Wavefun, Inc., California, USA). Structures were drawn in ACD Labs ChemsSketch (freeware), saved as '.skc' files and then opened in Spartan. Starting geometry was obtained using molecular mechanics MMFF minimum energy geometry optimisation.

All compounds were geometry optimised for deprotonation at all potential sites including carbons, using AM1 with following preferences: maximum ligand distance 3.60 Å; polar area range 1000 kJmol⁻¹; accessible area radius 1.000; 'Converge' was selected.

All calculations were undertaken with the explicit hydrogens on the molecule.

4.2.4. Assignment of product ions

Product ions of greater than approximately 8% of the most abundant product ion were structurally assigned. All percentages in the assignment tables are relative to the most abundant product ion (this may not be the base peak where there is a considerable amount of unfragmented precursor ion). In the results tables, bond length changes >0.025 Å adjacent to the site of cleavage, or that can feed into the cleavage site via a conjugated system, are highlighted in yellow and all bond length increases shown in red font.

4.3. RESULTS AND DISCUSSION

4.3.1. Dofetilide

The structure of dofetilide showing the sites of deprotonation modelled is shown in Figure 4.1. The negative ion product ion spectrum and the assignment of the product ions are shown in Figures 4.2 and Table 4.1. The AM1 modelled bond length changes are shown in Table 4.2. Only the sulphonamide cleavages are predicted on the basis of bond lengthening; the carbon-oxygen and carbon-nitrogen bond cleavages were not predicted. Sulphonamide bond cleavages were over-predicted as observed for the corresponding cations, discussed in Chapter 3. It appears that the sulphonamide groups in dofetilide are incorrectly predicted to cleave. The major ion in the product ion spectrum *m/z* 185 is the product of a rearrangement. Formation of product ions by

rearrangements frequently require less energy than simple bond cleavages because bond breaking may be partially compensated for by bond formation [255,256].

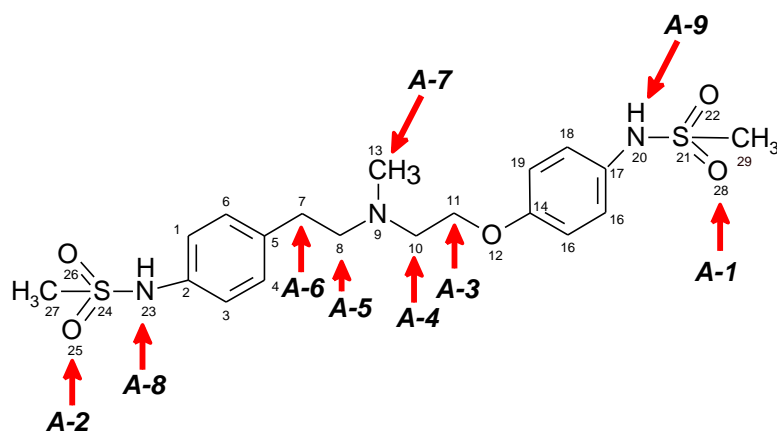


Figure 4.1 The structure of dofetilide with the potential anionic sites designated A-1 to A-9. The charge in the sulphonamide groups is delocalised over the whole sulphonamide group.

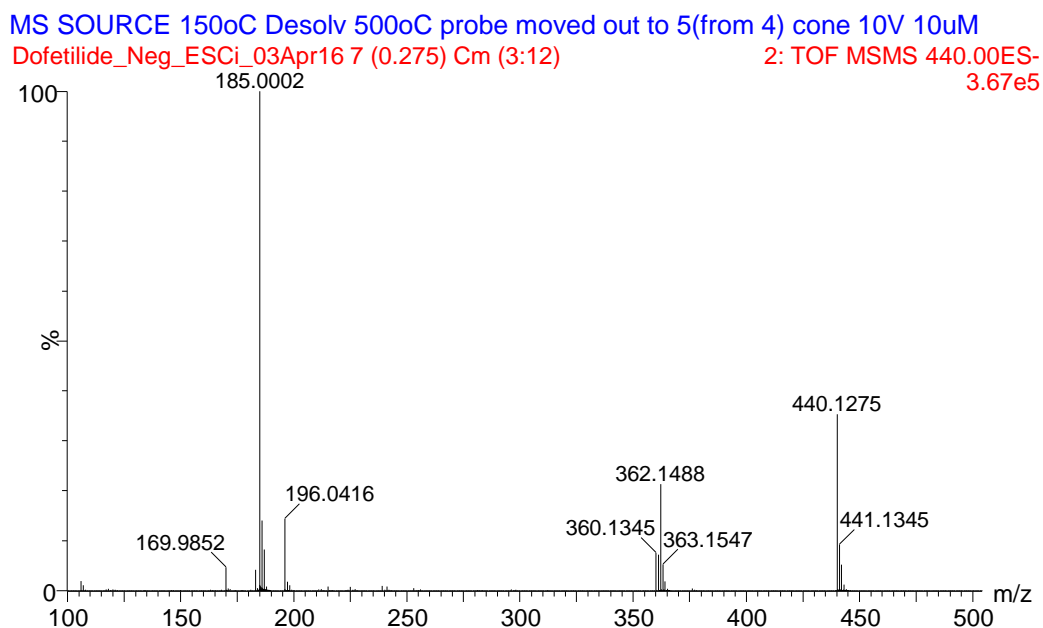


Figure 4.2 The negative product ion spectrum of deprotonated dofetilide.

Table 4.1 Proposed structures for the product ions observed in the negative ion CID spectrum of deprotonated dofetilide.

Relative Intensity	Experimental <i>m/z</i>	Proposed ion formula and calculated accurate mass	Error (ppm)	Proposed structure(s) of ion	Bond breaking
20%	362.1488	C ₁₈ H ₂₄ N ₃ O ₃ S 362.1538	14		S24,N23 S21,N20
15%	196.0416	C ₉ H ₁₀ NO ₂ S 196.0432	8		C8,N9
100%	185.0002	C ₆ H ₅ N ₂ O ₃ S 185.0002	<1		N9,C8 S24,C27 N9,C13 O12,C11 N9,C10

Table 4.2 Changes in bond length in of dofetilide resulting from deprotonation at the specified sites.

Bond	Bond length changes (?)									Bond observed to cleave in MS/MS spectrum?	Percent age of major product ion	Cleavage predicted on basis of bond lengthening?
	Anion A-1 (O25)	Anion A-2 (O28)	Anion A-3 (C11)	Anion A-4 (C10)	Anion A-5 (C8)	Anion A-6 (C7)	Anion A-7 (C13)	Anion A-8 (N23)	Anion A-9 (N20)			
S24,N23	0.113	-0.006	-0.012	-0.015	-0.023	-0.034	-0.014	0.027	0.001	Yes	20%	Yes
S24,O25	0.032	0.002	0.004	0.005	0.010	0.021	0.006	0.022	0.002	No	n/a	Yes
S24,O26	-0.262	-0.294	-0.292	-0.289	-0.289	-0.282	-0.291	0.065	0.001	No	n/a	Yes
S24,C27	0.077	0.296	0.297	0.296	0.299	0.307	0.295	-0.187	-0.006	Yes	100%	No
N23,C2	-0.034	0.003	0.006	0.007	0.010	0.005	0.007	-0.083	0.002	No	n/a	No
C5,C7	-0.003	0.000	-0.001	0.000	0.015	-0.120	-0.002	-0.002	0.002	No	n/a	No
C7,C8	0.000	-0.001	0.003	0.003	-0.078	-0.052	-0.004	-0.002	-0.002	No	n/a	No
C8,N9	0.003	0.000	-0.007	-0.003	-0.053	0.010	0.023	0.012	0.008	Yes	100%	No
N9,C13	0.000	0.001	-0.006	-0.002	0.011	0.003	-0.050	0.000	0.001	Yes	100%	No
N9,C10	0.004	0.010	0.030	-0.044	0.019	0.006	0.018	0.002	0.003	Yes	100%	No
C10,C11	0.002	-0.001	-0.080	-0.195	-0.007	0.002	-0.006	-0.001	-0.005	No	n/a	No
C11,O12	0.012	0.009	-0.061	1.885	0.016	0.013	0.031	0.003	-0.001	Yes	100%	No
O12,C14	-0.005	0.014	-0.006	-0.112	-0.011	-0.008	-0.019	-0.004	0.015	No	n/a	No
C17,N20	0.002	-0.035	0.007	0.004	0.006	0.003	0.005	0.002	-0.086	No	n/a	No
N20,S21	-0.006	0.113	-0.024	-0.030	-0.015	-0.008	-0.015	-0.004	-0.183	Yes	100%	Yes
S21,O28	0.001	0.028	0.006	0.009	0.004	0.001	0.003	0.001	0.026	No	n/a	Yes
S21,O22	0.003	0.023	0.013	0.018	0.007	0.004	0.007	0.002	0.021	No	n/a	No
S21,C29	0.003	-0.210	0.008	0.011	0.004	0.002	0.004	0.000	-0.063	No	n/a	No

4.3.2. Sulpiride

The structure of sulpiride showing the sites of deprotonation modelled is shown in Figure 4.3. The negative product ion spectrum and the assignment of the product ions are shown in Figures 4.4 and Table 4.3. The AM1 modelled bond length changes are shown in Table 4.4. As observed for dofetilide, only cleavage of the sulphonamide was predicted. The two carbon-oxygen bond cleavages were not predicted.

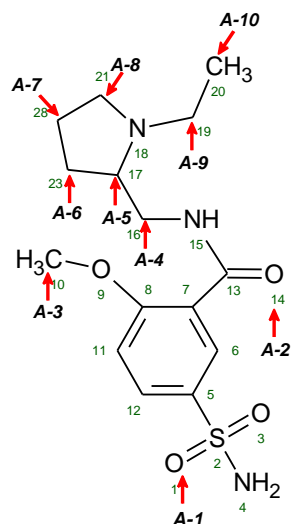


Figure 4.3 The structure of sulpiride with the potential anionic sites designated A-1 to A-10. The charge in the sulphonamide and amide groups is delocalised over the whole functional group.

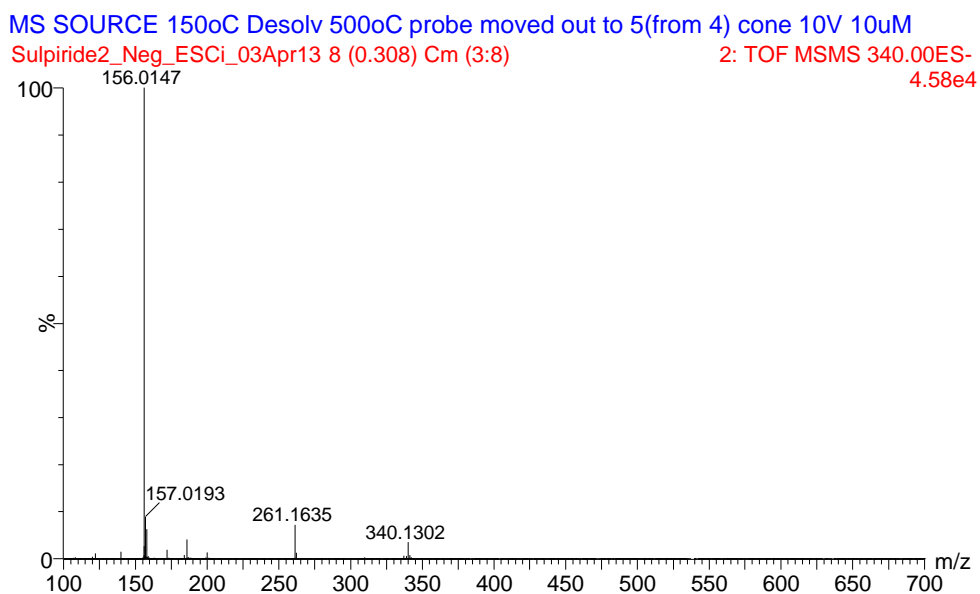


Figure 4.4 The negative product ion spectrum of deprotonated sulpiride.

Table 4.3 Proposed structures for the product ions observed in the negative ion CID spectrum of deprotonated sulpiride.

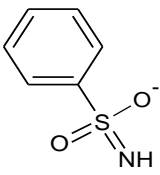
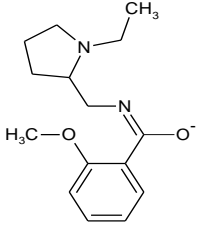
Relative Intensity	Experimental m/z	Proposed ion formula and calculated accurate mass	Error (ppm)	Proposed structure(s) of ion	Bond breaking
100%	156.0147	$C_6H_6NO_2S$ 156.0119	18		C8,O9 C7,C13
10%	261.1635	$C_{15}H_{21}N_2O_2$ 261.1603	12		C5,S2

Table 4.4 Changes in bond length in sulphiride resulting from deprotonation at the specified sites.

Bond	Bond length changes (?)										Bond observed to cleave in MS/MS spectrum?	Percentage of major product ion	Cleavage predicted on basis of bond lengthening?
	Anion A-1 (O1)	Anion A-2 (O14)	Anion A-3 (C10)	Anion A-4 (C16)	Anion A-5 (C17)	Anion A-6 (C21)	Anion A-7 (C28)	Anion A-8 (C23)	Anion A-9 (C19)	Anion A-10 (C20)			
O1,S2	-0.007	0.003	-0.023	-0.020	-0.021	-0.027	-0.028	-0.029	-0.027	0.000	No	n/a	No
S2,O3	-0.006	0.001	-0.029	-0.012	-0.029	-0.030	-0.031	-0.032	-0.031	0.001	No	n/a	No
S2,N4	-0.308	0.000	-0.068	-0.039	-0.085	-0.071	-0.071	-0.074	-0.074	0.000	No	n/a	No
S2,C5	0.078	-0.006	-0.102	-0.176	-0.088	-0.097	-0.095	-0.087	-0.092	-0.002	Yes	10%	Yes
C8,O9	0.022	-0.001	0.015	0.021	0.001	0.003	-0.007	0.010	-0.001	-0.006	Yes	100%	No
O9,C10	0.003	0.003	0.003	-0.002	0.000	0.010	0.002	0.009	0.001	-0.004	No	100%	No
C7,C13	-0.016	-0.007	0.013	-0.029	-0.003	0.002	-0.001	-0.003	0.001	-0.029	Yes	n/a	No
C13,O14	0.023	0.017	0.049	0.021	0.034	0.030	0.022	0.024	0.026	-0.001	No	n/a	No
C13,N15	0.013	-0.088	-0.040	0.036	-0.011	-0.021	0.002	-0.003	-0.006	-0.006	No	n/a	No
N15,C16	-0.022	0.010	-0.031	0.007	0.028	-0.016	-0.005	-0.005	-0.007	0.006	No	n/a	No
C16,C17	0.008	-0.004	0.012	0.005	-0.103	0.029	0.006	-0.003	0.000	-0.003	No	n/a	No
C17,N18	-0.007	0.005	-0.005	-0.001	-0.007	-0.037	-0.031	0.008	0.016	-0.013	No	n/a	No
N18,C19	-0.012	0.000	-0.021	-0.015	-0.030	0.024	0.010	0.017	-0.074	-0.019	No	n/a	No
C19,C20	-0.002	0.003	0.000	-0.002	-0.002	0.000	-0.001	-0.006	-0.072	-0.004	No	n/a	No
N18,C21	-0.006	-0.005	-0.008	-0.008	0.010	-0.002	0.017	-0.047	0.002	-0.005	No	n/a	No
C21,C22	0.025	0.013	0.024	0.025	0.031	0.038	-0.049	-0.048	0.025	0.014	No	n/a	No
C22,C23	0.005	0.007	0.008	0.006	0.018	-0.047	-0.069	0.018	0.007	0.004	No	n/a	No
C23,C17	0.003	-0.012	0.004	0.001	-0.060	-0.054	0.020	0.010	0.000	-0.013	No	n/a	No

4.3.3. Reserpine

The structure of reserpine showing the sites of deprotonation modelled is shown in Figure 4.5. Not all potential deprotonation sites are shown or modelled. The negative ion product ion spectrum and the assignment of the product ions are shown in Figure 4.6 and Table 4.5. The AM1 modelled bond length changes are shown in Table 4.6. Bond elongation did predict the cleavage of the two bonds to N13 and C33-C35 but did not predict the cleavage of C30-O32 the largest product ion at m/z 211 if it is assumed that the charge has to be resident on one of the atoms of the bond which broke as seen for cation fragmentation. However, deprotonation of C29, alpha to the bond and connected by a single bond, did result in extensive bond elongation (shown highlighted in pale green, in Table 4.6. As this effect was observed for a single bond in one compound it is not apparent if this suggests that the mechanism for bond cleavage is different for anions produced by deprotonation compared to cations formed by protonation.

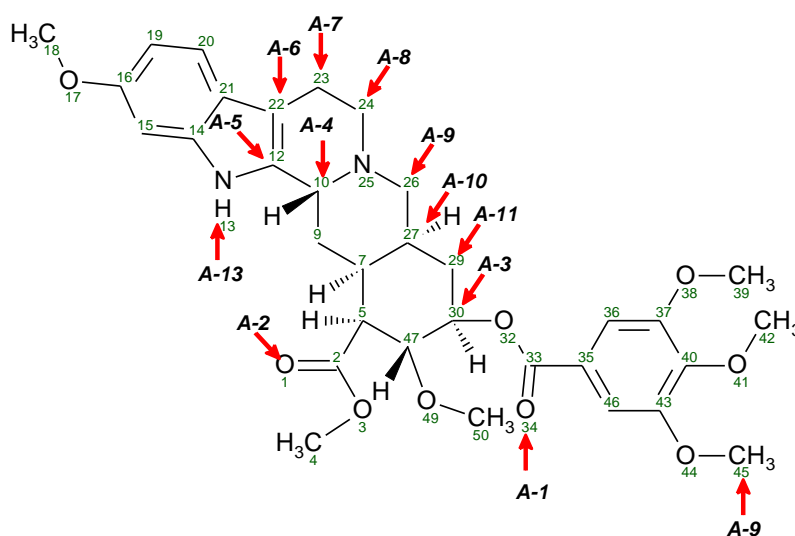


Figure 4.5 The structure of reserpine with the potential anionic sites designated A-1 to A-13. The charge on the carbonyl is modelled by removing the proton from the enol form.

MS SOURCE 150oC Desolv 500oC probe moved out to 5(from 4) cone 10V 10uM
 Reserpine_Neg_ESCI_03Apr14 9 (0.342) 2: TOF MSMS 607.00ES-385

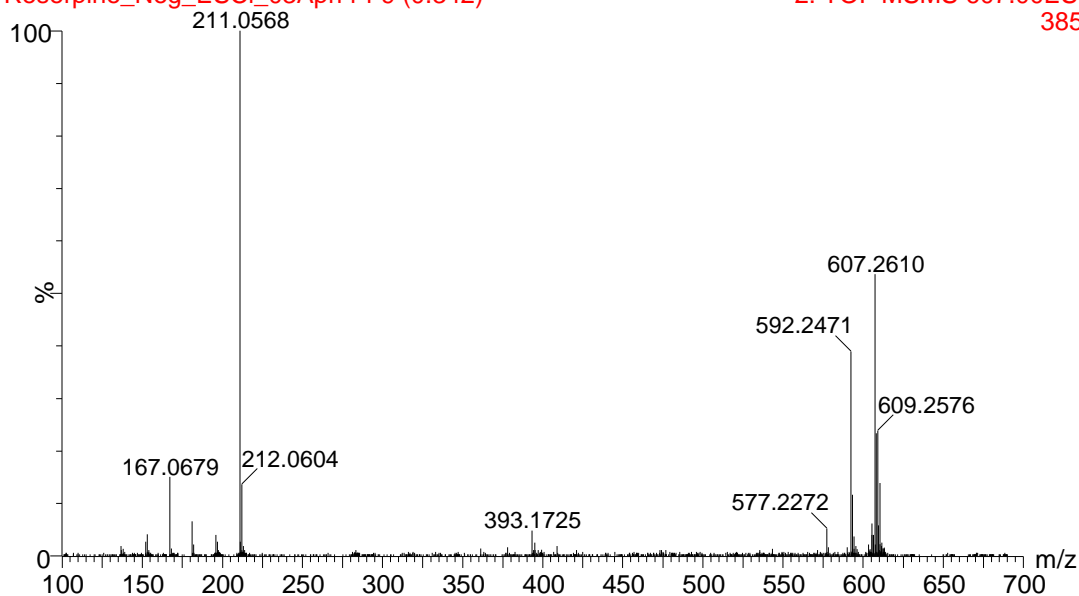


Figure 4.6 The negative product ion spectrum of deprotonated reserpine.

Table 4.5 Proposed structures for the product ions observed in the negative ion CID spectrum of deprotonated reserpine.

Relative Intensity	Experimental <i>m/z</i>	Proposed ion formula and calculated accurate mass	Error (ppm)	Proposed structure(s) of ion	Bond breaking
40%	592.2471	$C_{33}H_{38}NO_9$ 592.2547	12		N13,C14 N13C12
100%	211.0568	$C_{10}H_{11}O_5$ 211.0607	18		O32,C30
10%	167.0679	$C_9H_{11}O_3$ 167.0708	17		C35,C33

Table 4.6 Changes in bond length in of reserpine resulting from deprotonation at the specified sites.

Bond	Bond length changes (?)													Bond observed to cleave in MS/MS spectrum?	Percentage of major product ion	Cleavage predicted on basis of bond lengthening?
	Anion A-1	Anion A-2	Anion A-3	Anion A-4	Anion A-5	Anion A-6	Anion A-7	Anion A-8	Anion A-9	Anion A-10	Anion A-11	Anion A-12	Anion A-13			
	(O34)	(O1)	(C30)	(C10)	(C12)	(C22)	(C23)	(C24)	(C26)	(C27)	(C29)	(C4)	(N13)			
O1,C2	0.001	0.102	0.009	0.006	0.010	0.006	0.007	0.007	0.007	0.009	0.008	0.014	0.001	No	n/a	No
C2,O3	-0.002	-0.034	0.018	0.011	0.006	0.012	0.011	0.012	0.016	0.019	0.012	-0.004	-0.001	No	n/a	No
O3,C4	-0.001	-0.077	-0.006	-0.001	-0.001	-0.001	-0.001	-0.002	-0.003	-0.006	-0.002	-0.031	0.001	No	n/a	No
C2,C5	-0.001	-0.102	-0.016	-0.010	-0.009	-0.011	-0.010	-0.009	-0.013	-0.018	-0.012	-0.006	0.001	No	n/a	No
C5,C7	-0.005	-0.191	-0.016	-0.010	-0.011	-0.010	-0.010	-0.005	-0.013	0.018	-0.016	-0.021	-0.002	No	n/a	No
C7,C9	0.000	-0.191	-0.021	-0.016	-0.019	-0.010	-0.019	-0.018	-0.022	-0.016	-0.022	-0.023	-0.001	No	n/a	No
C9,C10	0.000	-0.210	-0.002	-0.050	0.005	-0.050	0.006	-0.001	-0.006	-0.005	-0.001	0.000	-0.001	No	n/a	No
C10,C12	0.000	-0.017	0.000	0.012	-0.025	-0.122	-0.024	-0.008	-0.008	0.003	0.000	0.000	0.000	No	n/a	No
C12,N13	0.000	0.031	0.030	0.071	0.065	0.068	0.065	0.047	0.036	0.031	0.031	0.030	0.031	Yes	40%	Yes
N13,C14	0.000	0.000	0.017	0.054	0.034	0.053	0.035	0.021	0.018	0.017	0.018	0.018	0.012	Yes	40%	Yes
C16,O17	0.000	0.000	0.018	0.005	0.023	0.026	0.023	0.022	0.021	0.019	0.017	0.017	-0.016	No	n/a	No
C18,O17	0.000	0.000	-0.003	-0.025	-0.005	0.000	-0.005	-0.004	-0.004	-0.003	-0.002	-0.002	0.002	No	n/a	No
C21,C22	0.000	-0.051	0.024	0.003	0.047	0.040	0.047	0.028	0.024	0.024	0.025	0.024	0.024	No	n/a	No
C22,C23	0.000	-0.110	-0.021	0.044	-0.022	0.048	-0.126	-0.005	-0.021	-0.021	-0.021	-0.021	0.007	No	n/a	No
C23,C24	0.000	-0.155	-0.013	-0.087	-0.066	-0.030	-0.066	-0.074	-0.011	-0.011	-0.013	-0.012	0.001	No	n/a	No
C24,N25	0.000	-0.110	-0.025	0.036	-0.020	-0.045	-0.019	-0.079	-0.019	-0.029	-0.025	-0.026	0.001	No	n/a	No
N25,C10	-0.001	-0.064	-0.011	0.052	-0.009	-0.054	-0.008	0.038	0.036	-0.017	-0.012	-0.012	-0.003	No	n/a	No
N25,C26	0.001	0.022	-0.005	0.059	-0.016	0.001	-0.016	-0.004	-0.060	0.004	-0.007	-0.009	0.002	No	n/a	No
C26,C27	0.000	-0.071	-0.003	0.001	0.002	-0.140	0.001	-0.005	-0.070	-0.074	-0.002	-0.004	-0.001	No	n/a	No
C27,C7	-0.006	-0.013	-0.013	-0.117	-0.012	-0.117	-0.012	-0.015	0.011	-0.085	-0.009	-0.006	0.001	No	n/a	No
C27,C29	-0.003	0.014	0.003	-0.110	-0.012	0.936	-0.012	-0.014	-0.007	-0.076	-0.041	-0.012	-0.001	No	n/a	No
C29,C30	-0.007	0.012	-0.064	-0.087	-0.010	-0.067	-0.006	-0.005	-0.006	0.015	-0.196	0.000	-0.003	No	n/a	No
C30,C47	-0.990	0.011	0.005	-0.181	-0.006	-0.028	-0.006	0.002	-0.007	0.001	-0.049	0.004	0.001	No	n/a	No
C47,C5	0.093	-0.100	1.062	-0.304	-0.003	-0.005	-0.005	-0.001	-0.001	-0.002	0.006	-0.004	0.004	No	n/a	No
C47,O49	0.018	-0.017	-0.001	0.033	-0.012	0.081	-0.021	-0.013	-0.012	-0.015	-0.014	-0.018	0.007	No	n/a	No
O49,C50	0.003	0.023	-0.013	-0.034	-0.004	0.116	-0.004	-0.004	-0.007	-0.006	0.003	-0.001	0.001	No	n/a	No
C30,O32	0.020	-0.090	-0.072	-0.017	0.001	-0.025	-0.003	0.003	-0.001	0.004	1.862	-0.005	0.000	Yes	100%	No
O32,C33	0.005	-0.134	0.014	0.032	0.010	0.063	0.009	0.018	0.003	-0.001	-0.089	0.023	0.005	No	n/a	No
C33,O34	0.100	0.266	0.020	0.015	0.014	0.015	0.015	0.012	0.016	0.017	0.046	0.011	-0.001	No	n/a	No
C33,C35	0.110	-0.116	0.003	-0.061	-0.010	-0.123	-0.011	-0.011	-0.007	-0.005	0.028	-0.009	-0.002	Yes	10%	Yes
C37,O38	0.000	0.056	0.014	0.011	0.010	-0.136	0.017	-0.001	0.011	0.012	0.017	-0.012	-0.009	No	n/a	No
O38,C39	-0.001	-0.055	-0.002	0.000	-0.001	0.050	0.003	0.011	0.000	-0.001	-0.004	0.010	-0.004	No	n/a	No
C40,O41	0.001	0.058	0.015	0.015	0.013	0.009	0.014	0.012	0.014	0.013	0.016	0.016	0.001	No	n/a	No
O41,C42	0.000	-0.059	-0.003	0.001	0.000	-0.005	0.001	-0.002	-0.001	-0.001	-0.004	-0.002	0.001	No	n/a	No
C43,O44	0.000	0.056	0.019	0.017	0.009	0.012	0.016	0.018	0.011	0.017	0.021	0.015	0.000	No	n/a	No
O44,C45	0.000	0.000	0.000	0.003	-0.001	0.002	0.002	0.001	-0.001	0.001	-0.001	-0.003	0.001	No	n/a	No

4.3.4. Sildenafil

The structure of sildenafil showing the sites of deprotonation modelled is shown in Figure 4.7. The negative product ion spectrum and the assignment of the product ions are shown in Figure 4.8 and Table 4.7. The AM1 modelled bond length changes are shown in Figure 4.8 and Table 4.7. The AM1 modelled bond length changes are shown in Table 4.8. Two bond cleavages were successfully predicted; the sulphonamide S2-C11 as a results of deprotonation at C10 adjacent to the sulphonamide nitrogen N4 and C14-N15 after formation of anion A-4 shown in Figure S-7 (the charge can feed through the conjugated system to N15). The cleavages O28-C29 and C14-N20 were not predicted. In the case of O28-C29 direct deprotonation of the bonding atom was not feasible as neither of them had a proton available to be removed.

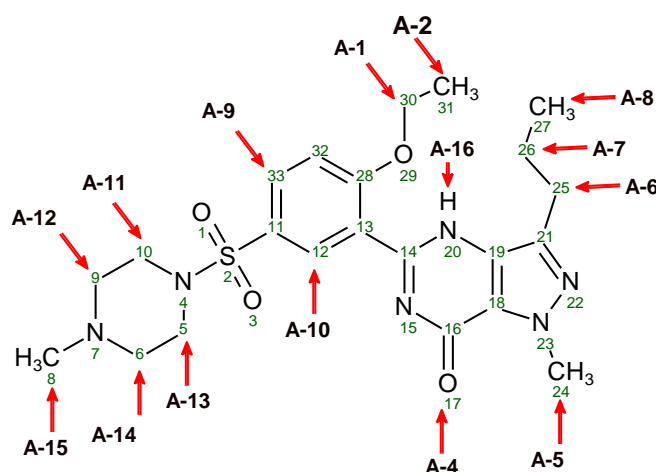


Figure 4.7 The structure of sildenafil with the potential anionic sites designated A-1 to A-15. The charge in the sulphonamide and amide groups is delocalised over the whole functional group.

MS SOURCE 150oC Desolv 500oC probe moved out to 5(from 4) cone 10V 10uM
 Sildenafil_Neg_ESCi_03Apr13 7 (0.274) Cm (6:9) 2: TOF MSMS 473.00ES-
 1.37e5

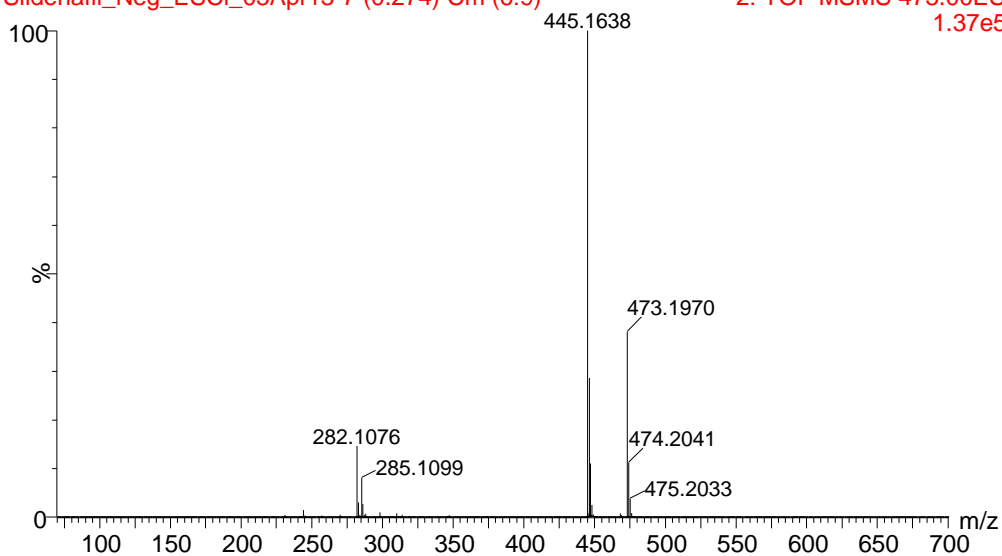


Figure 4.8 The negative product ion spectrum of deprotonated sildenafil.

Table 4.7 Proposed structures for the product ions observed in the negative ion CID spectrum of deprotonated reserpine.

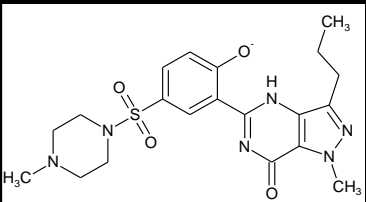
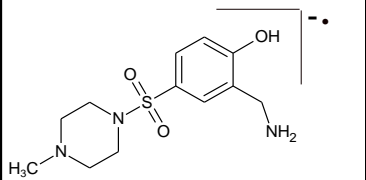
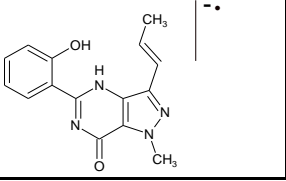
Relative Intensity	Experimental <i>m/z</i>	Proposed ion formula and calculated accurate mass	Error (ppm)	Proposed structure(s) of ion	Bond breaking
100%	445.1638	$C_{20}H_{25}N_6O_4S$ 445.1658	4		O29,C30
10%	285.1099	$C_{12}H_{19}N_3O_3S$ 285.1147	12		O29,C30 C14,N20 N15,C16
15%	282.1076	$C_{15}H_{14}N_4O_2$ 282.1117	14		O29,C30 C11,S2

Table 4.8 Changes in bond length in sildenafil resulting from deprotonation at the specified sites.

Bond	Bond length changes (?)																Bond observed to cleave in MS/MS spectrum?	Percentage of major product ion	Cleavage predicted on basis of bond lengthening?
	Anion A-1	Anion A-2	Anion A-3	Anion A-4	Anion A-5	Anion A-6	Anion A-7	Anion A-8	Anion A-9	Anion A-10	Anion A-11	Anion A-12	Anion A-13	Anion A-14	Anion A-15	Anion A-16			
	C30	C31	C32	O17	C26	C25	C26	C27	C33	C12	C10	C9	C8	C6	C5	N20			
O1,S2	0.007	-0.001	0.008	0.008	0.007	0.004	0.004	0.009	0.002	0.021	0.070	0.003	0.006	0.027	0.076	-0.007	No	n/a	Yes
S2,O3	0.003	0.010	0.012	0.002	0.001	0.000	0.005	0.009	0.021	0.005	0.074	0.021	0.007	0.025	0.069	-0.003	No	n/a	Yes
S2,N4	0.008	0.011	0.028	0.013	0.005	0.004	0.005	0.022	0.025	0.028	0.183	0.028	-0.032	-0.039	0.188	-0.011	No	n/a	Yes
N4,C5	0.000	-0.001	-0.006	-0.006	-0.003	-0.002	0.000	-0.005	-0.005	-0.007	-0.111	-0.004	0.005	0.000	0.014	0.002	No	n/a	No
C5,C6	-0.002	-0.001	0.000	0.003	-0.001	-0.001	-0.001	0.000	0.000	0.000	-0.051	-0.001	-0.001	0.000	-0.007	0.001	No	n/a	No
C6,N7	0.007	0.008	0.008	0.008	0.005	0.007	0.009	0.008	0.008	0.007	0.015	0.010	0.017	0.014	0.004	0.002	No	n/a	No
N7,C8	-0.003	0.001	0.000	0.000	-0.003	0.001	0.006	0.000	-0.002	0.000	0.000	-0.001	-0.061	0.007	-0.004	0.003	No	n/a	No
N7,C9	-0.002	0.000	0.002	-0.003	-0.001	0.000	0.001	0.002	0.000	0.002	0.001	0.000	0.020	-0.037	0.003	-0.006	No	n/a	No
C9,C10	-0.003	-0.003	-0.003	-0.003	-0.004	-0.003	-0.003	-0.003	0.000	-0.003	-0.006	-0.001	-0.006	-0.112	-0.054	0.001	No	n/a	No
C10,N4	-0.003	-0.002	-0.004	0.002	0.002	0.001	0.001	-0.002	-0.007	-0.003	0.015	-0.007	0.009	0.068	-0.113	0.003	No	n/a	No
S2,C11	-0.022	-0.023	-0.053	-0.027	-0.018	-0.008	-0.014	-0.053	-0.057	-0.060	0.076	-0.054	0.033	0.062	0.076	0.027	Yes	10%	Yes
C13,C14	0.008	0.006	-0.011	0.006	0.007	0.001	0.006	-0.007	-0.011	-0.009	-0.003	-0.011	-0.001	-0.002	-0.003	-0.002	No	n/a	No
C14,N15	0.034	0.037	0.008	0.042	-0.011	0.012	0.042	0.014	0.006	0.009	0.002	0.006	0.000	0.000	0.001	-0.041	Yes	n/a	Yes
N15,C16	-0.024	-0.026	-0.011	-0.028	0.026	-0.005	-0.030	-0.012	-0.009	-0.013	-0.004	-0.009	-0.001	-0.003	-0.005	0.028	No	n/a	No
C16,O17	0.016	0.019	0.006	0.019	0.010	0.010	0.021	0.007	0.005	0.008	0.003	0.005	0.001	0.002	0.003	-0.019	No	n/a	No
C16,C18	-0.004	-0.004	0.004	1.039	-0.042	-0.005	-0.005	0.003	0.004	0.004	0.003	0.005	0.002	0.003	0.004	0.004	No	n/a	No
C18,C19	0.005	0.006	-0.003	0.005	0.034	-0.004	0.006	-0.004	-0.003	-0.002	-0.003	-0.003	-0.002	-0.001	-0.002	-0.006	No	n/a	No
C19,N20	-0.018	-0.016	-0.005	-0.014	0.020	-0.003	-0.014	-0.007	-0.005	-0.009	-0.004	-0.005	-0.002	-0.004	-0.005	0.014	No	n/a	No
N20,C14	-0.031	-0.034	0.008	-0.038	0.014	-0.016	-0.038	0.000	0.009	0.010	0.008	0.010	0.006	0.006	0.007	0.037	Yes	n/a	No
C19,C21	0.012	0.013	0.003	0.014	-0.049	0.035	0.013	0.004	0.003	0.005	0.003	0.003	0.001	0.002	0.003	-0.013	No	n/a	No
C21,N22	-0.006	-0.006	-0.002	-0.007	0.043	0.028	-0.007	-0.003	-0.002	-0.002	-0.002	-0.001	-0.001	-0.001	-0.001	0.007	No	n/a	No
N22,N23	0.004	0.004	0.002	0.005	0.011	0.033	0.005	0.004	0.002	0.002	0.001	0.001	0.001	0.001	0.001	-0.005	No	n/a	No
N23,C24	-0.007	-0.008	-0.003	-0.008	-0.109	-0.003	-0.008	-0.004	-0.003	-0.005	-0.003	-0.003	-0.001	-0.002	-0.003	0.008	No	n/a	No
N23,C18	0.004	0.006	0.002	0.005	0.019	-0.001	0.005	0.002	0.002	0.003	0.002	0.002	0.001	0.001	0.002	-0.005	No	n/a	No
C14,N20	-0.031	-0.034	0.008	-0.038	0.014	-0.016	-0.038	0.000	0.009	0.010	0.008	0.010	0.006	0.006	0.007	-0.037	Yes	15%	No
O29,C30	-0.059	-0.010	-0.005	-0.001	-0.005	0.004	-0.004	-0.081	-0.010	-0.008	-0.007	-0.009	-0.003	-0.001	-0.005	-0.001	Yes	100%	No
C21,C25	-0.001	-0.001	0.000	-0.001	-0.003	-0.106	0.000	0.001	0.000	-0.001	0.000	-0.001	0.000	0.000	0.000	0.000	No	n/a	No
C25,C26	0.000	0.000	0.001	-0.009	0.002	-0.052	0.001	0.004	0.001	-0.001	0.001	0.001	0.001	0.000	0.000	0.001	No	n/a	No

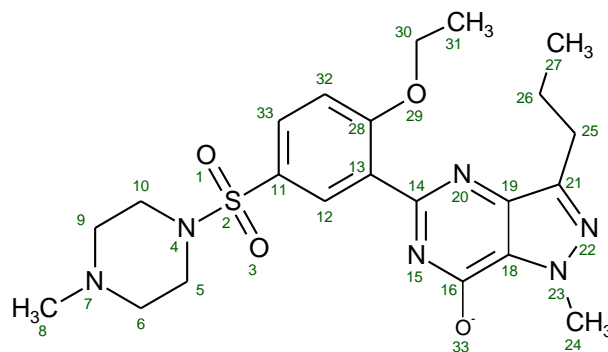


Figure 4.9 The structure of deprotonated sildenafil anion A-4.

4.3.5. Carboxylic acids and phosphates

None of the compounds considered so far have been carboxylic acids or phosphates i.e. compounds with an acidic group at which deprotonation is likely to occur. The negative ion spectra of a number of carboxylic acid molecules and one phosphate molecule were available in the literature. The author of this thesis modelled these molecules with AM1 and compared the results with the literature spectra. Only the neutral molecule and the anion produced by deprotonating the carboxylic acid or phosphate group were modelled.

For the four compounds shown in Figure 4.10, only the neutral molecule and the anion produced by deprotonating the carboxylic acid or phosphate group were modelled. The bond length changes calculated to result from deprotonation of the respective carboxylic acid and phosphate groups are shown in Table 4.9. Only the product ions associated with charge directed fragmentation at these acidic functional groups are shown. For aspirin and 1-palmitoyl lysophosphatidic acid, bond elongation did not predict which bonds cleaved in the CID spectra. In fact, the bonds which cleaved were predicted to contract. For the other two compounds, 6-oxoheptanoic acid and steric acid, conformational changes due to deprotonation did lead to significant elongation of the bonds which were observed to cleave in the CID spectra.

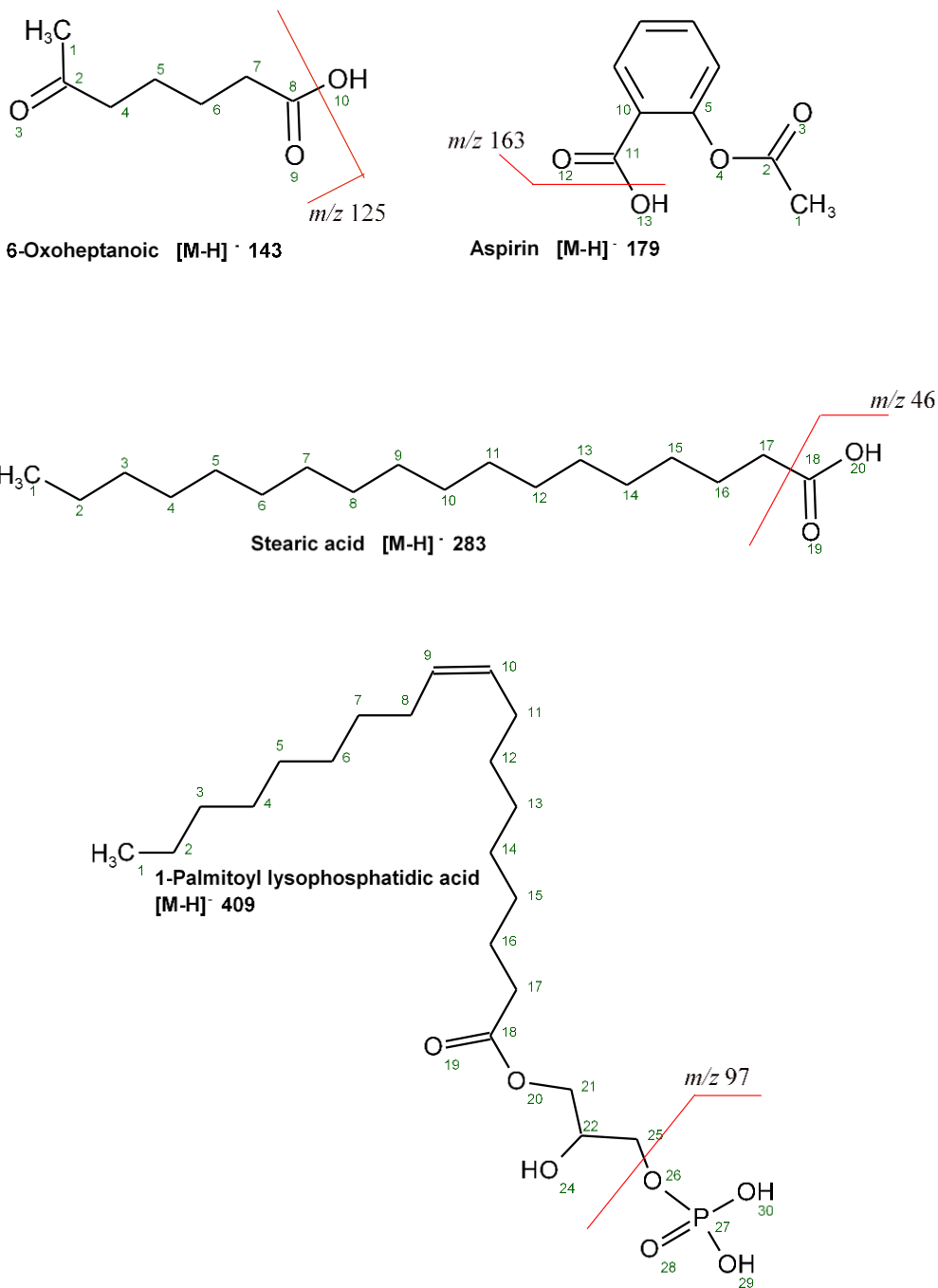


Figure 4.10 Structures of the four acidic compounds showing only the bonds observed to cleave in their CID spectra (6-oxoheptanoic acid^[257], aspirin^[258], 1-palmitoylphosphatidic acid and stearic acid (Scripps Center For Metabolomics and Mass Spectrometry - METLIN) as a result of deprotonation at the carboxylic acid or phosphate groups.

Table 4.9 Changes in bond length in of 6-oxoheptanoic acid, aspirin, 1-palmitoyl lysophosphatidic acid and stearic acid resulting from deprotonation at the carboxylic acid or phosphate groups.

Compound	Bond	Bond length changes (Å)		
		Anion	Bond proposed to cleave on the basis of product ions observed in CID spectrum?	Cleavage predicted on basis of bond lengthening?
6-Oxoheptanoic acid	C7,C8	0.035	Yes	Yes
	C8,O9	0.046	Yes	Yes
Aspirin	C11,O13	-0.096	Yes	No
1-Palmitoyl lysophosphatidic acid	C25,O26	-0.023	Yes	No
Stearic acid	C17,C18	0.045	Yes	Yes
	C18,O19	0.031	Yes	Yes

4.4. CONCLUSIONS

For the seven molecules modelled, overall 48% of the bonds proposed to cleave on the basis of the product ions observed were correctly flagged as likely to cleave on the basis of bond lengthening after deprotonation of one of the bonding atoms. Thus, it may be concluded that bond length change calculations are not effective predictors of CID bond cleavage of anions formed by deprotonation for these compounds. There are two possible reasons for this: the conformational changes are not being adequately modelled by AM1 or the mechanism for fragmentation in negative ion CID differs significantly from that of positive ion CID. AM1 has been reported to model adequately for anions^[260–263], therefore, it may be the latter which is the explanation for bond elongation not predicting bond cleavage in negative ion.

The main differences between anion and cation CID fragmentation are:

- Negative ion CID fragmentation has been reported to deviate from the even electron rule to a greater extent than positive ion CID. The even electron rule states that even electron species will not fragment into two odd-electron species but rather to a cation and a neutral molecule. For example, the deprotonated anion of (2-hydroxy-3-(3-methyl-2-but-enyl)-1,4-naphthoquinone) fragmented to two radicals ^[264]. Hence, there is an increased tendency to observed radicals in negative ion CID spectra relative to positive ion CID spectra ^[242,265]; organic sulphates ^[244], *N*-phenyl benzenesulphonamides ^[266], isoflavones ^[267] and a range of low molecular weight pharmaceutical compounds ^[258] all form radical product ions during CID. The majority of these radical product ions undergo resonance stabilisation. For small oxocarboxylic acids, it has been reported that the inability of a product to undergo resonance stabilisation inhibits its formation^[257]. This increased propensity for homolytic cleavage is unlikely to be the reason for the lack of correlation between bond elongations and bond cleavage in negative ion as the majority of the negative product ions observed in this study are even-electron species.
- The bond activation rule (BAR)^[185] states that protonation of the most electronegative atom of the bond results in an increase in the polarity of the bond, weakening it, by attracting the bonding electrons toward the positive charge. This process is reversed for deprotonated species, however. The electrons will be repelled away from the deprotonated negatively charged atom. This represents a fundamental difference in bond activation.
- It is not clear if a deprotonation site is as mobile as the corresponding situation in cations where the proton migrates allowing the charge to reach the dissociative site.

In summary, it may be concluded from the data presented here that the conformational changes induced by deprotonation do not consistently lead to bond elongations (as calculated by AM1) which are indicative of bond cleavage during CID. Therefore, this approach may not be applied to reliably predict negative product ion formation.

It is known that the properties of anions are significantly different from those of

cations and neutral molecules. For example, anions have large potential for polarisation and often have stronger van der Waals interactions with other molecules than cations of corresponding size. This is due to the weak binding of the valence electrons. Molecules generally lose energy on deprotonation as some of their internal energy is transferred, as vibrational energy with the proton as it forms a bond with another molecule, whereas protonation leads to increase in energy with the formation of the M-H⁺ bond in the other molecule. Therefore, even electron anions are inherently less energetic than their cationic counterparts^[268] and generally produce less fragmentation. However, electronically anions are less stable than cations^[268] as the anion 'wants' to lose the extra electron to increase stability. It may be, therefore, that fragmentation of anions is driven by their instability rather than the bond weakening as a result of charge-induced conformational changes. Another possibility is these anions do not always fragment by direct bond cleavage, but rather go via an intermediate(s), to a greater extent than occurs for the corresponding cations. Further studies looking at the effect of collision energy on the CID spectra of deprotonated ions and also the Ion Trap CID spectra where single step fragmentation predominates may shed some light on the mechanism of anion fragmentation.

Chapter 5: COMPARING APCI AND ESI SPECTRA

5.1. INTRODUCTION

CID spectra of ions produced by both APCI and ESI were obtained in order to see if there were any differences in the product ion spectra of ions formed by gas phase and liquid phase ionisation, respectively. During APCI, protonation occurs in the gas phase whereas during ESI the ions are pre formed in solution. Therefore, potentially, there may be differences in the CID spectra of compounds which are protonated at different atoms in the gas phase and in solution. If the proton migrates from the initial site of ionisation, however, the CID spectra may be qualitatively independent of the ionisation process.

The spectra were obtained with an ESCi source. An ESCi source uses both an electrospray capillary and a corona discharge needle. A baffle is automatically toggled to shield or uncover the discharge needle preventing or allowing APCI ionisation respectively. This provides alternating ESI and APCI ionisation modes. It has been shown that the CID spectra obtained on an ESCi source are essentially the same as the CID spectra obtained on an instrument fitted with separate APCI and ESI sources ^[269]. There is a difference between a dedicated APCI source and the APCI component of an ESCi source in that the dedicated APCI source requires significant additional heating at or near the sample inlet whereas the ESCi source does not. The geometry of the Waters' ESCi source and the use of gas turbulence, make additional heating during APCI unnecessary. Therefore, thermally labile compounds are more stable during ESCi ionisation than during conventional APCI. This increased stability may result in an increased abundance of precursor ion available to undergo CID but will not affect the product ions formed by CID.

The benefit of using an ESCi source for this study is that the ESI and APCI spectra for the same compound are obtained during one acquisition under the same conditions (mobile phase, orifice voltage, focussing lenses and collision energy), ensuring like-for-like comparisons.

5.2. EXPERIMENTAL

5.2.1. Chemicals

As described in section 3.2.1.

5.2.2. LC/MS

Data was acquired using a Waters Synapt G1 Q-TOF (quadrupole-time-of-flight) mass spectrometer (Waters Corporation, Manchester, UK) in ESI positive ion and V mode (resolution 15,000 FWHM), calibrated with sodium formate. Leucine enkephalin (MH^+ 556.277) was infused at 5 μ L/minute as the reference lock mass. Sample (10 μ L; 20 μ g/mL) was introduced via flow injection (0.5 mL/min 50/50 methanol/water 1% formic acid; no HPLC column). Methanol was chosen as the modifier as it has a lower proton affinity than the other common modifier, acetonitrile, potentially enhancing protonation of the analyte.

The following instrumental conditions were applied, they are slightly different to those described in section 3.2.2: capillary voltage 5 kV; corona discharge 5 kV; voltage extraction cone 5 V; sampling cone 35 V; transfer collision energy 10 eV; cone gas 150 L/h; desolvation gas 1800 L/h; source temperature 150°C; desolvation temperature 500°C; trap collision energy 25 to 35 eV (set on a compound by compound basis to obtain product ions spread across the mass range). The collision gas was argon.

The data acquisition settings are as follows: scan range m/z 50 to 700; scan rate 1 s, data are centroided.

5.2.3. Computational modelling

As described in section 4.2.3.

5.2.4. Assignment of product ions

As described in section 4.2.4.

5.3. RESULTS AND DISCUSSION

Qualitatively, the CID spectra were the same for all the eleven compounds which ionised by both ESI and APCI. This is consistent with the author's own experience and observations from the literature, for example the CID spectra of triacylglycerols are the same for both ESI and APCI ionised precursor ions^[270]. Also, CID spectral libraries are searchable for both ESI and APCI spectra^[271], suggesting that the spectra are generally the same irrespective of ionisation mode.

This was irrespective of whether the most basic centre of the molecule was the same in both solution and gas phase or if the most basic site was at different locations in solution and gas phase. Ionisation is achieved in APCI and ESI by different mechanisms: for ESI, ions are pre formed in solution but for APCI, ionisation occurs in the gas phase via ion-molecule charge transfer. Therefore, if the proton remained at the initial site of ionisation, the CID spectra of precursor ions produced by APCI and ESI would show differences for compounds which have differing basicities in the gas phase and in solution as charge directed fragmentation would result in different bond cleavages. The observation that the spectra did not show any differences provides evidence of proton migration from the initial site of ionisation to the dissociative site(s).

Example spectra are shown in this chapter, the remaining spectra are in shown in Appendix 3. The pKa's and gas phase basicities are shown in Appendices 1 and 2.

5.3.1. Compounds with APCI and ESI spectra are similar

5.3.1.1. *Similar Gas and liquid phase basicities*

The following compounds have the same basic centres in gas and liquid phase and also have similar ESI and APCI spectra: trimethoprim, reserpine, ziprasidone, 1,1-dimethyl biguanide, ephedrine, 1-methyl-2-pyrrolidinol, sildenafil and dofetilide. The APCI and ESI spectra are shown in Figure 5.1. The similarity of the spectra is expected as ionisation is proposed to occur on the same atom in the gas and liquid phases.

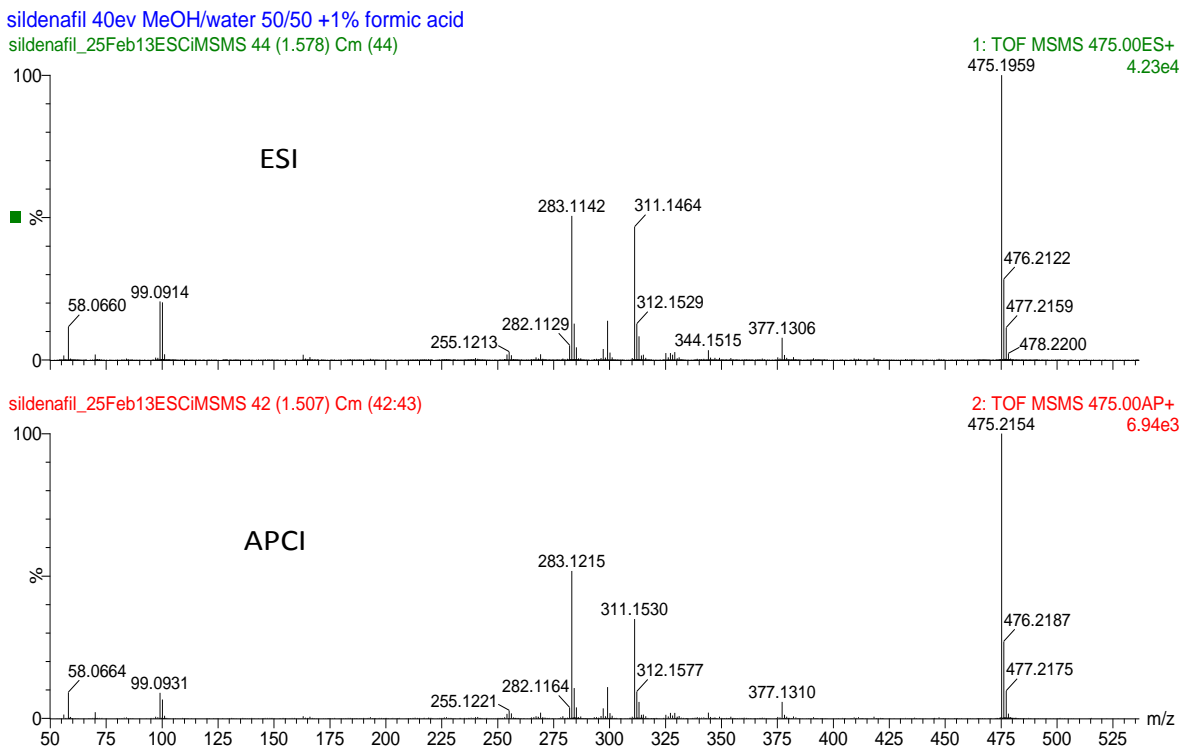


Figure 5.1 The ESI and APCI spectra of protonated sildenafil obtained with a Waters' ESCi ionisation source.

5.3.1.2. Different gas and liquid phase basicities

The following compounds have differing basic centres in gas and liquid phase but have similar ESI and APCI spectra: desipramine and maraviroc. The APCI and ESI spectra are qualitatively similar, as exemplified in Figure 5.2 for desipramine. However, the initial sites of ionisation are proposed to occur on different atoms by ESI and APCI, and this therefore suggests that the proton does not remain at the initial site of ionisation but moves to the dissociative site(s).

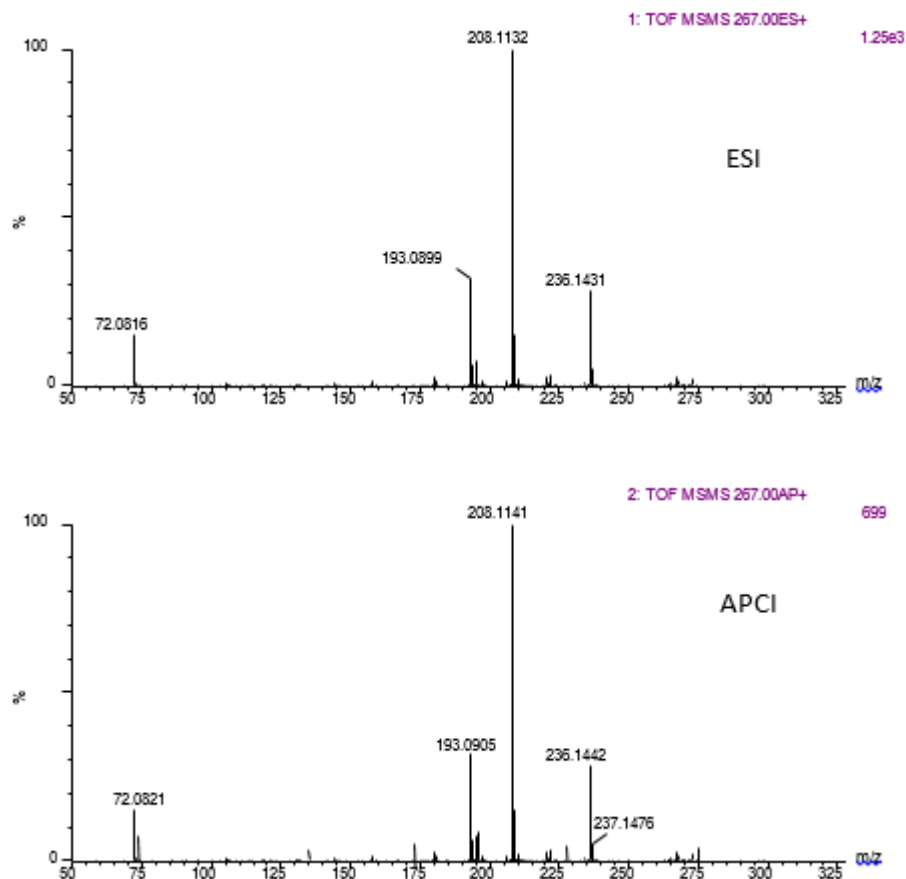


Figure 5.2 The ESI and APCI spectra of protonated desipramine obtained with the Waters' ESCi source.

5.3.1.3. Compounds for which APCI and ESI spectra differ

Cortisone, structure shown in Figure 5.3, is the only compound which showed a significant difference between its ESI and APCI spectra. Qualitatively the spectra are similar, but the amount of unfragmented precursor differed between the two ionisation techniques (Figure 5.4.). There is significantly more unfragmented precursor at m/z 361 in the APCI spectrum than in the ESI. The intensities of the base peak in both types of spectra were similar and of reasonable intensity ($4-8e^3$). This is consistent with the literature which report quantitative LC/MS assays for cortisone which utilise either ESI and APCI^[250,272-274] to obtain sufficient sensitivity.

As the collision energy was the same for both experiments the difference in the

amount of unchanged precursor ion is not due to differences in collision energy. In addition as the ionisation site is the same both in solution and gas phase, the precursor ions generated by APCI and ESI should have the same intrinsic energy. However, the fact that the APCI spectra contain significantly more unchanged precursor ion does suggest that the ESI precursor ion has a higher energy when entering the collision cell than the APCI generated ion. This increase in energy must be due to the ionisation process as the ions produced by APCI and ESI ions are proposed to be the same. It has been reported that ions produced by APCI have a higher internal energy than those produced by ESI but this comparison was made with conventional heated APCI where the extra energy is at least partly thermal^[275]. As the ESCi source is not heated, this additional thermal energy is not available to the precursor ion. The capillary voltage and corona discharge voltage were both set to 5 kV. The observation that the precursor ion generated by ESI undergoes more extensive fragmentation does suggest that the conversion of applied voltage into internal energy of the ions may be more efficient in ESI than APCI in the ESCi source.

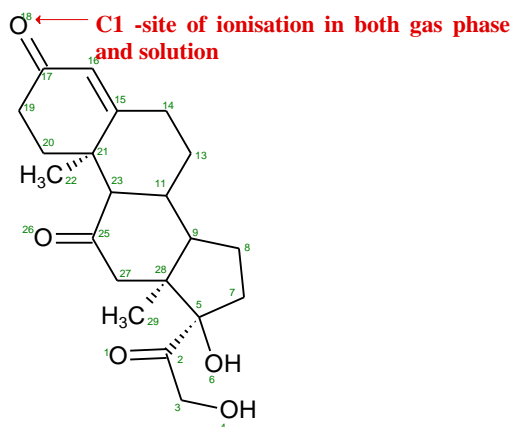


Figure 5.3. The structure of cortisone showing the most basic centre in solution and gas phase.

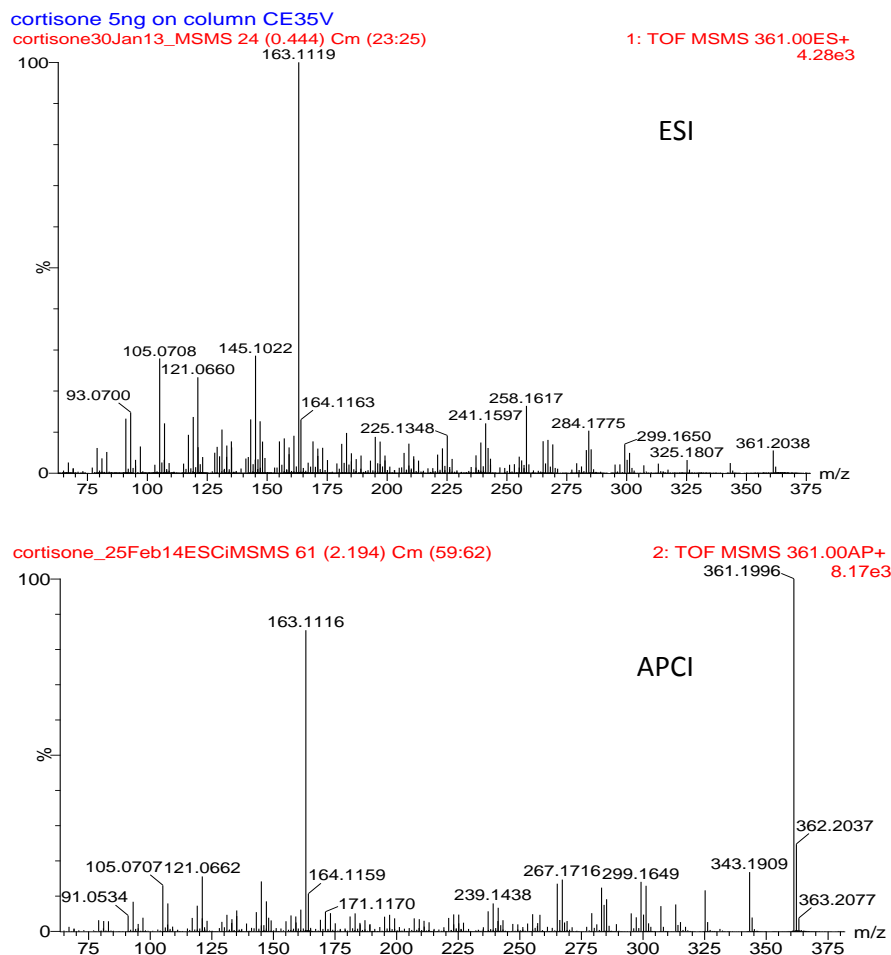


Figure 5.4 The ESI and APCI spectra of cortisone (Waters' ESCi source).

5.3.2. Relative intensity of APCI and ESI spectra

The intensity of the APCI spectrum of desipramine in Figure 5.2 is significantly less than that of the ESI spectrum. Although it is widely reported that API performs better for nonpolar compounds and ESI performs better for polar compounds with an overlap for compounds of moderate polarity (Figure 5.5)^[276], in the author's experience it is not always possible to rationalise why a compound ionise best by one ionisation method than another. Desipramine has a $\log D_{7.4}$ 1.6 suggesting that it may be ionised well by both APCI and ESI. The difference in sensitivity may be due to additional optimisation of the instrument parameters being required to maximise the APCI response; generic conditions were used for acquisition as the interest in the data was primarily qualitative.

In general, the relative response of the compounds by APCI and ESI (spectra in Appendix 3) were as expected on the basis of Figure 5.5. Reserpine ($\log D_{7.4}$ 3.9) and ziprasidone ($\log D_{7.4}$ 3.4) are relatively non-polar and respond well by APCI. Also, cortisone ($\log D_{7.4}$ 1.5) is in the medium polarity range and may be expected to give a similar response by APCI and ESI, as is observed. The polar compounds 1-methyl-2-pyrrolidinol ($\log D_{7.4}$ -1.8) and 1,1-dimethylbiguanidine ($\log D_{7.4}$ -3.4) are significantly more sensitive when analysed by ESI. Ephedrine is an anomaly, however, as it is polar ($\log D_{7.4}$ -0.8) and so would be expected to respond better by ESI but its response is similar by both ionisation methods.

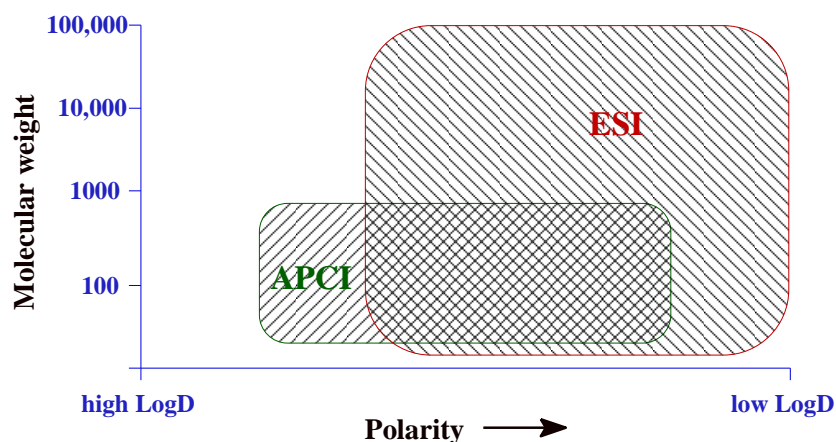


Figure 5.5 Schematic showing the polarity and molecular weight requirements for efficient APCI and ESI ionisation.

It has been reported that at the flow rate of 0.5 mLmin^{-1} such as those used in this study, diphenhydramine gives a considerably higher response with APCI than with ESI ^[269]. This flow rate dependence may be compound dependent, however, and may not reflect the situation with compounds investigated here.

5.4. CONCLUSIONS

The observation that there were no qualitative differences between the ESI and APCI spectra, irrespective of which site is more basic in the gas phase or solution, provides evidence that proton migration from the initial site of ionisation to the dissociative site(s) does occur.

Chapter 6: EFFECT OF COLLISION ENERGY ON PROTON MIGRATION

6.1. INTRODUCTION

The mobile proton model has been commonly applied to explain the fragmentation of protonated peptides. This model^[277] assumes that the peptide is initially protonated during ionisation at the most thermodynamically stable site, that is the most basic sites such as the N-terminus or basic amino acids (arginine, lysine and histidine). This proton can move to less thermodynamically, less basic, sites during ion activation to initiate charge directed fragmentation. The classic example of this behaviour exhibited by peptides and proteins, arises from the observation that the loss of ammonia from amides requires protonation on the nitrogen even though the oxygen is both the most energetically favoured protonation site, and the observed initial protonation site^[207,278]. Evidence for the validity of the mobile proton model includes the statistical analysis of product ion spectra from a large number of compounds^[279,280], the observation of the movement of deuterium across selectively deuterated peptides^[281,282] and quantum chemical modelling showing that the energy required for a proton to migrate across peptide does not present a barrier to proton movement, typically 0.5 to 1.5 eV^[213]. Proton migration was initially considered to mainly occur in larger molecules because they were considered flexible enough to accommodate internal hydrogen bonds without significant strain; cyclic intermediates are formed. For internal proton transfer to occur between proximal basic centres, the intermediate structure with the internal hydrogen bond may be strained^[213], potentially to such an extent that short distance direct proton migration may not be energetically feasible. Transfer of the proton between atoms via the formation of an ion-molecule transition state, termed 'proton-transport catalysis'^[283,284], may lower the barrier to proton movement. Molecules which have been reported to catalyse proton transfer include molecules derived from a typical mobile phase, water and ammonia. For example, the activation energy for the rearrangement of isoformyl cation to the formyl cation, requiring a 1,2-proton migration, is reduced by 500% if the proton transfer occurs via interaction with a

water molecule^[214].

Increasingly, the mobile proton is also considered a suitable model for explaining fragmentation of small molecules. There is significant evidence to support this. There are publications on a range of non-peptidic molecules which exhibit fragmentation behaviour which may be explained by charge directed fragmentation having occurred as a result of the proton moving from the initial, most basic, site of ionisation. For example, it has been reported that isobaric ions^[187,285] in the same product ion spectrum could only be explained if they were derived from precursor ions protonated on different atoms. Kaufmann^[187] studied the fragmentation of difloxacin, finding evidence, including differing effects of cone voltage on sampling of the isobaric molecular ions, that a mixture of singly charged protonated species was formed in the ion source.

There are examples of proton migration for many classes of compounds: The product ion spectrum of penicillin contains ions, resulting from cleavage of the β -lactam bond after transfer of the proton from the carbonyl to the lactam nitrogen^[286]; dibenzyl ether^[192], the pharmaceutical compounds maraviroc and dofetilide^[91,233] dialkylphosphoric acid esters^[210] and thiourea/urea compounds^[287] have all been reported to undergo proton migration prior to fragmentation. Internal proton transfer to C-3 of 4-hydroxy coumarin is not thermodynamically favourable but is required to trigger bond cleavage^[288]. *N*-(2-pyridinylmethyl) indole cleavage requires an internal proton migration to the dissociative site^[289]. Fragmentation of protonated 5-methyl benzylmethylenedihydrazine dithiocarboxylate is due to migration of both the external proton and the thiocarbamide hydrogen^[290]. The loss of CO and H₂O from 5-methylpyranopelargonidin requires migration of a proton from a carbon on the 'C' ring to one on the 'B' ring^[291]. It is not just polarised bonds that are proposed to cleave after proton migration; proton migration has also been proposed to initiate carbon-carbon bond cleavage in mono-substituted aromatic molecules^[292]. Internal transfers of larger groups are also possible; it has been reported that loss of benzene from *N*-benzylindoline results from benzyl cation transfer rather than proton transfer^[293].

Proton migration may occur by the proton overcoming the energy barrier to

movement or by proton tunnelling, a quantum process, in which it passes through the energy barrier rather than going over it^[205]. Proton tunnelling transfer times are in the nano second range^[294] and so are well within the transit times of the ion through the mass spectrometer (QTOF in this study), typically 45-57 microseconds^[255] and so quantum tunnelling is a possible mechanism for the proton's movement.

Protonation-induced bond cleavage is reported to be the result of bond lengthening, and hence weakening, resulting from conformational changes induced by protonation. Protonation needs to have occurred on the most electronegative atom in the bond which goes on to cleave, which is charge directed cleavage at the 'dissociative site'. The bond weakening (via lengthening) results from an increase in polarity of the bond by the addition of a proton to the most electronegative atom. This is consistent with the bond activation rule (BAR) proposed by Alcamí et al. ^[183-185], the presence of the proton on the electronegative centre pulls the bonding electrons toward the charged centre, reducing the electron density in the bonding region, with cleavage occurring if there is sufficient difference in electronegativity between the basic centre and the atom bonded to it. For heterolytic bond cleavage, the bond dissociation energy decreases with the increasing electronegativity difference between the bonding atoms (the reverse trend is observed for homolytic bond cleavage). If the bond becomes sufficiently elongated, it has the potential to cleave. Guy Bouchoux has suggested that structures in which a bond elongation is particularly large may be better considered an ion-neutral complex^[213].

In previous studies^[91,92,233], the authors have shown that the dissociative sites can be visualised using quantum chemistry software to flag which polarised bonds elongated to the greatest extent as a result of protonation on one of the bonding atoms. This can be used predictively as the computational analysis of the structure is only required to find the bonds with the potential to cleave. In one study,^[295] 15 compounds (98 observed bond cleavages and over 8000 bond length calculations) were used to confirm that significant bond elongation (>0.040 Å for these compounds) may be used as a descriptor for cleavage of polarised bonds during CID. In this study a 100% success rate was achieved in the prediction of polarised

bond cleavage. In addition, it has been shown that the semi-empirical computational approach AM1 (Austin Model 1) is effective in calculating these bond length changes as it gives very similar results to those obtained by DFT, the quantum computational method most often applied to mass spectral data. AM1 calculations have the advantage that they are rapid, taking seconds to minutes, compared with the hours often taken for the DFT calculations. Over-prediction of bond cleavage was only 34% in this study, a significant improvement to the over-prediction of product ion formation by many spectral interpretation software packages; one commercial package over-predicted by 200% for the same compounds^[233].

Having established the potential for using semi empirical quantum chemistry software for predicting CID fragmentation, the author wanted to investigate the potential for predicting the collision energy at which fragmentation occurs based on quantum calculations rather than experimental data. It has been reported that it is that possible to predict CE_{50} (the collision energy at which the precursor ion provides 50% of the total ion current) for compounds in a homologous series based on experimental data, for at least two members of the series as the relationship between m/z of precursor and CE_{50} is often linear. ^[161] In order to do this, a further understanding of the mechanism by which the proton moves around the molecule during CID and the relationship between proton migration and collision energy need to be established. In particular, answers to the following questions were sought:

- I. Does fragmentation resulting from protonation at sites other than the most basic increase with collision energy, suggesting that the proton starts at the most basic site and becomes more mobile as the collision energy is increased?
- II. Does the distance that a proton has to migrate affect the abundance of the product ions?
- III. Is there any correlation between the relative stabilities of the protonated precursor molecules and the collision energy at which fragmentation occurs?
- IV. Do the activation energies of internal proton transfer to the dissociative site correlate with the collision energy applied i.e. is the applied collisional energy necessary for proton migration?

- V. Does proton transfer occur at energies below the activation energy barrier, suggesting proton tunnelling?
- VI. Is there any correlation between the physicochemical properties of these molecules and the collision energies at which fragmentation occurs?

6.2. EXPERIMENTAL

6.2.1. Chemicals

As described in section 4.2.1. The 16 test compounds are listed in the tables in Appendix 5.

6.2.2. LC/MS

As described in section 3.2.2.

Spectra were acquired at collision energies of 5, 10, 15, 20, 15, 30, 35, 40, 45, 50 eV. The calculated maximum gain in internal energies at these collision energies are shown in Appendix 5.

6.2.3. Computational modelling

All 16 compounds were modelled (as described in section 5.2.3.) to determine the energy minimised structures of the molecules protonated at each potential site.

The procedures for calculating activation energies for internal proton transfer are shown in Appendix 6. The activation energies of only certain proton transfers were calculated. These were selected intramolecular proton transfers within 1, 1-dimethyl biguanidine, dofetilide, amlodipine and doxazosin. These proton transfers were chosen to represent transfer between the most basic centre in solution (and in the gas phase in the case of amlodipine) and the dissociative site leading to single bond cleavage. Single bond cleavages only were modelled to facilitate interpretation of results.

6.2.4. Assignment of product ions

As described in section 3.2.4. The assignments are listed in Appendix 7 and in Table 2.3 in Chapter 2.

6.2.5. Physicochemical properties

The physicochemical properties, with the exception of dipole moment, were obtained via the RSC Chemspider website (<http://www.chemspider.com>) using the ACD predicted values. The values were those predicted at pH 7.4. The value of the dipole moment was taken from the DFT energy minimised structures calculated as described in 5.2.3.

6.3. RESULTS

The results obtained were analysed in terms of answering the question posed in the introduction to this chapter:

- I. Does fragmentation resulting from protonation at sites other than the most basic site increase with collision energy? *and*
- II. Does the distance that a proton has to migrate affect the abundance of the product ions?

Tables 1 to 5 show the product ions formed at the collisions energies stated (in the range 5 eV to 50 eV) for five of the test compounds. These are based on the ESI spectra only. The distance 'hopped' by the proton from the most basic site is also stated. The highest mass in each table is the $[M+H]^+$ ion. The ions derived from the protonation at the most basic centre are highlighted in yellow.

Table 6.1 The percentage abundance of product ions of protonated desipramine at the stated collision energies.

Ion (m/z)	Collision energy (eV)										No. atoms between most basic and dissociative site
	5	10	15	20	25	30	35	40	45	50	
267	100%	80%	100%	30%	10%	0%	0%	0%	0%	0%	n/a
236	0%	10%	10%	40%	30%	10%	10%	0%	0%	0%	0
208	0%	5%	10%	100%	100%	100%	100%	30%	10%	30%	0
193	0%	0%	0%	20%	20%	90%	90%	100%	100%	100%	4
72	5%	10%	30%	100%	12%	10%	10%	5%	5%	2%	4

Table 6.2 The percentage abundance of product ions of protonated dofetilide at the stated collision energies.

Ion (m/z)	Collision energy (eV)										No. atoms between most basic and dissociative site
	5	10	15	20	25	30	35	40	45	50	
442	100%	100%	100%	100%	100%	40%	20%	0%	0%	0%	n/a
255	0%	15%	50%	60%	60%	25%	20%	0%	0%	0%	3
198	0%	20%	100%	50%	0						
179	0%	5%	20%	30%	25%	10%	10%	0%	0%	0%	3
120	0%	0%	20%	20%	20%	70%	45%	100%	70%	100%	6
119	0%	0%	25%	40%	35%	60%	55%	70%	60%	50%	6
118	0%	0%	0%	15%	10%	40%	30%	70%	50%	60%	6
91	0%	0%	0%	0%	0%	0%	5%	20%	15%	30%	3,7

Table 6.3 The percentage abundance of product ions of protonated doxazosin at the stated collision energies.

Ion (m/z)	Collision energy (eV)										No. atoms between most basic and dissociative sites
	5	10	15	20	25	30	35	40	45	50	
452	100%	100%	100%	100%	100%	100%	100%	40%	20%	0%	n/a
344	0%	0%	5%	5%	85%	85%	85%	100%	95%	40%	8,10
326	0%	0%	0%	0%	10%	10%	10%	20%	20%	15%	8,10
310	0%	0%	0%	0%	0%	0%	0%	15%	20%	30%	5,8,10
290	0%	0%	0%	0%	0%	0%	0%	50%	60%	30%	4
247	0%	0%	0%	0%	20%	20%	20%	95%	100%	100%	4
231	0%	0%	0%	0%	0%	0%	0%	30%	40%	85%	4,5
221	0%	0%	0%	0%	10%	10%	10%	30%	40%	30%	2

Table 6.4 The percentage abundance of product ions of protonated maraviroc at the stated collision energies.

Ion (<i>m/z</i>)	Collision energy (eV)										No. atoms between most basic and dissociative sites	
	5	10	15	20	25	30	35	40	45	50		
514	100%	100%	100%	80%	50%	10%	0%	0%	0%	0%		n/a
389	0%	80%	95%	100%	100%	90%	90%	10%	10%	0%		4
280	0%	10%	10%	90%	95%	100%	100%	100%	100%	70%		0
117	0%	0%	0%	0%	5%	45%	35%	70%	65%	100%		4
106	0%	0%	0%	0%	3%	35%	25%	50%	50%	70%		4

Table 6.5 The percentage abundance of product ions of protonated amlodipine at the stated collision energies. The ions at *m/z* 170 and 142 are rearrangement products potentially formed by several roots and there the number of atoms 'hopped' by the proton is variable and so is designated 'n/a' in the Table.

Ion (<i>m/z</i>)	Collision energy (eV)										No. atoms between most basic and dissociative sites	
	5	10	15	20	25	30	35	40	45	50	Liquid	Gas
	409	100%	80%	45%	15%	10%	0%	0%	0%	0%	n/d	n/a
377	0%	40%	40%	70%	60%	20%	10%	0%	0%	n/d	10	6
320	0%	10%	10%	20%	30%	30%	5%	5%	0%	n/d	3,8	5
294	30%	85%	65%	70%	70%	30%	20%	5%	0%	n/d	3,8	5
288	0%	0%	0%	0%	20%	45%	30%	20%	15%	n/d	7,8,9,10	5,6,8
238	40%	100%	100%	85%	100%	40%	30%	0%	0%	n/d	7,8,9	6,8,10
220	0%	10%	0%	50%	30%	70%	60%	30%	50%	n/d	7,8,9	6,8,10
208	0%	10%	5%	65%	50%	100%	100%	90%	100%	n/d	7,8,9	6,8,10
206	0%	35%	10%	100%	55%	100%	90%	40%	60%	n/d	5	6
170	0%	8%	0%	35%	20%	85%	70%	65%	80%	n/d	n/a	n/a
142	0%	0%	0%	5%	0%	60%	30%	30%	65%	n/d	n/a	n/a

Table 6.6 The percentage abundance of ions of protonated 1,1-dimethyl biguanidine at the stated collision energies.

Ion (m/z)	Collision energy (eV)										No. atoms between most basic and dissociative sites
	5	10	15	20	25	30	35	40	45	50	
130	100%	100%	100%	100%	100%	60%	50%	10%	n/d	n/d	n/a
113	0%	0%	10%	40%	80%	90%	100%	50%	n/d	n/d	4
88	0%	0%	8%	40%	40%	50%	60%	40%	n/d	n/d	2
85	0%	0%	8%	40%	50%	50%	60%	30%	n/d	n/d	2
71	3%	20%	8%	50%	50%	100%	100%	100%	n/d	n/d	2
68	0%	0%	0%	10%	10%	30%	15%	30%	n/d	n/d	1,4
60	10%	40%	18%	60%	20%	30%	10%	20%	n/d	n/d	2

Table 6.7. The percentage abundance of ions of protonated sildenafil at the stated collision energies.

Ion (m/z)	Collision energy (eV)										No. atoms between most basic and dissociative site
	5	10	15	20	25	30	35	40	45	50	
475	100%	100%	100%	100%	100%	100%	100%	40%	10%	0%	n/a
377	0%	0%	0%	0%	0%	2%	5%	8%	5%	0%	3
311	0%	0%	0%	0%	0%	10%	20%	20%	20%	8%	5
299	0%	0%	0%	0%	0%	5%	5%	20%	20%	20%	5,9
283	0%	0%	0%	0%	0%	0%	20%	100%	100%	100%	5,9
100	0%	0%	0%	0%	0%	20%	20%	20%	18%	5%	3
99	0%	0%	0%	0%	0%	18%	18%	20%	18%	8%	3

The product ion intensity data in these tables show that fragmentation at sites other than the most basic centre does not increase with collision energy i.e. initial fragmentation is not due to the protonation at the most basic atom followed by the proton then moving onto other atoms as the collision energy increases. For example, none of the product ions listed in Tables 3, 4, 5 and 6 (doxazosin, amlodipine, 1,1-dimethyl biguanidine and sildenafil) result from protonation on the most basic sites in either gas phase or solution. This suggests that intramolecular proton migration occurs freely and is not collision energy dependent or kinetically hindered.

It has been reported that both proton migration and the mechanism of fragmentation are independent of collision energy during the SID (surface-induced

dissociation) of the peptide octoglycine^[296]. The route of fragmentation was reported to be dependent on the number of atoms which the proton has to 'hop' to reach the dissociative site. In order to see if the distance of proton migration did correlate with the abundance of product ions produced in our non-peptidic molecules, the number of atoms 'hopped' for five compounds is listed against percentage abundance in Tables 2 to 5. The data for these five compounds does not show any correlation between product ion abundance and distance in terms of atoms travelled. This lack of correlation may differ from the observations made for octoglycine because, for octoglycine, the same bond type is being cleaved throughout whereas the molecules investigated in this manuscript undergo fragmentation via cleavage of different bond types. Also, SID and CID do tend to give similar product ions but the intensity of these ions differ between the two techniques^[297] suggesting there are differences between the mechanism of the two techniques.

The lack of dependence of the charge directed fragmentation on the distance the proton have moved from its initial position is not kinetically limited.

III. Is there any correlation between the relative stabilities of the protonated precursor molecules, the product ions formed and the collision energy at which fragmentation occurs?

Potentially, the stability of the protonated precursor molecule may affect its fragmentation in one of two ways: less stable protonated molecules may be more likely to fragment; alternatively, considering the kinetics, the more stable the molecule, the longer it has for proton-induced fragmentation to occur. For the compounds investigated in this study, the relative stability of the molecules protonated at different sites are compared to the collision energy at which fragmentation occurs and the abundance of the product ions. An example, maraviroc, is shown in Table 6.8. The results of the other compounds are in Tables 6.9 to Table 6.14. Maraviroc has different basic centres in the gas and liquid phase; for completeness, both protonation in gas phase and in solution are considered. The

product ions at m/z 389 and m/z 280 are both base peaks in the CID spectra. The ion at m/z 389 is formed as a result of protonation at a significantly less stable site, C3; less stable by 42 kcal mol⁻¹ in solution and 54 kcal mol⁻¹ in the gas phase. The ion at m/z 280, however, results from protonation at C4, the most thermodynamically stable site in solution or a moderately less stable site (by 12 kcal mol⁻¹) in gas phase. It should also be noted that m/z 389 is most abundant at a lower collision energy than that of the collision energy required for m/z 280 to be maximal, in spite of m/z 389 being formed via a significantly less energetically favourable protonation. This suggests that the additional collision energy is not required to allow the proton to move to thermodynamically less favourable sites.

Therefore, it may be concluded the relative stabilities of the protonated precursor molecules do not affect their CID fragmentation. Similar observations were made for the other six molecules. From Table 6.9 to Table 6.14 it may be seen that there is no correlation between the relative stabilities of the precursor ions, the product ions formed or the collision energy required to form these ions.

Table 6.8 The relative energies of maraviroc cations protonated at the initial ionisation site(s) compared to the cations formed by protonation at the dissociative sites yielding product ions at the collision energies stated.

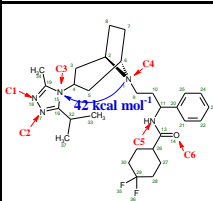
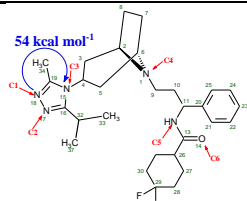
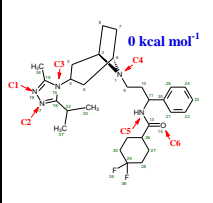
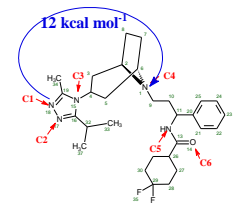
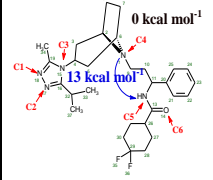
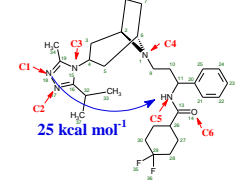
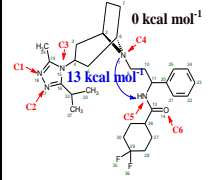
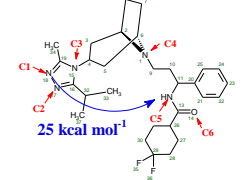
Ion abundance (25 eV collision energy)	Product ion nominal mass (m/z)	Dissociative site (cation no.)	Relative energy		Ion first observed		Ion most abundant	
			Between ionisation site in solution and dissociative site	Between gas phase ionisation site in and dissociative site	Collision Energy (eV)	Calculated δ internal energy (kcal mol ⁻¹)	Collision Energy (eV)	Calculated δ internal energy (kcal mol ⁻¹)
100%	389	C3			10	17	20	33
95%	280	C4			15	25	30	50
5%	117	C4, C5			25	42	50	83
3%	106	C4, C5			25	42	50	83

Table 6.9 The relative energies of desipramine cations protonated at the initial ionisation site compared to the cations (s) formed by protonation at the dissociative site yielding product ions at the collision energies stated.

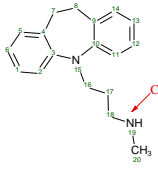
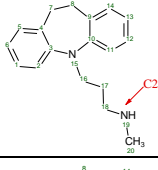
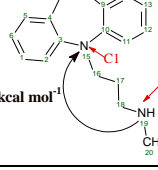
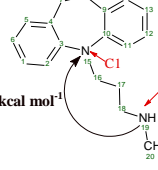
Ion abundance (25 eV collision energy)	Product ion nominal mass (<i>m/z</i>)	Dissociative site (cation no.)	Relative energy between ionisation site in solution/gas phase and dissociative site	Ion first observed		Ion most abundant		No. atoms between most basic and dissociative site
				Collision Energy (eV)	Calculated δ internal energy (kcal mol ⁻¹)	Collision Energy (eV)	Calculated δ internal energy (kcal mol ⁻¹)	
30%	236	C2		10	30	20	61	0
100%	208	C2 & carbon-carbon cleavage		10	30	20	61	0
20%	193	C1		20	61	40	122	4
12%	72	C1		5	15	20	61	4

Table 6.10 The relative energies of doxazosin cations, protonated at the initial ionisation site compared to the structures formed by protonation at the dissociative site yielding product ions at the collision energies stated.

Ion abundance (25 eV collision energy)	Product ion nominal mass (m/z)	Dissociative site (cation no.)	Relative energy between ionisation site in solution/gas phase and dissociative site	Ion first observed		Ion most abundant	
				Collision Energy (eV)	Calculated δ internal energy (kcal mol ⁻¹)	Collision Energy (eV)	Calculated δ internal energy (kcal mol ⁻¹)
85%	344	C9, C10		15	28	40	75
10%	326	C9, C10		25	47	40	75
0%	310	C3, C9, C10		40	75	50	94
0%	290	C7		40	75	45	84
20%	247	C7		25	47	45	84
0%	231	C3, C7		40	75	50	94
10%	221	C6		25	47	45	84

Table 6.11 The relative energies of amlodipine cations protonated at the initial ionisation site compared to the cations (s) formed by protonation at the dissociative site yielding product ions at the collision energies stated.

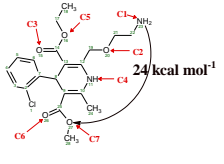
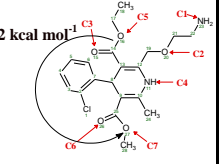
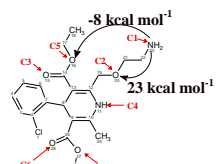
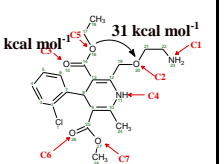
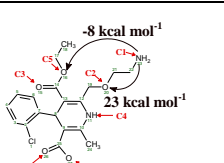
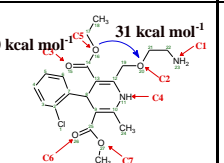
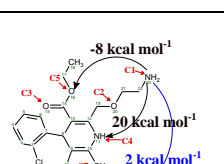
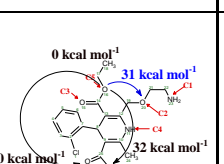
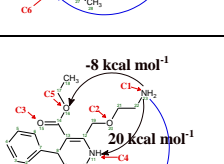
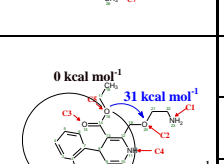
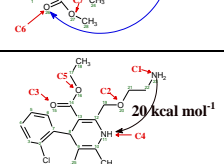
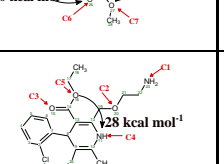
Ion abundance (25 eV collision energy)	Product ion nominal mass (<i>m/z</i>)	Dissociative site (cation no.)	Relative energy		Ion first observed		Ion most abundant	
			Between ionisation site in solution and dissociative site	Between gas phase ionisation site in and dissociative site	Collision Energy (eV)	Calculated δ internal energy (kcal mol ⁻¹)	Collision Energy (eV)	Calculated δ internal energy (kcal mol ⁻¹)
60%	377	C7			10	20	20	41
30%	320	C2, C5			10	20	25	51
70%	294	C2, C5			5	10	10	20
20%	288	C2, C5, C6, C7			25	51	30	61
100%	238	C4, C5, C6			5	10	10	20
30%	220	C4, C5, C6			10	20	30	61
50%	208	C4, C5, C6			10	20	30	61
55%	208	C4 & carbon-carbon cleavage			10	20	30	61
20%	170	n/a	n/a	n/a	10	20	30	61
0%	142	n/a	n/a	n/a	20	41	45	92

Table 6.12 The relative energies of sildenafil cations, protonated at the initial ionisation site(s), compared to the structures formed by protonation at the dissociative sites yielding product ions at the collision energies stated.

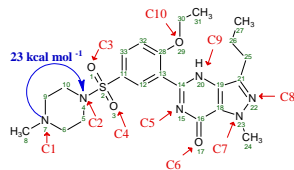
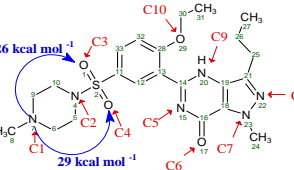
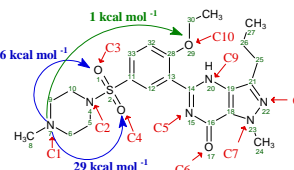
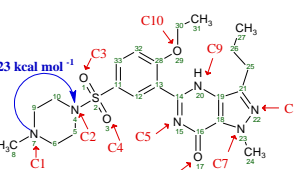
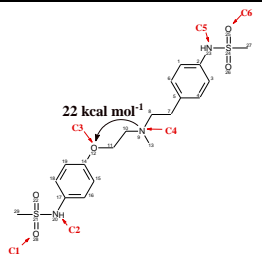
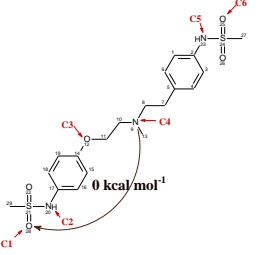
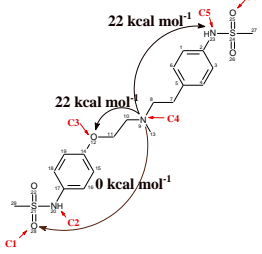
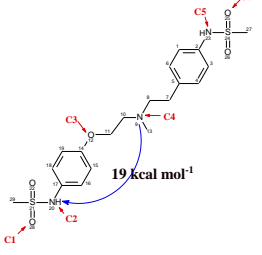
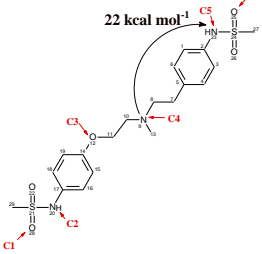
Ion abundance (25 eV collision energy)	Product ion nominal mass (<i>m/z</i>)	Dissociative site (cation no.)	Relative energy between ionisation site in solution/gas phase and dissociative site	Ion first observed		Ion most abundant	
				Collision Energy (eV)	Calculated δ internal energy (kcal mol ⁻¹)	Collision Energy (eV)	Calculated δ internal energy (kcal mol ⁻¹)
0%	377	C2		30	52	40	69
0%	311	C3, C4		30	52	35	63
0%	299	C3, C4, C10		30	52	40	69
0%	283	C3, C4, C10		35	63	40	69
0%	100	C2		30	52	35	63
0%	99	C2		30	52	40	69

Table 6.13 The relative energies of 1,1-dimethylbiguanide cations, protonated at the initial ionisation site(s), compared to the structures formed by protonation at the dissociative sites yielding product ions at the collision energies stated.

Ion abundance (25 eV collision energy)	Product ion nominal mass (<i>m/z</i>)	Dissociative site (cation no.)	Relative energy between ionisation site in solution/gas phase and dissociative site	Ion first observed		Ion most abundant	
				Collision Energy (eV)	Calculated δ internal energy (kcal mol ⁻¹)	Collision Energy (eV)	Calculated δ internal energy (kcal mol ⁻¹)
80%	113	C2 or C5		15	81	35	189
40%	88	C1		15	81	35	189
50%	85	C3 or C4		15	81	35	189
50%	71	C1		5	27	30	162
10%	68	C2 or C5		20	108	30	162
20%	60	C1		5	27	20	108

Table 6.14 The relative energies of dofetilide cations, protonated at the initial ionisation site(s), compared to the structures formed by protonation at the dissociative sites yielding product ions at the collision energies stated.

Ion abundance (25 eV collision energy)	Relative energy between ionisation site in solution/gas phase and dissociative site	Dissociative site (cation no.)	Relative energy between ionisation site in solution/gas phase and dissociative site	Ion first observed		Ion most abundant	
				Collision Energy (eV)	Calculated δ internal energy (kcal mol ⁻¹)	Collision Energy (eV)	Calculated δ internal energy (kcal mol ⁻¹)
60%	255	C3		10	19	25	48
100%	198	C1		10	19	15	29
25%	179	C1, C3, C5		10	19	20	38
20%	120	C2, C4		15	29	40	76
35%	119			15	29	40	76
10%	118			20	38	40	76
0%	91	C5, carbon-carbon bond cleavage		35	67	50	95

- IV. Do the activation energies of internal proton transfer to the dissociative site correlate with the collision energy applied i.e. is the applied collisional energy necessary for proton migration? and**
- V. Does proton transfer occur at energies below the activation energy barrier, suggesting proton tunnelling?**

The activation energies for certain internal proton transfers within 1,1-dimethyl biguanidine, dofetilide, amlodipine and doxazosin are shown in Table 6.9. These activation energies were of narrow range, 2 to 4 eV, and were lower than the collision energies required to observe the product ions arising from these proton transfers. Therefore, it may be concluded that internal proton migration does not offer a barrier to CID fragmentation and internal proton movements are independent of the applied collision energy. Thus there is no evidence of proton tunnelling. This is consistent with literature reports that the barriers to proton migration are lower than those to fragmentation in peptides^[298]. Several protonated forms of *N*-acetyl-*O*-methyl proline were calculated to have low barriers to internal proton migration, maximum 2.5 eV^[189]. The energy barrier to intramolecular proton transfer in cationised glycine and its derivatives is less than 0.1 eV^[299], whilst in tryptophan and its derivatives the activation energy for internal proton migration was reported to be approximately 0.7 eV^[300].

The transition structures modelled were often strained to achieve proton transfer, via hydrogen bond formation, over relatively short distances. It is possible, therefore, that the actual proton transfer may occur via an ion-neutral complex, potentially involving a mobile phase component molecule such as water^[214]. Potential ion-neutral complexes were not modelled in this study as direct internal hydrogen transfer was calculated to be energetically favourable at collision energies of greater than 5 eV and so possible existence of a lower energy mode of proton transfer does not contradict the conclusion that proton movement is Independent of collision energy.

Table 6.15 The activation energies for the internal proton transfer from the starting and final cations of 1,1-dimethyl biguanidine, dofetilide, amlodipine and doxazosin. The activation energies for the internal proton transfers were calculated in both directions. The collision energies at which the product ions resulting from the stated proton transfers are observed are also listed.

Compound	Starting cation most basic in solution (Aq) and/or gas Phase (GP)	Direction of reaction	Energies (eV)						
			Starting cation	Transition state	Final cation	Activation energy	Collision energy at which product ion observed		
1,1-Dimethyl biguanidine	Aq/GP	Forward	C4	-11788.95	-11784.98	C1	-11786.82	3.97	5
1,1-Dimethyl biguanidine	Aq/GP	Back	C1	-11786.82	-11784.85	C4	-11788.95	-4.10	5
Dofetilide	Aq/GP	Forward	C4	-56525.21	-56522.71	C3	-56524.25	2.50	10
Dofetilide	Aq/GP	Back	C3	-56524.25	-56522.79	C4	-56525.21	-2.42	10
Amlodipine	Aq	Forward	C1	-46896.75	-46893.45	C7	-46895.72	3.30	10
Amlodipine	Aq	Back	C7	-46895.72	-46894.15	C1	-46896.75	-2.60	10
Amlodipine	GP	Forward	C5	-46897.1	-46893.18	C7	-46895.72	3.92	10
Amlodipine	GP	Back	C7	-46895.72	-46894.15	C5	-46897.1	-2.95	10
Doxazosin	Aq/GP	Forward	C5	-41955.16	-41951.24	C6	-41954.48	3.92	25
Doxazosin	Aq/GP	Back	C6	-41954.48	-41951.21	C5	-41955.16	-3.95	25

VI. Is there a correlation between the physicochemical properties of these molecules and the collision energies at which fragmentation occurs?

Table 6.16 shows the physicochemical properties of all sixteen compounds together with the CE_{50} values quoted to the nearest 5 eV. Appendix 8 contains graphical plots of each physicochemical property against the CE_{50} . These graphs do not show any significant correlation between the physicochemical properties and collision energy. These observations are consistent with a literature report based on determining the CE_{50} 's of 56 compounds which found a similar lack of correlation^[152]. Therefore, it may be concluded the properties of the molecule which dictate the collision energy at which it fragments are interdependent and so individual physicochemical properties may not be used to predict optimal collision energies.

Table 6.16 Physicochemical properties of the test compounds compared to the CE₅₀ (the collision energy at which the survival yield is 50%; the values quoted are rounded up or down to the nearest 5 eV).

Compound	[M+H] ⁺ (Da)	pKa most basic centre	Log P	Log D _{7.4}	Polarizability	Dipole moment (debye)	HBD	HBA	Number of rings	Number rotatable bonds	CE ₅₀ (eV)
1-Methyl-2-pyrrolidinol	n/a	8.6	0.3	-1.8	11.4	1.3	1	2	1	0	n/a
1,1- Dimethyl biguanidine	20	12.3	0.0	-3.4	13.0	2.4	0	2	0	0	35
Ephedrine	10	9.5	1.3	-0.8	49.7	3.0	2	2	1	3	10
Desipramine	10	10.0	3.9	1.6	31.7	0.8	1	2	3	4	20
Trimethaprim	25	7.2	1.3	1.0	29.7	2.0	2	7	2	5	30
Sulpiride	20	8.4	0.2	-1.0	36.2	5.5	2	5	2	6	40
Cortisone	20	-3.2	2.1	1.5	42.3	6.5	1	5	4	4	30
Trichlormethiazide	5	-4.1	-2.8	0.3	-1.8	3.6	3	5	2	2	20
Amlodipine	5	9.5	1.6	1.9	-3.4	4.2	2	5	2	10	15
Ziprasidone	25	7.1	4.3	3.4	45.0	3.0	1	4	5	4	30
Dofetilide	15	9.0	0.2	0.8	46.1	4.5	2	6	2	0	30
Doxazosin	20	7.1	2.1	1.5	46.6	6.4	1	9	5	4	40
Sildenafil	35	5.9	-1.8	1.8	51.2	9.9	0	10	4	11	40
CEN025-014	25	8.4	0.7	4.6	57.4	6.0	1	6	5	7	30
Maraviroc	10	9.4	3.6	1.1	55.6	7.8	1	4	5	8	50
Sampatrilat	15	10.4	-2.4	1.0	57.5	3.9	17	13	1	16	40
Reserpine	35	7.3	3.5	3.9	64.3	3.7	1	8	6	10	40

6.3.1. Interesting observation on fragmentation of desipramine.

It should be noted that the ions at m/z 72 and m/z 193 (Figure 6.1) represent the different products of the same bond cleavage (i.e. N15-C16). However m/z 72 is the result of heterolytic bond cleavage and m/z 193 results from homolytic cleavage, resulting in a radical ion (Appendix 7, Table 7.13).

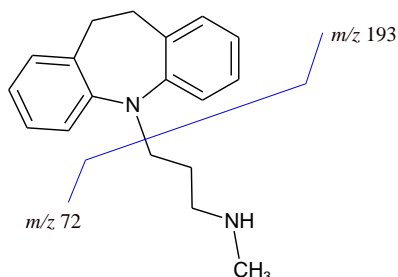


Figure 6.1 The product ions of desipramine, m/z 72 and m/z 193, formed by cleavage of N15 and C16.

The ion at m/z 72 was the first detected ion at a low collision energy of 5 eV and became the major ion at a collision energy of 10eV. However, the ion at m/z 193 was not present in the spectra until the collision energy is increased to 20 eV. Heterolytic bond cleavage requires more energy than homolytic bond cleavage due to the additional energy needed for charge separation^[213,301]. Therefore, it may be expected that the homolytic product ion at m/z 193 would be the first to be detected at the lower collision energy. This is not the case, suggesting that it is the stability of the product ion at m/z 72 formed by heterolytic cleavage which makes this fragmentation route most favoured at low collision energies. Therefore, m/z 72 is likely to be the product of a rearrangement rather than the linear structure drawn in Table A-7.13.

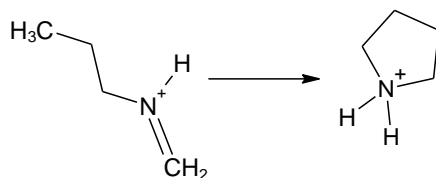


Figure 6.2 The product at m/z 72 formed by heterolytic cleavage of N15-C1

6.4. CONCLUSIONS

There is clear evidence from the literature, as discussed in the introduction, that proton migration from the initial site of protonation to a ‘dissociative site’ may be required to initiate charged direct fragmentation in small (<1000 Da) molecules. For the molecules investigated in this study, the proton is fully mobile in the range 5 to 50 eV collision energy. The evidence for this is that proton migration was shown to be independent of the collision energy applied:

- Fragmentation at sites other than the most basic site does not increase with collision energy i.e. initial fragmentation is not due to the protonation at the most basic atom followed by proton migration onto other atoms as the collision energy increases.
- There appears to be no relationship between the stability of the precursor cations, the nature and abundance of product ions and the collision energy at which fragmentation occurs. This may be expected if the proton is fully mobile at collision energies as low as 5 eV, rendering the stability of individual protonated species less relevant.
- The calculation activation energies for intramolecular proton migration leading to single bond cleavage were significantly lower than 5 eV.

Therefore, it may be concluded that the protonation induced bond elongation is required for fragmentation during CID; however on its own is not sufficient to trigger bond cleavage. Fragmentation is collision energy dependent but proton migration does not depend on collision energy. There are two possible

explanations for this:

- In addition to stretching the bond, its vibrational energy must also be increased for it to cleave. Applying a voltage across the collision cell supplies this additional molecular internal energy.
- Bond elongation alone is sufficient to initiate cleavage but does so at a rate greater than the residence time of the ion in the collision cell. Application of the collision energy leads to a 'kinetic shift' leading to an increase in reaction rate allowing decomposition to occur within the experimental conditions^[145]. Gregg et al. modelled the fragmentation of ions by surface-induced dissociation (SID). SID may be considered as analogous to CID with a target gas of infinite mass. They calculated the activation energy for transfer of a proton from the amide nitrogen to the carbonyl oxygen to initiate amide cleavage to be 0.1 to 0.2 eV by DFT and 0.8 eV by AM1. In this simulation, 90% fragmentation was achieved in 1.5 ps at 110 eV whereas it took 2.5 ps to reach the same extent of fragmentation at 30 eV. Thus the additional collision energy produced a kinetic shift.

Thus, the role of the applied collision energy in CID fragmentation appears to be to increase the internal energy of the analyte molecules and not to enable proton migration. Therefore, it does not appear to be feasible to predict the collision energy at which fragmentation occurs by using quantum chemistry calculations to determine the energy required to mobilise the proton. In addition, individual physicochemical properties did not correlate with the collision energies at which fragmentation occurred and therefore cannot be used predictively.

Chapter 7: CONCLUSIONS AND FUTURE WORK

The aim of this thesis was to test the hypothesis that the bonds which cleaved during CID MSMS of cations may be predicted by modelling protonation-induced bond lengthening within the precursor ion using quantum chemistry software. A pilot study was undertaken on the antiarrhythmic agent, dofetilide and four methylated analogues. The modelling approach used for this work was DFT (B3LYP, basis set 6-31G**). The reason for selecting DFT is that it is considered a 'gold standard' approach delivering high accuracy thermodynamic data. It is also the computational approach most mentioned in the literature in connection with mass spectra; although these literature studies differ from the work in this thesis in that DFT is usually applied to determine the energy profiles for formation of product ions, not calculating bonds lengths.

The product ion spectra of dofetilide and its analogues are consistent with fragmentation having occurred via charge directed cleavage; one of the major ions formed after migration of the proton from its initial site of ionisation, the tertiary nitrogen, to the phenolic oxygen.

The calculated bond length changes in this dofetilide study supported the initial hypothesis. Bond elongation was successful in determining which bonds cleaved to form the product ions. False negatives were not produced; all the bonds which cleaved were predicted to elongate significantly as a results of protonation; none of the cleavages observed were for bonds which were calculated to contract or remain the same. False positives, however, were observed; some bonds which elongated were not observed to cleave. The effect of introducing additional methyl groups into the dofetilide template suggests that steric and kinetic factors may also influence fragmentation.

There is a potential for these type of quantum chemistry calculations to be used predictively as an aid for the interpretation of mass spectra, as they highlight the centres around which charge-direct cleavage is likely to occur, i.e. the sites at which protonation has the greatest effect on bond lengthening. Compared to the conventional approach reported in the literature in which the activation energies for formation of the product ions are calculated by DFT in order to determine the most energetically favourable fragmentation routes, this approach is computationally economical; only bond length changes need to be calculated. Also, calculation of the

gas phase basicities is not required to successfully identify sites of bond cleavage as the proton may move from the initial ionisation site

In addition, this approach limits the number of predicted possible product ions to only those which are thermodynamically likely in terms of bond elongation. In particular, quantum chemistry methods may be applied to improve software packages designed to assist with the assignment of product ions, by both contributing to a greater understanding of the 'rules' of CID fragmentation and also offering the possibility of incorporating quantum descriptors, such as bond lengths, into interpretational software. The only disadvantage to using DFT for calculating bond lengths which may limit its appeal for routine use by mass spectrometrists, is the time it takes for these high accuracy calculations to be completed. For example the dofetilide structures took approximately 3 hours per structure (i.e for the six protonated and the neutral molecules, the total time was 21 hours).

In order to see if the hypothesis can be successfully applied to a wider range of molecules a study was undertaken in order to obtain a larger data set. Sixteen pharmaceutically active compounds (molecular weights 101 to 608 Da) were selected on the basis of their range of functional groups and availability. In this study, the positive product ion spectra were obtained for all sixteen compounds and quantum chemistry software used to calculate bond length changes resulting from protonation at each of the heteroatoms. Both DFT and the semi-empirical quantum chemistry approach AM1 were used to perform these calculations.

In total, 102 bond cleavages were observed and over 8000 bond lengths calculated. As in the case of dofetilide, the CID spectra are consistent with the product ions being formed by charge direct cleavage, sometimes initiated by migration of the proton to a less thermodynamically likely site.

The results obtained fully support the original hypothesis; elongations of polarised bonds calculated to be significant (greater 0.039 Å calculated by AM1) corresponded to the bonds which were observed to cleave in the CID product ion spectra. This represented 100% success rate in the prediction of polarised bond cleavage for these 16 compounds. In addition, over-prediction of bond cleavage was only 34% overall, a significant improvement over the over-prediction of product ion formation by many commercial spectral interpretation software packages.

The same bonds calculated to elongate significantly by DFT were also predicted

by AM1. This may be because only large bond length changes are of interest so the high accuracy of DFT is not required. The ability to use AM1 calculations make this approach accessible to mass spectrometrists as the calculations are rapid (2 minutes total for calculation on all seven protonated and neutral molecules of dofetilide) and do not require a high specification computer. It also makes its incorporation into interpretive software packages more feasible.

There was one type of bond cleavage which was not successfully predicted on the basis of bond elongation, and that was the cleavage of non-polarised carbon-carbon bonds, even if the charge on one of the bonding carbons were modelled. For unpolarised bonds, it may be that the stabilities of the product ions dictate fragmentation pathways.

Having established that AM1 may be successfully applied to predict polarised bond cleavage in cations, a study was undertaken to investigate if this approach would also work for anions. Four of the compounds studied were taken from the set of sixteen pharmaceutical compounds to allow direct comparison with the cation results. In addition, three carboxylic acids and one phosphate were modelled. For this anion modelling AM1 only was used. This was because AM1 proved to be successful in our studies to date in modelling bond length changes in cations and, also, *in silico* modelling of anions is more challenging than modelling cations or neutral species, but AM1 models anions more accurately than DFT.

It was found that bond length change calculations are not effective in predicting CID bond cleavage of anions formed by deprotonation for these compounds. Only 48% of the bonds observed to cleave became significantly longer after deprotonation. Possibly, the conformational changes are not being effectively modelled by AM1 or the mechanism for fragmentation, in negative ion CID, differs significantly from that of positive ion CID. AM1 has been reported to model adequately for anions^[260–263], therefore it may be the latter which is the explanation for bond elongation not predicting bond cleavage in negative ions.

Having established that AM1 has the potential to be used to aid mass spectral interpretation by identifying the 'dissociative' sites, i.e. the atoms around which the bonds are lengthened significantly as a result of protonation on these atoms, further investigations were made into the nature of the proton migration which initiates some fragmentation.

In order to provide additional evidence for proton migration during CID fragmentation, product ion spectra were obtained for the sixteen pharmaceutical compounds after ionisation by both APCI and ESI using an ESCi source. Not all compounds gave APCI spectra under the conditions of analysis used. Of those which gave both APCI and ESI spectra, the product ion spectra were qualitatively similar, even for the compounds which have different basic centres in the gas phase and solution. Thus it may be inferred that the proton must have moved from the initial site of ionisation.

Next, the effect of collision energy on proton movement and the distances the proton has to migrate were studied. It was found that the activation energy of internal proton migration was calculated (by DFT) to be generally low, significantly less than 5 eV; hence it appears that the proton is fully mobile across the molecule at collision energies of 5 eV or greater. For the molecules studied here, little or no fragmentation was observed at 5 eV. Therefore, protonation alone does not lead to fragmentation; an input of internal energy, in the form of an applied collision voltage, is also required, probably to increase the bonds' vibrational energies and/or increase the rate of decomposition of the molecule to within its residence time in the collision cell. In summary, thermodynamics predicts that the proton is able to range freely across the molecule and initiate fragmentation at sites where it causes the greatest bond elongations (and hence weakening), if the molecule also has sufficient internal energy to enable fragmentation. This is represented schematically in Figure 7.1.

The distance that the proton has to migrate from the most basic site does not affect the abundance of the product ions observed in the CID spectra. This is also consistent with the proposal that the proton is freely mobile, not thermodynamically or kinetically limited, and, therefore equally likely to be on any atom within the structure of the cation.

In this research we have successfully shown that bonds which are liable to be formed during the CID process of cations, produced by ESI or APCI, may be predicted using AM1 quantum chemistry software. Further work is needed to both to improve the predictive nature of application of quantum chemistry software to mass spectral interpretation and to gain a deeper understanding of the drivers for fragmentation. In particular, the work presented here does not predict product ion intensity or the collision energy at which the fragmentation occurs, nor does it explain non polarised bond cleavage or anion fragmentation. These apparent shortfalls in complete

prediction may be due to the fact that this work has only examined how the thermodynamic properties of ions and neutral molecules can be modelled and used to predict CID fragmentation. It is clear from the work presented in this thesis that thermodynamics alone cannot be the sole influence on fragmentation, and other effects need to be considered and modelled to obtain a complete *in silico* prediction of the CID fragmentation of drug like molecules and ions. The kinetics of fragmentation may also play a part in the process and therefore need to be considered as part of this approach. For example, there is a reported relationship between product ion intensity and kinetics of bond cleavage^[302,303]. It is intended in future studies to model the kinetics of certain of the bond cleavages reported here, at collision energies 5 eV to 50 eV, to gain an understanding of whether the collision energy is required to produce a kinetic shift or to increase bond vibrational energy (or both). There are software packages available for this, such as MassKinetics^[162]. In addition, future work will include modelling the stability of product ions, by DFT for cations and AM1 for anions. The aims will be to ascertain to what extent cation product ion stability correlates with product ion intensity and to establish if the stability of all potential anionic product ions dictates which product ions are actually formed. Further studies looking at the effect of collision energy on the CID spectra of deprotonated ions and also the Ion Trap CID spectra, where single step fragmentation predominates, may shed some light on the mechanism of anion fragmentation.

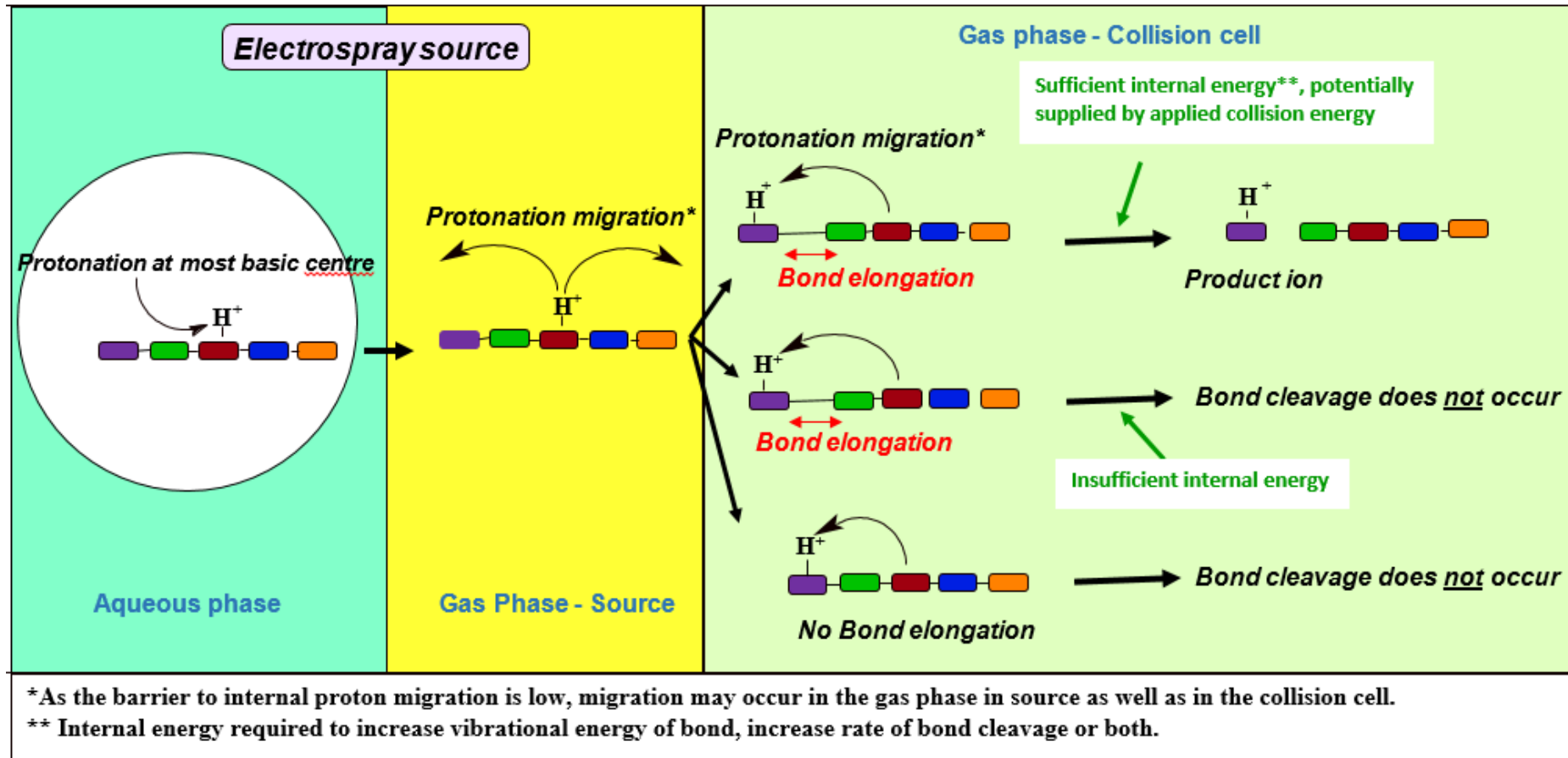


Figure 7.1 Schematic illustrating the proposal that protonation induced bond elongation initiates bond cleavage if the molecule has sufficient internal energy.

REFERENCES

- [1] A. El-Aneed, A. Cohen, J. Banoub. Mass Spectrometry, Review of the Basics: Electrospray, MALDI, and Commonly Used Mass Analyzers. *Appl. Spectrosc. Rev.* **2009**, *44*, 210.
- [2] E. R. Amstalden van Hove, D. F. Smith, R. M. A. Heeren. A concise review of mass spectrometry imaging. *J. Chromatogr. A* **2010**, *1217*, 3946.
- [3] W. M. A. Niessen. *Liquid Chromatography-Mass Spectrometry, Third Edition*. CRC Press, **2006**.
- [4] H. Awad, M. M. Khamis, A. El-Aneed. Mass Spectrometry, Review of the Basics: Ionization. *Appl. Spectrosc. Rev.* **2014**, 158.
- [5] D. I. Carroll, I. Dzidic, R. N. Stillwell, K. D. Haegele, E. C. Horning. Atmospheric pressure ionization mass spectrometry. Corona discharge ion source for use in a liquid chromatograph-mass spectrometer-computer analytical system. *Anal. Chem.* **1975**, *47*, 2369.
- [6] A. P. Bruins. Liquid chromatography-mass spectrometry with ionspray and electrospray interfaces in pharmaceutical and biomedical research. *J. Chromatogr. A* **1991**, *554*, 39.
- [7] P. Favetta, J. Guitton, C. . Degoute, L. Van Daele, R. Boulieu. High-performance liquid chromatographic assay to detect hydroxylate and conjugate metabolites of propofol in human urine. *J. Chromatogr. B Biomed. Sci. Appl.* **2000**, *742*, 25.
- [8] R. Ramanathan, R. Zhong, N. Blumenkrantz, S. K. Chowdhury, K. B. Alton. Response normalized liquid chromatography nanospray ionization mass spectrometry. *J. Am. Soc. Mass Spectrom.* **2007**, *18*, 1891.
- [9] G. Taylor. Disintegration of Water Drops in an Electric Field. *Proc. R. Soc. A Math. Phys. Eng. Sci.* **1964**, *280*, 383.
- [10] M. Dole. Molecular Beams of Macroions. *J. Chem. Phys.* **1968**, *49*, 2240.
- [11] B. A. Thomson, J. V. Iribarne. Field induced ion evaporation from liquid surfaces at atmospheric pressure. *J. Chem. Phys.* **1979**, *71*, 4451.
- [12] L. Konermann, A. D. Rodriguez, J. Liu. On the formation of highly charged gaseous ions from unfolded proteins by electrospray ionization. *Anal. Chem.* **2012**, *84*, 6798.

- [13] P. Kebarle, M. Peschke. On the mechanisms by which the charged droplets produced by electrospray lead to gas phase ions. *Anal. Chim. Acta* **2000**, 406, 11.
- [14] M. A. Kelly, M. M. Vestling, C. C. Fenselau, P. B. Smith. Electrospray analysis of proteins: A comparison of positive-ion and negative-ion mass spectra at high and low pH. *Org. Mass Spectrom.* **1992**, 27, 1143.
- [15] S. Zhou, K. Cook. Protonation in electrospray mass spectrometry: wrong-way-round or right-way-round? *J. Am. Soc. Mass Spectrom.* **2000**, 11, 961.
- [16] C. L. Gatlin, F. Turecek. Acidity Determination in Droplets Formed by Electrospraying Methanol-Water Solutions. *Anal. Chem.* **1994**, 66, 712.
- [17] C. Delatour, L. Leclercq. Positive electrospray liquid chromatography/mass spectrometry using high-pH gradients: a way to combine selectivity and sensitivity for a large variety of drugs. *Rapid Commun. Mass Spectrom.* **2005**, 19, 1359.
- [18] A. M. Kamel, P. R. Brown, B. Munson. Effects of Mobile-Phase Additives, Solution pH, Ionization Constant, and Analyte Concentration on the Sensitivities and Electrospray Ionization Mass Spectra of Nucleoside Antiviral Agents. *Anal. Chem.* **1999**, 71, 5481.
- [19] X. J. Yang, Y. Qu, Q. Yuan, P. Wan, Z. Du, D. Chen, C. Wong. Effect of ammonium on liquid- and gas-phase protonation and deprotonation in electrospray ionization mass spectrometry. *Analyst* **2012**, 138, 659.
- [20] R. Guevremont, K. W. M. Siu, J. C. Y. Blanc, S. S. Berman. Are the electrospray mass spectra of proteins related to their aqueous solution chemistry? *J. Am. Soc. Mass Spectrom.* **1992**, 3, 216.
- [21] A. P. Bruins. Atmospheric-pressure-ionization mass spectrometry. *TrAC Trends Anal. Chem.* **1994**, 13, 37.
- [22] H. Keski-Hynnilä, M. Kurkela, E. Elovaara, L. Antonio, J. Magdalou, L. Luukkanen, J. Taskinen, R. Kostianen. Comparison of Electrospray, Atmospheric Pressure Chemical Ionization, and Atmospheric Pressure Photoionization in the Identification of Apomorphine, Dobutamine, and Entacapone Phase II Metabolites in Biological Samples. *Anal. Chem.* **2002**, 74, 3449.
- [23] R. B. Cody, J. A. Laramée, H. D. Durst. Versatile new ion source for the analysis of materials in open air under ambient conditions. *Anal. Chem.* **2005**, 77, 2297.
- [24] Z. Takáts, J. M. Wiseman, B. Gologan, R. G. Cooks. Mass spectrometry sampling under ambient conditions with desorption electrospray ionization. *Science* **2004**, 306, 471.

- [25] M. Karas, D. Bachmann, F. Hillenkamp. Influence of the wavelength in high-irradiance ultraviolet laser desorption mass spectrometry of organic molecules. *Anal. Chem.* **1985**, *57*, 2935.
- [26] H. Wang, J. Liu, R. G. Cooks, Z. Ouyang. Paper Spray for Direct Analysis of Complex Mixtures Using Mass Spectrometry. *Angew. Chemie* **2010**, *122*, 889.
- [27] J. P. Williams, V. J. Patel, R. Holland, J. H. Scrivens. The use of recently described ionisation techniques for the rapid analysis of some common drugs and samples of biological origin. *Rapid Commun. Mass Spectrom.* **2006**, *20*, 1447.
- [28] B. Shrestha, Y. Li, A. Vertes. Rapid analysis of pharmaceuticals and excreted xenobiotic and endogenous metabolites with atmospheric pressure infrared MALDI mass spectrometry. *Metabolomics* **2008**, *4*, 297.
- [29] J. M. Wiseman, D. R. Ifa, Y. Zhu, C. B. Kissinger, N. E. Manicke, P. T. Kissinger, R. G. Cooks. Desorption electrospray ionization mass spectrometry: Imaging drugs and metabolites in tissues. *Proc. Natl. Acad. Sci. U. S. A.* **2008**, *105*, 18120.
- [30] B. Prideaux, D. Staab, M. Stoeckli. Applications of MALDI-MSI to pharmaceutical research. *Methods Mol. Biol.* **2010**, *656*, 405.
- [31] W. Paul, H. Steinwedel. Ein neues Massenspektrometer ohne Magnetfeld. *Zeitschrift Naturforsch. Tl. A* **1953**, *8*, 448.
- [32] S. Guan, A. G. Marshall. Equilibrium space charge distribution in a quadrupole ion trap. *J. Am. Soc. Mass Spectrom.* **1994**, *5*, 64.
- [33] D. J. Douglas, A. J. Frank, D. Mao. Linear ion traps in mass spectrometry. *Mass Spectrom. Rev.* **24**, 1.
- [34] M. Zhu, L. Ma, D. Zhang, K. Ray, W. Zhao, W. G. Humphreys, G. Skiles, M. Sanders, H. Zhang. Detection and characterization of metabolites in biological matrices using mass defect filtering of liquid chromatography/high resolution mass spectrometry data. *Drug Metab. Dispos.* **2006**, *34*, 1722.
- [35] M. M. Wolff, W. E. Stephens. A Pulsed Mass Spectrometer with Time Dispersion. *Rev. Sci. Instrum.* **1953**, *24*, 616.
- [36] B. A. Mamyurin, V. I. Karataev, D. V. Shmikk, V. A. Zagulin. The mass-reflectron, a new nonmagnetic time-of-flight mass spectrometer with high resolution. *Sov. J. Exp. Theor. Phys.* **1973**, *37*, 45.
- [37] M. B. Comisarow, A. G. Marshall. Fourier transform ion cyclotron resonance spectroscopy. *Chem. Phys. Lett.* **1974**, *25*, 282.

- [38] Q. Hu, R. J. Noll, H. Li, A. Makarov, M. Hardman, R. Graham Cooks. The Orbitrap: a new mass spectrometer. *J. Mass Spectrom.* **2005**, *40*, 430.
- [39] G. L. Glish, D. E. Goeringer. A tandem quadrupole/time-of-flight instrument for mass spectrometry/mass spectrometry. *Anal. Chem.* **1984**, *56*, 2291.
- [40] M. Wrona, T. Mauriala, K. P. Bateman, R. J. Mortishire-Smith, D. O'Connor. "All-in-one" analysis for metabolite identification using liquid chromatography/hybrid quadrupole time-of-flight mass spectrometry with collision energy switching. *Rapid Commun. Mass Spectrom.* **2005**, *19*, 2597.
- [41] C. Hopley, T. Bristow, A. Lubben, A. Simpson, E. Bull, K. Klagkou, J. Herniman, J. Langley. Towards a universal product ion mass spectral library – reproducibility of product ion spectra across eleven different mass spectrometers. *Rapid Commun. Mass Spectrom.* **2008**, *22*, 1779.
- [42] B.K. Cho, D. M. Hercules, T. Zhang, and A.I. Gusev. Comparison of quadrupole, time-of-flight, and Fourier transform mass analyzers for LC-MS applications. *LC GC Mag. Am. Sep. Sci.* 195, 514-524 **2001**, *15*, 514.
- [43] T. Rousu, J. Herttuainen, A. Tolonen. Comparison of triple quadrupole, hybrid linear ion trap triple quadrupole, time-of-flight and LTQ-Orbitrap mass spectrometers in drug discovery phase metabolite screening and identification in vitro--amitriptyline and verapamil as model compounds. *Rapid Commun. Mass Spectrom.* **2010**, *24*, 939.
- [44] J. Dearden, A. Worth. In silico prediction of physicochemical properties. can be found under http://ihcp.jrc.ec.europa.eu/our_labs/predictive_toxicology/doc/EUR_23051_EN.pdf, **2007**.
- [45] S. H. Yalkowsky, S. C. Valvani. Solubility and partitioning I: Solubility of nonelectrolytes in water. *J. Pharm. Sci.* **1980**, *69*, 912.
- [46] S. Caetano, T. Decaestecker, R. Put, M. Daszykowski, J. Van Bocxlaer, Y. Vander Heyden. Exploring and modelling the responses of electrospray and atmospheric pressure chemical ionization techniques based on molecular descriptors. *Anal. Chim. Acta* **2005**, *550*, 92.
- [47] R. Todeschini, V. Consonni. *Handbook of Molecular Descriptors (Google eBook)*. John Wiley & Sons, **2008**.
- [48] D. A. Winkler. The role of quantitative structure - activity relationships (QSAR) in biomolecular discovery. *Brief. Bioinform.* **2002**, *3*, 73.

- [49] Han van de Waterbeemd and Eric Gifford. ADMET in silico modelling: towards prediction paradise? *Nat. Rev. Drug Discov.* **2003**, 192, 192.
- [50] ACD/Labs.com :: ACD/Percepta Predictors. can be found under <http://www.acdlabs.com/products/percepta/predictors.php>,
- [51] Simulations Plus - Modeling & Simulation Software and Consulting Services for Pharmaceutical Research. <http://www.simulations-plus.com/>,
- [52] ChemSilico Homepage. <http://www.chemsilico.com/>,
- [53] Pipeline Pilot | Accelrys graphical scientific workflow authoring application. <http://accelrys.com/products/pipeline-pilot/>,
- [54] Sparc On-Line Calculator. <http://archemcalc.com/sparc/smiles/smiles.cfm?CFID=811885&CFTOKEN=40255081>,
- [55] P. A. Smith, M. J. Sorich, L. S. C. Low, R. A. McKinnon, J. O. Miners. Towards integrated ADME prediction: past, present and future directions for modelling metabolism by UDP-glucuronosyltransferases. *J. Mol. Graph. Model.* **2004**, 22, 507.
- [56] A. Long, J. D. Walker. Quantitative structure-activity relationships for predicting metabolism and modelling cytochrom P450 enzyme activities. *Environ. Toxicol. Chem.* **2003**, 22, 1894.
- [57] D. F. V Lewis. Quantitative structure-activity relationships (QSARs) within the cytochrome P450 system: QSARs describing substrate binding, inhibition and induction of P450s. *Inflammopharmacology* **2003**, 11, 43.
- [58] K. K. Chohan, S. W. Paine, N. J. Waters. Advancements in Predictive In Silico Models for ADME. *Curr. Chem. Biol.* **2008**, 2, 14.
- [59] P. J. Goodford. A computational procedure for determining energetically favorable binding sites on biologically important macromolecules. *J. Med. Chem.* **1985**, 28, 849.
- [60] Molnar-Institut. <http://www.molnar-institut.com/HP/index.php>,
- [61] ChromSword — HPLC method development, HPLC method development software, method development and validation, hplc software, analytical method development, automated method development, robustness. <http://www.chromsword.com/en/products/>,

- [62] L. R. Snyder, J. W. Dolan. *High-Performance Gradient Elution: The Practical Application of the Linear-Solvent-Strength Model*. John Wiley & Sons, **2007**.
- [63] ACD/Labs.com :: ACD/ChromGenius.
http://www.acdlabs.com/products/com_iden/meth_dev/chromgen/,
- [64] E. Tyrkkö, A. Pelander, I. Ojanperä. Prediction of liquid chromatographic retention for differentiation of structural isomers. *Anal. Chim. Acta* **2012**, 720, 142.
- [65] K. Klagkou, F. Pullen, M. Harrison, A. Organ, A. Firth, G. J. Langley. Fragmentation pathways of sulphonamides under electrospray tandem mass spectrometric conditions. *Rapid Commun. Mass Spectrom.* **2003**, 17, 2373.
- [66] S. J. Barry, J.-C. Wolff. Identification of isobaric amino-sulfonamides without prior separation. *Rapid Commun. Mass Spectrom.* **2012**, 26, 419.
- [67] S. W. Holman, P. Wright, G. J. Langley. A rapid methodology for the characterization of dialkyl tertiary amine-N-oxide metabolites using structurally dependent dissociation pathways and reconstructed ion current chromatograms. *Anal. Chem.* **2010**, 82, 2347.
- [68] P. Wright, A. Alex, D. Gibson, R. Jones, P. Macrae. Characterisation of sulphoxides by atmospheric pressure ionisation mass spectrometry. *Rapid Commun. Mass Spectrom.* **2005**, 19, 2005.
- [69] L. J. Kangas, T. O. Metz, G. Isaac, B. T. Schrom, B. Ginovska-Pangovska, L. Wang, L. Tan, R. R. Lewis, J. H. Miller. In silico identification software (ISIS): a machine learning approach to tandem mass spectral identification of lipids. *Bioinformatics* **2012**, 28, 1705.
- [70] Mass Frontier™. <http://www.highchem.com/massfrontier/mass-frontier.html>,
- [71] ACD/Labs.com :: ACD/MS Fragmenter.
http://www.acdlabs.com/products/adh/ms/ms_frag/,
- [72] Mass Spec Calculator. <http://www.chemsw.com/Software-and-Solutions/Laboratory-Software/Chromatography-and-Mass-Spec-Tools/Mass-Spec-Calculator-Professional.aspx>,
- [73] M. Heinonen, A. Rantanen, T. Mielikäinen, J. Kokkonen, J. Kiuru, R. A. Ketola, J. Rousu. FiD: a software for ab initio structural identification of product ions from tandem mass spectrometric data. *Rapid Commun. Mass Spectrom.* **2008**, 22, 3043.

- [74] S. Wolf, S. Schmidt, M. Müller-Hannemann, S. Neumann. In silico fragmentation for computer assisted identification of metabolite mass spectra. *BMC Bioinformatics* **2010**, *11*, 148.
- [75] H. Horai, M. Arita, S. Kanaya, Y. Nihei, T. Ikeda, K. Suwa, Y. Ojima, K. Tanaka, S. Tanaka, K. Aoshima, Y. Oda, Y. Kakazu, M. Kusano, T. Tohge, et al. MassBank: a public repository for sharing mass spectral data for life sciences. *J. Mass Spectrom.* **2010**, *45*, 703.
- [76] MassBank | High Quality Mass Spectral Database. <http://www.massbank.jp/?lang=en>,
- [77] MetWorks* Automated Metabolite Identification Software Thermo Scientific. http://www.thermoscientific.com/ecommerce/servlet/productsdetail_11152___11961727_-1,
- [78] MetabolitePilot™ Software | Simple, Clear Data Review | AB SCIEX. <http://www.absciex.com/products/software/metabolitepilot-software>,
- [79] LightSight® Software | Ultimate Tool to Find Metabolites | AB SCIEX. <http://www.absciex.com/products/software/lightsight-software>,
- [80] Overview | Bruker Corporation. <http://www.bruker.com/en/products/mass-spectrometry-and-separations/software/metabolitertools/overview.html>,
- [81] Waters: MetaboLynx XS. <http://www.waters.com/waters/nav.htm?cid=513803>,
- [82] K. Burke. Perspective on density functional theory. *J. Chem. Phys.* **2012**, *136*, 150901.
- [83] Schrödinger - Product Suites - List of All Products - Jaguar - Publications. <http://www.schrodinger.com/productpublications/14/7/>
- [84] COSMOlogic, computational chemistry and fluid phase thermodynamics from chemical engineering to life science. <http://www.cosmologic.de/index.php>,
- [85] C. Liao, M. C. Nicklaus. Comparison of nine programs predicting pK(a) values of pharmaceutical substances. *J. Chem. Inf. Model.* **2009**, *49*, 2801.
- [86] V. S. Bryantsev, M. S. Diallo, W. A. Goddard. pKa calculations of aliphatic amines, diamines, and aminoamides via density functional theory with a Poisson-Boltzmann continuum solvent model. *J. Phys. Chem. A* **2007**, *111*, 4422.
- [87] M. Borówko, S. Sokołowski, T. Staszewski. A density functional approach to retention in chromatography with chemically bonded phases. *J. Chromatogr. A* **2011**, *1218*, 711.

- [88] B.-H. Kim, J. Jung, Y.-K. Han. Liquid chromatographic enantiomer separation of racemic amine using chiral crown ether stationary phase. *J. Chromatogr. Sci.* **2006**, *44*, 27.
- [89] M. Szalaniec, A. Dudzik, M. Pawul, B. Kozik. Quantitative structure enantioselective retention relationship for high-performance liquid chromatography chiral separation of 1-phenylethanol derivatives. *J. Chromatogr. A* **2009**, *1216*, 6224.
- [90] N. Marchand-geneste, C. Lacoste, H. Budzinski, A. Carpy. Quantum Mechanics Calculations on PASH: Attempts to Correlate Thermodynamic Properties to Chromatographic Behaviour and/or Relative Abundance or Presence in Petroleum Samples. *Polycycl. Aromat. Compd.* **2001**, *19*, 37.
- [91] P. Wright, A. Alex, T. Nyaruwata, T. Parsons, F. Pullen. Using density functional theory to rationalise the mass spectral fragmentation of maraviroc and its metabolites. *Rapid Commun. Mass Spectrom.* **2010**, *24*, 1025.
- [92] A. Alex, S. Harvey, T. Parsons, F. S. Pullen, P. Wright, J.-A. Riley. Can density functional theory (DFT) be used as an aid to a deeper understanding of tandem mass spectrometric fragmentation pathways? *Rapid Commun. Mass Spectrom.* **2009**, *23*, 2619.
- [93] A. Alex. *Comprehensive Medicinal Chemistry II*. Elsevier, **2007**.
- [94] E. G. Lewars. *Computational Chemistry: Introduction to the Theory and Applications of Molecular and Quantum Mechanics (Google eBook)*. Springer, **2010**.
- [95] F. Jensen. *Introduction to Computational Chemistry (Google eBook)*. John Wiley & Sons, **2007**.
- [96] J. Sadowski, J. Gasteiger. From atoms and bonds to three-dimensional atomic coordinates: automatic model builders. *Chem. Rev.* **1993**, *93*, 2567.
- [97] J. Boeyens*. Molecular mechanics: theoretical basis, rules, scope and limits. *Coord. Chem. Rev.* **2001**, *212*, 3.
- [98] J. D. Durrant, J. A. McCammon. Molecular dynamics simulations and drug discovery. *BMC Biol.* **2011**, *9*, 71.
- [99] L. de Broglie. Waves and Quanta. *Nature* **1923**, *112*, 540.
- [100] H. P. Robertson. The Uncertainty Principle. *Phys. Rev.* **1929**, *34*, 163.

- [101] W. Heisenberg, C. Eckart, F. C. Hoyt. *The Physical Principles of the Quantum Theory*. New York: Dover Publications. Dover Publications, New York, **1949**.
- [102] F. Hund. Zur Deutung der Molekelspektren Part IV . *Zeitschrift für Phys.* **1928**, 51, 759.
- [103] Hund. F. Zur Deutung der Molekelspektren Part III . *Zeitschrift für Phys.* **1927**, 43, 805.
- [104] F. Hund. Zur Deutung der Molekelspektren Part II . *Zeitschrift für Phys.* **1927**, 42, 93.
- [105] F. Hund. Zur Deutung der Molekelspektren Part V . *Zeitschrift für Phys.* **1930**, 63, 719.
- [106] R. S. Mulliken. Electronic states. IV. Hund's theory; second positive nitrogen and Swan bands; alternate intensities. *Phys. Rev.* **1927**, 29, 637.
- [107] R. S. Mulliken. The assignment of quantum numbers for electrons in molecules. **1928**, 32, 186.
- [108] J. Slater. Atomic Shielding Constants. *Phys. Rev.* **1930**, 36, 57.
- [109] W. J. Hehre, R. F. Stewart, J. A. Pople. Self-Consistent Molecular-Orbital Methods. I. Use of Gaussian Expansions of Slater-Type Atomic Orbitals. *J. Chem. Phys.* **1969**, 51, 2657.
- [110] E. Schrödinger. An Undulatory Theory of the Mechanics of Atoms and Molecules. *Phys. Rev.* **1926**, 28, 1049.
- [111] N. M. Harrison. *Computational Materials Science*. IOS Press, **2003**.
- [112] J. C. Slater. Hartree. *Phys. Rev.* **1930**, 210, 35.
- [113] V. Fock. Hartree. *Z.Physik* **1930**, 61, 126.
- [114] M. Born, J. R. Oppenheimer. Born-Oppenheimer approximation. *Ann. Phys.* **1927**, 84, 457.
- [115] J. A. Pople, R. K. Nesbet. Self-Consistent Orbitals for Radicals. *J. Chem. Phys.* **1954**, 22, 571.
- [116] C. Møller, M. S. Plesset. Note on an Approximation Treatment for Many-Electron Systems. *Phys. Rev.* **1934**, 46, 618.

- [117] M. Head-Gordon, J. A. Pople, M. J. Frisch. MP2 energy evaluation by direct methods. *Chem. Phys. Lett.* **1988**, *153*, 503.
- [118] M. J. S. Dewar, W. Thiel. A semiempirical model for the two-center repulsion integrals in the NDDO approximation. *Theor. Chim. Acta* **1977**, *46*, 89.
- [119] M. J. S. Dewar. A Molecular Orbital Theory of Organic Chemistry. I. General Principles. *J. Am. Chem. Soc.* **1952**, *74*, 3341.
- [120] C. Cojocaru, A. Rotaru, V. Harabagiu, L. Sacarescu. Molecular structure and electronic properties of pyridylindolizine derivative containing phenyl and phenacyl groups: Comparison between semi-empirical calculations and experimental studies. *J. Mol. Struct.* **2013**, *1034*, 162.
- [121] T. R. Sharp. Calculated carbon-hydrogen bond dissociation enthalpies for predicting oxidative susceptibility of drug substance molecules. *Int. J. Pharm.* **2011**, *418*, 304.
- [122] E. Klein, M. Matis, V. Lukeš, Z. Cibulková. The applicability of AM1 and PM3 semi-empirical methods for the study of N–H bond dissociation enthalpies and ionisation potentials of amine type antioxidants. *Polym. Degrad. Stab.* **2006**, *91*, 270.
- [123] M. J. S. Dewar, E. G. Zoebisch, E. F. Healy, J. J. P. Stewart. Development and use of quantum mechanical molecular models. 76. AM1: a new general purpose quantum mechanical molecular model. *J. Am. Chem. Soc.* **1985**, *107*, 3902.
- [124] N. T. Anh, G. Frison, A. Solladié-Cavallo, P. Metzner. Some difficulties encountered with AM1 and PM3 calculations. *Tetrahedron* **1998**, *54*, 12841.
- [125] G. Zheng, S. Irle, K. Morokuma. Performance of the DFTB method in comparison to DFT and semiempirical methods for geometries and energies of C₂₀–C₈₆ fullerene isomers. *Chem. Phys. Lett.* **2005**, *412*, 210.
- [126] S. Rajak, N. Islam, D. Ghosh. Modeling of the Chemico-Physical Process of Protonation of Molecules Entailing Some Quantum Chemical Descriptors. *J. Quantum Inf. Sci.* **2011**, *1*, 87.
- [127] S. Huzinaga. Basis sets for molecular calculations. *Comput. Phys. Reports* **1985**, *2*, 281.
- [128] R. Van Noorden, B. Maher, R. Nuzzo. The top 100 papers. *Nature* **2014**, *514*, 550.
- [129] P. Hohenberg, W. Kohn. Inhomogeneous Electron Gas. *Phys. Rev.* **1964**, *136*, B864.

- [130] W. Kohn, L. J. Sham. Self-Consistent Equations Including Exchange and Correlation Effects. *Phys. Rev.* **1965**, *140*, A1133.
- [131] C. Lee, W. Yang, R. G. Parr. Development of the Colle-Salvetti correlation-energy formula into a functional of the electron density. *Phys. Rev. B* **1988**, *37*, 785.
- [132] A. D. Becke. Density-functional exchange-energy approximation with correct asymptotic behavior. *Phys. Rev. A* **1988**, *38*, 3098.
- [133] P. E. M. Siegbahn. The performance of hybrid DFT for mechanisms involving transition metal complexes in enzymes. *J. Biol. Inorg. Chem.* **2006**, *11*, 695.
- [134] M. Orio, D. A. Pantazis, F. Neese. Density functional theory. *Photosynth. Res.* **2009**, *102*, 443.
- [135] S. Tsuzuki, H. P. Lüthi. Interaction energies of van der Waals and hydrogen bonded systems calculated using density functional theory: Assessing the PW91 model. *J. Chem. Phys.* **2001**, *114*, 3949.
- [136] R. B. Murphy, M. D. Beachy, R. A. Friesner, M. N. Ringnalda. Pseudospectral localized Møller–Plesset methods: Theory and calculation of conformational energies. *J. Chem. Phys.* **1995**, *103*, 1481.
- [137] R. A. Friesner. Ab initio quantum chemistry: methodology and applications. *Proc. Natl. Acad. Sci. U. S. A.* **2005**, *102*, 6648.
- [138] A. Saeed, I. Arshad, U. UlrichFlörke. Synthesis, Crystal Structure, and DFT Study of N'-(2,4-Dinitrophenyl)-2-Fluorobenzohydrazide. *J. Chem.* **2013**, *2013*, 1.
- [139] F. Jensen. Describing Anions by Density Functional Theory: Fractional Electron Affinity. *J. Chem. Theory Comput.* **2010**, *6*, 2726.
- [140] A. J. Cohen, P. Mori-Sánchez, W. Yang. Challenges for density functional theory. *Chem. Rev.* **2012**, *112*, 289.
- [141] S. Ehrlich, J. Moellmann, S. Grimme. Dispersion-corrected density functional theory for aromatic interactions in complex systems. *Acc. Chem. Res.* **2013**, *46*, 916.
- [142] S. I. Sandler. Quantum mechanics: a new tool for engineering thermodynamics. *Fluid Phase Equilib.* **2003**, *210*, 147.
- [143] C. Wittekindt, A. Klamt. COSMO-RS as a Predictive Tool for Lipophilicity. *QSAR Comb. Sci.* **2009**, *28*, 874.

- [144] M. Schäfer, M. Dray, A. Springer, P. Zacharias, K. Meerholz. Radical Cations in Electrospray Mass Spectrometry: Formation of Open-Shell Species, Examination of the Fragmentation Behaviour in ESI-MSn and Reaction Mechanism Studies by Detection of Transient Radical Cations. *European J. Org. Chem.* **2007**, 2007, 5162.
- [145] K. Vékey. Internal Energy Effects in Mass Spectrometry. *J. Mass Spectrom.* **1996**, 31, 445.
- [146] L. Drahos, K. Vékey. Determination of the thermal energy and its distribution in peptides. *J. Am. Soc. Mass Spectrom.* **1999**, 10, 323.
- [147] C. Collette, E. De Pauw. Calibration of the internal energy distribution of ions produced by electrospray. *Rapid Commun. Mass Spectrom.* **1998**, 12, 165.
- [148] L. Drahos, R. Heeren, C. Collette, De Pauw E, K. Vekey. Thermal energy distribution observed in electrospray ionization. *J. Mass Spectrom.* **1999**, 34, 1373.
- [149] J. Naban-Maillet, D. Lesage, A. Bossée, Y. Gimbert, J. Sztáray, K. Vékey, J.-C. Tabet. Internal energy distribution in electrospray ionization. *J. Mass Spectrom.* **2005**, 40, 1.
- [150] D. Rondeau, L. Drahos, K. Vékey. Internal energy distribution in electrospray ionization: Towards the evaluation of a thermal-like distribution from the multiple-collision model. *Rapid Commun. Mass Spectrom.* **2014**, 28, 273.
- [151] F. Ichou, D. Lesage, X. Machuron-Mandard, C. Junot, R. B. Cole, J.-C. Tabet. Collision cell pressure effect on CID spectra pattern using triple quadrupole instruments: a RRKM modeling. *J. Mass Spectrom.* **2013**, 48, 179.
- [152] T. M. Kertesz, L. H. Hall, D. W. Hill, D. F. Grant. CE50: quantifying collision induced dissociation energy for small molecule characterization and identification. *J. Am. Soc. Mass Spectrom.* **2009**, 20, 1759.
- [153] R. D. Voyksner. Atmospheric Pressure Ionization LC/M. *Environ. Sci. Technol.* **1994**, 28, 118A.
- [154] I. Marginean, J. S. Page, A. V Tolmachev, K. Tang, R. D. Smith. Achieving 50% ionization efficiency in subambient pressure ionization with nanoelectrospray. *Anal. Chem.* **2010**, 82, 9344.
- [155] V. Gabelica, E. De Pauw, M. Karas. Influence of the capillary temperature and the source pressure on the internal energy distribution of electrosprayed ions. *Int. J. Mass Spectrom.* **2004**, 231, 189.

- [156] C. M. Whitehouse, R. N. Dreyer, M. Yamashita, J. B. Fenn. Electrospray interface for liquid chromatographs and mass spectrometers. *Anal. Chem.* **1985**, *57*, 675.
- [157] C. Cunningham, G. L. Glish, D. J. Burinsky. High amplitude short time excitation: a method to form and detect low mass product ions in a quadrupole ion trap mass spectrometer. *J. Am. Soc. Mass Spectrom.* **2006**, *17*, 81.
- [158] A. Kuki, L. Nagy, A. Memboeuf, L. Drahos, K. Vékey, M. Zsuga, S. Kéki. Energy-dependent collision-induced dissociation of lithiated polytetrahydrofuran: effect of the size on the fragmentation properties. *J. Am. Soc. Mass Spectrom.* **2010**, *21*, 1753.
- [159] Á. Kuki, B. Biri, L. Nagy, G. Deák, J. Kalmár, A. Mándi, M. Nagy, M. Zsuga, S. Kéki. Collision induced dissociation study of the major components of silymarin. *Int. J. Mass Spectrom.* **2012**, *315*, 46.
- [160] T. M. Kertesz, L. H. Hall, D. W. Hill, D. F. Grant. CE50: quantifying collision induced dissociation energy for small molecule characterization and identification. *J. Am. Soc. Mass Spectrom.* **2009**, *20*, 1759.
- [161] A. Memboeuf, A. Nasioudis, S. Indelicato, F. Pollreisz, A. Kuki, S. Kéki, O. F. van den Brink, K. Vékey, L. Drahos. Size effect on fragmentation in tandem mass spectrometry. *Anal. Chem.* **2010**, *82*, 2294.
- [162] L. Drahos, K. Vékey. MassKinetics: a theoretical model of mass spectra incorporating physical processes, reaction kinetics and mathematical descriptions. *J. Mass Spectrom.* **2001**, *36*, 237.
- [163] J. M. Wells, S. A. McLuckey. Collision-induced dissociation (CID) of peptides and proteins. *Methods Enzymol.* **2005**, *402*, 148.
- [164] A. Cartoni, M. Altamura, F. Animati, G. Balacco, R. Cosi, A. Ettorre, A. Madami, A. Triolo. An unusual rearrangement of Zofenopril, a new ACE inhibitor drug: mass spectrometric and conformational studies. *J. Mass Spectrom.* **2002**, *37*, 1258.
- [165] L. Sleno, D. A. Volmer. Ion activation methods for tandem mass spectrometry. *J. Mass Spectrom.* **2004**, *39*, 1091.
- [166] E. de Hoffmann. Tandem mass spectrometry: A primer. *J. Mass Spectrom.* **1996**, *31*, 129.
- [167] K. Vékey. Mass spectrometry and mass-selective detection in chromatography. *J. Chromatogr. A* **2001**, *921*, 227.

- [168] P. Wright, A. Alex, F. Pullen. 3D thinking: computational aids for the bioanalyst. *Bioanalysis* **2013**, 5, 395.
- [169] K. Scheubert, F. Hufsky, S. Böcker. Computational mass spectrometry for small molecules. *J. Cheminform.* **2013**, 5, 12.
- [170] M. Szaleniec, A. Dudzik, M. Pawul, B. Kozik. Quantitative structure enantioselective retention relationship for high-performance liquid chromatography chiral separation of 1-phenylethanol derivatives. *J. Chromatogr. A* **2009**, 1216, 6224.
- [171] S. K. Rajak, D. C. Ghosh. Correlating the site selectivity of protonation in some ambidentate molecules in terms of the dual descriptor. *Eur. Phys. J. D* **2012**, 66, 66.
- [172] M. Z. Griffiths, I. Alkorta, P. L. A. Popelier. Predicting p K a Values in Aqueous Solution for the Guanidine Functional Group from Gas Phase Ab Initio Bond Lengths. *Mol. Inform.* **2013**, 32, 363.
- [173] R. D. Bowen, B. J. Stapleton, D. H. Williams. Non-concerted unimolecular reactions of ions in the gas phase: isomerisation of weakly co-ordinated carbonium ions. *J. Chem. Soc. Chem. Commun.* **1978**, 24.
- [174] R. D. Bowen, D. H. Williams, H. Schwarz, C. Wesdemiotis. Energy barriers for isomerization of gaseous C₃H₅⁺ ions. *J. Am. Chem. Soc.* **1979**, 101, 4681.
- [175] Z. You, Y. Wen, K. Jiang, Y. Pan. Fragmentation mechanism of product ions from protonated proline-containing tripeptides in electrospray ionization mass spectrometry. *Chinese Sci. Bull.* **2012**, 57, 2051.
- [176] F. Li, X. Zhang, H. Zhang, K. Jiang. Gas-phase fragmentation of the protonated benzyl ester of proline: intramolecular electrophilic substitution versus hydride transfer. *J. Mass Spectrom.* **2013**, 48, 423.
- [177] A. Škríba, Š. Janková, J. Váňa, P. Barták, P. Bednář, P. Fryčák, L. Kučera, O. Kurka, K. Lemr, P. Macíková, E. Marková, P. Nováková, B. Papoušková, J. Skopalová, et al. Protonation sites and fragmentations of para-aminophenol. *Int. J. Mass Spectrom.* **2013**, 337, 18.
- [178] R. Vessecchi, F. S. Emery, N. P. Lopes, S. E. Galembeck. Electronic structure and gas-phase chemistry of protonated α - and β -quinonoid compounds: a mass spectrometry and computational study. *Rapid Commun. Mass Spectrom.* **2013**, 27, 816.

- [179] E. Kraka, D. Cremer. Characterization of CF bonds with multiple-bond character: bond lengths, stretching force constants, and bond dissociation energies. *Chemphyschem* **2009**, *10*, 686.
- [180] L. Pauling. The Dependence of Bond Energy on Bond Length. *J. Phys. Chem.* **1954**, *58*, 662.
- [181] L. Pauling. *The Nature of the Chemical Bond and the Structure of Molecules and Crystals: An Introduction to Modern Structural Chemistry*. Cornell University Press, Ithaca, NY, **1960**.
- [182] P. Wright, A. Alex, T. Nyaruwata, T. Parsons, F. Pullen. Using density functional theory to rationalise the mass spectral fragmentation of maraviroc and its metabolites. **2010**, 1025.
- [183] M. Alcamí, O. Mó, M. Yáñez. Computational chemistry: a useful (sometimes mandatory) tool in mass spectrometry studies. *Mass Spectrom. Rev.* **2001**, *20*, 195.
- [184] M. Alcamí, O. Mó, M. Yáñez, J.-L. M. Abboud, J. Elguero. Bond activation by protonation in the gas phase. *Chem. Phys. Lett.* **1990**, *172*, 471.
- [185] M. Alcamí, O. Mó, M. Yáñez. Modeling intrinsic basicities and acidities. *J. Phys. Org. Chem.* **2002**, *15*, 174.
- [186] J.-L. M. Abboud, M. Esseffar, M. Herreros, O. Mó, M. T. Molina, R. Notario, M. Yáñez. Protonation of S₄, S₆, and S₈ Sulfur Cycles. A Quantitative Study. *J. Phys. Chem. A* **1998**, *102*, 7996.
- [187] A. Kaufmann, P. Butcher, K. Maden, M. Widmer, K. Giles, D. Uría. Are liquid chromatography/electrospray tandem quadrupole fragmentation ratios unequivocal confirmation criteria? *Rapid Commun. Mass Spectrom.* **2009**, *23*, 985.
- [188] S. W. Holman, P. Wright, G. J. Langley. High-throughput approaches towards the definitive identification of pharmaceutical drug metabolites . 2 . An example of how unexpected dissociation behaviour could preclude correct assignment of sites of metabolism. **2009**, 2017.
- [189] I. Komáromi, Á. Somogyi, V. H. Wysocki. Proton migration and its effect on the MS fragmentation of N-acetyl OMe proline: MS/MS experiments and ab initio and density functional calculations. *Int. J. Mass Spectrom.* **2005**, *241*, 315.
- [190] V. H. Wysocki, G. Tsaprailis, L. L. Smith, L. A. Breci. Mobile and localized protons: a framework for understanding peptide dissociation. *J. Mass Spectrom.* **2000**, *35*, 1399.

- [191] S. Bourcier, Y. Hoppilliard. Use of diagnostic neutral losses for structural information on unknown aromatic metabolites: an experimental and theoretical study. *Rapid Commun. Mass Spectrom.* **2009**, *23*, 93.
- [192] Y.-P. Tu. Dissociative protonation and fragmentation: Retro-Friedel–Crafts reactions of heterocyclic drug and metabolite molecules in mass spectrometry. *Int. J. Mass Spectrom.* **2012**, *316-318*, 40.
- [193] J. R. Joyce, D. S. Richards. Kinetic control of protonation in electrospray ionization. *J. Am. Soc. Mass Spectrom.* **2011**, *22*, 360.
- [194] A. Kaufmann, P. Butcher, K. Maden, M. Widmer, K. Giles, D. Uría. Are liquid chromatography/electrospray tandem quadrupole fragmentation ratios unequivocal confirmation criteria? *Rapid Commun. Mass Spectrom.* **2009**, *23*, 985.
- [195] A. M. Kamel, P. R. Brown, B. Munson. Effects of Mobile-Phase Additives, Solution pH, Ionization Constant, and Analyte Concentration on the Sensitivities and Electrospray Ionization Mass Spectra of Nucleoside Antiviral Agents. *Anal. Chem.* **1999**, *71*, 5481.
- [196] M. A. Kelly, M. M. Vestling, C. C. Fenselau, P. B. Smith. Electrospray analysis of proteins: A comparison of positive-ion and negative-ion mass spectra at high and low pH. *Org. Mass Spectrom.* **1992**, *27*, 1143.
- [197] Z. Tian, S. R. Kass. Gas-phase versus liquid-phase structures by electrospray ionization mass spectrometry. *Angew. Chem. Int. Ed. Engl.* **2009**, *48*, 1321.
- [198] B. M. Ehrmann, T. Henriksen, N. B. Cech. Relative importance of basicity in the gas phase and in solution for determining selectivity in electrospray ionization mass spectrometry. *J. Am. Soc. Mass Spectrom.* **2008**, *19*, 719.
- [199] C. R. Mallet, Z. Lu, J. R. Mazzeo. A study of ion suppression effects in electrospray ionization from mobile phase additives and solid-phase extracts. *Rapid Commun. Mass Spectrom.* **2004**, *18*, 49.
- [200] F. Beaudry, P. Vachon. Electrospray ionization suppression, a physical or a chemical phenomenon? *Biomed. Chromatogr.* **2006**, *20*, 200.
- [201] R. King, R. Bonfiglio, C. Fernandez-Metzler, C. Miller-Stein, T. Olah. Mechanistic investigation of ionization suppression in electrospray ionization. *J. Am. Soc. Mass Spectrom.* **2000**, *11*, 942.
- [202] B. K. Matuszewski, M. L. Constanzer, C. M. Chavez-Eng. Strategies for the Assessment of Matrix Effect in Quantitative Bioanalytical Methods Based on HPLC–MS/MS. *Anal. Chem.* **2003**, *75*, 3019.

- [203] S. F. Campbell. *Proceedings XIVth International Symposium on Medicinal Chemistry*. Elsevier, **1997**.
- [204] M. Alcamí, O. Mó, M. Yáñez, J.-L. M. Abboud, J. Elguero. Bond activation by protonation in the gas phase. *Chem. Phys. Lett.* **1990**, 172, 471.
- [205] R. P. Bell. *The Tunnel Effect in Chemistry*. Chapman And Hall, London, **1980**.
- [206] F. Madeja, M. Havenith. High resolution spectroscopy of carboxylic acid in the gas phase: Observation of proton transfer in (DCOOH)₂. *J. Chem. Phys.* **2002**, 117, 7162.
- [207] K. A. Cox, S. J. Gaskell, M. Morris, A. Whiting. Role of the site of protonation in the low-energy decompositions of gas-phase peptide ions. *J. Am. Soc. Mass Spectrom.* **1996**, 7, 522.
- [208] H.-Y. Lin, D. P. Ridge, E. Uggerud, T. Vulpius. Unimolecular Chemistry of Protonated Formamide. Mass Spectrometry and ab Initio Quantum Chemical Calculations. *J. Am. Chem. Soc.* **1994**, 116, 2996.
- [209] C. K. Fagerquist, A. R. Lightfield, S. J. Lehotay. Confirmatory and quantitative analysis of beta-lactam antibiotics in bovine kidney tissue by dispersive solid-phase extraction and liquid chromatography-tandem mass spectrometry. *Anal. Chem.* **2005**, 77, 1473.
- [210] Y. Zeng, X. Chen, D. Zhao, H. Li, Y. Zhang, X. Xiao. Estimation of pKa values for carboxylic acids, alcohols, phenols and amines using changes in the relative Gibbs free energy. *Fluid Phase Equilib.* **2012**, 313, 148.
- [211] F. Falvo, L. Fiebig, F. Dreiocker, R. Wang, P. B. Armentrout, M. Schäfer. Fragmentation reactions of thiourea- and urea-compounds examined by tandem MS-, energy-resolved CID experiments, and theory. *Int. J. Mass Spectrom.* **2012**, 330-332, 124.
- [212] D. J. Harvey. A new charge-associated mechanism to account for the production of fragment ions in the high-energy CID spectra of fatty acids. *J. Am. Soc. Mass Spectrom.* **2005**, 16, 280.
- [213] G. Bouchoux. From the mobile proton to wandering hydride ion: mechanistic aspects of gas-phase ion chemistry. *J. Mass Spectrom.* **2013**, 48, 505.
- [214] A. J. Chalk, L. Radom. Proton-Transport Catalysis: A Systematic Study of the Rearrangement of the Isoformyl Cation to the Formyl Cation. *J. Am. Chem. Soc.* **1997**, 119, 7573.

- [215] Y. Chai, C. Guo, K. Jiang, Y. Pan, C. Sun. C α -C β and C α -N bond cleavage in the dissociation of protonated N-benzylactams: dissociative proton transfer and intramolecular proton-transport catalysis. *Org. Biomol. Chem.* **2012**, *10*, 791.
- [216] A. Djandé, B. Sessouma, F. B. Kini, L. Kaboré, B. Karifa, P. I. Guissou, A. Saba. AM1 and electron impact mass spectrometry study of the fragmentation of 4-acyl isochroman-1,3-diones. *Bull. Chem. Soc. Ethiop.* **2012**, *26*, DOI 10.4314/bcse.v26i2.15.
- [217] Y.-P. Tu. Dissociative protonation sites: reactive centers in protonated molecules leading to fragmentation in mass spectrometry. *J. Org. Chem.* **2006**, *71*, 5482.
- [218] S. T. Schneebeli, M. L. Hall, R. Breslow, R. Friesner. Quantitative DFT modeling of the enantiomeric excess for dioxirane-catalyzed epoxidations. *J. Am. Chem. Soc.* **2009**, *131*, 3965.
- [219] A. Shukla, J. Futrell. Tandem mass spectrometry: dissociation of ions by collisional activation. *J. Mass Spectrom.* **2000**, *35*, 1069.
- [220] S. A. McLuckey. Principles of collisional activation in analytical mass spectrometry. *J. Am. Soc. Mass Spectrom.* **1992**, *3*, 599.
- [221] T. Covey, D. J. Douglas. Collision cross sections for protein ions. *J. Am. Soc. Mass Spectrom.* **1993**, *4*, 616.
- [222] J. M. Wells, S. A. McLuckey. Collision-induced dissociation (CID) of peptides and proteins. *Methods Enzymol.* **2005**, *402*, 148.
- [223] V. H. Wysocki, H. I. Kenttämaa, R. G. Cooks. Internal energy distributions of isolated ions after activation by various methods. *Int. J. Mass Spectrom. Ion Process.* **1987**, *75*, 181.
- [224] A. Shukla, J. Futrell. Tandem mass spectrometry: dissociation of ions by collisional activation. *J. Mass Spectrom.* **2000**, *35*, 1069.
- [225] F. W. McLafferty. Mass Spectrometric Analysis. Molecular Rearrangements. *Anal. Chem.* **1959**, *31*, 82.
- [226] J. H. Beynon, G. R. Lester, A. E. Williams. Some Specific Molecular Rearrangements in the Mass Spectra of Organic Compounds. *J. Phys. Chem.* **1959**, *63*, 1861.
- [227] F. P. Boer, T. W. Shannon, F. W. McLafferty. Electronic structure of the six-membered cyclic transition state in some γ -hydrogen rearrangements. *J. Am. Chem. Soc.* **1968**, *90*, 7239.

- [228] I. Auzmendi-Murua, S. Charaya, J. W. Bozzelli. Thermochemical Properties of Methyl Substituted Cyclic Alkyl Ethers and Radicals for Oxiranes, Oxetanes and Oxolanes: C-H Bond Dissociation Enthalpy Trends with Ring Size and Ether Site. *J. Phys. Chem. A* **2012**, DOI 10.1021/jp309775h.
- [229] J. Ben Ari, I. Navon, A. Mandelbaum. The effect of steric hindrance on the relative rates of anchimerically assisted alcohol eliminations from MH⁺ ions of 2-substituted 1,4-dialkoxybutanes upon CI and CID. *Int. J. Mass Spectrom.* **2006**, 249-250, 433.
- [230] V. Vais, A. Etinger, A. Mandelbaum. Steric hindrance and the kinetic nature of the protonation process in 4-amino-1-methoxycyclohexanes upon chemical ionization. *Eur. Mass Spectrom.* **1999**, 5, 449.
- [231] A. Weisz, A. Mandelbaum, J. Shabanowitz, D. F. Hunt. The effect of configuration of gas phase protonated ethenedicarboxylates on their low energy collision induced dissociation behaviour. *Org. Mass Spectrom.* **1984**, 19, 238.
- [232] J. Yu, Kate; Castro-Perez, Jose; Schockar. MassFrag Method for structural elucidation in Metabolite identification using exact Mass Measurements. <http://www.waters.com/webassets/cms/library/docs/720002572en.pdf>, **2008**.
- [233] P. Wright, A. Alex, S. Harvey, T. Parsons, F. Pullen. Understanding collision-induced dissociation of dofetilide: a case study in the application of density functional theory as an aid to mass spectral interpretation. *Analyst* **2013**, 138, 6861.
- [234] C. Cojocaru, A. Rotaru, V. Harabagiu, L. Sacarescu. Molecular structure and electronic properties of pyridylindolizine derivative containing phenyl and phenacyl groups: Comparison between semi-empirical calculations and experimental studies. *J. Mol. Struct.* **2013**, 1034, 162.
- [235] P. J. Amorim Madeira, P. D. Vaz, R. J. N. Bettencourt da Silva, M. H. Florêncio. Can Semi-empirical Calculations Help Solve Mass Spectrometry Problems? Protonation Sites and Proton Affinities of Amino Acids. *Chempluschem* **2013**, 78, 1149.
- [236] C. K. Kim, S. G. Cho, C. K. Kim, M.-R. Kim, H. W. Lee. Prediction of Physicochemical Properties of organic Molecules Using Semi-Empirical Methods. *Bull. Korean Chem. Soc.* **2013**, 34, 1043.
- [237] C. Baldauf, R. Günther, H.-J. Hofmann. Conformational properties of sulfonamido peptides. *J. Mol. Struct. Theochem* **2004**, 675, 19.

- [238] T. Pechan, S. R. Gwaltney. Calculations of relative intensities of fragment ions in the MSMS spectra of a doubly charged penta-peptide. *BMC Bioinformatics* **2012**, *13 Suppl 1*, S13.
- [239] A. Galezowska, M. W. Harrison, J. M. Herniman, C.-K. Skylaris, G. J. Langley. A predictive science approach to aid understanding of electrospray ionisation tandem mass spectrometric fragmentation pathways of small molecules using density functional calculations. *Rapid Commun. Mass Spectrom.* **2013**, *27*, 964.
- [240] C. K. Fagerquist, A. R. Lightfield. Confirmatory analysis of beta-lactam antibiotics in kidney tissue by liquid chromatography/electrospray ionization selective reaction monitoring ion trap tandem mass spectrometry. *Rapid Commun. Mass Spectrom.* **2003**, *17*, 660.
- [241] C. Cheng, M. L. Gross. Applications and mechanisms of charge-remote fragmentation. *Mass Spectrom. Rev.* **2000**, *19*, 398.
- [242] J. H. Bowie. The fragmentations of even-electron organic negative ions. *Mass Spectrom. Rev.* **1990**, *9*, 349.
- [243] E. de Hoffmann, V. Stroobant. Mass Spectrometry: Principles and Applications. <http://eu.wiley.com/WileyCDA/WileyTitle/productCd-047003310X.html>, **2007**.
- [244] A. B. Attygalle, S. García-Rubio, J. Ta, J. Meinwald. Collisionally-induced dissociation mass spectra of organic sulfate anions. *J. Chem. Soc. Perkin Trans. 2* **2001**, 498.
- [245] M. K. Kumar, B. Sateesh, S. Prabhakar, G. N. Sastry, M. Vairamani. Generation of regiospecific carbanions under electrospray ionisation conditions and their selectivity in ion-molecule reactions with CO₂. *Rapid Commun. Mass Spectrom.* **2006**, *20*, 987.
- [246] T. T. N. Tran, T. Wang, S. Hack, J. H. Bowie. Fragmentations of [M-H]⁻ anions of peptides containing tyrosine sulfate. Does the sulfate group rearrange? A joint experimental and theoretical study. *Rapid Commun. Mass Spectrom.* **2013**, *27*, 1135.
- [247] P. Garcia, M. A. Popot, F. Fournier, Y. Bonnaire, J. C. Tabet. Gas-phase behaviour of negative ions produced from thiazidic diuretics under electrospray conditions. *J. Mass Spectrom.* **2002**, *37*, 940.
- [248] B. Kanawati, M. Harir, P. Schmitt-Kopplin. Exploring rearrangements along the fragmentation pathways of diuron anion: A combined experimental and computational investigation. *Int. J. Mass Spectrom.* **2009**, *288*, 6.

- [249] J. Zaia, M. J. C. Miller, J. L. Seymour, C. E. Costello. The role of mobile protons in negative ion CID of oligosaccharides. *J. Am. Soc. Mass Spectrom.* **2007**, *18*, 952.
- [250] K. M. Wooding, R. M. Barkley, J. A. Hankin, C. A. Johnson, A. P. Bradford, N. Santoro, R. C. Murphy. Mechanism of formation of the major estradiol product ions following collisional activation of the molecular anion in a tandem quadrupole mass spectrometer. *J. Am. Soc. Mass Spectrom.* **2013**, *24*, 1451.
- [251] F.-F. Hsu, J. Turk. Charge-driven fragmentation processes in diacyl glycerophosphatidic acids upon low-energy collisional activation. A mechanistic proposal. *J. Am. Soc. Mass Spectrom.* **2000**, *11*, 797.
- [252] I. Ferrer, E. M. Thurman. Measuring the mass of an electron by LC/TOF-MS: a study of "twin ions". *Anal. Chem.* **2005**, *77*, 3394.
- [253] L. E. Greene, J. S. Grossert, R. L. White. Correlations of ion structure with multiple fragmentation pathways arising from collision-induced dissociations of selected α -hydroxycarboxylic acid anions. *J. Mass Spectrom.* **2013**, *48*, 312.
- [254] J. Kalcher. Gas-phase stabilities of small anions. *Annu. Reports Sect. "C" (Physical Chem.* **2001**, *97*, 149.
- [255] J. H. Gross. *Mass Spectrometry*. Springer Berlin Heidelberg, Berlin, Heidelberg, **2011**.
- [256] N.-E. Es-Safi, L. Kerhoas, J. Einhorn, P.-H. Ducrot. Application of ESI/MS, CID/MS and tandem MS/MS to the fragmentation study of eriodictyol 7-O-glucosyl-(1 \rightarrow 2)-glucoside and luteolin 7-O-glucosyl-(1 \rightarrow 2)-glucoside. *Int. J. Mass Spectrom.* **2005**, *247*, 93.
- [257] B. Kanawati, S. Joniec, R. Winterhalter, G. K. Moortgat. Mass spectrometric characterization of small oxocarboxylic acids and gas phase ion fragmentation mechanisms studied by electrospray triple quadrupole-MS/MS-TOF system and DFT theory. *Int. J. Mass Spectrom.* **2007**, *266*, 97.
- [258] J. P. Williams, N. M. M. Nibbering, B. N. Green, V. J. Patel, J. H. Scrivens. Collision-induced fragmentation pathways including odd-electron ion formation from desorption electrospray ionisation generated protonated and deprotonated drugs derived from tandem accurate mass spectrometry. *J. Mass Spectrom.* **2006**, *41*, 1277.
- [259] Scripps Center For Metabolomics and Mass Spectrometry - METLIN.
<http://metlin.scripps.edu/index.php>,

- [260] J. H. Bowie, C. S. Brinkworth, S. Dua. Collision-induced fragmentations of the (M-H)- parent anions of underivatized peptides: an aid to structure determination and some unusual negative ion cleavages. *Mass Spectrom. Rev.* **21**, 87.
- [261] D. Bilusich, J. H. Bowie. Fragmentations of (M-H)- anions of underivatized peptides. Part 2: Characteristic cleavages of Ser and Cys and of disulfides and other post-translational modifications, together with some unusual internal processes. *Mass Spectrom. Rev.* **28**, 20.
- [262] T. Sotomatsu, Y. Murata, T. Fujita. Correlation analysis of substituent effects on the acidity of benzoic acids by the AM1 method. *J. Comput. Chem.* **1989**, *10*, 94.
- [263] S. A. Chacko, P. G. Wenthold. The negative ion chemistry of nitric oxide in the gas phase. *Mass Spectrom. Rev.* **25**, 112.
- [264] R. Vessecchi, F. S. Emery, S. E. Galembeck, N. P. Lopes. Fragmentation studies and electrospray ionization mass spectrometry of lapachol: protonated, deprotonated and cationized species. *Rapid Commun. Mass Spectrom.* **2010**, *24*, 2101.
- [265] W. M. A. Niessen. Fragmentation of toxicologically relevant drugs in negative-ion liquid chromatography-tandem mass spectrometry. *Mass Spectrom. Rev.* **2011**, *31*, 626.
- [266] J. A. Hibbs, F. B. Jariwala, C. S. Weisbecker, A. B. Attygalle. Gas-phase fragmentations of anions derived from N-phenyl benzenesulfonamides. *J. Am. Soc. Mass Spectrom.* **2013**, *24*, 1280.
- [267] R. Vessecchi, G. J. Zocolo, D. R. Gouvea, F. Hübner, B. Cramer, M. R. R. de Marchi, H.-U. Humpf, N. P. Lopes. Re-examination of the anion derivatives of isoflavones by radical fragmentation in negative electrospray ionization tandem mass spectrometry: experimental and computational studies. *Rapid Commun. Mass Spectrom.* **2011**, *25*, 2020.
- [268] A. Dreuw, L. S. Cederbaum. Multiply Charged Anions in the Gas Phase. *Chem. Rev.* **2002**, *102*, 181.
- [269] R. T. Gallagher, M. P. Balogh, P. Davey, M. R. Jackson, I. Sinclair, L. J. Southern. Combined Electrospray Ionization-Atmospheric Pressure Chemical Ionization Source for Use in High-Throughput LC-MS Applications. *Anal. Chem.* **2003**, *75*, 973.
- [270] W. C. Byrdwell, W. E. Neff. Dual parallel electrospray ionization and atmospheric pressure chemical ionization mass spectrometry (MS), MS/MS and MS/MS/MS for the analysis of triacylglycerols and triacylglycerol oxidation products. *Rapid Commun. Mass Spectrom.* **2002**, *16*, 300.

- [271] P. Wurtinger, H. Oberacher. Evaluation of the performance of a tandem mass spectral library with mass spectral data extracted from literature. *Drug Test. Anal.* **2012**, 4, 235.
- [272] T. Koal, D. Schmiederer, H. Pham-Tuan, C. Röhring, M. Rauh. Standardized LC-MS/MS based steroid hormone profile-analysis. *J. Steroid Biochem. Mol. Biol.* **2012**, 129, 129.
- [273] J. A. Ray, M. M. Kushnir, A. L. Rockwood, A. W. Meikle. Analysis of cortisol, cortisone and dexamethasone in human serum using liquid chromatography tandem mass spectrometry and assessment of cortisol: cortisone ratios in patients with impaired kidney function. *Clin. Chim. Acta.* **2011**, 412, 1221.
- [274] X. Zhai, F. Chen, C. Zhu, Y. Lu. A simple LC-MS/MS method for the determination of cortisol, cortisone and tetrahydro-metabolites in human urine: assay development, validation and application in depression patients. *J. Pharm. Biomed. Anal.* **2015**, 107, 450.
- [275] V. Gabelica, E. De Pauw. Internal energy and fragmentation of ions produced in electrospray sources. *Mass Spectrom. Rev.* **2004**, 24, 566.
- [276] M. Herderich, E. Richling, R. Roscher, C. Schneider, W. Schwab, H.-U. Humpf, P. Schreier. Application of atmospheric pressure ionization HPLC-MS-MS for the analysis of natural products. *Chromatographia* **1997**, 45, 127.
- [277] R. Boyd, A. Somogyi. The mobile proton hypothesis in fragmentation of protonated peptides: a perspective. *J. Am. Soc. Mass Spectrom.* **2010**, 21, 1275.
- [278] V. H. Wysocki, G. Tsaprailis, L. L. Smith, L. A. Breci. Mobile and localized protons: a framework for understanding peptide dissociation. *J. Mass Spectrom.* **2000**, 35, 1399.
- [279] E. A. Kapp, F. Schütz, G. E. Reid, J. S. Eddes, R. L. Moritz, R. A. J. O'Hair, T. P. Speed, R. J. Simpson. Mining a Tandem Mass Spectrometry Database To Determine the Trends and Global Factors Influencing Peptide Fragmentation. *Anal. Chem.* **2003**, 75, 6251.
- [280] Y. Huang, J. M. Triscari, G. C. Tseng, L. Pasa-Tolic, M. S. Lipton, R. D. Smith, V. H. Wysocki. Statistical characterization of the charge state and residue dependence of low-energy CID peptide dissociation patterns. *Anal. Chem.* **2009**, 77, 5800.
- [281] T. J. D. Jørgensen, H. Gårdsvoll, M. Ploug, P. Roepstorff. Intramolecular migration of amide hydrogens in protonated peptides upon collisional activation. *J. Am. Chem. Soc.* **2005**, 127, 2785.

- [282] M. Cydzik, M. Rudowska, P. Stefanowicz, Z. Szewczuk. The competition of charge remote and charge directed fragmentation mechanisms in quaternary ammonium salt derivatized peptides--an isotopic exchange study. *J. Am. Soc. Mass Spectrom.* **2011**, 22, 2103.
- [283] D. K. Bohme. Proton transport in the catalyzed gas-phase isomerization of protonated molecules. *Int. J. Mass Spectrom. Ion Process.* **1992**, 115, 95.
- [284] C. Knight, G. A. Voth. The curious case of the hydrated proton. *Acc. Chem. Res.* **2012**, 45, 101.
- [285] S. W. Holman, P. Wright, G. J. Langley. The low-energy collision-induced dissociation product ion spectra of protonated beta-blockers reveal an analogy to fragmentation behaviour under electron ionisation conditions. *J. Mass Spectrom.* **2011**, 46, 1182.
- [286] C. K. Fagerquist, A. R. Lightfield, S. J. Lehotay. Confirmatory and quantitative analysis of beta-lactam antibiotics in bovine kidney tissue by dispersive solid-phase extraction and liquid chromatography-tandem mass spectrometry. *Anal. Chem.* **2005**, 77, 1473.
- [287] F. Falvo, L. Fiebig, F. Dreiocker, R. Wang, P. B. Armentrout, M. Schäfer. Fragmentation reactions of thiourea- and urea-compounds examined by tandem MS-, energy-resolved CID experiments, and theory. *Int. J. Mass Spectrom.* **2012**, 330-332, 124.
- [288] J. Zhang, Y. Chai, K. Jiang, H. Yang, Y. Pan, C. Sun. Gas phase retro-Michael reaction resulting from dissociative protonation: fragmentation of protonated warfarin in mass spectrometry. *J. Mass Spectrom.* **2012**, 47, 1059.
- [289] Z. You, C. Guo, Y. Pan. An experimental and theoretical study on fragmentation of protonated N-(2-pyridinylmethyl)indole in electrospray ionization mass spectrometry. *Rapid Commun. Mass Spectrom.* **2012**, 26, 2509.
- [290] K. Jiang, G. Bian, N. Hu, Y. Pan, G. Lai. Coordinated dissociative proton transfers of external proton and thiocarbamide hydrogen: MS experimental and theoretical studies on the fragmentation of protonated S-methyl benzenylmethylenhydrazine dithiocarboxylate in gas phase. *Int. J. Mass Spectrom.* **2010**, 291, 17.
- [291] O. Kurka, J. Roithová, P. Bednář. Examination of small molecule losses in 5-methylpyranopelargonidin MS/MS CID spectra by DFT calculations. *J. Mass Spectrom.* **2014**, 49, 1314.
- [292] M. Li, M. Lin, A. M. Rustum. Gas-phase formation of protonated benzene during collision-induced dissociation of certain protonated mono-substituted aromatic

- molecules produced in electrospray ionization. *Rapid Commun. Mass Spectrom.* **2010**, *24*, 1707.
- [293] C. Guo, L. Yue, M. Guo, K. Jiang, Y. Pan. Elimination of benzene from protonated N-benzylindoline: benzyl cation/proton transfer or direct proton transfer? *J. Am. Soc. Mass Spectrom.* **2013**, *24*, 381.
- [294] F. Madeja, M. Havenith. High resolution spectroscopy of carboxylic acid in the gas phase: Observation of proton transfer in (DCOOH). *J. Chem. Phys.* **2002**, *117*, 7162.
- [295] P. Wright, A. Alex, F. Pullen. Predicting collision-induced dissociation spectra: Semi-empirical calculations as a rapid and effective tool in software-aided mass spectral interpretation. *Rapid Commun. Mass Spectrom.* **2014**, *28*, 1127.
- [296] Z. Gregg, W. Ijaz, S. Jannetti, G. L. Barnes. The Role of Proton Transfer in Surface-Induced Dissociation. *J. Phys. Chem. C* **2014**, *118*, 22149.
- [297] S. H. Lee, D. W. Choi. Comparison between Source-induced Dissociation and Collision-induced Dissociation of Ampicillin, Chloramphenicol, Ciprofloxacin, and Oxytetracycline via Mass Spectrometry. *Toxicol. Res.* **2013**, *29*, 107.
- [298] N. Bache, K. D. Rand, P. Roepstorff, M. Ploug, T. J. D. Jørgensen. Hydrogen atom scrambling in selectively labeled anionic peptides upon collisional activation by MALDI tandem time-of-flight mass spectrometry. *J. Am. Soc. Mass Spectrom.* **2008**, *19*, 1719.
- [299] S. Pulkkinen, M. Noguera, L. Rodríguez-Santiago, M. Sodupe, J. Bertran. Gas phase intramolecular proton transfer in cationized glycine and chlorine substituted derivatives (M-Gly, M = Na⁺, Mg²⁺, Cu⁺, Ni⁺, and Cu²⁺): existence of Zwitterionic structures? *Chemistry* **2000**, *6*, 4393.
- [300] H. Lioe, R. A. J. O'Hair, G. E. Reid. A mass spectrometric and molecular orbital study of H₂O loss from protonated tryptophan and oxidized tryptophan derivatives. *Rapid Commun. Mass Spectrom.* **2004**, *18*, 978.
- [301] P. B. Armentrout, J. Simons. Understanding heterolytic bond cleavage. *J. Am. Chem. Soc.* **1992**, *114*, 8627.
- [302] M. M. Bursey, F. W. McLafferty. Substituent Effects in Unimolecular Ion Decompositions. II. A Linear Free Energy Relationship between Acyl Ion Intensities in the Mass Spectra of Substituted Acylbenzenes 1,2. *J. Am. Chem. Soc.* **1966**, *88*, 529.
- [303] W. A. Tao, F. C. Gozzo, R. G. Cooks. Mass Spectrometric Quantitation of Chiral Drugs by the Kinetic Method. *Anal. Chem.* **2001**, *73*, 1692.

APPENDIX 1: THE PKA'S OF THE TEST COMPOUNDS

The pKa's were calculated using ChemAxon MarvinView. The values shown in blue describe dissociation to the conjugated acid and the values shown in red describe dissociation to the conjugated base.

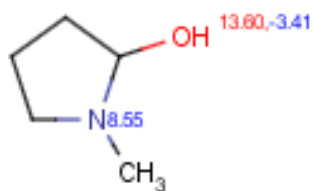


Figure A-1.1 Methyl-2-pyrrolidinol

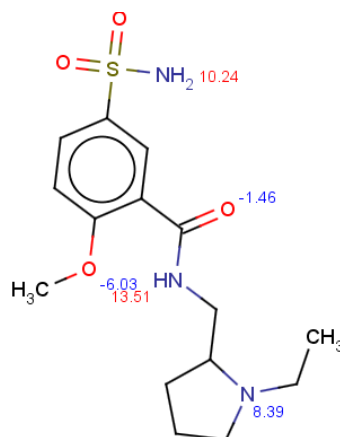


Figure A-1.2 Sulpiride

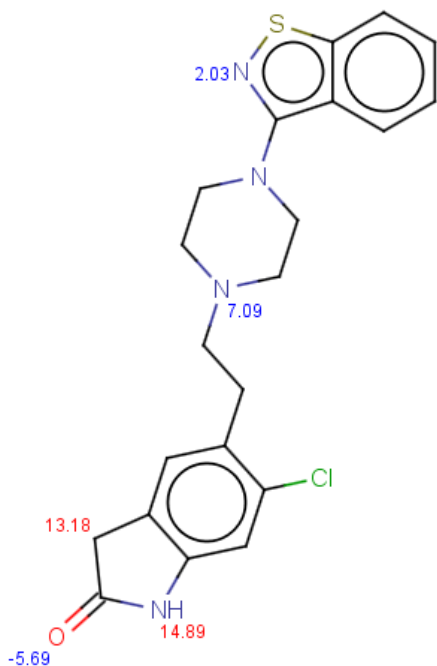


Figure A-1.3 Ziprasidone

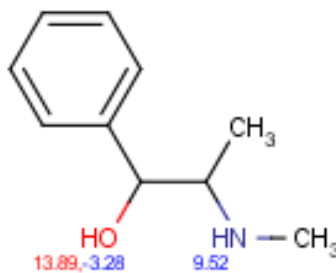


Figure A-1.4 Ephedrine

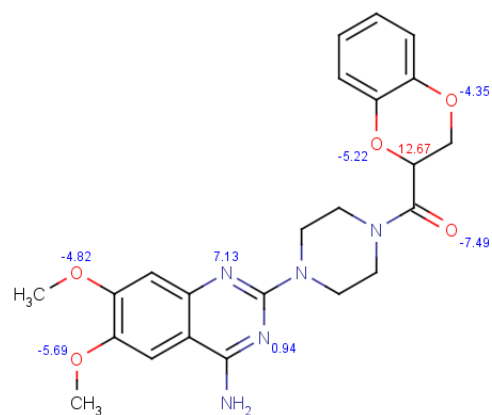


Figure A-1.5 Doxazosin

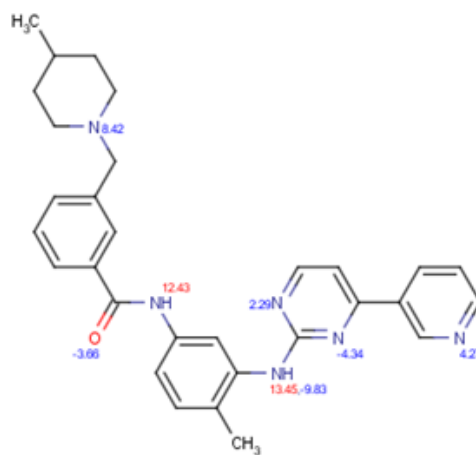


Figure A-1.6 CEN025-014

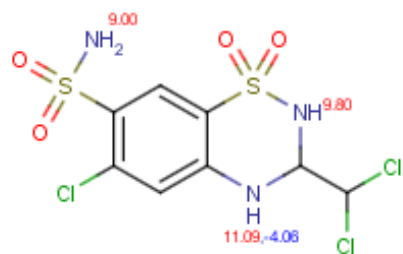


Figure A-1.7 Trichlormethiazide

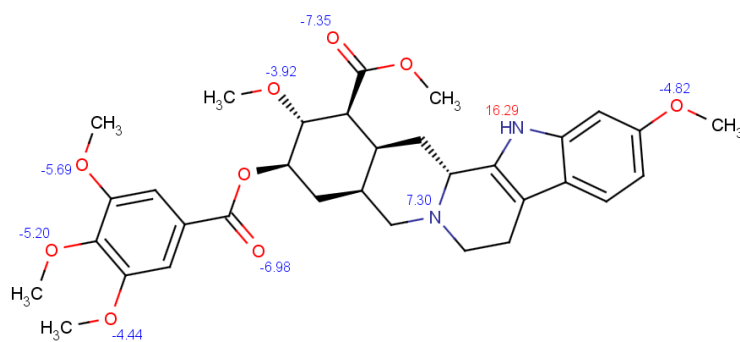


Figure A-1.8 Reserpine

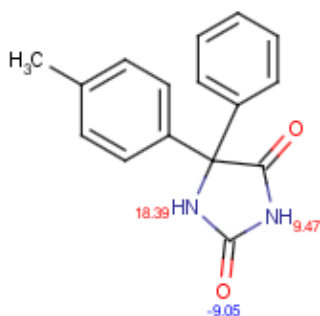


Figure A-1.9 5-(p-Methylphenyl)-Phenylhydantoin

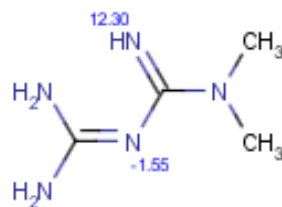


Figure A-1.10 1,1-Dimethyl biguanidine

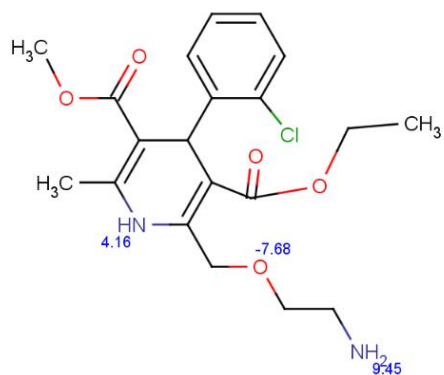


Figure A-1.11 Amlodipine

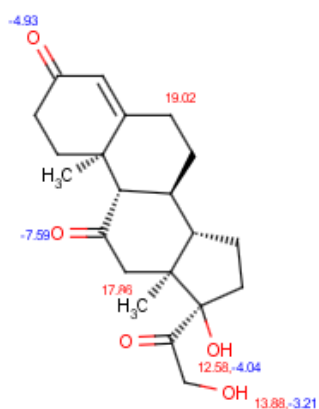


Figure A-1.12 Cortisone

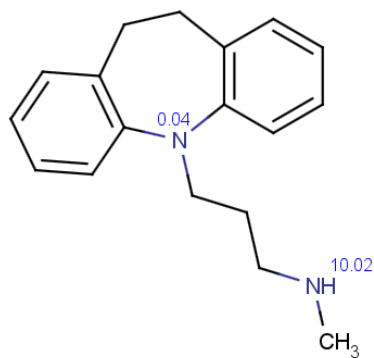


Figure A-1.13 Desipramine

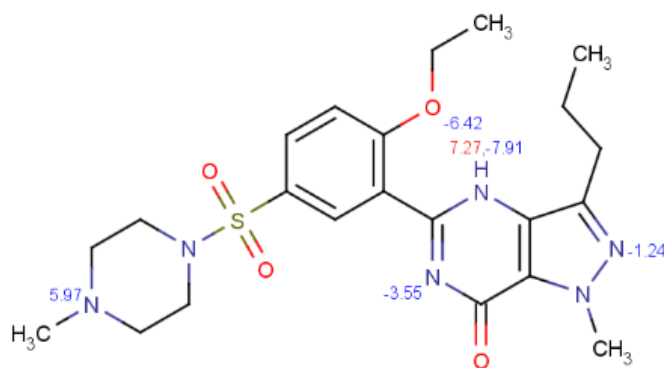


Figure A-1.14 Sildenafil

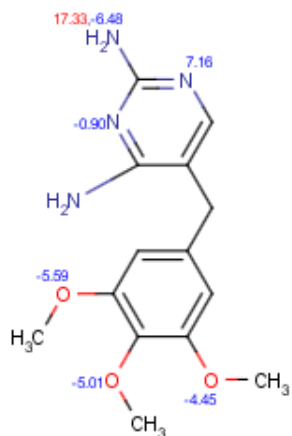


Figure A-1.15 Trimethoprim

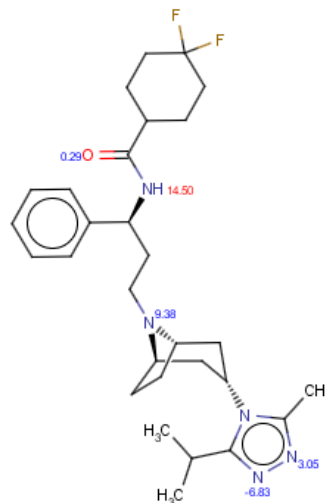


Figure A-1.16 Maraviroc

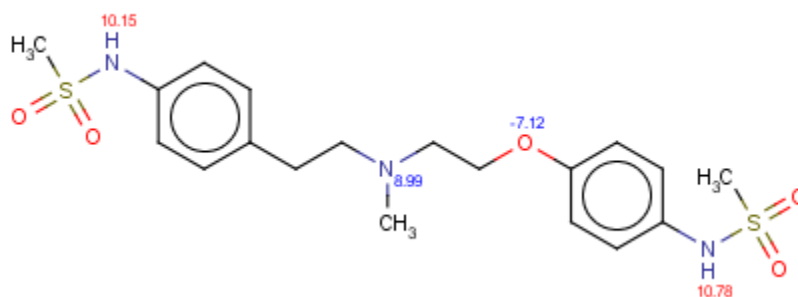


Figure A-1.17 Dofetilide

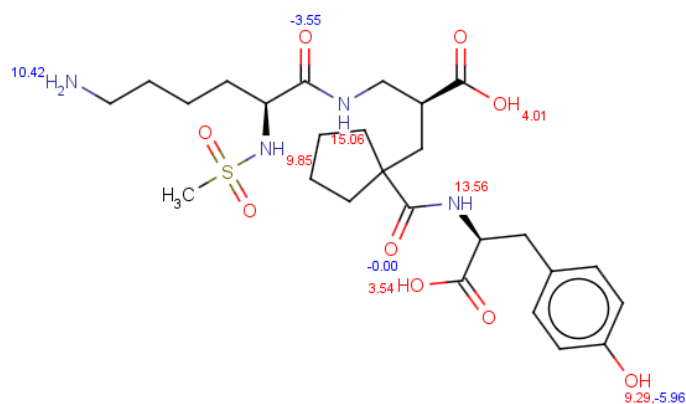


Figure A-1.18 Sampatrilat

APPENDIX 2: THE RELATIVE STABILITIES OF THE CATIONS PROTONATED AT HETEROATOMS IN TEST COMPOUNDS

Relative stabilities were calculated using DFT Spartan'10, basis set 6.31G*. The stabilities of the different possible protonation sites reflect their relative gas phase basicities.

Table A-2.1 1-Methyl-2-pyrrolidinol.

<i>E</i> (kcal mol ⁻¹)			Energy Difference between Cation C2 and Cation C1 (kcal mol ⁻¹)			
AM1	DFT 6.31G**	DFT 6.31++G**	AM1	DFT 6.31G**	DFT 6.31++G**	
412	-328	-328	0	0	0	Cation 2
455	-328	-328	2	4	3	Cation 1
-220	-327	-327	n/a	n/a	n/a	Neutral

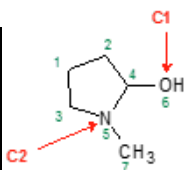


Table A-2.2 Sulpiride.

<i>E</i> (kcal mol ⁻¹)		Energy Difference between most stable cation and others (kcal mol ⁻¹)	<i>E</i> (Kcal mol ⁻¹)		Energy Difference between most stable cation and others (kcal mol ⁻¹)
AM1			DFT 6.31G**		
-123	Neutral	n/a	-909102	Neutral	n/a
15	Cation2	0	-909358	Cation2	0
20	Cation1	4	-909358	Cation1	1
23	Cation4	8	-909348	Cation4	11
30	Cation3	14	-909325	Cation5	33
30	Cation5	15	-909325	Cation7	33
32	Cation6	17	-909319	Cation6	39
43	Cation7	28	-904902	Cation3	44

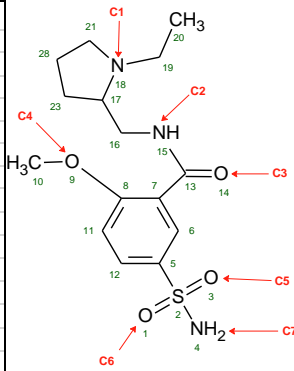


Table A-2.3 Ziprasidone.

E (kcal mol ⁻¹)		Energy Difference between most stable cation and others (kcal mol ⁻¹)	E (Kcal/mol ⁻¹)		Energy Difference between most stable cation and others (kcal mol ⁻¹)
AM1			DFT 6.31G**		
61	Neutral	n/a	-1233396.9	Neutral	n/a
204	Cation 3	0	-1233643.2	Cation 4	0
204	Cation 4	0	-1233639	Cation 2	4
205	Cation 2	1	-1233634.3	Cation 3	9
223	Cation 1	19	-1233604.5	Cation 6	26
228	Cation 6	24	-1233607.7	Cation 8	36
229	Cation 8	25	-1233602.5	Cation 1	39
230	Cation 5	25	-1233602.5	Cation 5	41
267	Cation 7	63	-1233564.9	Cation 7	78

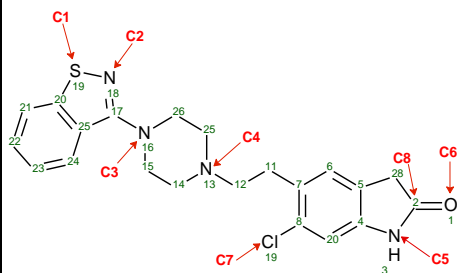


Table A-2.4 Ephedrine.

E (kcal mol ⁻¹)		Energy Difference between Cation C2 and Cation C1 (kcal mol ⁻¹)		
AM1	DFT 6.31G**	AM1	DFT 6.31G**	
115	-326600	0	0	Cation 2
143	-326604	29	4	Cation 1
-31	-326357	n/a	n/a	Neutral

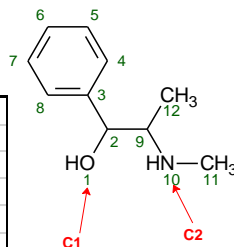


Table A-2.5 Doxazosin

E (kcal mol ⁻¹)		Energy Difference between most stable cation and others (kcal mol ⁻¹)	E (kcal mol ⁻¹)		Energy Difference between most stable cation and others (kcal mol ⁻¹)
AM1			DFT 6.31G**		
0	Cation3	0	-967510	Cation5	0
132	Cation5	32	-967497	Cation4	12
255	Cation4	61	-967494	Cation6	16
280	Cation6	67	-967491	Cation10	19
304	Cation10	73	-967477	Cation3	33
321	Cation8	77	-967481	Cation8	17
342	Cation7	82	-967476	Cation7	33
404	Cation2	96	-967467	Cation2	43
437	Cation1	104	-967460	Cation1	49
463	Cation9	111	-967455	Cation9	55

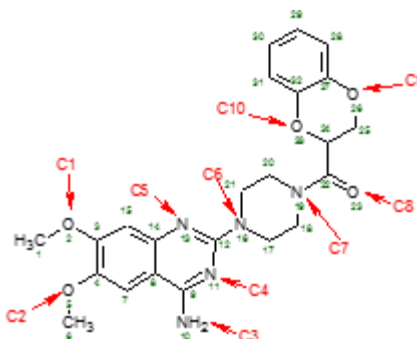


Table A-2.6 CEN025-014.

E (kcal mol ⁻¹)		Energy Difference between most stable cation and others (kcal mol ⁻¹)	E (Kcal/mol)		Energy Difference between most stable cation and others (kcal mol ⁻¹)
AM1			DFT 6.31G**		
98	Neutral		98	Neutral	
237	Cation 6	0	-983114	Cation6	0
245	Cation 1	7	-983110	Cation 1	4
245	Cation 2	8	-983108	Cation2	5
247	Cation 5	10	-983095	Cation4	18
247	Cation7	10	-983087	Cation5	27
251	Cation 4	13	-983075	Cation3	38
254	Cation3	16	-983056	Cation7	57

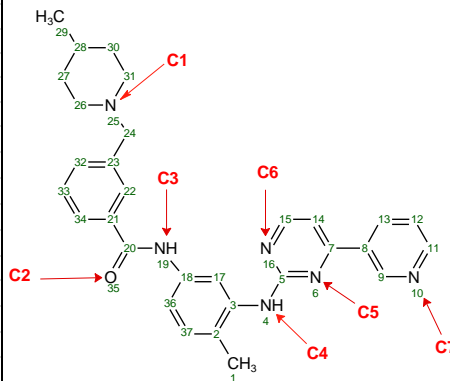


Table A-2.7 Trichlormethiazide

<i>E (kcal mol⁻¹)</i>		<i>Energy Difference between most stable cation and others (kcal mol⁻¹)</i>	<i>E (kcal mol⁻¹)</i>		<i>Energy Difference between most stable cation and others (kcal mol⁻¹)</i>
AM1			DFT 6.31G**		
-112	Neutral	n/a	-1852184	Neutral	n/a
41	Cation7	0	-1852402	Cation5	0
43	Cation6	2	-1852397	Cation7	5
49	Cation4	8	-1852394	Cation2	8
49	Cation3	9	-1852393	Cation6	9
53	Cation5	13	-1852390	Cation4	12
67	Cation1	26	-1852390	Cation3	12
69	Cation2	28	-1852387	Cation1	15

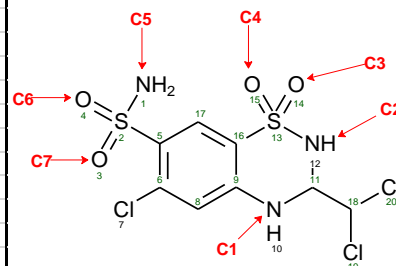


Table A-2.8 Reserpine

<i>Energy (kcal mol⁻¹)</i>		<i>Energy Difference between most stable cation and others (kcal mol⁻¹)</i>	<i>Energy (kcal mol⁻¹)</i>		<i>Energy Difference between most stable cation and others (kcal mol⁻¹)</i>
AM1			DFT 6.31G**		
-278	Neutral	n/a	-1297781	Neutral	n/a
-137	Cation9	0	-1298031	Cation9	0
-121	Cation8	16	-1298011	Cation4	20
-118	Cation3	19	-1298009	Cation3	22
-116	Cation4	20	-1298003	Cation8	28
-108	Cation2	29	-1298000	Cation10	31
-102	Cation10	35	-1297999	Cation5	33
-100	Cation11	36	-1297996	Cation2	35
-99	Cation5	38	-1297995	Cation6	36
-97	Cation1	39	-1297991	Cation1	41
-97	Cation6	40	-1297990	Cation7	41
-93	Cation7	43	-1297987	Cation11	44

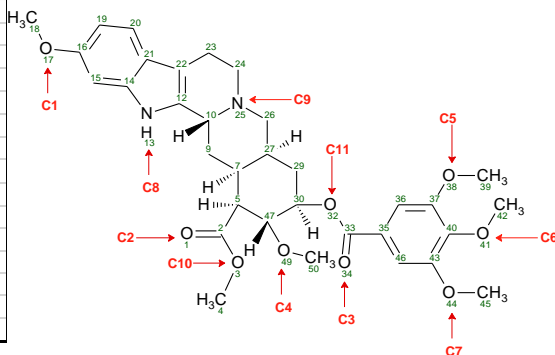


Table A-2.9 5-(*p*-Methylphenyl)- 5-phenylhydantoin

E (kcal mol ⁻¹)		Energy Difference between most stable Cation and others (kcal mol ⁻¹)	E (kcal mol ⁻¹)		Energy Difference between most stable Cation and others (kcal mol ⁻¹)
AM1			DFT 6.31G**		
1	Neutral	n/a	-551050	Neutral	n/a
164	Cation1	0	-551268	Cation3	0
164	Cation3	1	-551263	Cation1	5
172	Cation4	8	-5521249	Cation2	14
174	Cation2	11	-54878	Cation4	3391

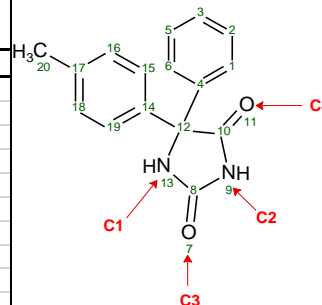


Table A-2.10 1,1-Dimethyl biguanidine

E (kcal mol ⁻¹)		Energy Difference between most stable cation and others (kcal mol ⁻¹)	E (kcal mol ⁻¹)		Energy Difference between most stable cation and others (kcal mol ⁻¹)	E (kcal mol ⁻¹)		Energy Difference between most stable cation and others (kcal mol ⁻¹)
AM1			DFT 6.31G**			DFT 6.31++G**		
59	Neutral	n/a	-271591	Neutral	n/a	-271669	Neutral	n/a
190	Cation 4	0	-271882	Cation 3	0	-271925	Cation 5	0
189	Cation 5	0	-271860	Cation 4	23	-271925	Cation 4	0
221	Cation 2	32	-271857	Cation 5	25	-271882	Cation 3	42
223	Cation 3	34	-271811	Cation 1	72	-271879	Cation 1	45
224	Cation 1	35	-271794	Cation 2	88	-271811	Cation 2	113

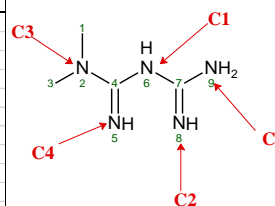


Table A-2.11 Amlodipine

E (kcal mol ⁻¹)		Energy Difference between most stable cation and others (kcal mol ⁻¹)	E (kcal mol ⁻¹)		Energy Difference between most stable Cation and others (kcal mol ⁻¹)
AM1			DFT 6.31G**		
-172	Neutral	n/a	-1081222	Neutral	n/a
-33	Cation1	0	-1081473	Cation5	0
-27	Cation6	6	-1081465	Cation1	8
-24	Cation3	8	-1081465	Cation3	8
-10	Cation7	23	-1081463	Cation6	10
-9	Cation4	23	-1081445	Cation4	28
-5	Cation5	28	-1081443	Cation2	31
5	Cation2	38	-1081441	Cation7	32

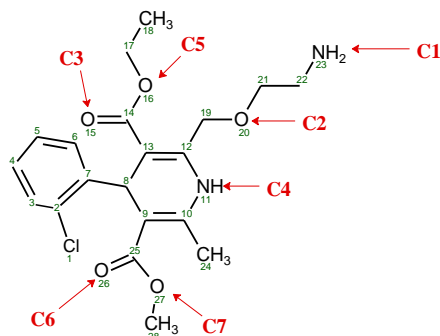


Table A-2.12 Cortisone

E (kcal mol ⁻¹)		Energy Difference between most stable cation and others (kcal mol ⁻¹)	E (kcal mol ⁻¹)		Energy Difference between most stable Cation and others (kcal mol ⁻¹)
AM1			DFT 6.31G**		
-217	Neutral	n/a	-748766.1	Neutral	n/a
-60	Cation1	0	-748997	Cation1	0
-47	Cation2	13	-748980	Cation2	17
-44	Cation4	16	-748980	Cation4	17
-44	Cation3	16	-748980	Cation3	17
-36	Cation5	24	-748974	Cation5	23

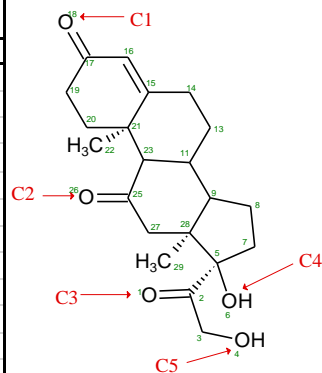


Table A-2.13 Desipramine

E (kcal mol ⁻¹)		Energy Difference between most stable cation and others (kcal mol ⁻¹)	E (kcal mol ⁻¹)		Energy Difference between most stable cation and others (kcal mol ⁻¹)
AM1			DFT 6.31G**		
55	Neutral	n/a	-507458	Neutral	n/a
202	Cation1	0	-507698	Cation1	0
205	Cation2	2	-507699	Cation2	2

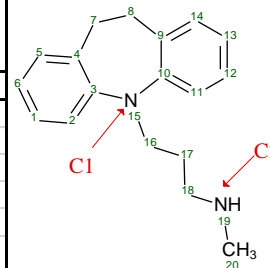


Table A-2.14 Sildenafil

E (kcal mol ⁻¹)		Energy Difference between most stable cation and others (kcal mol ⁻¹)	E (kcal mol ⁻¹)		Energy Difference between most stable Cation and others (kcal mol ⁻¹)
AM1			DFT 6.31G**		
-16	Neutral	n/a	-1182207	Neutral	n/a
119	Cation5	0	-1182469	Cation1	0
123	Cation6	3	-1182469	Cation10	1
123	Cation1	4	-1182467	Cation5	2
123	Cation10	4	-1182466	Cation6	2
134	Cation4	11	-1182446	Cation2	23
134	Cation3	11	-1182442	Cation8	28
145	Cation8	26	-1182441	Cation3	26
148	Cation2	25	-1182438	Cation4	29
151	Cation9	32	-1182427	Cation7	40
156	Cation7	32	-1182422	Cation9	48

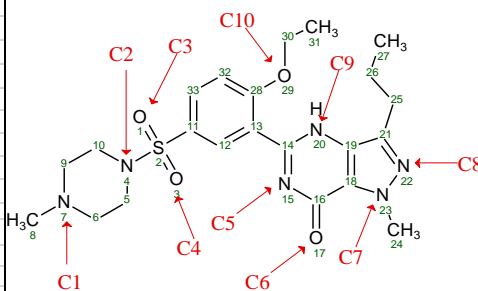


Table A-2.15 Trimethoprim

<i>E</i> (kcal mol ⁻¹)			<i>E</i> (kcal mol ⁻¹)		
Energy Difference between most stable cation and others (kcal mol ⁻¹)			Energy Difference between most stable Cation and others (kcal mol ⁻¹)		
AM1			DFT 6.31G**		
-43	Neutral	n/a	-620620	Neutral	n/a
95	Cation2	0	-620870	Cation2	0
99	Cation3	4	-620862	Cation3	8
112	Cation4	17	-620846	Cation4	24
115	Cation1	20	-620845	Cation1	25
131	Cation6	36	-620838	Cation6	32
137	Cation7	42	-620829	Cation5	41
137	Cation5	42	-620829	Cation7	41

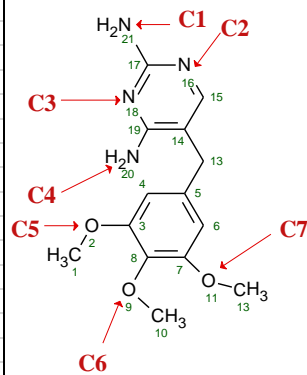


Table A-2.16 Maraviroc

<i>E</i> (kcal mol ⁻¹)			<i>E</i> (kcal mol ⁻¹)		
Energy Difference between most stable cation and others (kcal mol ⁻¹)			Energy Difference between most stable Cation and others (kcal mol ⁻¹)		
AM1			DFT 6.31G**		
-321	Neutral	n/a		Neutral	n/a
301	Cation2	0	-1679	Cation1	0
311	Cation1	10	-1679	Cation2	1
343	Cation6	43	-1679	Cation4	12
375	Cation5	74	-1679	Cation6	13
427	Cation3	127	-1679	Cation5	25
707	Cation4	407	-1679	Cation3	54

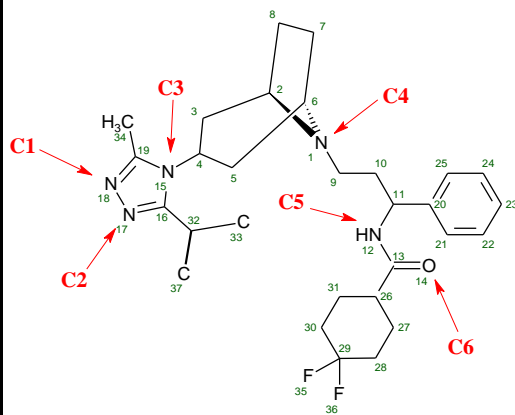


Table A-2.17 Sampatrilat

E (kcal mol ⁻¹)		Energy Difference between most stable cation and others (kcal mol ⁻¹)	E (kcal mol ⁻¹)		Energy Difference between most stable Cation and others (kcal mol ⁻¹)
AM1			DFT 6.31G**		
-395	Neutral	n/a	-1448958	Neutral	n/a
-241	Cation8	0	-1449198	Cation2	0
-238	Cation6	3	-1449196	Cation6	2
-235	Cation7	6	-1449186	Cation7	13
-230	Cation5	11	-1449184	Cation4	15
-230	Cation2	11	-1449181	Cation5	17
-226	Cation3	15	-1449168	Cation3	30
-225	Cation4	16	-1449164	Cation8	34
-204	Cation1	37	-1449150	Cation1	48

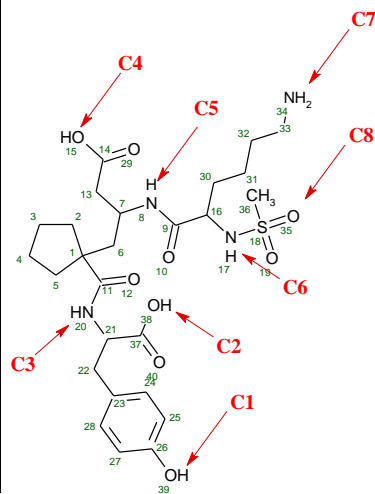
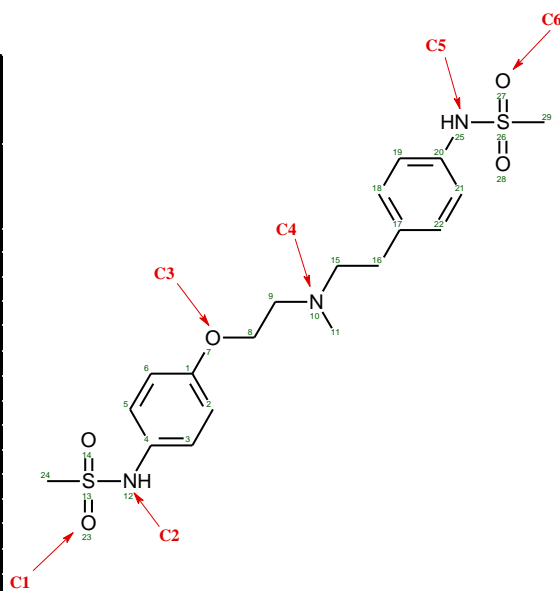


Table A-2.18 Dofetilide

E (kcal mol ⁻¹)		Energy Difference between most stable cation and others (kcal mol ⁻¹)	E (kcal mol ⁻¹)		Energy Difference between most stable Cation and others (kcal mol ⁻¹)
AM1			DFT 6.31G**		
-119	Neutral	n/a	-1303471	Neutral	n/a
-176	Cation3	0	-1303503	Cation4	0
-94	Cation4	82	-1303503	Cation1	0
33	Cation1	209	-1303484	Cation2	19
43	Cation5	219	-1303481	Cation3	22
55	Cation2	231	-1303480	Cation5	22
58	Cation6	233	-1303471	Cation6	31



APPENDIX 3: THE APCI AND ESI POSITIVE ION SPECTRA OF TEST COMPOUNDS

(ESI spectrum is the top panel and the APCI spectrum is the bottom panel).

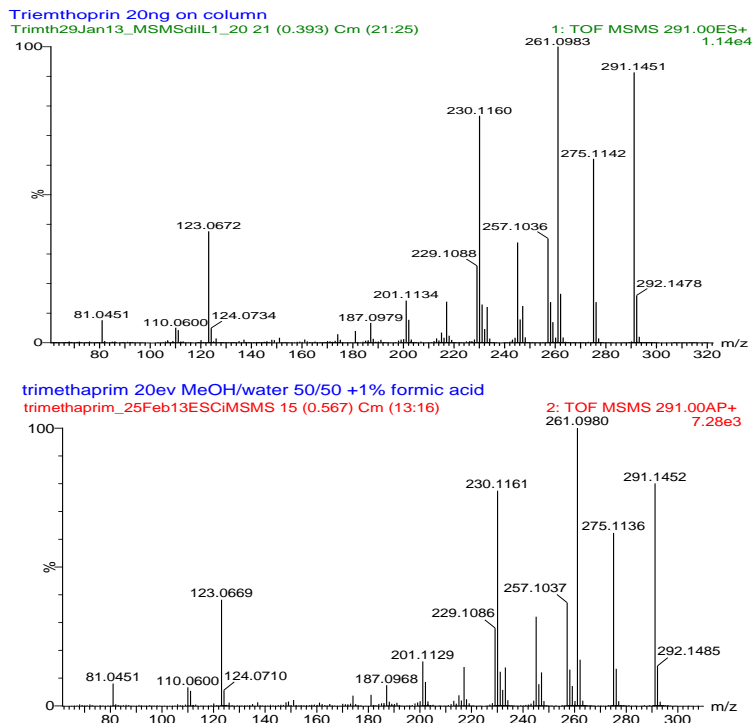


Figure A-3.1 Trimethoprim

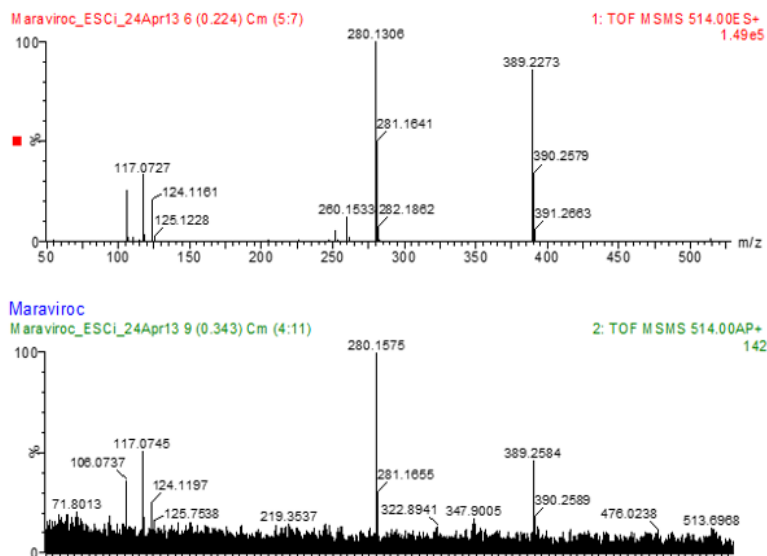


Figure A-3.2 Maraviroc

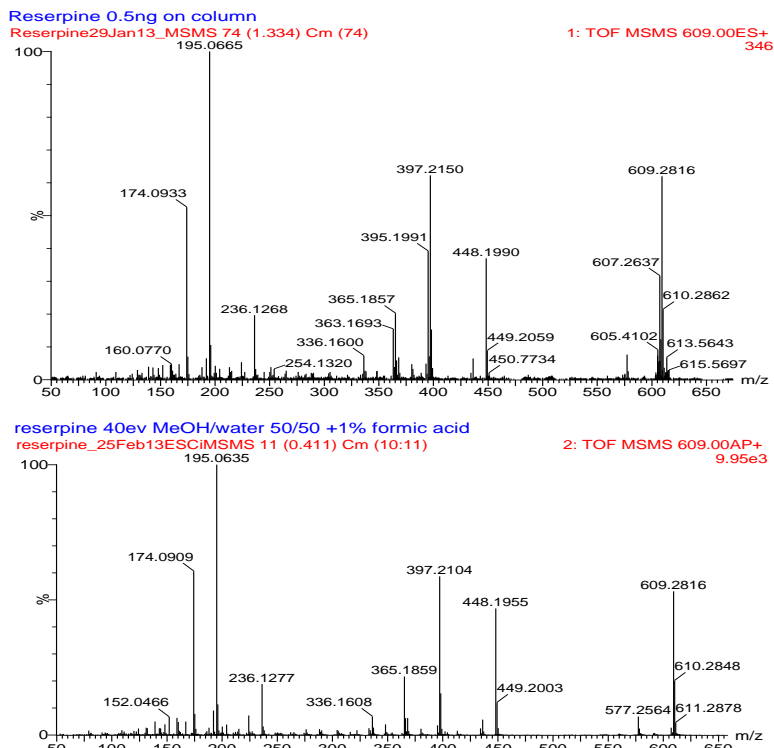


Figure A-3.3 Reserpine

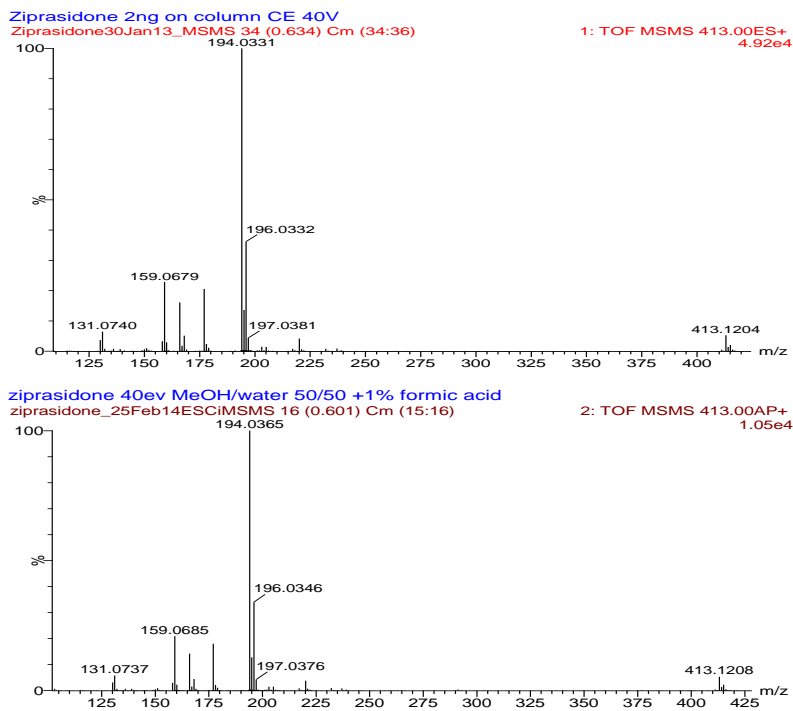


Figure A-3.4 Ziprasidone

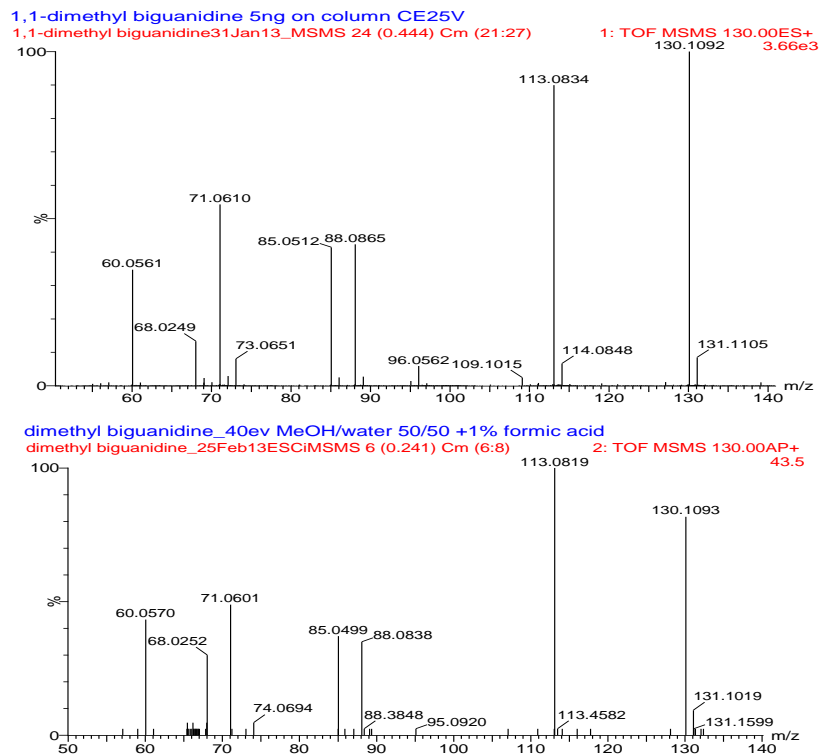


Figure A-3.5 1,1,-Dimethyl biguanidine

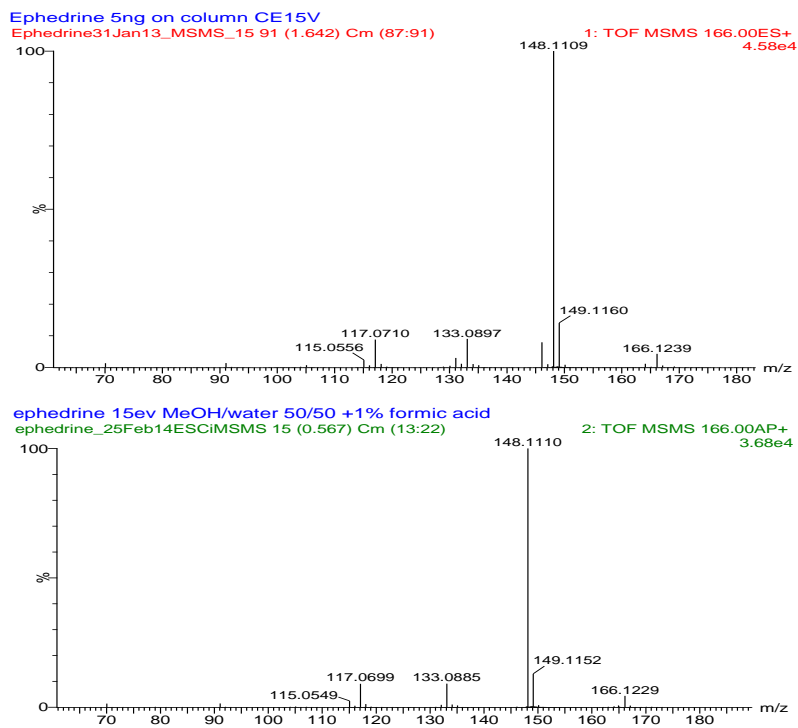


Figure A-3.6 Ephedrine

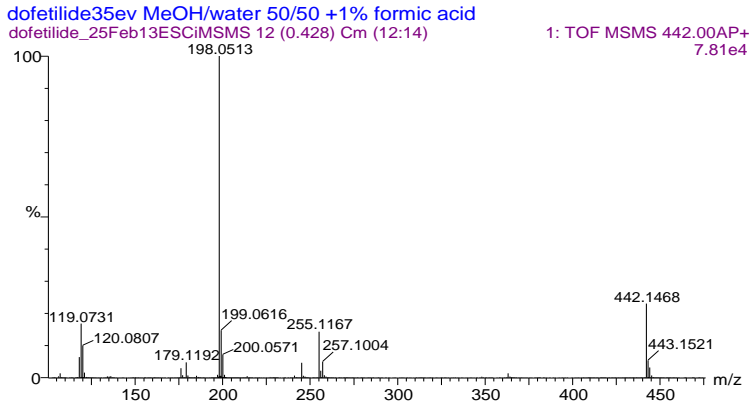
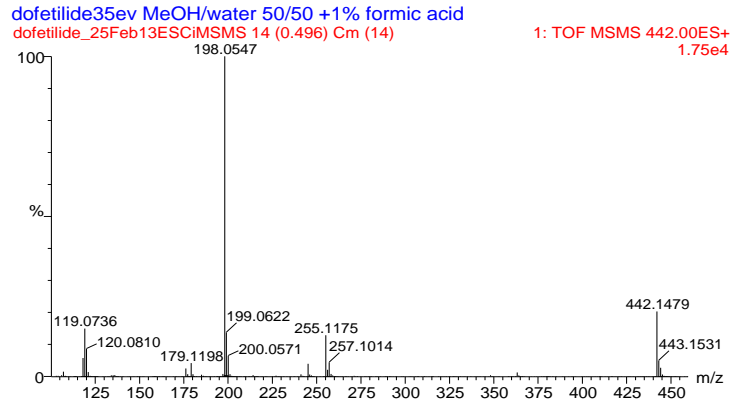


Figure A-3.7 Dofetilide

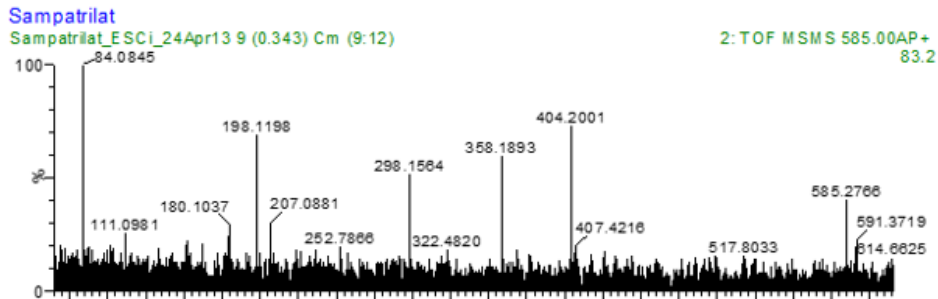
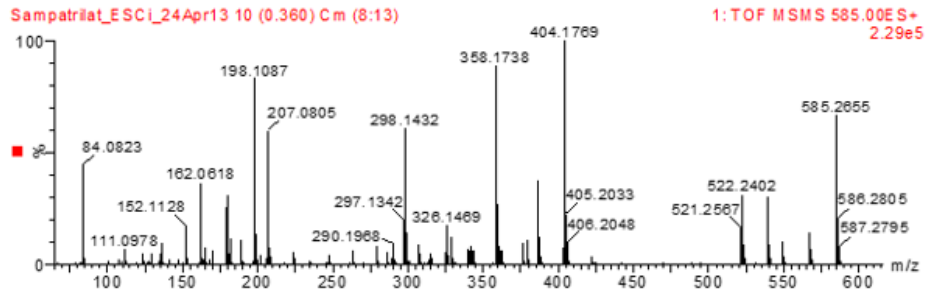
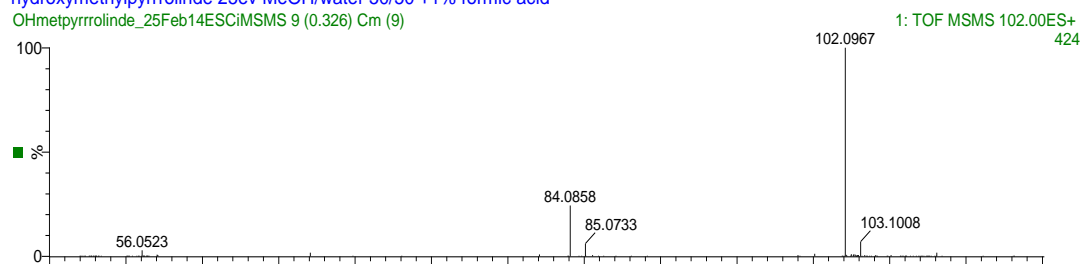


Figure A-3.8 Sampatrilate

hydroxymethylpyrrolidine 25ev MeOH/water 50/50 +1% formic acid
OHmetpyrrolidine_25Feb14ESiMSMS 9 (0.326) Cm (9)



OHmetpyrrolidine_25Feb14ESiMSMS 7 (0.275) Cm (7)

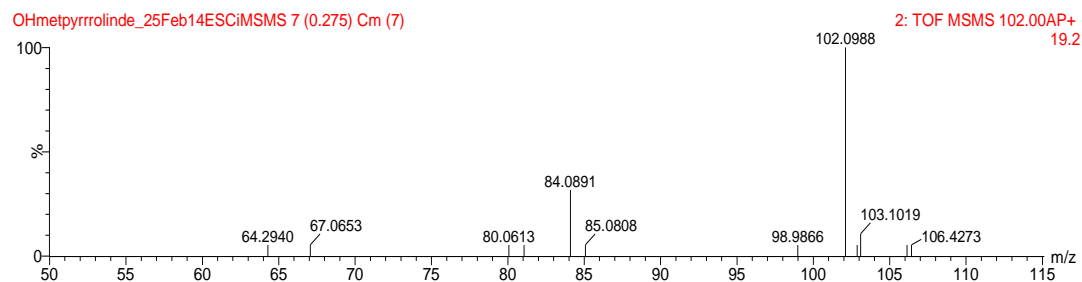
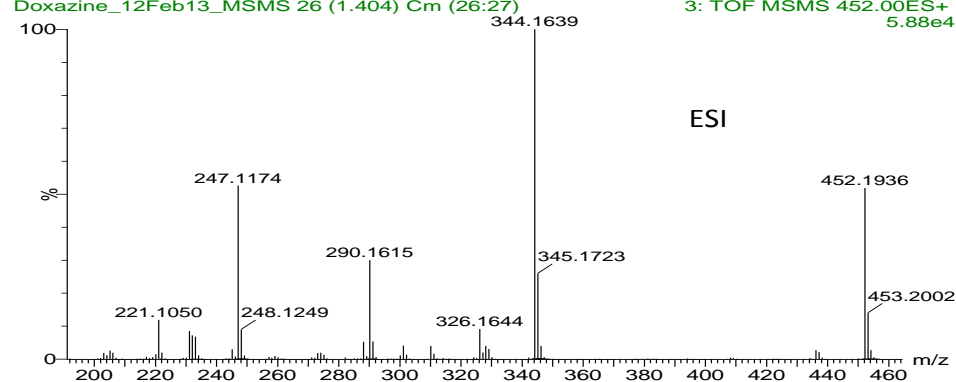


Figure A-3.9 1-Methyl-2-pyrrolidinol

Doxazine

Doxazine_12Feb13_MSMS 26 (1.404) Cm (26:27)

3: TOF MSMS 452.00ES+ 5.88e4

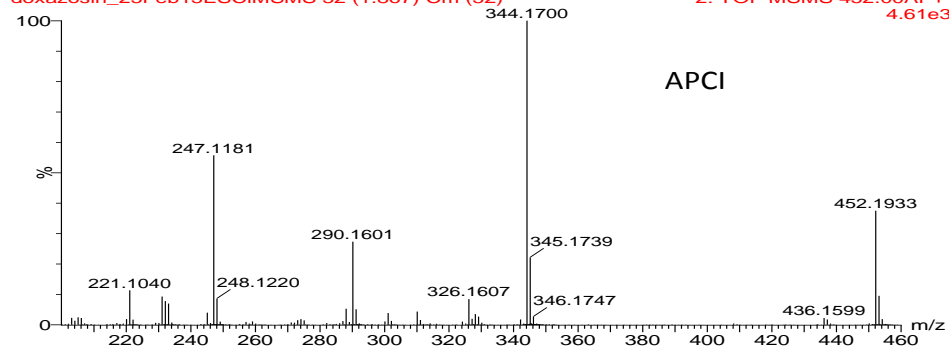


ESI

doxazosin 40ev MeOH/water 50/50 +1% formic acid

doxazosin_25Feb15ESiMSMS 52 (1.867) Cm (52)

2: TOF MSMS 452.00AP+ 4.61e3



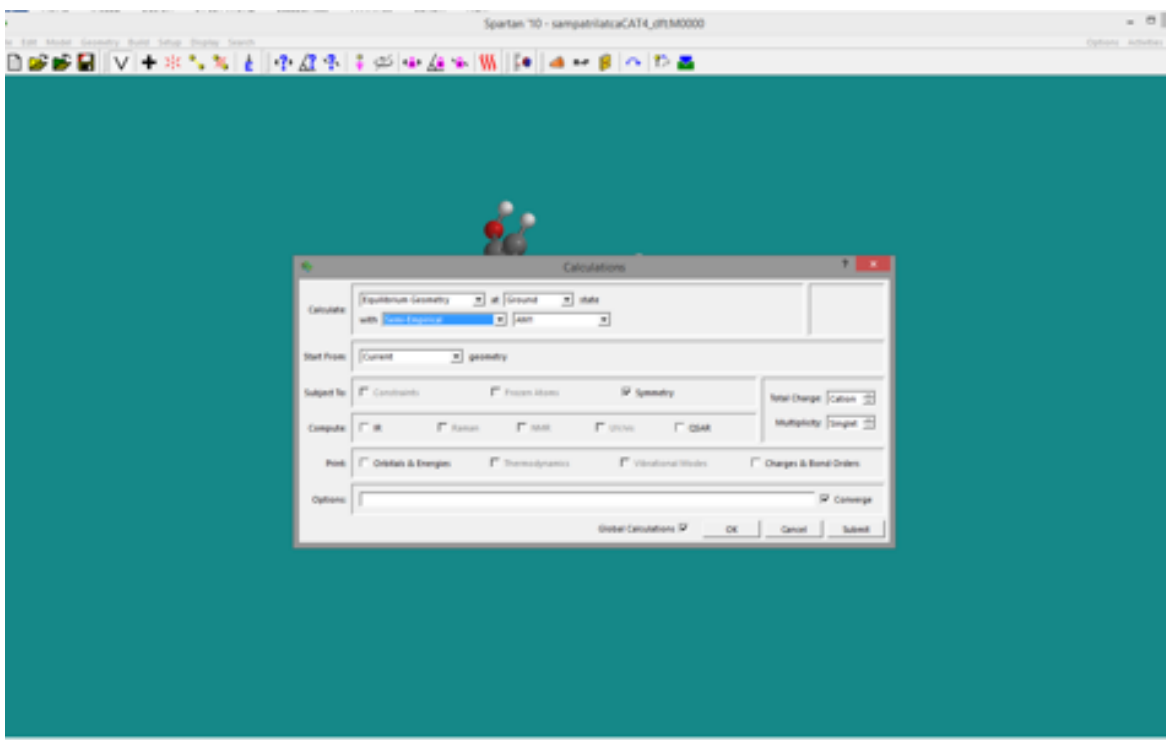
APCI

Figure A-3.10 Doxazosin

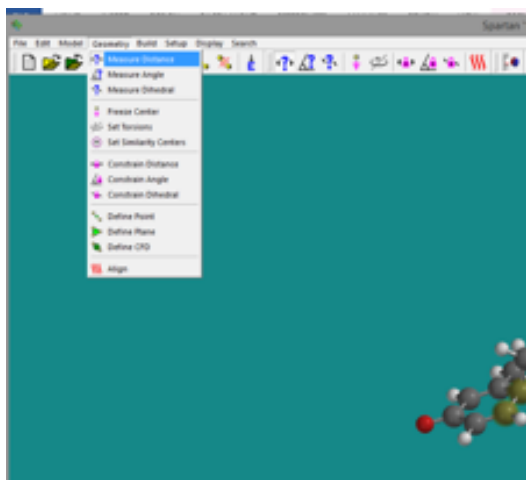
APPENDIX 4: THE WORK FLOW FOR CALCULATING THE BOND ELONGATIONS USING SPARTAN '10

For neutral structure and all protonated forms (protonated at each heteroatoms) of the molecules.

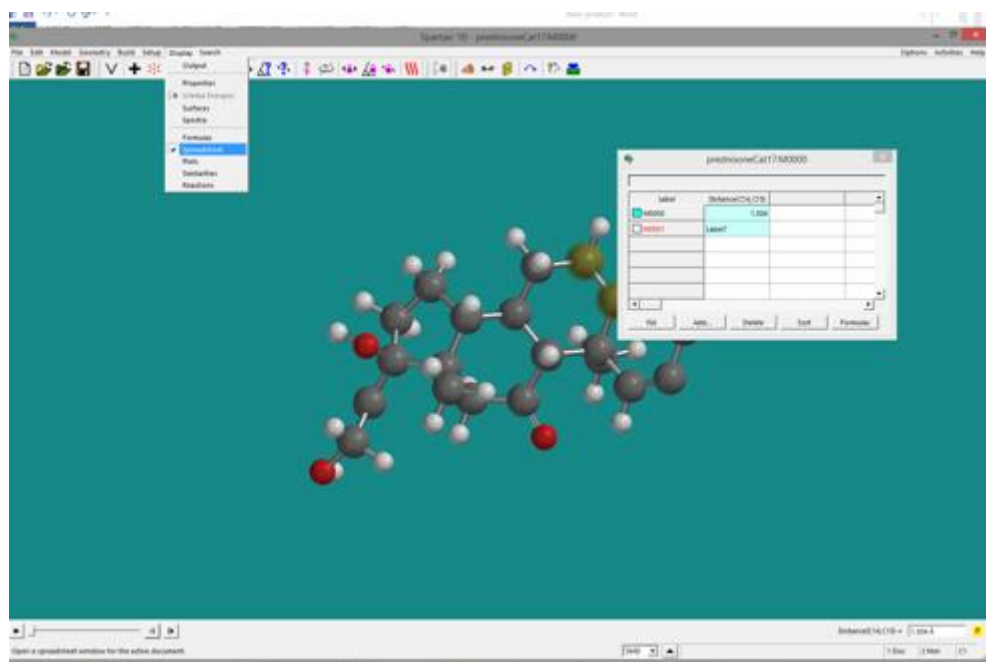
1. Structure generated or imported (as MOL file) into ChemSketch (ACD/Labs)
2. Saved as '.skc' file
3. Open Spartan Graphical interface
4. 'File', 'open' the '.skc' file
5. 'Build', 'Minimise' to perform an initial molecular mechanics energy minimisation
6. 'Set up', 'Calculation', select 'AM1' . Ensure 'converge' and 'global calculation' are selected.



7. Chose charge state
8. 'Submit'
9. Name file appropriately and proceed.
10. After calculation complete measure bond lengths as follows
 - a. 'Geometry', 'measure distance'
 - b. Use mouse to click on each end of bond to be measured (bonds in phenyl rings do not cleave therefore their bond lengths do not need to be calculated).



- c. 'P' (yellow box in bottom RH corner next to bond length value) to input bond length into spreadsheet
- d. 'Display', 'Spreadsheet' to view bond lengths
- a. 'P' (yellow box in bottom RH corner next to bond length value)



11. Copy bond lengths with bond identifiers from the spreadsheet within Spartan into Excel, being careful to ensure that all bond lengths for the neutral and all protonated molecules are in the correct columns.
12. Subtract the bond lengths of the neutral molecule from those of the corresponding bonds in each protonated form of the molecule.
13. Flag bonds which significantly elongate ($>0.025 \text{ \AA}$)* as a result of the proton being on one of the bonding atoms or the proton being available to one of the bonding atoms via an aromatic system.

APPENDIX 5: THE MAXIMUM INTERNAL ENERGY GAIN FOR EACH MOLECULE AT THE STATED COLLISIONS ENERGIES CALCULATED USING THE EQUATION S-2 IN CHAPTER 2.

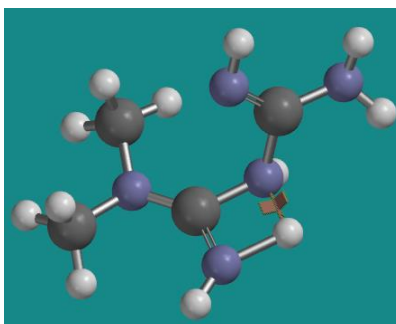
Collision Energy		5 eV	10 eV	15 eV	20 eV	25 eV	30 eV	35 eV	40 eV	45 eV	50 eV
Compound	[M+H] ⁺ (Da)	Internal energy gain (eV)									
1-methyl-2-pyrrolidinol	102	1.4	2.8	4.2	5.6	7.0	8.5	9.9	11.3	12.7	14.1
Dimethyl biguanidine	130	1.2	2.4	3.5	4.7	5.9	7.1	8.2	9.4	10.6	11.8
Ephedrine	166	1.0	1.9	2.9	3.9	4.9	5.8	6.8	7.8	8.7	9.7
Desipramine	267	0.7	1.3	2.0	2.6	3.3	4.0	4.6	5.3	6.0	6.6
Trimethaprim	291	0.6	1.2	1.8	2.4	3.0	3.6	4.2	4.8	5.4	6.0
Cortisone	342	0.5	1.0	1.6	2.1	2.6	3.1	3.7	4.2	4.7	5.2
Trichloromethiazide	361	0.5	1.0	1.5	2.0	2.5	3.0	3.5	4.0	4.5	5.0
Amlodipine	409	0.4	0.9	1.3	1.8	2.2	2.7	3.1	3.6	4.0	4.5
Ziprasidone	413	0.4	0.9	1.3	1.8	2.2	2.6	3.1	3.5	4.0	4.4
Dofetilide	442	0.4	0.8	1.2	1.7	2.1	2.5	2.9	3.3	3.7	4.1
Doxasine	452	0.4	0.8	1.2	1.6	2.0	2.4	2.8	3.3	3.7	4.1
Sildenafil	475	0.4	0.8	1.2	1.6	1.9	2.3	2.7	3.1	3.5	3.9
CEN025-14	493	0.4	0.8	1.1	1.5	1.9	2.3	2.6	3.0	3.4	3.8
Maraviroc	514	0.4	0.7	1.1	1.4	1.8	2.2	2.5	2.9	3.2	3.6
Sampatrilat	585	0.3	0.6	1.0	1.3	1.6	1.9	2.2	2.6	2.9	3.2
Reserpine	609	0.3	0.6	0.9	1.2	1.5	1.8	2.2	2.5	2.8	3.1

Collision Energy		5 eV	10 eV	15 eV	20 eV	25 eV	30 eV	35 eV	40 eV	45 eV	50 eV
Compound	[M+H] ⁺ (Da)	Internal energy gain (kcal mol ⁻¹)									
1-Methyl-2-pyrrolidinol	102	32	65	97	130	162	194	227	259	292	324
Dimethyl biguanidine	130	27	54	81	108	135	162	189	216	244	271
Ephedrine	166	22	45	67	89	112	134	156	179	201	223
Desipramine	267	15	30	46	61	76	91	107	122	137	152
Trimethaprim	291	14	28	42	56	69	83	97	111	125	139
Cortisone	342	12	24	36	48	60	72	84	96	108	120
Trichloromethiazide	361	11	23	34	46	57	69	80	92	103	115
Amlodipine	409	10	20	31	41	51	61	72	82	92	102
Ziprasidone	413	10	20	30	41	51	61	71	81	91	102
Dofetilide	442	10	19	29	38	48	57	67	76	86	95
Doxasine	452	9	19	28	37	47	56	65	75	84	93
Sildenafil	475	9	18	27	36	45	54	63	71	80	89
CEN025-14	493	9	17	26	35	43	52	60	69	78	86
Maraviroc	514	8	17	25	33	42	50	58	66	75	83
Sampatrilat	585	7	15	22	29	37	44	52	59	66	74
Reserpine	609	7	14	21	28	35	43	50	57	64	71

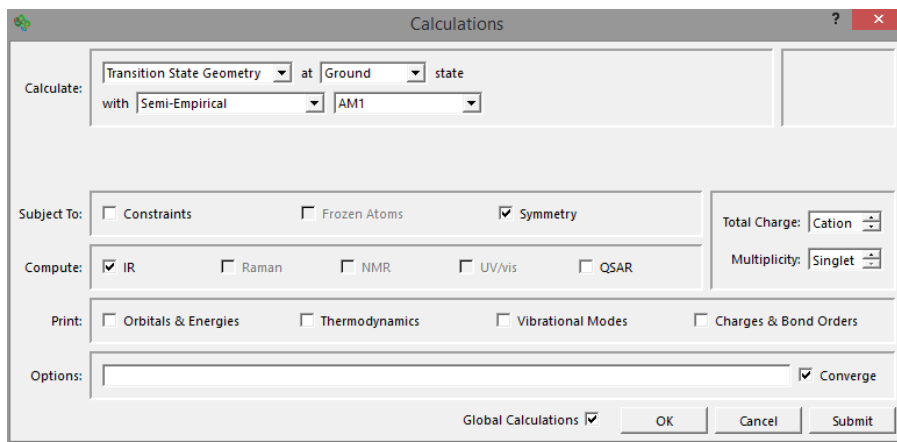
APPENDIX 6: CALCULATING THE ACTIVATION ENERGIES FOR INTERNAL PROTON TRANSFER

1. As steps 1 to 5 in Appendix 5.
2. Draw in the internal hydrogen bond. Constrain the bond lengths of the internal hydrogen bond so that both bonds to the hydrogen are approximately equidistant. An example is given in the figure immediately below where the bond length for an internal hydrogen bond in m/z 193 was be entered into the interactive box on the bottom right hand side of the screen:

Constraint(Con1) =   1.080 Å Profile



3. The energy of the structure was then minimised using the molecular mechanics icon  on the toolbar.
4. From the toolbar, 'Setup' then 'Calculations' were selected, followed by 'Transition State Geometry', 'Semi-empirical' and 'AM1'. The charge was 'Cation' and 'Compute IR' was selected. Then 'Submit' the calculation.



- On completion of the calculation, 'Display' then 'Spectra' was used to verify that the results represent a true transition state. A transition state has only one imaginary vibration, shown with an 'i' before the frequency. Selecting this 'i' frequency showed the bonds to the migrating hydrogen vibrating.
- To calculate the energy of the transition state, from the toolbar 'Setup' then 'Calculations' were selected, followed by 'Energy' with 'DFT', settings as shown below:

- The energies of the starting and product cations (cation 4 and cation 1, respectively in the example of 1,1-dimethyl biguanidine) were available from previous DFT calculations allowing a reaction profile to be constructed and the activation energy calculated.
- The proton transfer was modelled in reverse (i.e. product cation to starting cation) to check the calculations.

APPENDIX 7. PROPOSED STRUCTURAL ASSIGNMENTS FOR PRODUCT IONS AND THEIR RELATIVE INTENSITIES

Table A-7.1 1-Methyl-2-pyrrolidinol

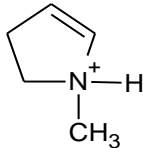
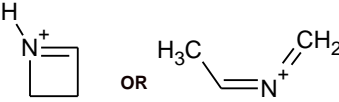
Relative intensity (%)	Experimental <i>m/z</i>	Proposed ion formula and calculated accurate mass	Error (ppm)	Proposed structure(s) of ion	Bond cleaved
100	84.082	C ₅ H ₁₀ N 84.0813	4.8		C4,O6
20	56.0506	C ₃ H ₆ N 56.050024	10.0		N5, C7 and/or N5,C3 and/or N5,C4 and/or C2,C4 and/or C1,C2 and/or C1,C3

Table A-7.2 Sulpiride

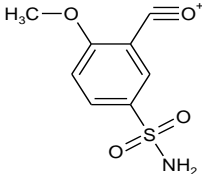
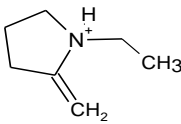
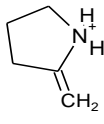
Experimental <i>m/z</i>	Proposed ion formula and calculated accurate mass	Error (ppm)	Proposed structure(s) of ion	Bond cleaved
214.0128	C ₈ H ₈ SO ₄ N 214.0174	21		C13,N15
112.1113	C ₇ H ₁₄ N 112.1126	11	 <i>m/z</i> 112	N15,C16
84.0803	C ₅ H ₁₀ N 84.0813	12	 <i>m/z</i> 84	N15,C16 N18,C19

Table A-7.3 Ziprasidone

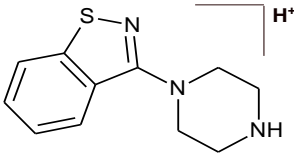
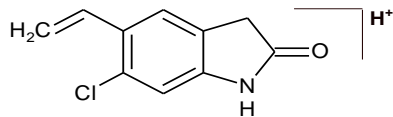
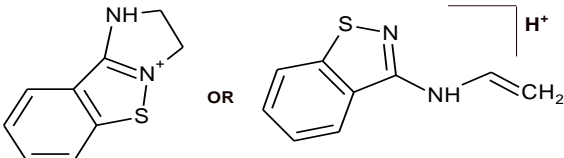
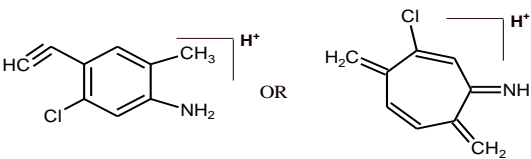
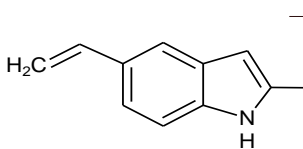
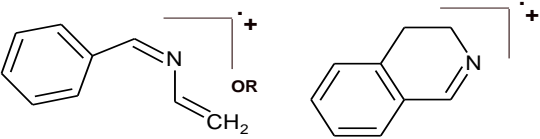
Relative intensity (%)	Experimental <i>m/z</i>	Proposed ion formula and calculated accurate mass	Error (ppm)	Proposed structure(s) of ion	Bond cleaved
5%	220.0924	C ₁₁ H ₁₄ N ₃ S 220.0908	7		N13,C12
100%	194.0331	C ₁₀ H ₉ ClNO 194.0373	22		N13,C12
23%	177.0487	C ₉ H ₉ N ₂ S 177.0486	<1		N13,C25 N13,C14 N16,C15 N16,C26
20%	166.0427	C ₉ H ₉ ClN 166.0424	2		N13,C12 C2,C28 C2,N3
25%	159.0678	C ₁₀ H ₉ NO 159.0684	4		N13,C12 C8,C19
8%	131.0738	C ₉ H ₉ N 131.0735	2		S19,C20 N18,C17 N16,C25 N16,C13 N13,C14 N13,C25

Table A-7.4 Ephedrine

Relative intensity (%)	Experimental <i>m/z</i>	Proposed ion formula and calculated accurate mass	Error (ppm)	Proposed structure(s) of ion	Bond cleaved
100	148.1109	C ₁₀ H ₁₄ N 148.1126	12		O1,C2
10	133.0897	C ₉ H ₁₁ N 133.0892	4		O1,C2 N10,C11
10	117.0710	C ₉ H ₉ 117.0704	5		O1,C2 N10,C9

Table A-7.5 Doxazosin

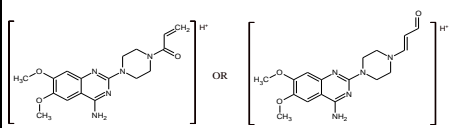
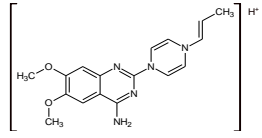
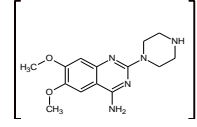
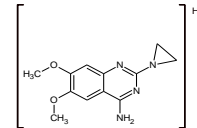
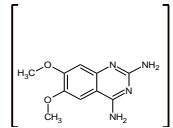
Relative intensity (%)	Experimental <i>m/z</i>	Proposed ion formula and calculated accurate mass	Error (ppm)	Proposed structure(s) of ion	Bond cleaved
100	344.1723	344.1723 C ₁₇ H ₂₂ N ₅ O ₃	24.0		C27,O26 C25,O26 C24,O33 C22,O23
10	326.1644	326.1617 C ₁₇ H ₂₀ N ₅ O ₂	8.0		C25,O26 C24,O33 C22,O23
27	290.1615	290.1617 C ₁₄ H ₂₀ N ₅ O ₂	<1		N19,C22
50	247.1174	C ₁₂ H ₁₅ N ₄ O ₂ 247.1195	8.0		N19,C20 N19,C18
10	221.105	221.1039 C ₁₀ H ₁₃ N ₄ O ₂	5.0		N16,C21 N16,C17

Table A-7.6 CEN025-14

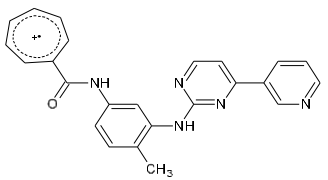
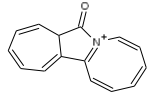
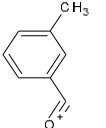
Relative intensity (%)	Experimental <i>m/z</i>	Proposed ion formula and calculated accurate mass	Error (ppm)	Proposed structure(s) of ion	Bond cleaved
100%	394.1680	C ₂₄ H ₂₀ N ₅ O 394.1668	3		N25,C24
10%	222.0952	C ₁₅ H ₁₂ NO 222.0919	15		N25,C24 N4,C3
10%	119.0516	C ₈ H ₇ O 119.0497	16		N25,C24 C20,N19

Table A-7.7 Trichlormethiazide

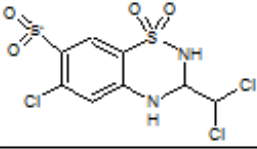
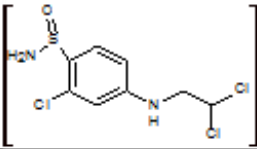
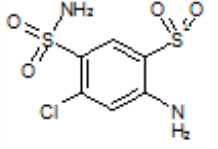
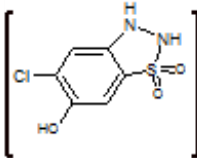
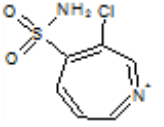
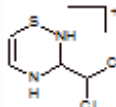
Relative Intensity	Experimental m/z	Proposed ion formula and calculated accurate mass	Error (ppm)	Proposed structure(s) of ion	Bond cleaved
40%	362.8833	$C_9H_7Cl_3N_2O_4S_2$ 362.8835	<1		N1, S2
40%	286.9586	$C_8H_{10}Cl_2N_2OS$ 286.9579	2		S2, O3 or S2, O4 S13, C16 N12, C11
100%	268.9464	$C_8H_8ClN_2O_4S_2$ 268.9458	2		S13, N12 C11, N10
20%	220.9764	$C_8H_7ClN_2O_3S$ 220.9736	10		S2, O3 S2, O4 S13, N12
40%	204.9843	$C_8H_7ClN_2O_3S$ 204.9839	2		S13, C16 C11, N10
10%	183.9639	$C_4H_6Cl_2N_2S$ 183.9629	5		S13, O15 S13, O14 C16, C17 C9, C8

Table A-7.8 Reserpine

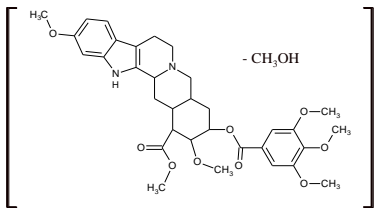
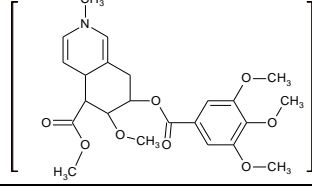
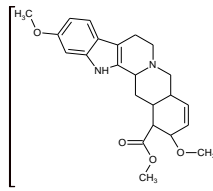
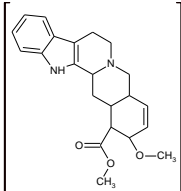
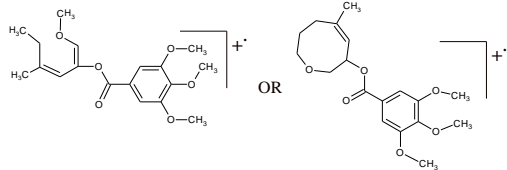
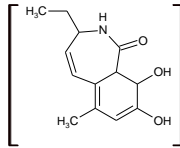
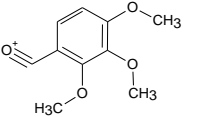
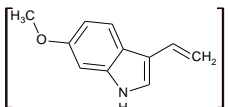
Relative intensity	Experimental <i>m/z</i>	Proposed ion formula and calculated accurate mass	Error (ppm)	Proposed structure(s) of ion	Bond cleaved
10%	577.2564	C ₃₂ H ₃₇ N ₂ O ₉ 577.255	2	 $\left[\text{Reserpine} - \text{CH}_3\text{OH} \right]^+ \text{H}^+$	O17, C16 O38, C37 O41, C40 O44, C43 O49, C47
40%	448.1190	C ₂₃ H ₃₀ NO ₈ 448.1971	4	 $\left[\text{Reserpine} - \text{CH}_3 \right]^+ \text{H}^+$	C10, C12 C24, C23
60%	397.2150	C ₂₃ H ₂₈ N ₂ O ₄ 397.2127	6	 $\left[\text{Reserpine} - \text{OCH}_3 \right]^+ \text{H}^+$	O38, C37 O41, C40 O44, C43 O32, C33
20%	365.1857	C ₂₂ H ₂₄ N ₂ O ₃ 365.1846	2	 $\left[\text{Reserpine} - \text{CH}_3 \right]^+ \text{H}^+$	O38, C37 O41, C40 O44, C43 O32, C33 O17, C16
10%	336.1600	C ₁₈ H ₂₄ NO ₆ 336.1572	8	 $\left[\text{Reserpine} - \text{Fragment} \right]^+ \text{H}^+$	C47, C45 C5, C7 C26, N25 C9, C10
20%	236.1268	C ₁₃ H ₁₈ NO ₃ 236.1287	8	 $\left[\text{Reserpine} - \text{CH}_3 \right]^+ \text{H}^+$	C22, C21 N13, C14 O32, C33
100%	195.0665	C ₁₀ H ₁₁ O ₄ 195.0657	6	 $\left[\text{Reserpine} - \text{CH}_3 \right]^+ \text{H}^+$	O32, C33
50%	174.0933	C ₁₁ H ₁₁ NO 174.0919	8	 $\left[\text{Reserpine} - \text{CH}_3 \right]^+ \text{H}^+$	C10, C12 C24, C23

Table A-7.9 5-(*p*-Methylphenyl)-5-phenylhydantoin

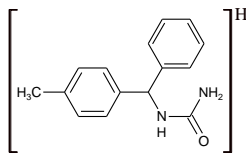
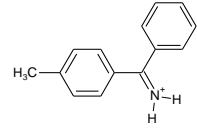
Relative Intensity	Experimental <i>m/z</i>	Proposed ion formula and calculated accurate mass	Error (ppm)	Proposed structure(s) of ion	Bond cleaved
8%	239.1200	C ₁₅ H ₁₅ N ₂ O 239.1184	7		N13,C8 C8,N9
100%	196.1108	C ₁₄ H ₁₄ N 196.1126	10		C12,C10 N13,C8
8%	104.0505	C ₇ H ₆ N 104.0500	5		C12,C14 C12,C10 N13,C8

Table A-7.10 1,1-Dimethyl biguanidine

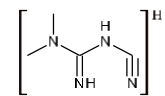
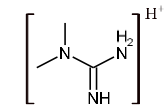
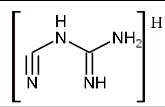
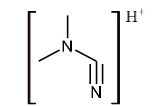
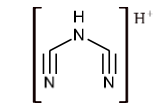
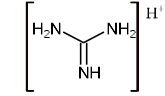
Relative intensity (%)	Experimental <i>m/z</i>	Proposed ion formula and calculated accurate mass	Error (ppm)	Proposed structure(s) of ion	Bond cleaved
90%	113.0834	C ₄ H ₈ N ₄ 113.0827	6		C7,N9 or N8,C7
40%	88.0865	C ₃ H ₉ N ₃ 88.0875	11		N6,C7
40%	85.0512	C ₂ H ₄ N ₄ 85.0514	3		N2,C4 or N5,C4 N2,C3 N2,C1
55%	71.0610	C ₃ H ₆ N ₂ 71.0609	1		C4,N6
15%	68.2490	C ₂ H ₂ N ₃ 68.0249	<1		C7,N9 N8,C7
35%	60.0561	CH ₆ N ₃ 60.0562	1		C4,N6 or N2,C1 N2,C3 N6,N7

Table A-7.11 Amlodipine

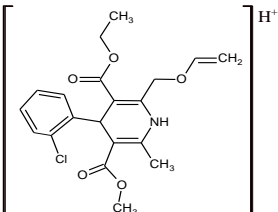
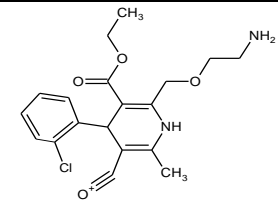
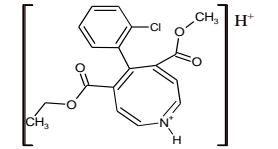
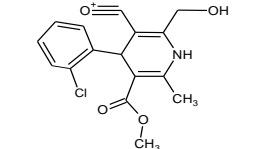
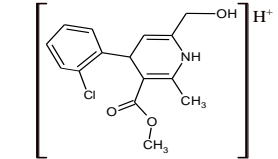
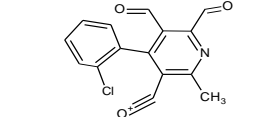
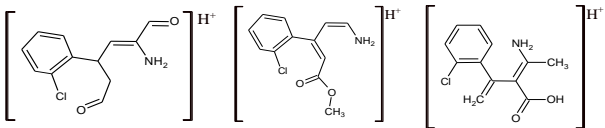
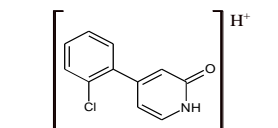
Relative intensity	Experimental <i>m/z</i>	Proposed ion formula and calculated accurate mass	Error (ppm)	Proposed structure(s) of ion	Bond breaking
10%	392.1281	C ₂₀ H ₂₃ ClNO ₅ 392.1264	4		N23,C22
40%	377.1299	C ₁₉ H ₂₂ ClN ₂ O ₄ 377.1268	8		C25,027
10%	346.0836	C ₁₈ H ₁₇ ClNO ₄ 346.0846	3		O20,C19
20%	320.0682	C ₁₆ H ₁₅ ClNO ₄ 320.0689	2		O20,C21 C14,016 or C19,O20 O16,C17
75%	294.0928	C ₁₅ H ₁₇ ClNO ₃ 294.089697	10		O20,C21 C14,016
10%	286.0321	C ₁₅ H ₉ ClNO ₃ 286.0271	17		O27,C26 O16,C14 O20,C21
100%	238.0652	C ₁₂ H ₁₃ ClNO ₂ 238.0635	7		C12,C19 C14,016 C13,C14 C9,C10 C10,N11 or O20,C21 N11,C10 C10, C9 C14,016
10%	206.0390	C ₁₁ H ₈ ClNO 206.037266	8		C9,C10 C19,C20 N11,C10 C13,C14

Table A-7.12 Cortisone

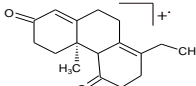
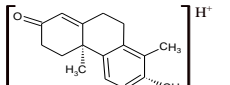
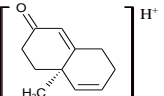
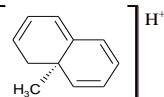
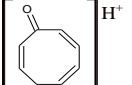
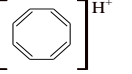
Relative intensity (%)	Experimental <i>m/z</i>	Proposed ion formula and calculated accurate mass	Error (ppm)	Proposed structure(s) of ion	Bond cleaved
15%	258.1617	C ₁₇ H ₂₂ O ₂ 258.1620	1		C7,C5 C28,C5
10%	241.1597	C ₁₇ H ₂₁ O 241.1592	2		C7,C8 C28,C5 C2,O1
100%	163.1119	C ₁₁ H ₁₅ O 163.1123	2		C23,C25 C9,C8 C5,C28
30%	145.1022	C ₁₁ H ₁₃ 145.1017	3		C23,C25 C9,C11 C17,O18
25%	121.0660	C ₈ H ₉ O 121.0653	5		C23,C21 C13,C14
30%	105.0708	C ₈ H ₉ 105.0708	4		C23,C21 C14,C13 C17,O18
15%	93.0700	C ₇ H ₉ 93.0704	5		C23,C21 C14,C13 C17,O18

Table A-7.13 Desipramine

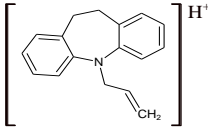
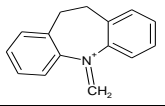
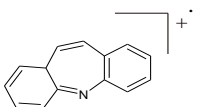
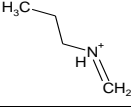
Relative Intensity	Experimental <i>m/z</i>	Proposed ion formula and calculated accurate mass	Error (ppm)	Proposed structure(s) of ion	Bond cleaved
30%	236.1423	C ₁₇ H ₁₈ N 236.1439	6		N19,C18
100%	208.1121	C ₁₅ H ₁₄ N 208.1126	3		N15,C6 N19,C20
20%	193.0900	C ₁₄ H ₁₁ N 193.0891	5		N15,C16
10%	72.0817	C ₄ H ₁₀ N 72.081324	5		N15,C16

Table A-7.14 Sildenafil

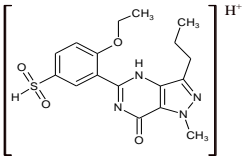
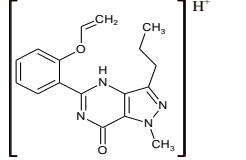
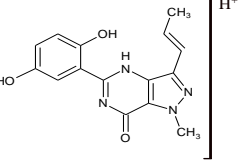
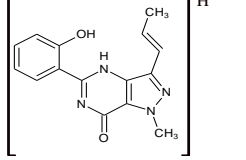
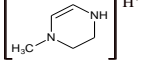
Relative Intensity	Experimental <i>m/z</i>	Proposed ion formula and calculated accurate mass	Error (ppm)	Proposed structure(s) of ion	Bond cleaved
10%	377.1289	C ₁₇ H ₂₁ N ₄ O ₄ S 377.1284	1		S2,N4
30%	311.1526	C ₁₇ H ₁₉ N ₄ O ₂ 311.1508	6		S2,C11
10%	299.1165	C ₁₅ H ₁₅ N ₄ O ₃ 299.1144	7		S2,C11 S2,01 S2,02 029,C30
50%	283.1215	C ₁₅ H ₁₅ N ₄ O ₂ 283.1195	7		S2,C11 029,C30
10%	99.0928	C ₅ H ₁₂ N ₂ 99.0922	6		S2,N4

Table A-7.15 Dofetilide (see also Table 2.3 in Chapter 2).

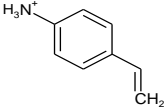
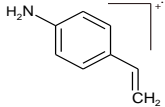
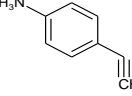
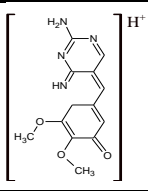
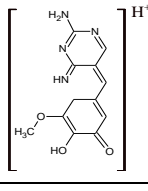
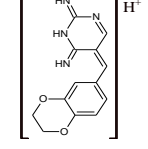
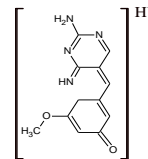
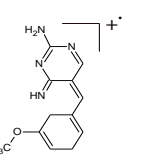
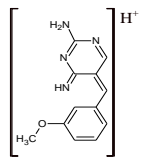
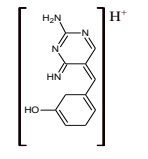
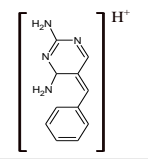
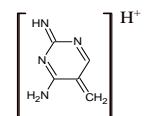
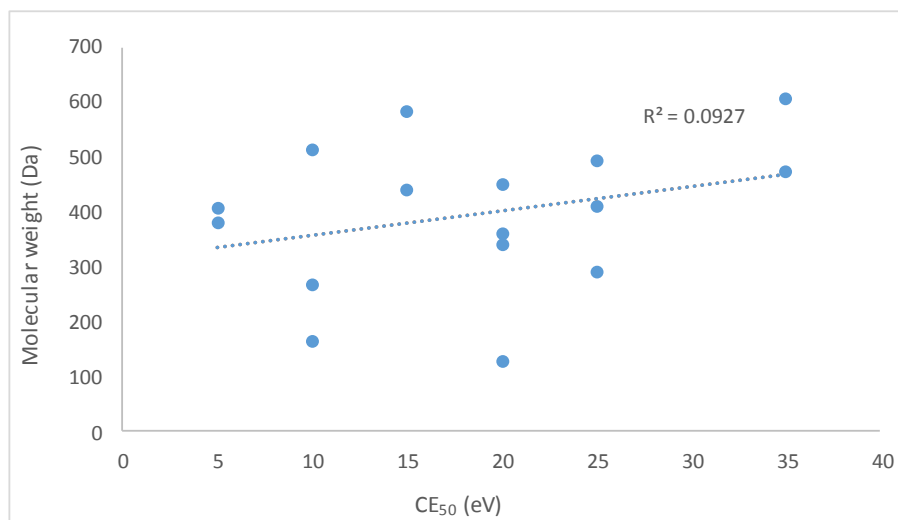
Experimental <i>m/z</i>	Proposed ion formula and calculated accurate mass	Error (ppm)	Proposed structure(s) of ion
120.8100	C ₈ H ₁₀ N 120.0813	2	
119.0725	C ₈ H ₉ N 119.735	8	
118.0647	C ₈ H ₈ N 118.0657	2	

Table A-7.16 Trimethoprim

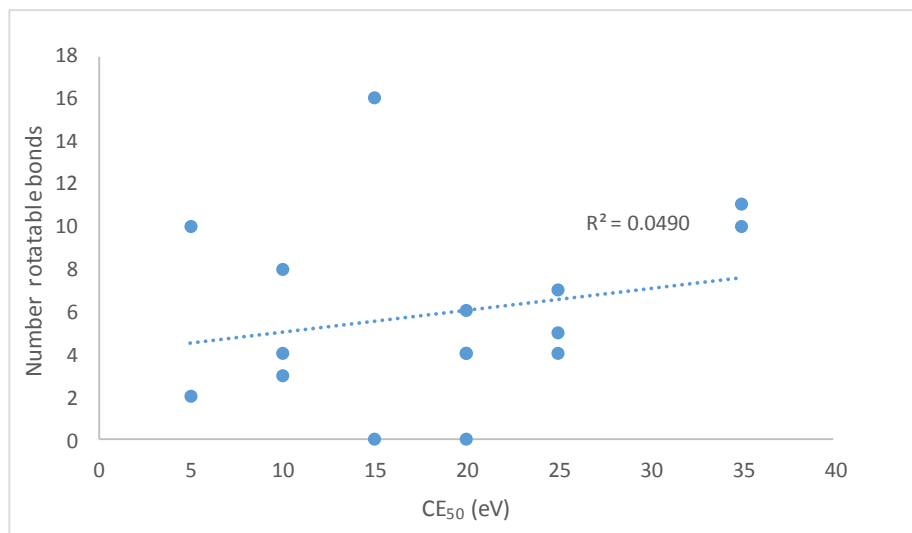
Relative intensity (%)	Experimental <i>m/z</i>	Proposed ion formula and calculated accurate mass	Error (ppm)	Proposed structure(s) of ions	Bond breaking
65%	275.1142	C ₁₃ H ₁₅ N ₄ O ₃ 275.1144	<1		O11,C12 O9,C10 O2,C1
100%	261.0963	C ₁₂ H ₁₃ N ₄ O ₃ 261.0988	2		O11,C12 O9,C10 O2,C1
35%	257.1036	C ₁₃ H ₁₃ N ₄ O ₂ 257.103851	1		C7,O11 C3,O2
35%	245.1031	C ₁₂ H ₁₃ N ₄ O ₂ 245.1039	3		C7,O11 C8,O9 C3,O2
80%	230.1160	C ₁₂ H ₁₄ N ₄ O 230.1168	3		C7,O11 C8,O9 C3,O2
30%	229.1088	C ₁₂ H ₁₃ N ₄ O 229.1089	<1		C7,O11 C8,O9 C3,O2
15%	217.1082	C ₁₁ H ₁₂ N ₄ O 217.1089	3		C7,O11 C8,O9 C3,O2 O11,C12 O9,C10 O2,C1
15%	201.1134	C ₁₁ H ₁₃ N ₄ 201.1140	3		C7,O11 C8,O9 C3,O2
40%	123.0672	C ₅ H ₇ N ₄ 123.0671	< 1		C5,C13

APPENDIX 8. PLOTS OF PHYSICOCHEMICAL PROPERTIES VERSUS CE₅₀ (THE COLLISION ENERGY AT WHICH THE SURVIVAL YIELD IS 50%)

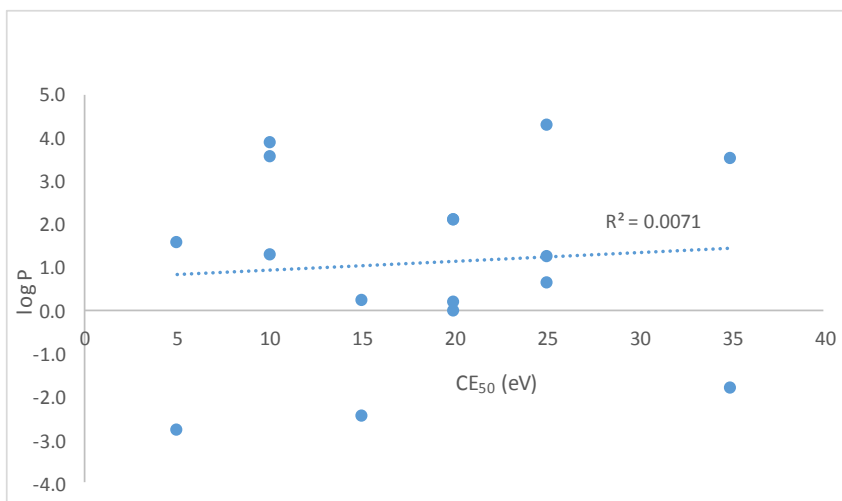
a) Molecular weight



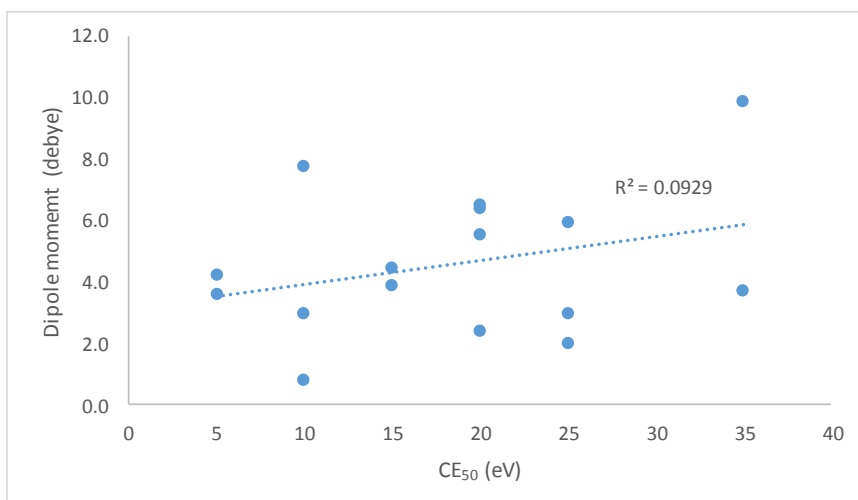
b) Number of rotatable bonds



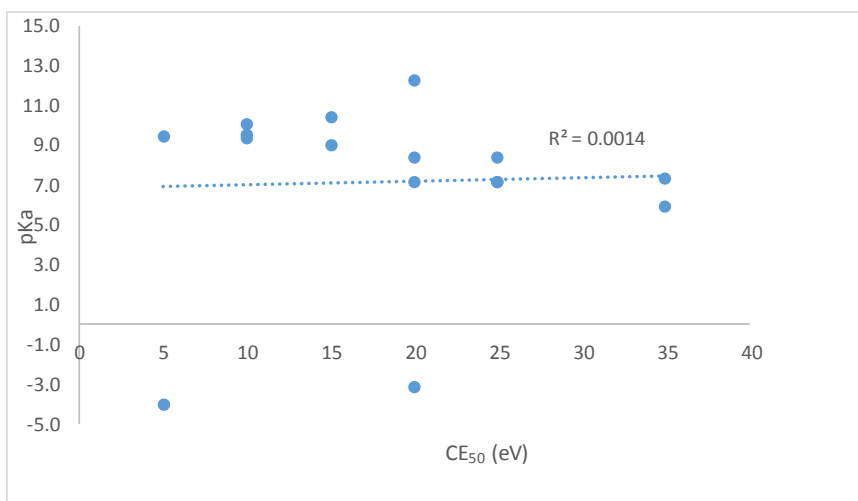
c) LogP



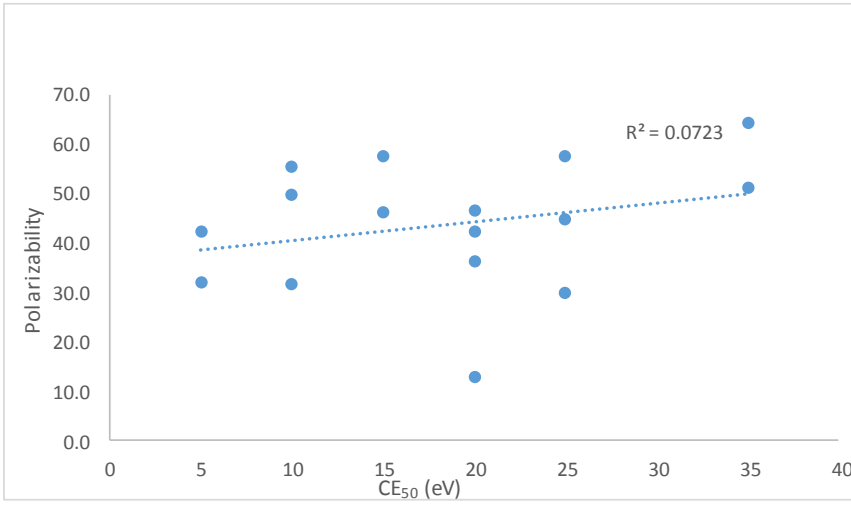
d) Dipole moment



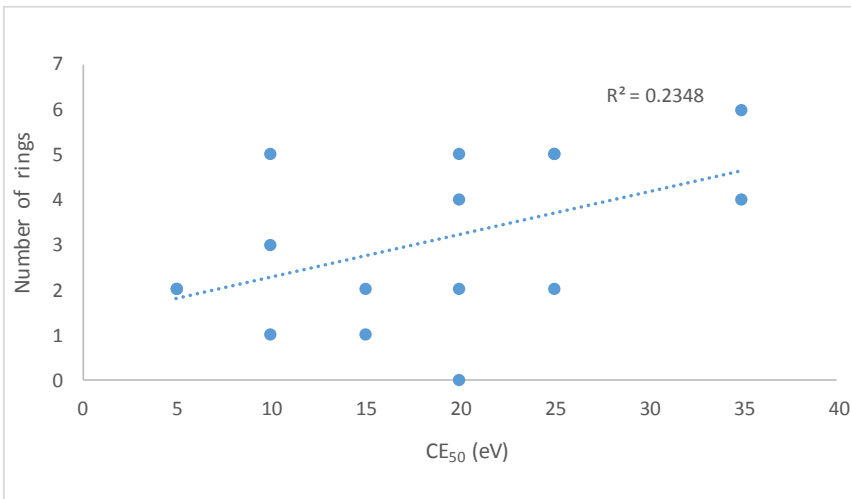
e) pKa



f) Polarizability



g) Number of rings



h) LogD

